

Technical Report No. 32-458

Mars Atmosphere Entry Parametric Study

J. M. Brayshaw

M. G. Comuntzis
M. G. Comuntzis, Acting Chief
Spacecraft Design Section

JET PROPULSION LABORATORY
CALIFORNIA INSTITUTE OF TECHNOLOGY
PASADENA, CALIFORNIA

September 15, 1963

**Copyright © 1963
Jet Propulsion Laboratory
California Institute of Technology**

**Prepared Under Contract No. NAS 7-100
National Aeronautics & Space Administration**

CONTENTS

I. Introduction	1
A. Constant Conditions	2
B. Variable Conditions	2
C. Results	3
II. Description of plots A-1 through A-384	5
Nomenclature	6
References	7
Appendix. Mars Atmosphere Entry Parameters	9

TABLES

1. Some properties of model atmospheres for Mars	2
2. Table of plots	6

FIGURES

1. Model atmospheres for Mars—temperature profile	3
2. Model atmospheres for Mars—density profile	3
3. Trajectory geometry	3
4. Summary plot--extreme QS_{\max} and ACX_{\max}	4
5. Summary plot--surface impact velocity (no parachute)	4
6. Summary plot--altitude for possible parachute deployment (Mach No. = 3, extreme VE = 21,700 ft/sec)	5
A-1 through A-384	10

ABSTRACT

In anticipation that the many technical disciplines involved in a Mars planetary entry program will require such information for design studies and preliminary design decisions, a fairly complete parametric study of the Mars atmospheric entry was performed. The expected extreme model atmospheres¹ as well as the anticipated extremes of initial entry velocity, entry angle and ballistic coefficient were included. As functions of these variables, the following parameters are plotted in graphical form:

1. Flight path acceleration vs altitude
2. Mach No. vs altitude
3. Dynamic pressure vs altitude
4. Heating rate vs altitude
5. Flight path angle vs altitude
6. Atmospheric velocity vs altitude
7. Altitude vs time
8. Altitude vs planet centered angle

In addition, summary plots of peak heating rate, peak acceleration, unretarded impact velocity, and altitude for parachute deployment are shown as a function of entry angle for the extremes of ballistic coefficient and model atmosphere.

The material is presented for reference use only, and no attempt is made to analyze the significance of the relationships depicted for a particular mission.

¹New planet spectrographic observations now under evaluation at JPL tentatively indicate a considerably lower limit on the density-altitude profile band.

I. INTRODUCTION

In order to assess the vehicle design problems involved in entering the atmosphere of Mars, to weigh compromise solutions to these problems, and to provide the terminal extension of planet approach space trajectories, a parametric study varying initial trajectory conditions,

planet atmosphere models, and vehicle ballistic coefficient was performed. The Jet Propulsion Laboratory powered flight entry program (Refs. 1 and 2) was used on the IBM 7090 computer. This is a point-mass trajectory solution, i.e., it considers only the translatory motion of the vehicle.

A. Constant conditions

1. Motion confined to equatorial plane, counter to planet rotation
2. Mars rotation velocity
3. Mars diameter
4. Mars gravity, surface
5. Initial altitude: 1,000,000 ft above surface
6. Vehicle drag coefficient (hypersonic): 0.7 with Mach No. variation
7. Atmosphere fixed to planet: no wind

8. Vehicle maximum diameter: 2.75 ft

9. Angle of attack: 0°

B. Variable conditions

1. Model atmosphere (Ref. 3): A, B, C and F as defined in Table 1 and Figs. 1 and 2
2. Initial velocity with respect to atmosphere: 15,200 to 37,000 ft/sec
3. Initial angle, flight path to local horizon: 20 to 90 deg
4. Ballistic coefficient or $\frac{m}{C_p A}$: 0.5 to 5.0, corresponding to gross weights of 67 to 670 lb

Table 1. Some properties of model atmospheres for Mars

Model designation	A	B	C	D	E	F
Composition (by volume)						
N ₂	86.8	97.25	98.7	86.8	97.25	98.7
CO ₂	7.2	1.9	0.7	7.2	1.9	0.7
A	6.0	0.85	0.6	6.0	0.85	0.6
Molecular weight	29.9	28.4	28.2	29.9	28.4	28.2
Surface pressure lb/ft ²	113	196	284	113	196	284
millibar	54	94	136	54	94	136
Ratio of specific heats	1.41	1.41	1.42	1.41	1.41	1.41
Temperature in stratosphere						
°R	410	320	230	230	410	410
°K	230	180	130	130	230	230
Temperature near surface						
°R	470	410	380	470	410	470
°K	260	230	210	260	230	260
Scale height*						
ft × 10 ⁻³	59	41	29	29	59	56
km	18	12.5	9	9	18	17
Reciprocal scale height*						
ft ⁻¹ × 10 ⁵	1.7	2.4	3.4	3.4	1.7	1.8
km ⁻¹ × 10 ²	5.6	8.0	11.0	11.0	5.6	5.9
Lapse rate						
°R ft ⁻¹ × 10 ³	-1.96	-2.04	-2.13	-1.96	0	-1.96
°K km ⁻¹	-3.43	-3.75	-4.10	-3.43	0	-3.43
Surface density						
slugs × ft ⁻³ × 10 ⁴	1.4	2.7	4.3	1.4	2.7	3.4
gm × cm ⁻³ × 10 ⁴	0.75	1.4	2.2	0.75	1.4	1.8
Acceleration of gravity						
ft/sec ²	11.8	12.3	12.8	12.8	11.8	12.8
cm/sec ²	360	375	390	390	360	390

* stratosphere

C. Results

The results give atmospheric ballistic entry variations of certain design parameters versus altitude or time (see

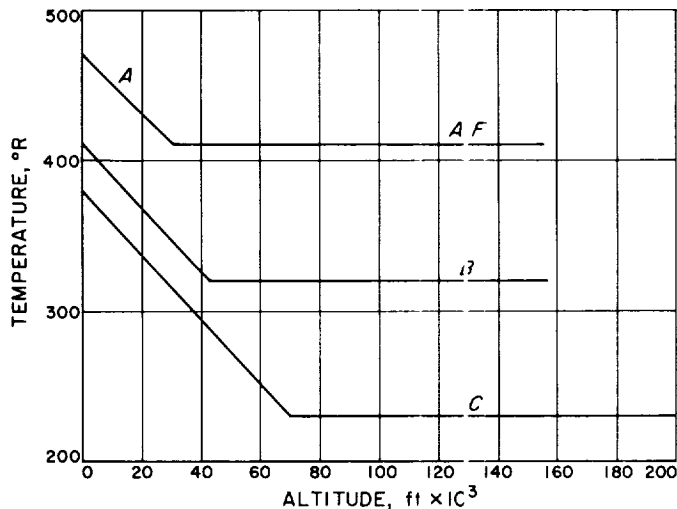


Fig. 1. Model atmospheres for Mars—temperature profile

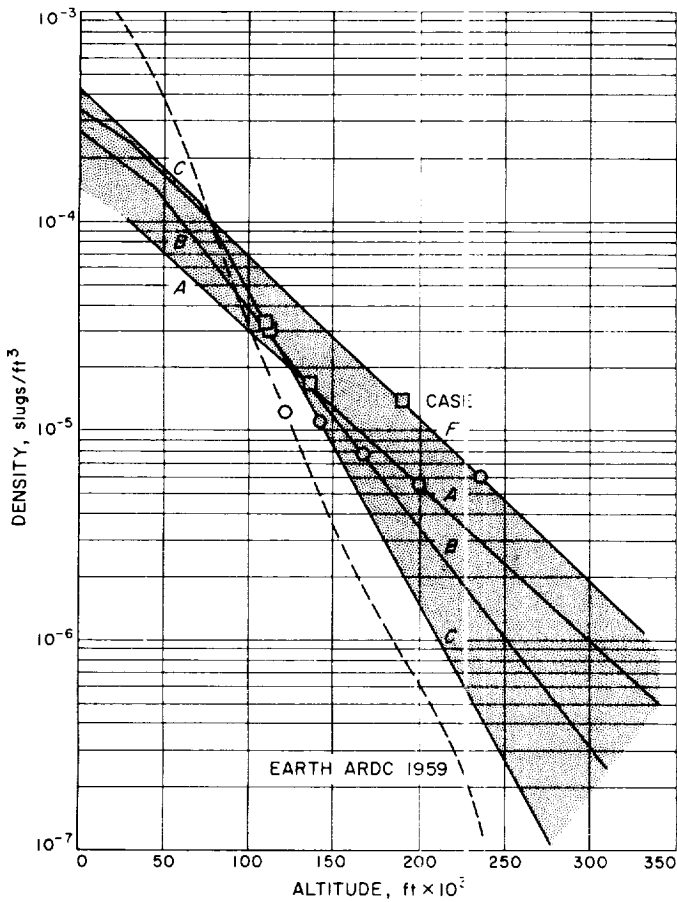


Fig. 2. Model atmospheres for Mars—density profile

nomenclature). Terminal motion under the influence of an auxiliary decelerator may be approximated by the assumption of a vertical trajectory starting at the desired Mach number and corresponding altitude. Results presented here (except for heating rates) also apply to vehicles having the same ballistic coefficients, but different combinations of diameter, weight, and drag coefficient (except in the low velocity terminal portion).

The atmosphere models chosen for use in this program span the expected temperature and density bands (see Figs. 1 and 2).

The initial velocity range extends from slightly less than escape velocity to a high value typical of short flight-time, low-payload missions. The most practical initial VE will probably fall between the two middle values.

At the highest ballistic coefficient and initial velocity it can be noted that the initial flight path angle of 20 deg below horizon is a marginal or overshoot condition. Depending on the atmosphere assumption, the vehicle is correspondingly captured immediately, captured after a reversal in rate of altitude change, or it escapes the planet. This is most easily seen in the plot of altitude vs ARC , which may be interpreted as ground range expressed in multiples of planet radius. The ALT vs ARC plot is thus a physical picture (with mismatched scales) of the trajectory. Figure 3 graphically defines trajectory geometry.

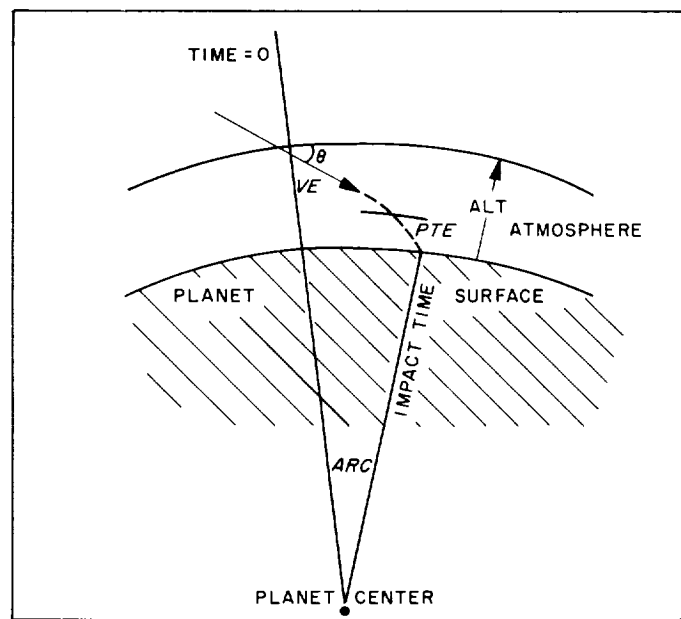


Fig. 3. Trajectory geometry

For purposes of comparison, all plot scales are the same. The percentage definition of small values suffers correspondingly. Printed output data and plotting tapes are available for fine-grained reexamination of any por-

tion of this study. Some of the extreme conditions possible within these bands of parameters are presented in Figs. 4, 5, and 6.

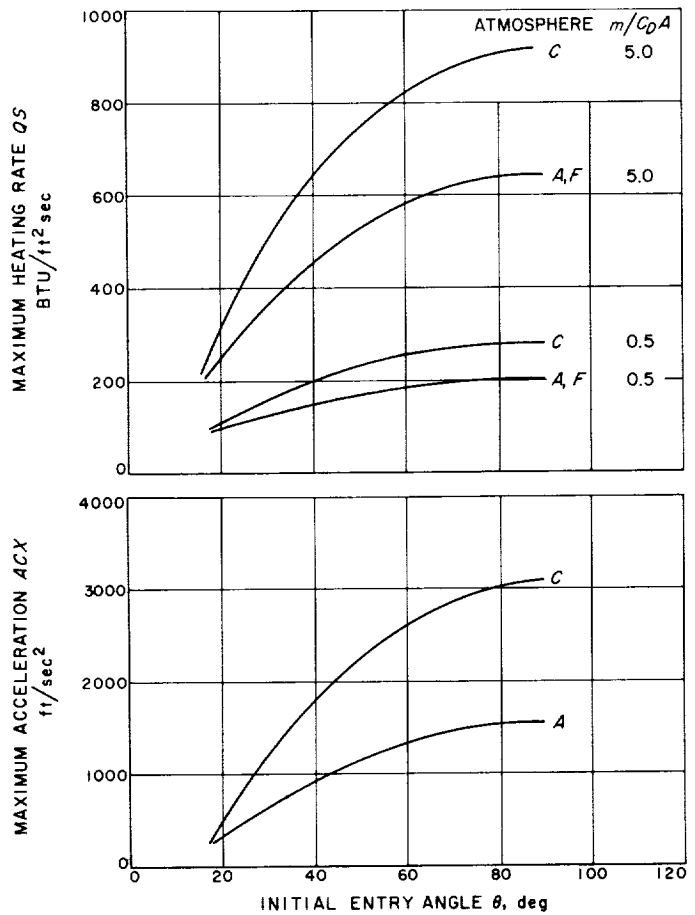


Fig. 4. Summary plot—extreme QS_{max} and ACX_{max}

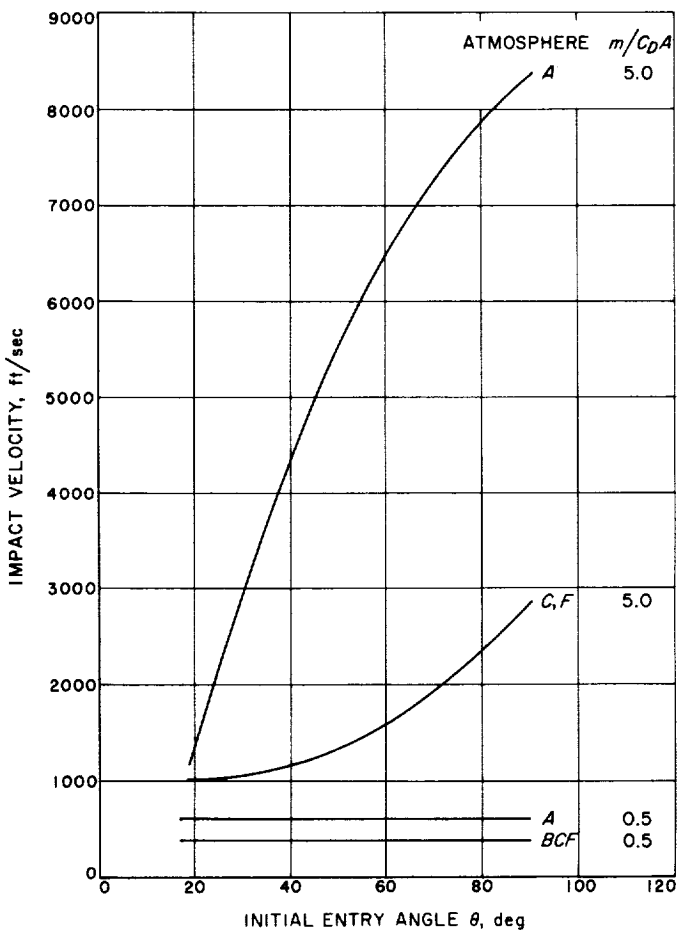


Fig. 5. Summary plot—surface impact velocity
(no parachute)

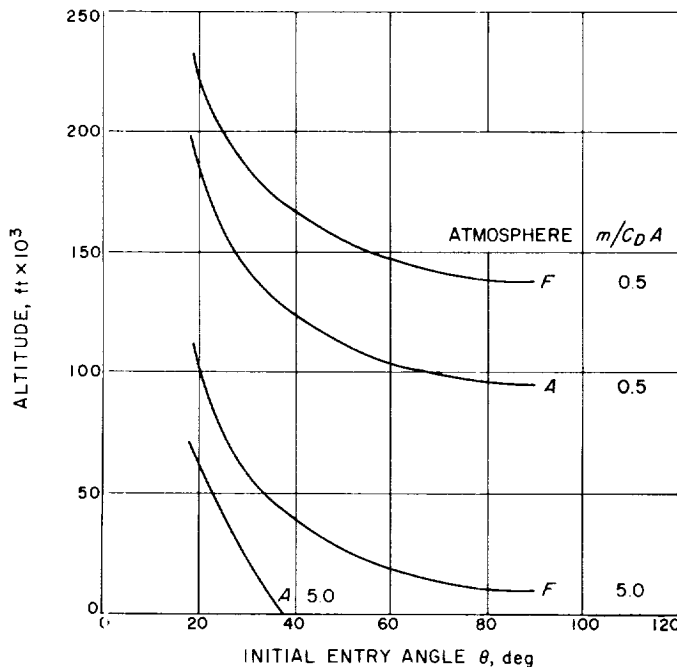


Fig. 6. Summary plot—altitude for possible parachute deployment (Mach No. = 3, extreme $VE = 21,700 \text{ ft/sec}$)

II. DESCRIPTION OF PLOTS

Quantities Plotted (see Table 2)

ACX	} vs ALT
Mach	
Q	
QS	
PTE	
VE	
ALT	vs TIM
ALT	vs ARC

Each of the four curves on a given plot (see Appendix) represents a different initial velocity (VE) of

15,200
21,700
29,300
or 37,000 ft/sec

The automatic plotting process does not allow machine labelling of curves. However, in most cases the identity

of the curves is evident, i.e., highest peak ACX , Q , QS , lowest initial decay rate of PTE vs ALT , and highest initial decay rate of ALT vs TIM correspond to highest initial VE .

The WEIGHT, which is a constant for each plot, corresponds to the following ballistic coefficients ($m/C_D A$), and densities. The density range is roughly that between balsa wood and water.

WEIGHT, lb	$m/C_D A$	Gross Density, lb/ft ³
67	0.5	5.7
200	1.5	17.1
400	3.0	34.2
667	5.0	57.0

The 200 lb, 21,700 ft/sec combination has received considerable attention at JPL in the past.

Table 2. Table of plots

Figure number	Ordinate	Abscissa	Weight	$m/C_D A$	ϕ	Atmosphere
A-1	ALT	TIM	67	0.5	20	A
A-2	VE	ALT	67	0.5	20	A
A-3	Mach	ALT	67	0.5	20	A
A-4	QS	ALT	67	0.5	20	A
A-5	Q	ALT	67	0.5	20	A
A-6	ACX	ALT	67	0.5	20	A
A-7	PTE	ALT	67	0.5	20	A
A-8	ALT	ARC	67	0.5	20	A
A-9 through A-16	Same as (A-1 through A-8)		200	1.5	20	A
A-17 through A-24	Same as (A-1 through A-8)		400	3.0	20	A
A-25 through A-32	Same as (A-1 through A-8)		667	5.0	20	A
A-33 through A-64	Same as (A-1 through A-8)		Same as (A-1 through A-32)	40		A
A-65 through A-96	Same as (A-1 through A-8)		Same as (A-1 through A-32)	90		A
A-97 through A-192	Same as (A-1 through A-8)		Same as (A-1 through A-32)	Same as (A-1 through A-96)		B
A-193 through A-288	Same as (A-1 through A-8)		Same as (A-1 through A-32)	Same as (A-1 through A-96)		C
A-289 through A-384	Same as (A-1 through A-8)		Same as (A-1 through A-32)	Same as (A-1 through A-96)		F

NOMENCLATURE

A	Vehicle projected frontal area, π (max. diam) 2 /4, ft/sec 2	Mach	Mach number, ratio of VE to local ambient sonic velocity
ACX	Acceleration along flight path direction, ft/sec 2	PTE	Local angle between VE and local horizon, rad
ALT	Length of perpendicular from vehicle to planet surface, ft	Q	Dynamic pressure, $(VE)^2 \rho /2$, lb/ft 2 /10.76
ARC	Planet centered angle between initial and current vehicle positions, $\frac{\text{Surface range}}{\text{Mars radius}}$	QS	Stagnation point heating rate, $2.15 \times 10^{-8} R_n^{-0.5} \rho^{0.5} V^{3.0}$, BTU/ft 2 sec
ATMOS	Atmosphere models defined in Table 1 and Figs. 1 and 2	R _n	Vehicle nose radius (max. diam)/2, ft
C _D	Drag coefficient drag force/QA	THETA	Initial angle between VE and local horizon, deg
m	Gross vehicle mass, slugs	TIM	Time after initial time, sec
		VE	Velocity of vehicle with respect to atmosphere, ft/sec
		WEIGHT	Gross vehicle weight on Earth, lb
		ρ	Atmosphere local density, slugs/ft 3

REFERENCES

1. Gianopoulos, G. N., *Generalized Powered Flight Trajectory Program*, Technical Report No. 32-38, Jet Propulsion Laboratory, Pasadena, California, September 28, 1960.
2. Kohlhase, C. E., *Additions to JPL Powered Flight Trajectory Program to Permit Planet Entry Simulation*, Jet Propulsion Laboratory Interoffice Memorandum, September 18, 1961.
3. Schilling, G. F., "Extreme Model Atmospheres of Mars," Report RM-2782-JPL, Rand Corporation, June 22, 1961.

APPENDIX

Mars Atmosphere Entry Parameters

The values for varied initial trajectory conditions, planet atmosphere models, and vehicle ballistic coefficients are presented in Figs. A-1 through A-384.

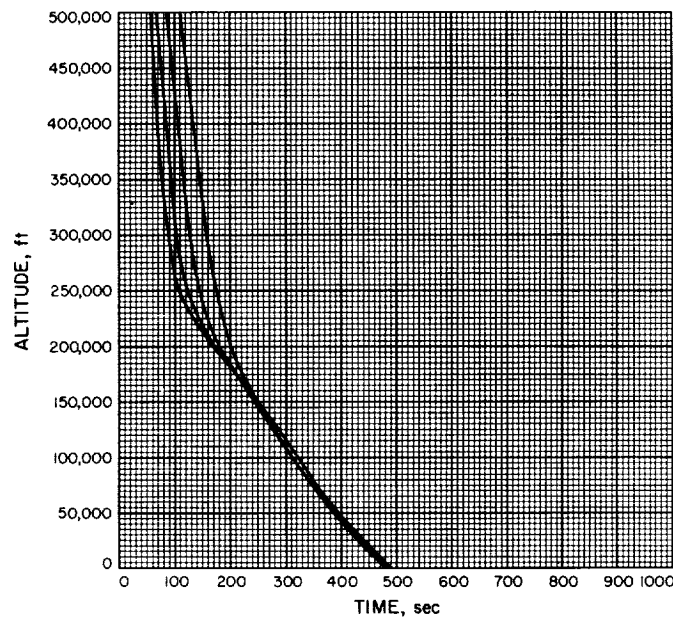


Fig. A-1

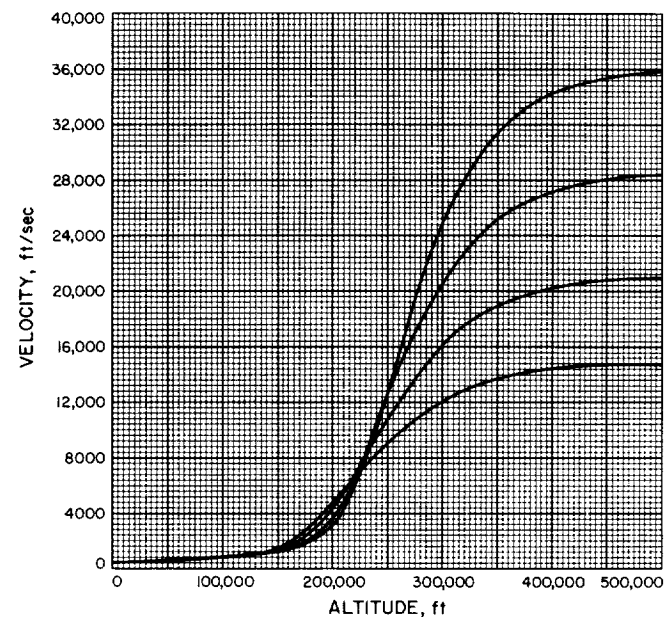


Fig. A-2

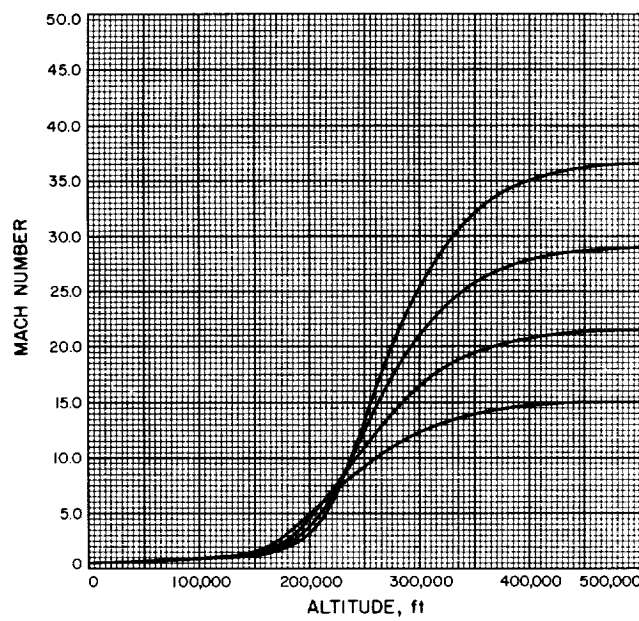


Fig. A-3

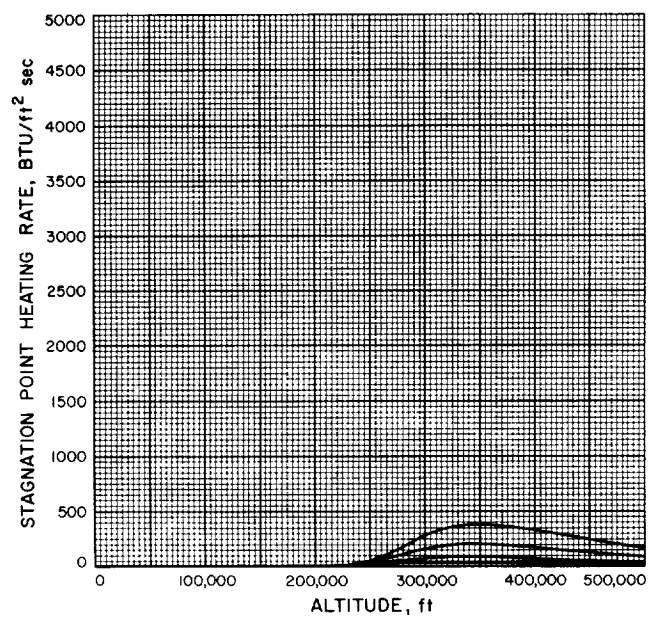


Fig. A-4

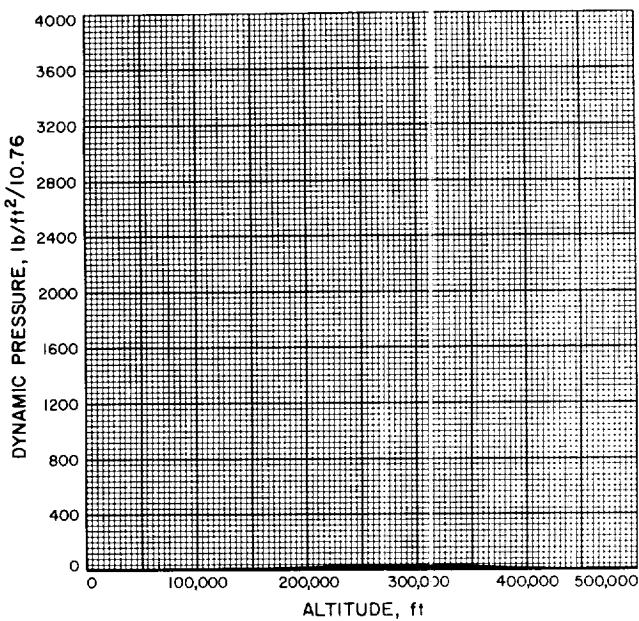


Fig. A-5

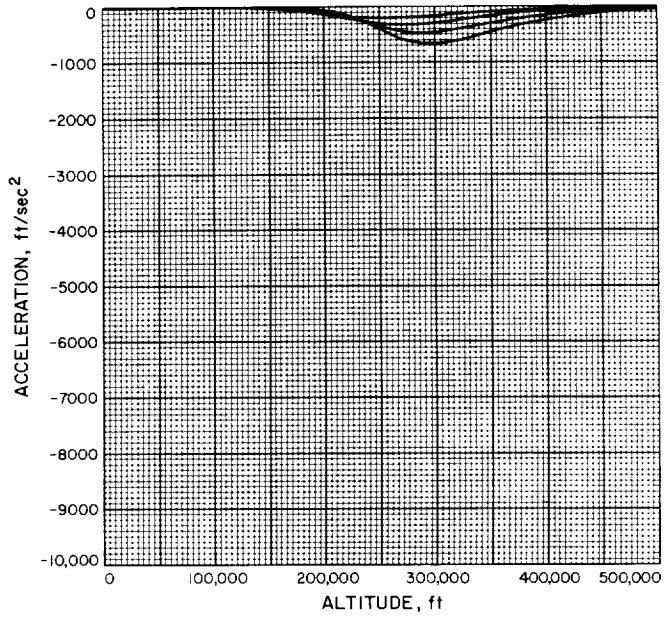


Fig. A-6

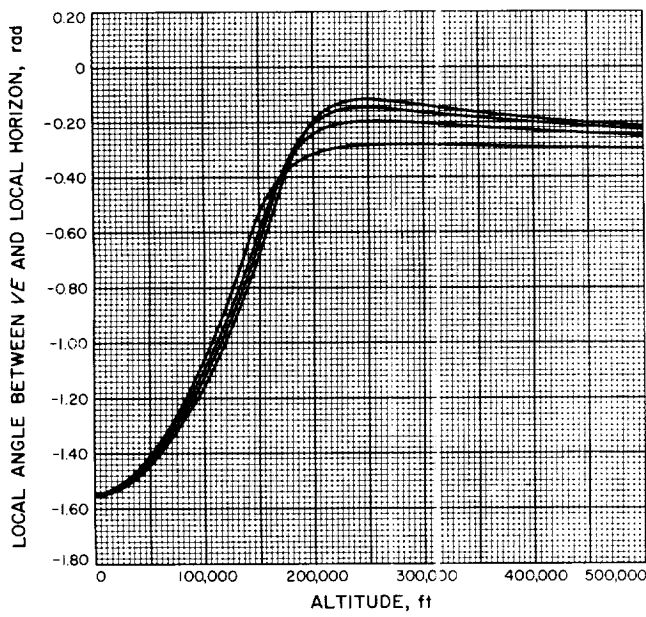


Fig. A-7

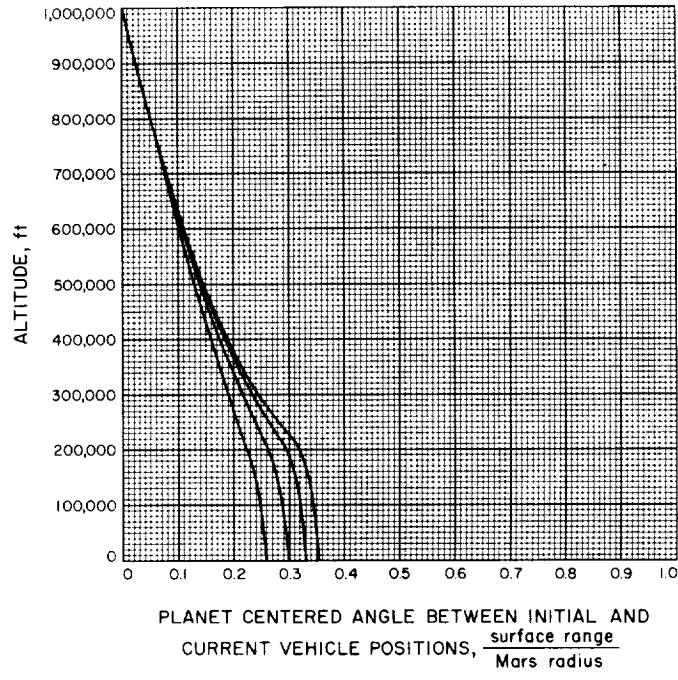


Fig. A-8

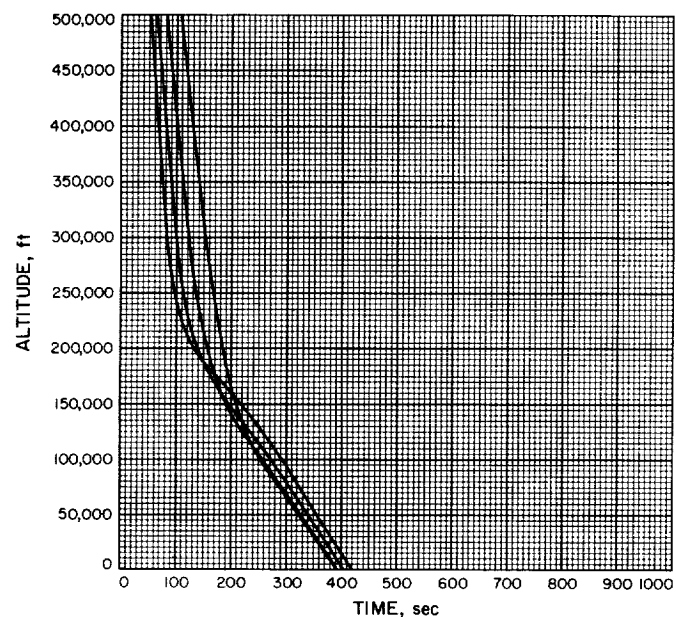


Fig. A-9

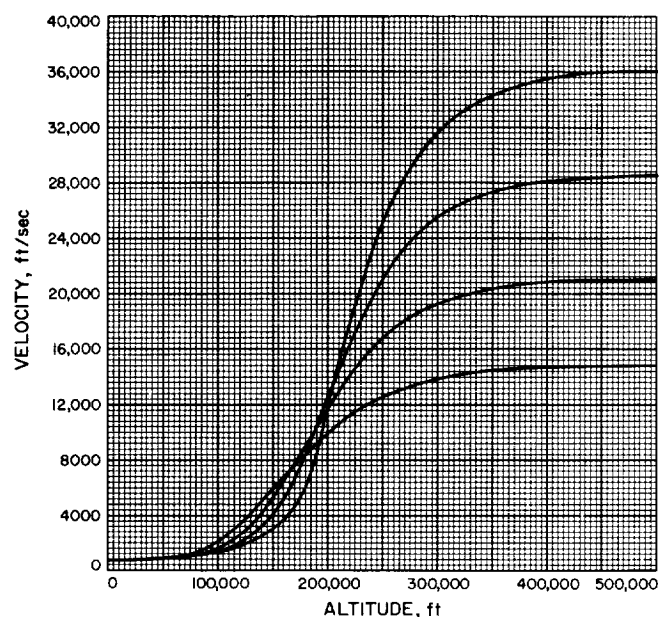


Fig. A-10

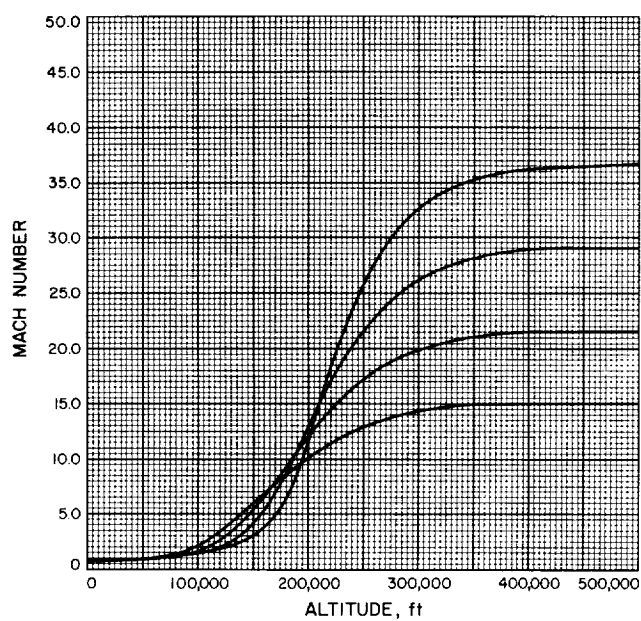


Fig. A-11

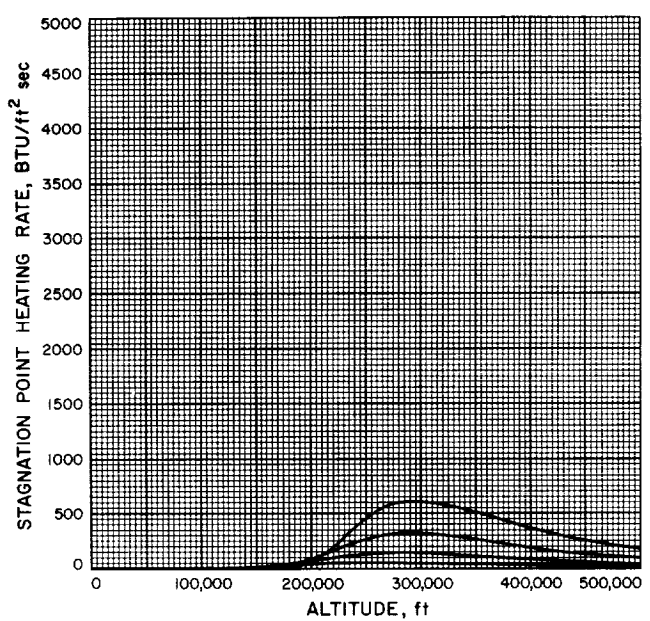


Fig. A-12

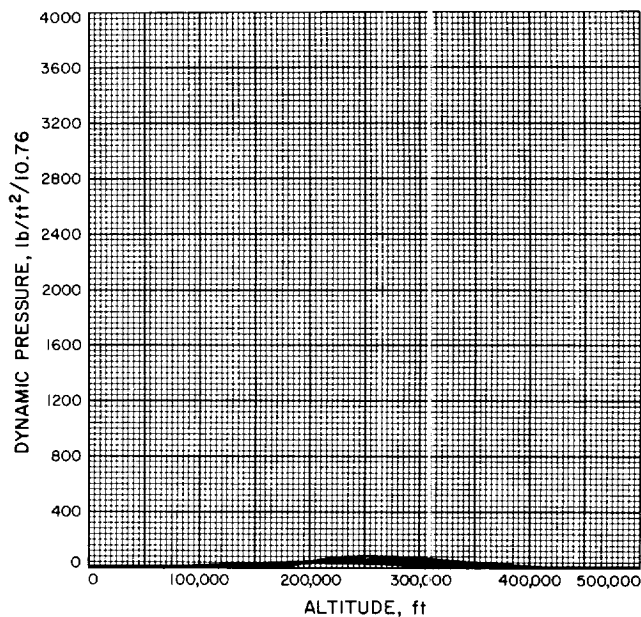


Fig. A-13

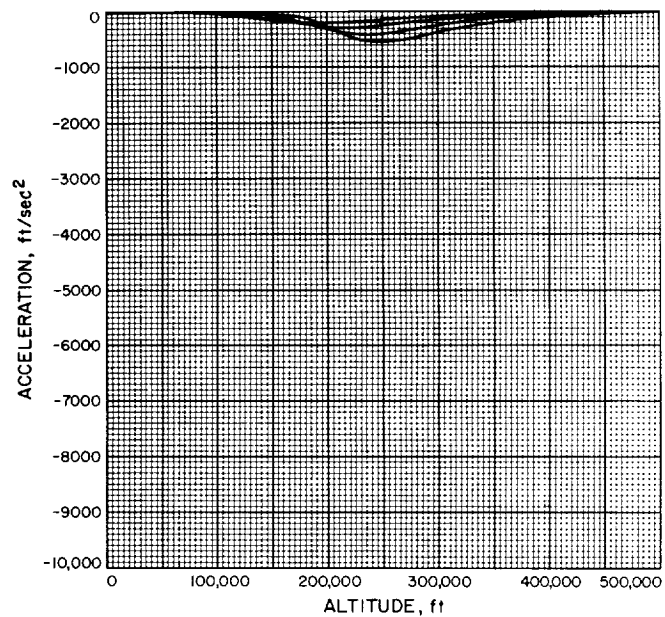


Fig. A-14

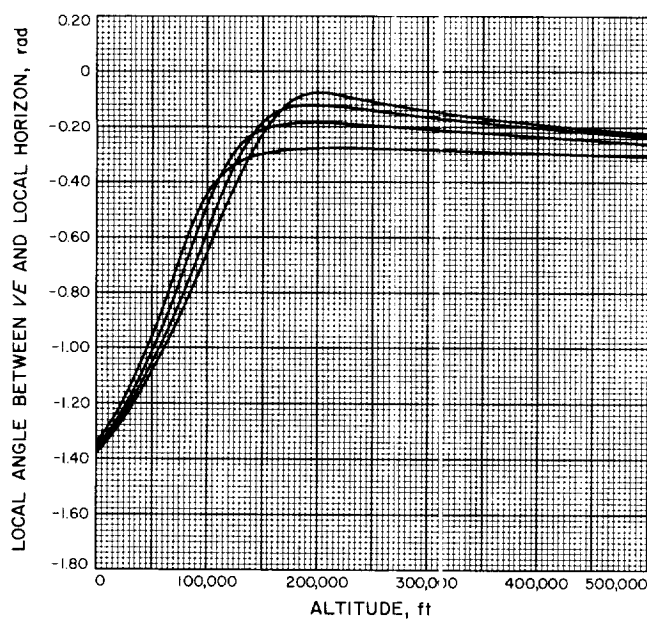


Fig. A-15

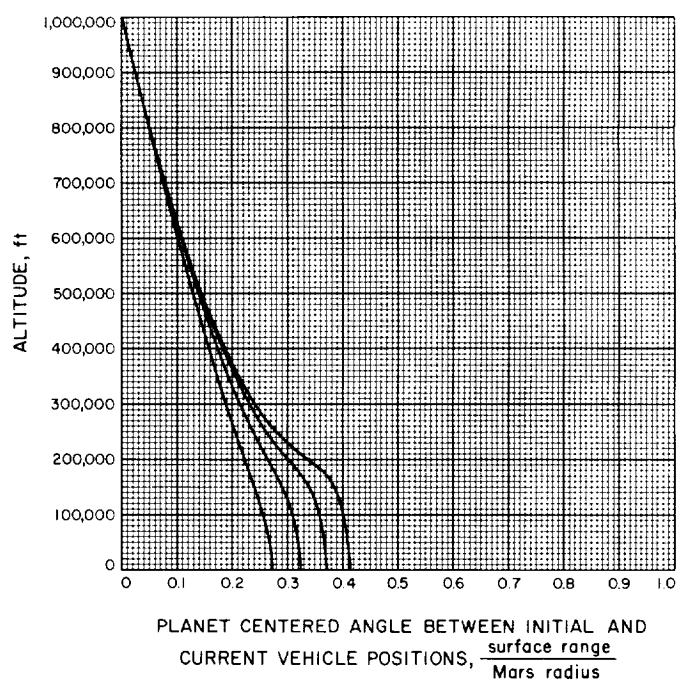


Fig. A-16

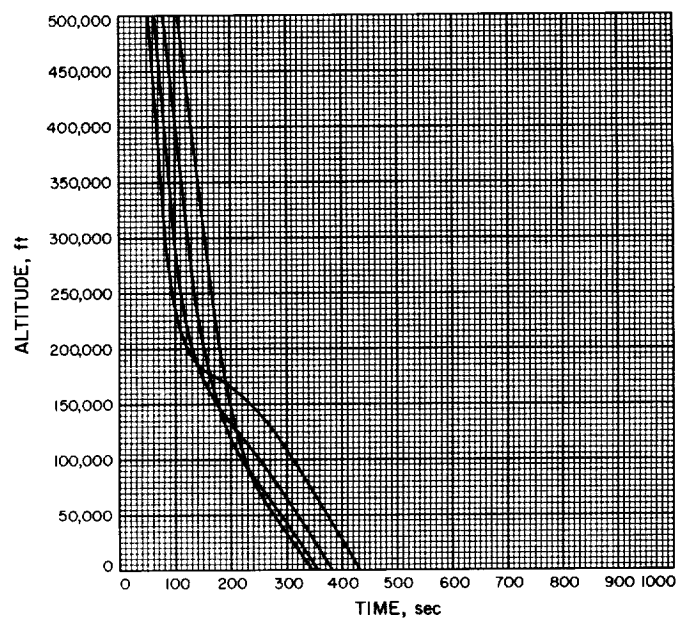


Fig. A-17

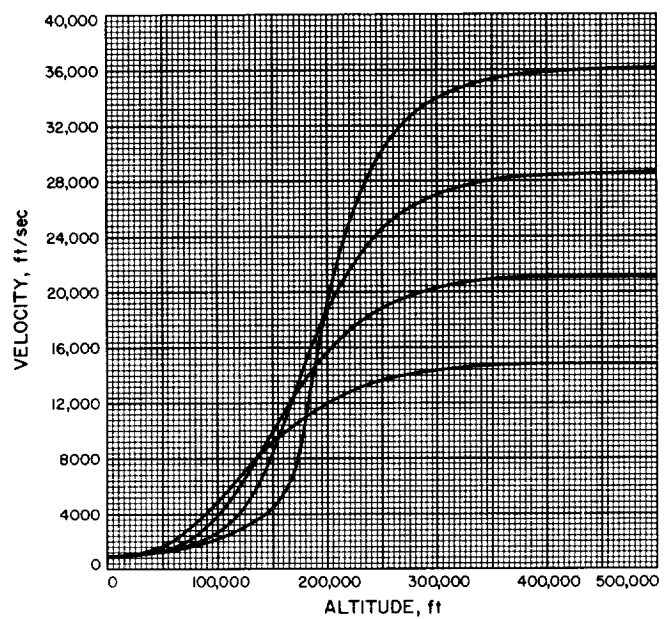


Fig. A-18

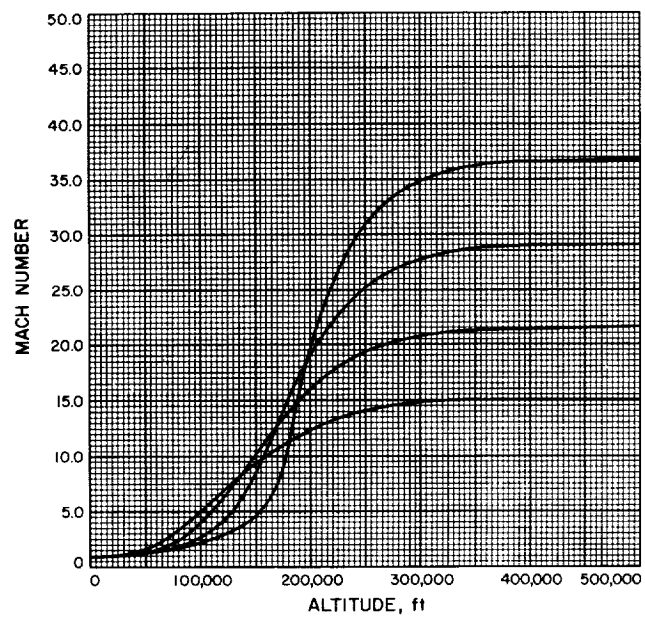


Fig. A-19

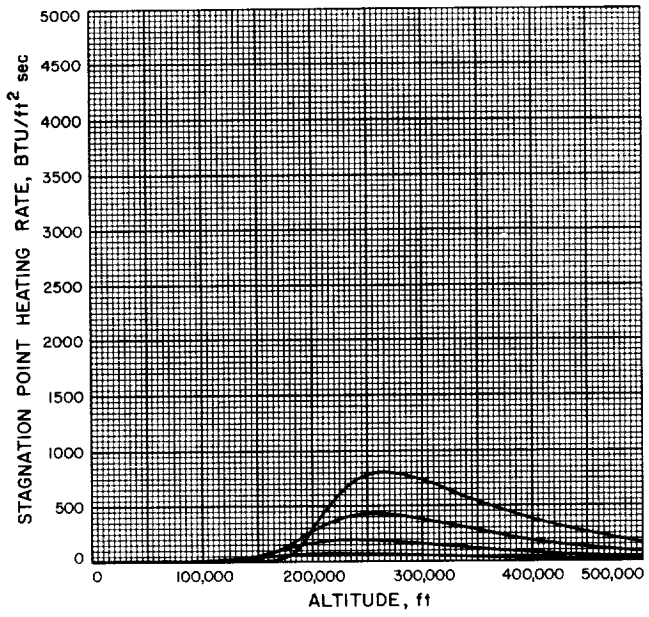


Fig. A-20

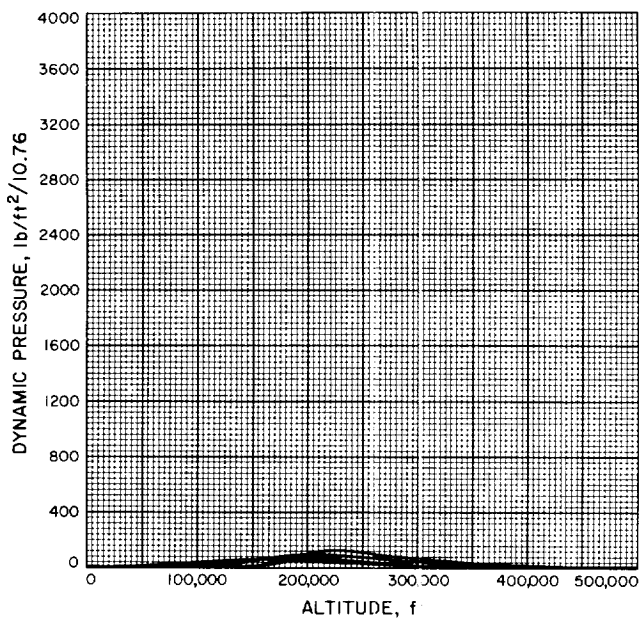


Fig. A-21

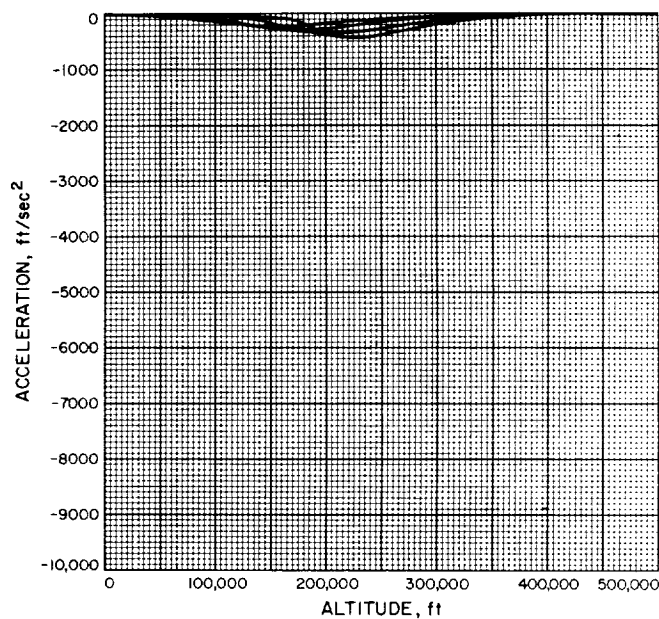


Fig. A-22

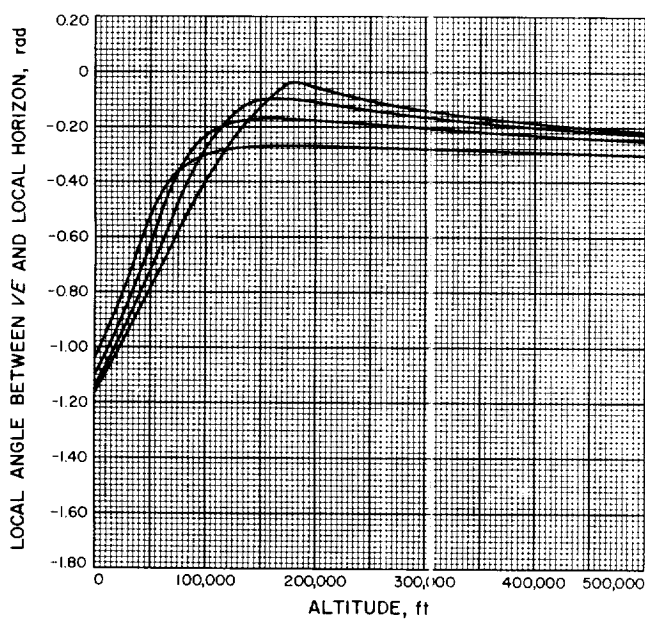


Fig. A-23

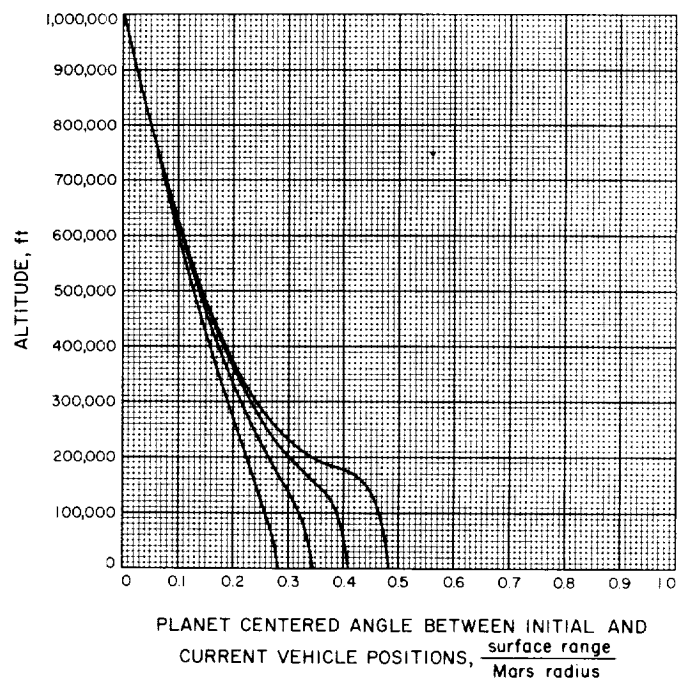


Fig. A-24

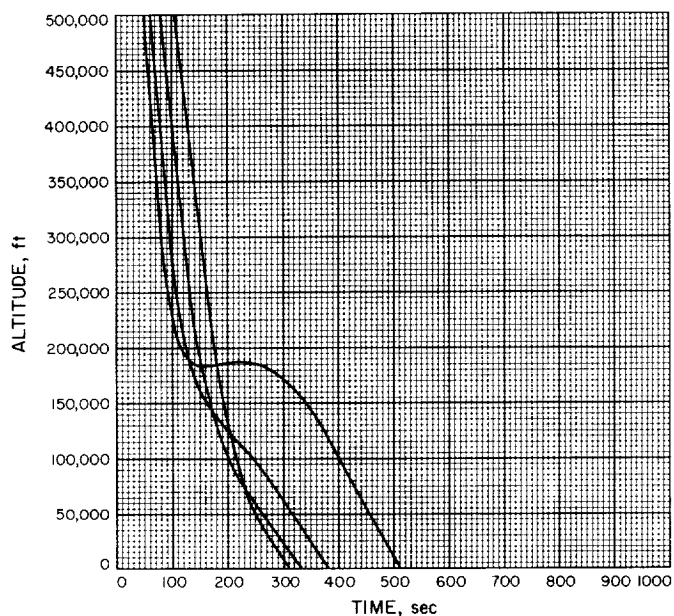


Fig. A-25

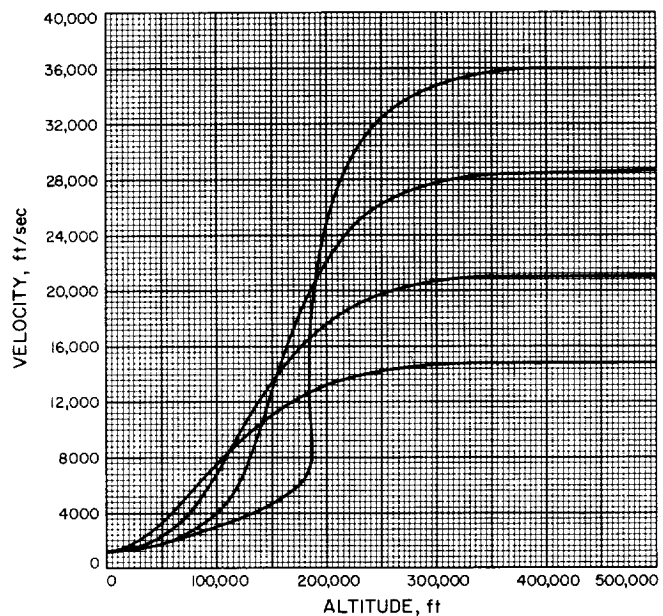


Fig. A-26

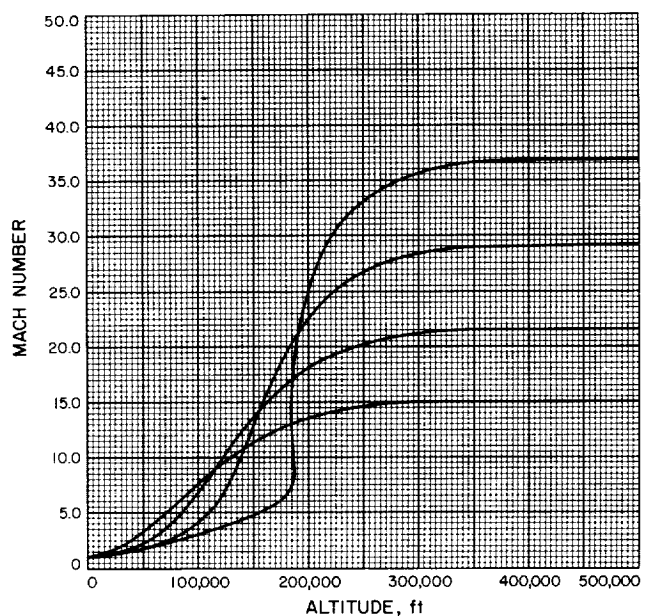


Fig. A-27

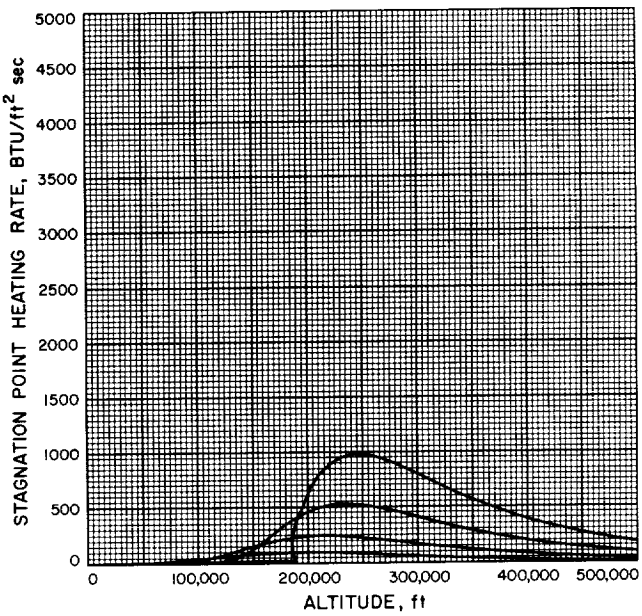


Fig. A-28

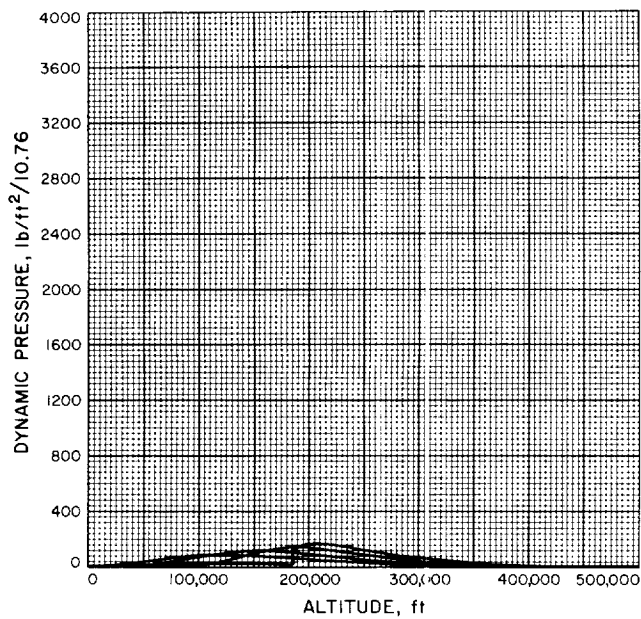


Fig. A-29

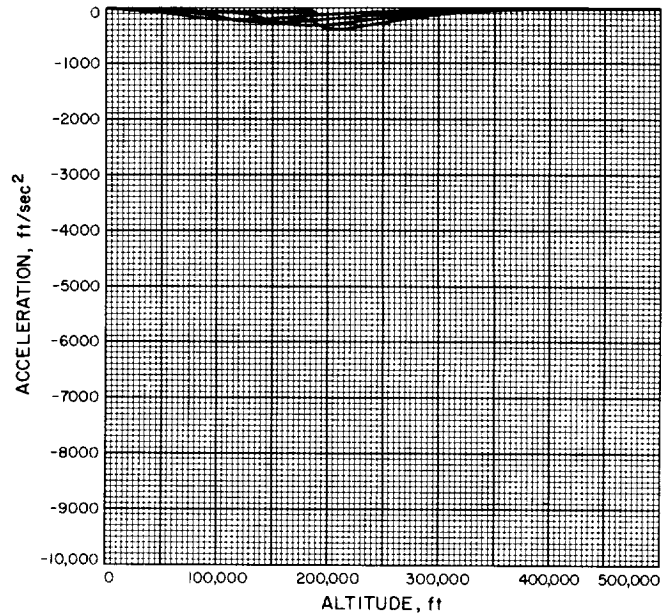


Fig. A-30

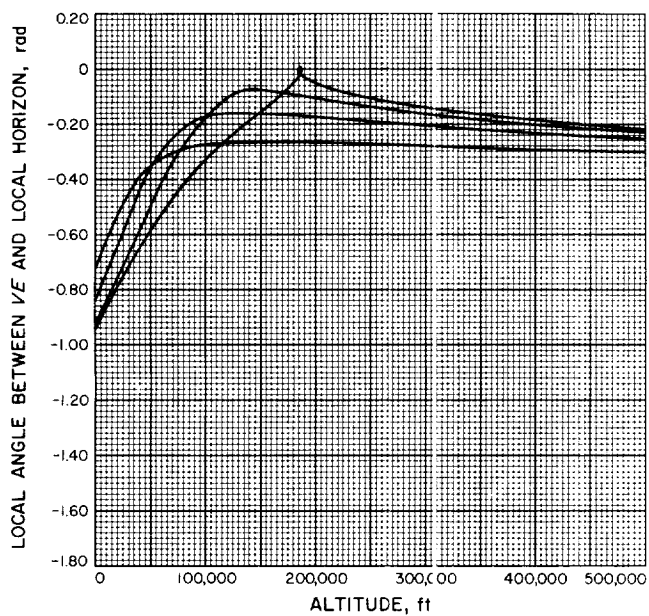
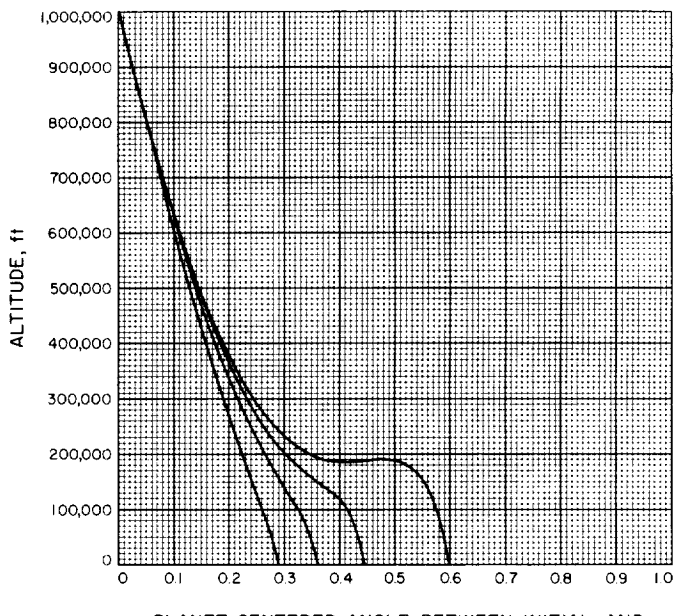


Fig. A-31



PLANET CENTERED ANGLE BETWEEN INITIAL AND
CURRENT VEHICLE POSITIONS, $\frac{\text{surface range}}{\text{Mars radius}}$

Fig. A-32

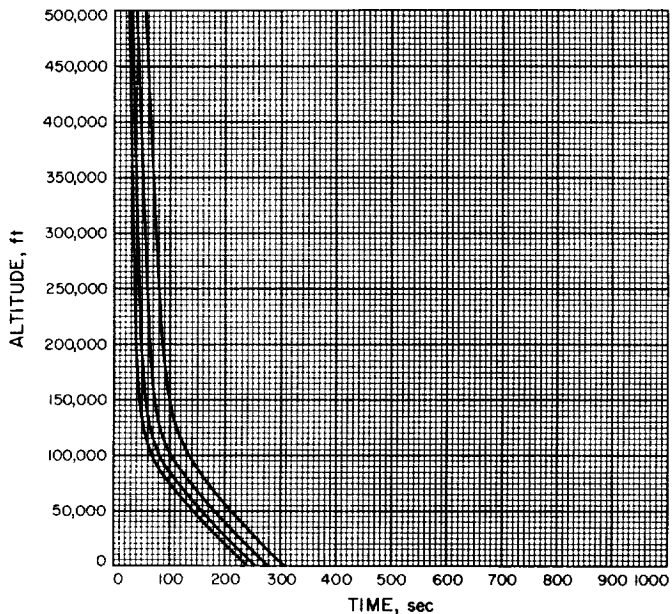


Fig. A-33

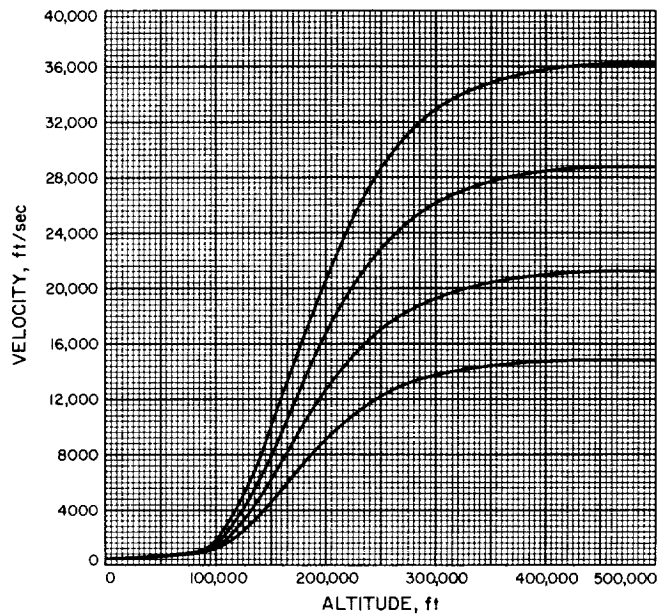


Fig. A-34

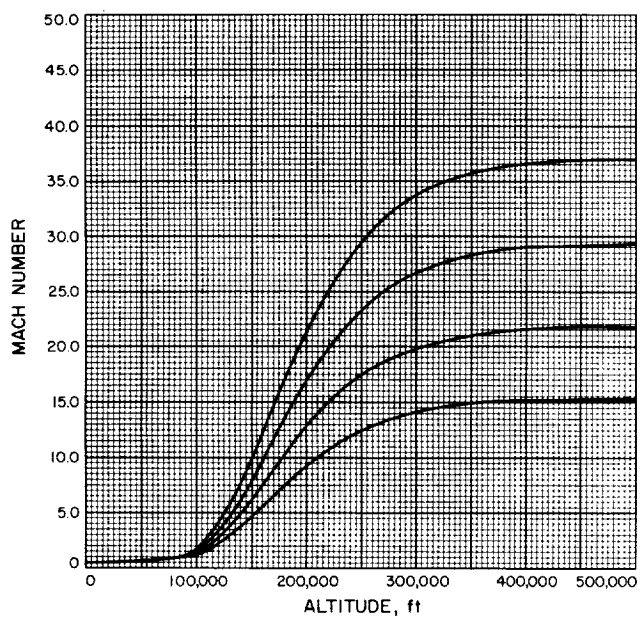


Fig. A-35

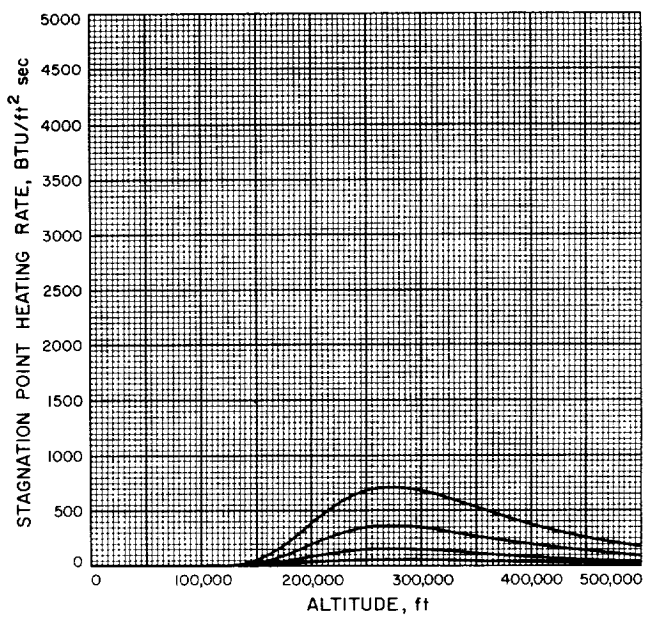


Fig. A-36

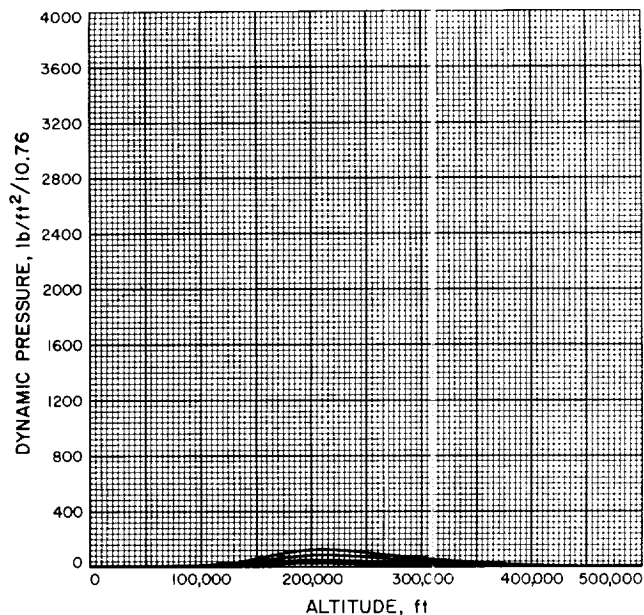


Fig. A-37

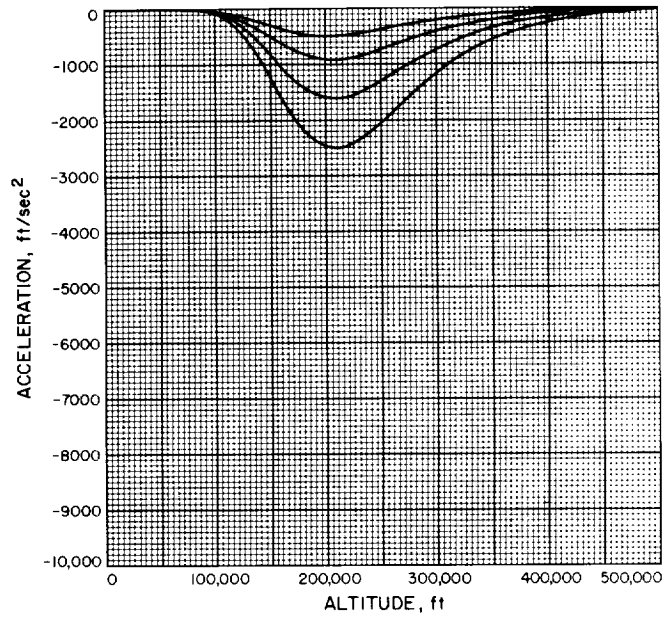


Fig. A-38

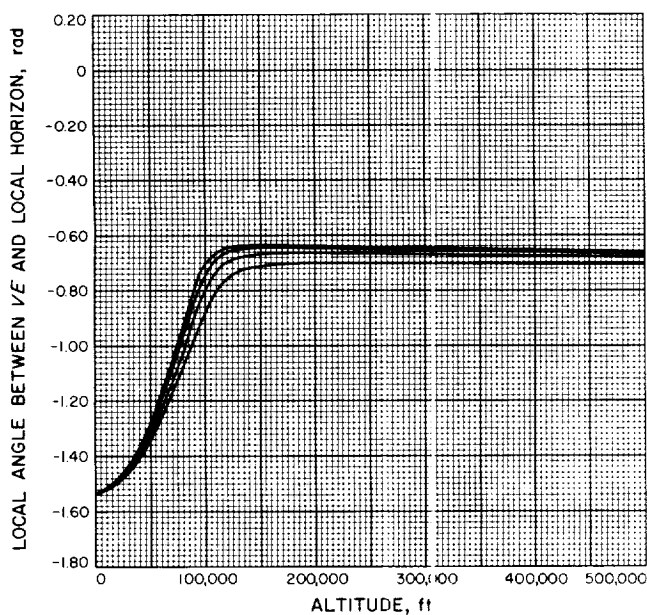


Fig. A-39

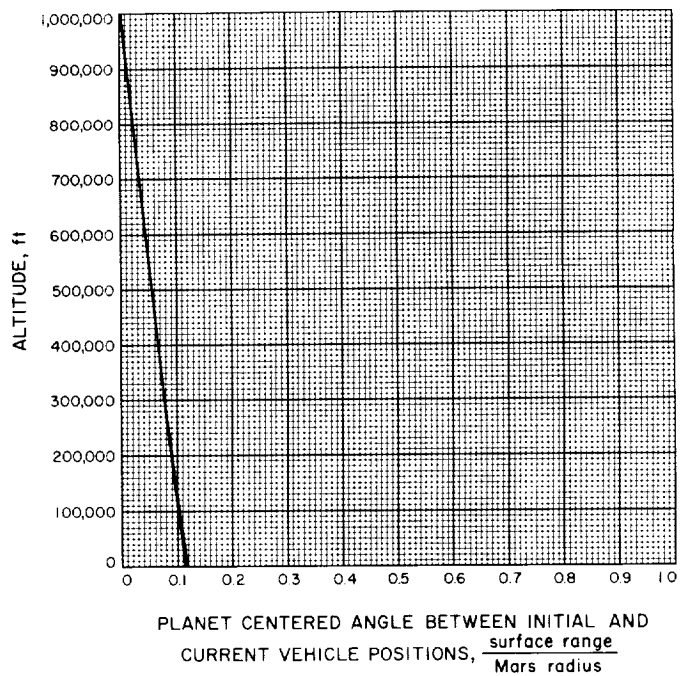


Fig. A-40

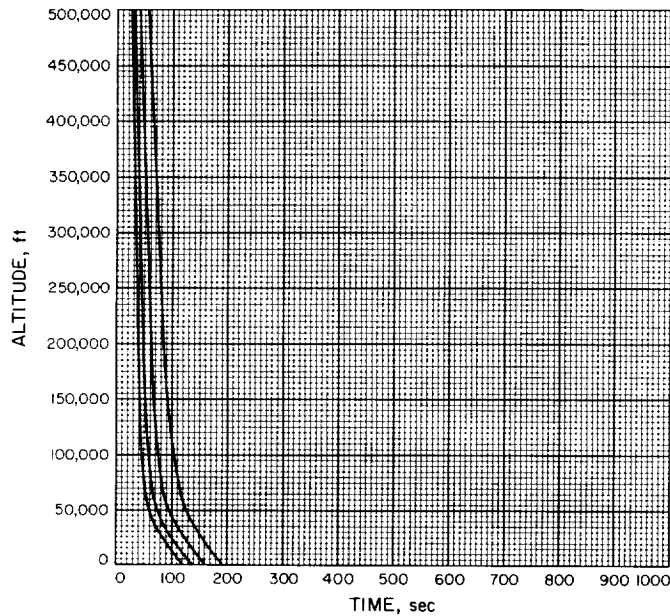


Fig. A-41

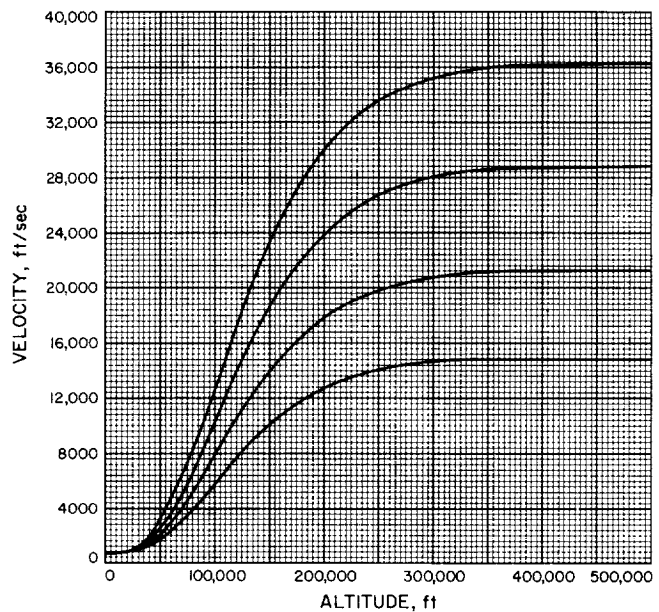


Fig. A-42

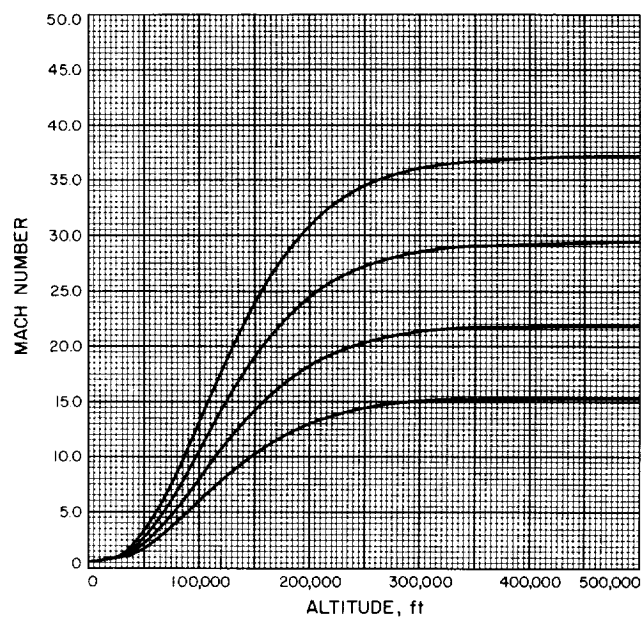


Fig. A-43

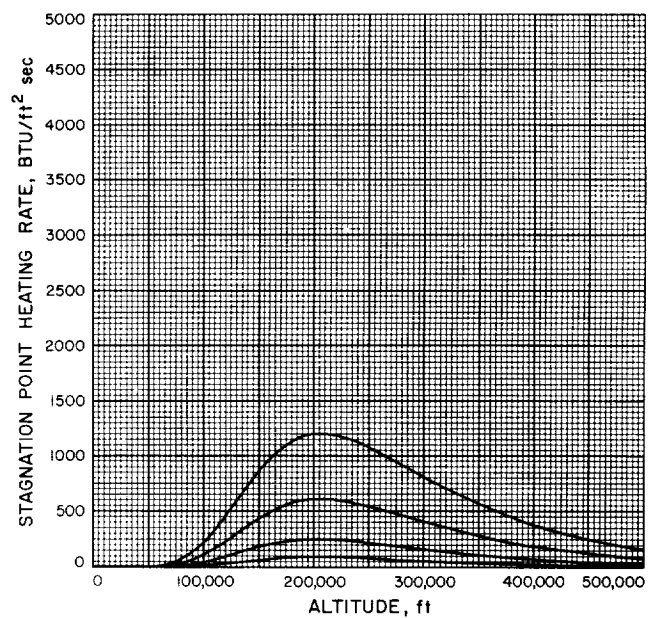


Fig. A-44

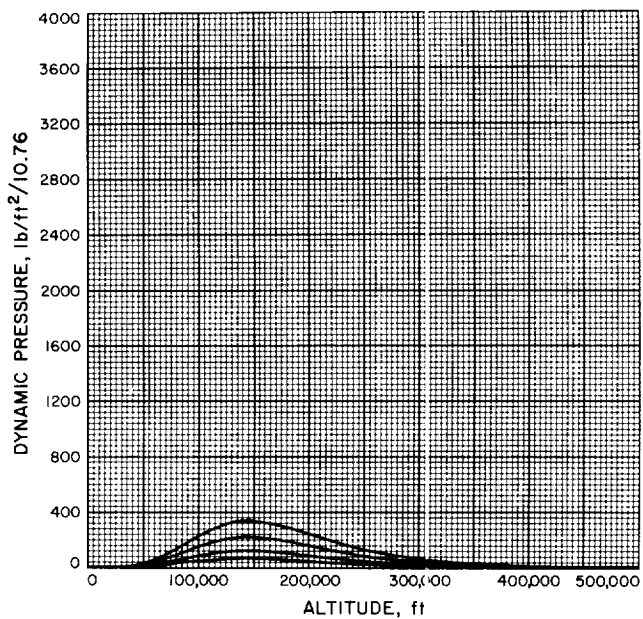


Fig. A-45

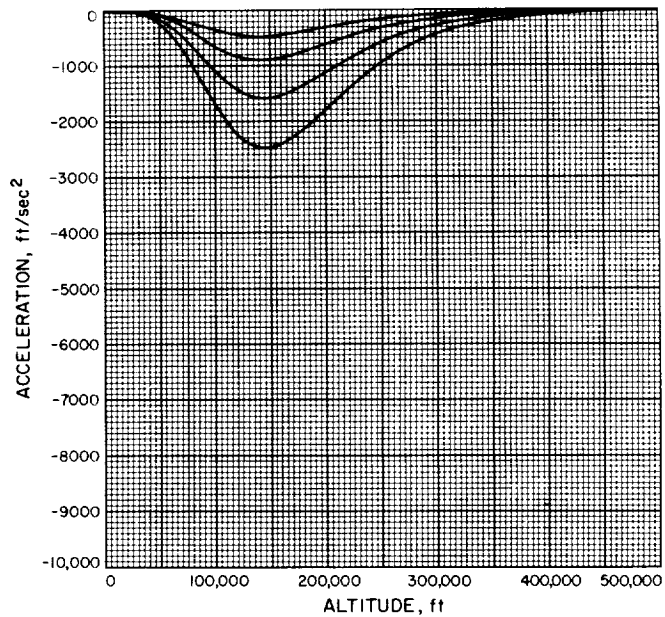


Fig. A-46

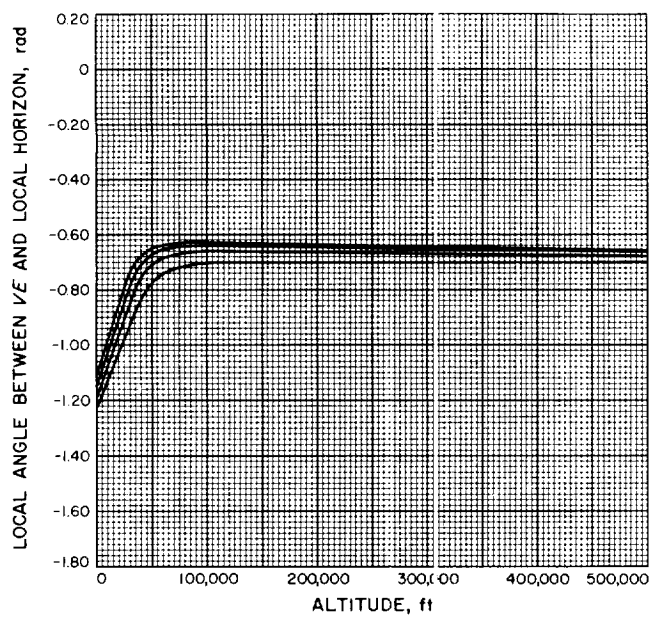
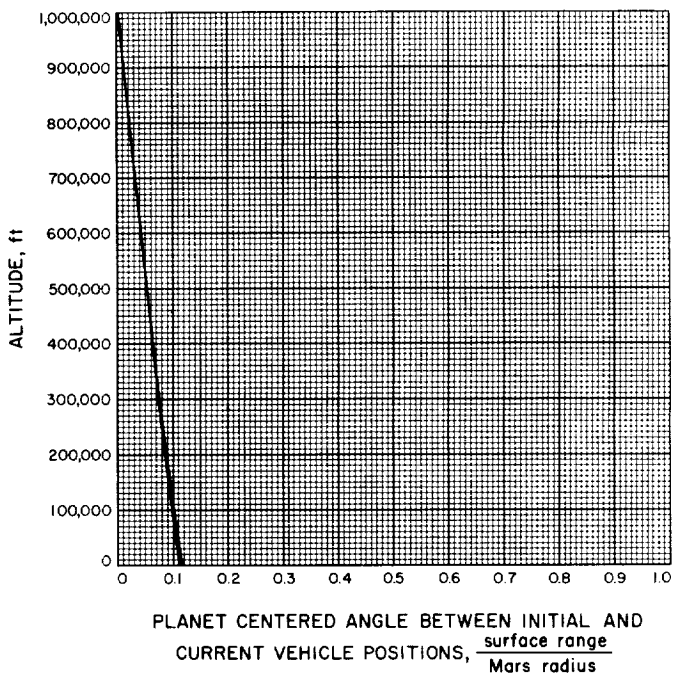


Fig. A-47



PLANET CENTERED ANGLE BETWEEN INITIAL AND

CURRENT VEHICLE POSITIONS, $\frac{\text{surface range}}{\text{Mars radius}}$

21

Fig. A-48

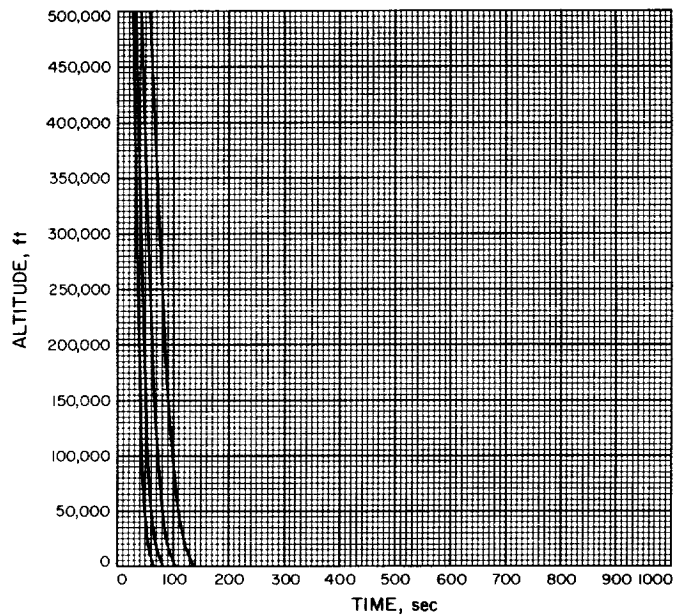


Fig. A-49

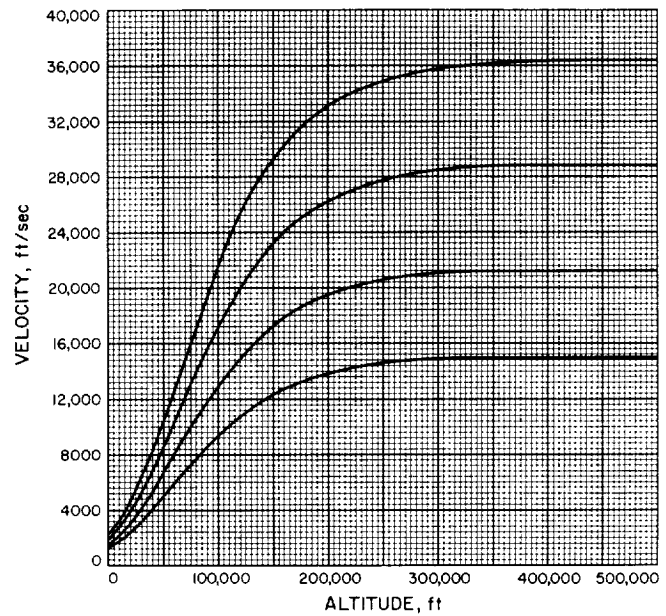


Fig. A-50

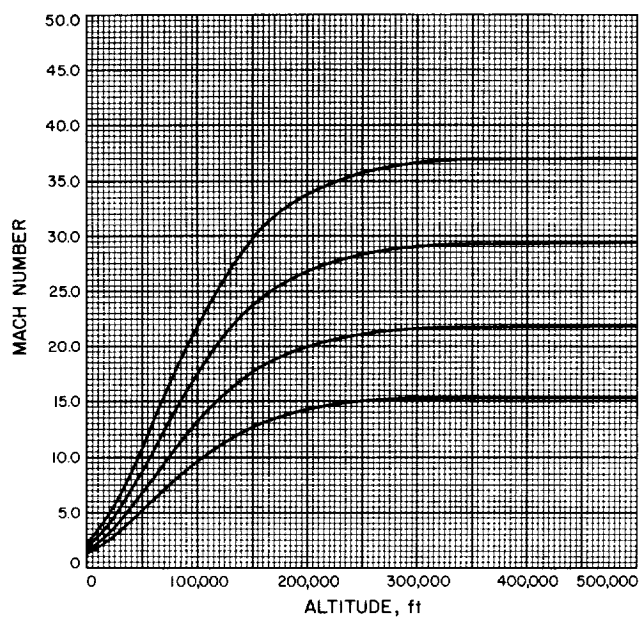


Fig. A-51

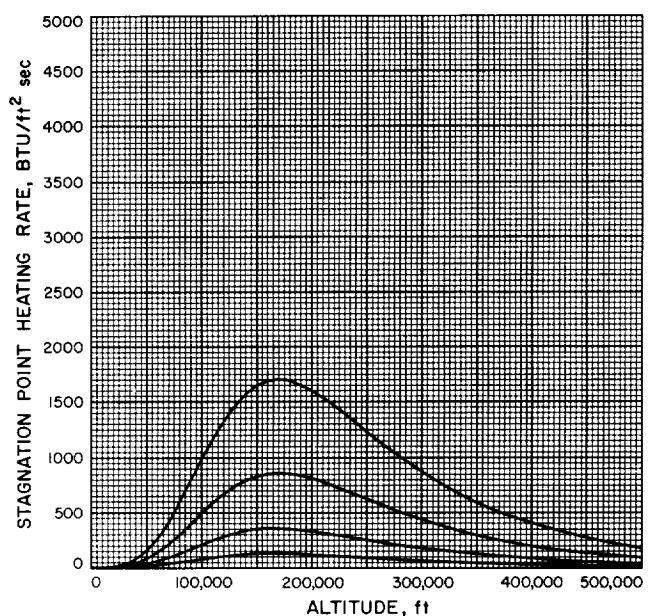


Fig. A-52

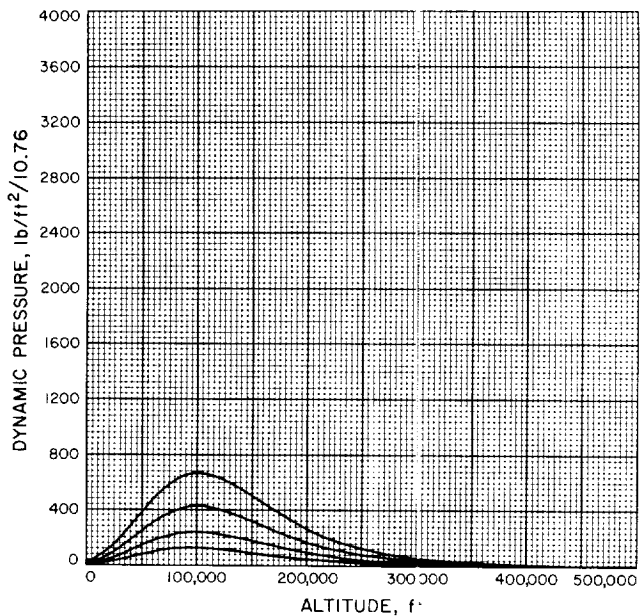


Fig. A-53

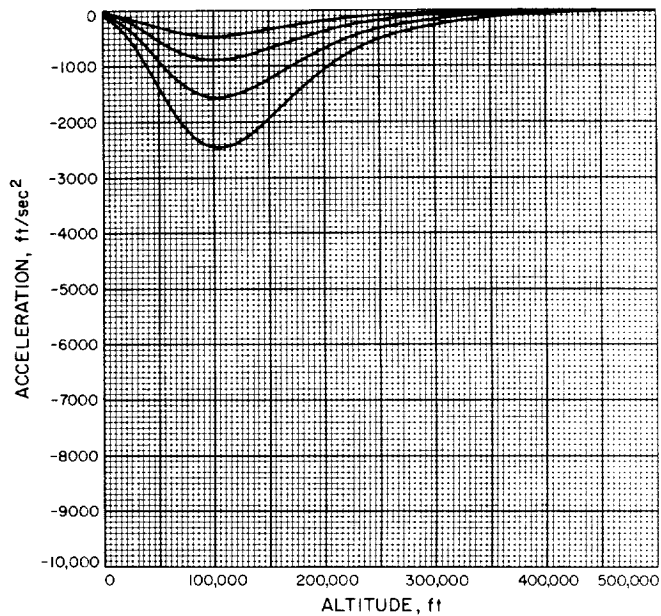


Fig. A-54

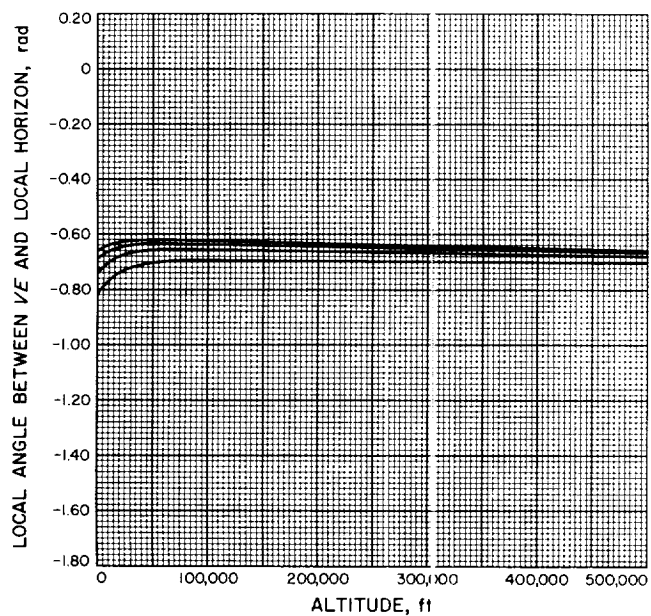
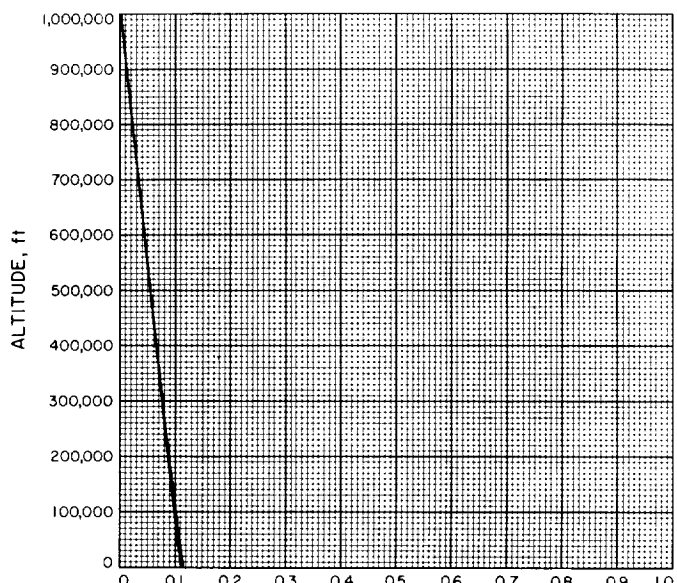


Fig. A-55



PLANET CENTERED ANGLE BETWEEN INITIAL AND
CURRENT VEHICLE POSITIONS, $\frac{\text{surface range}}{\text{Mars radius}}$

Fig. A-56

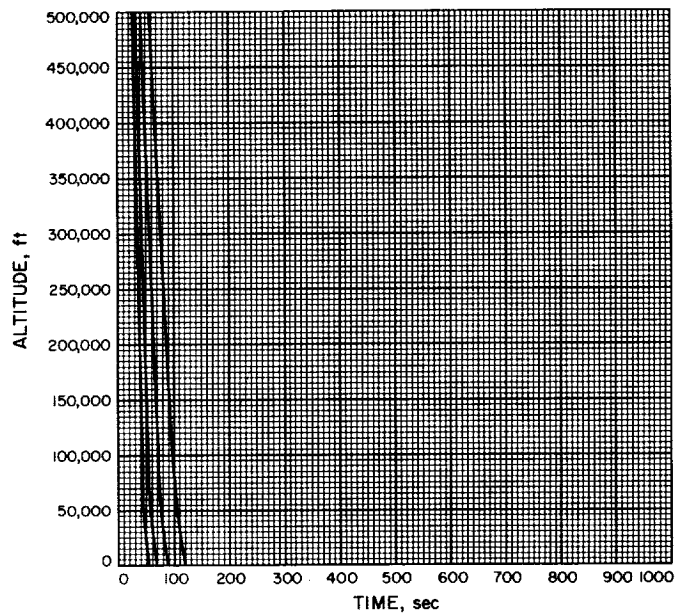


Fig. A-57

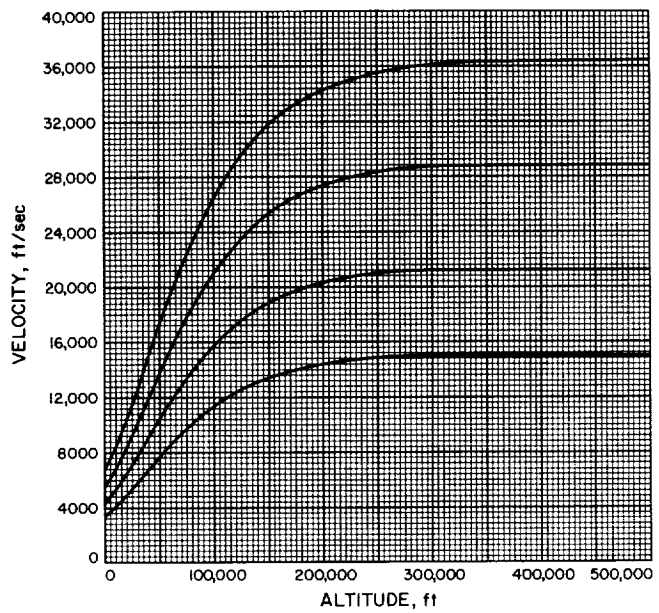


Fig. A-58

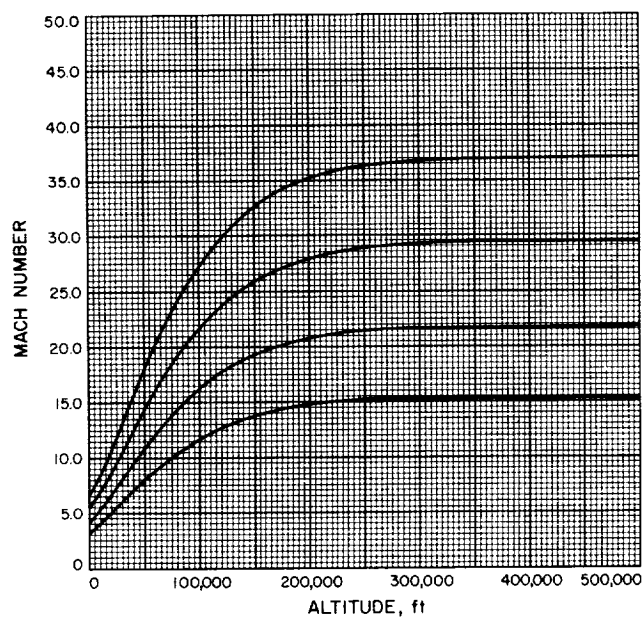


Fig. A-59

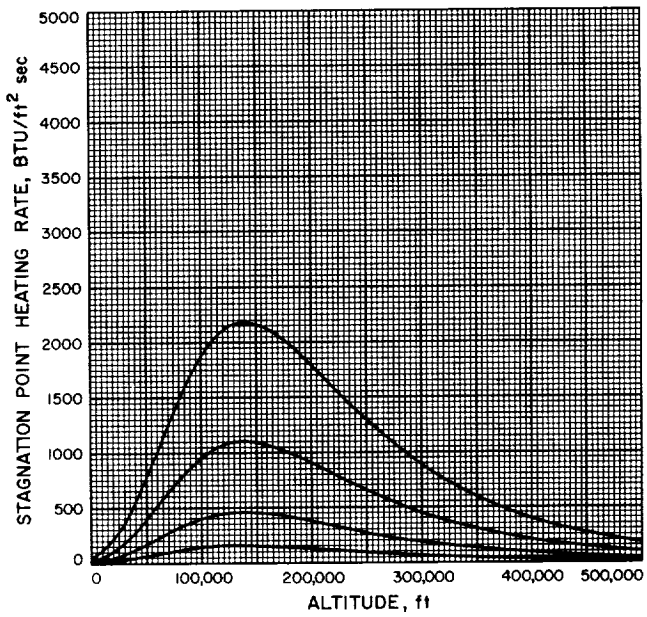


Fig. A-60

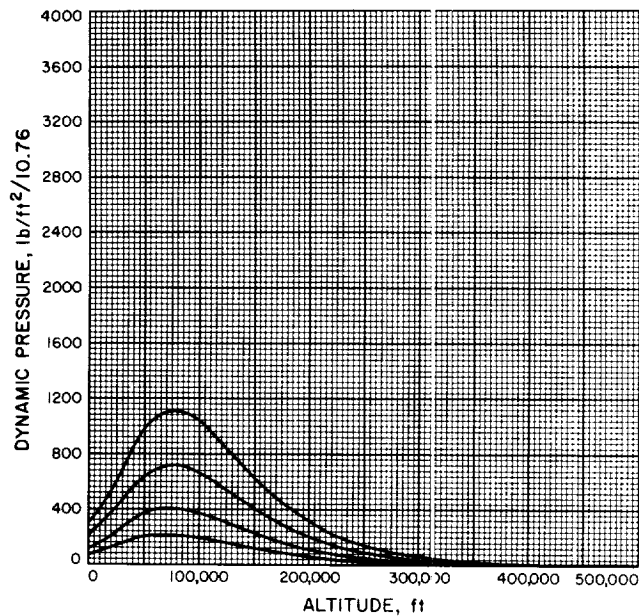


Fig. A-61

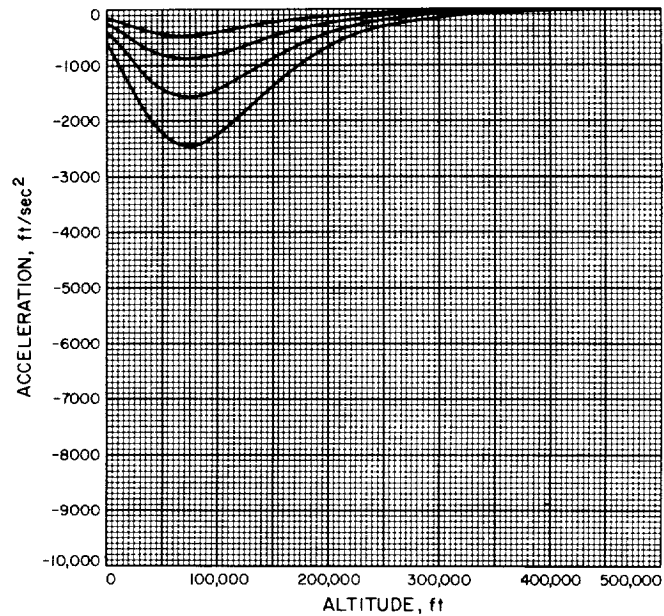


Fig. A-62

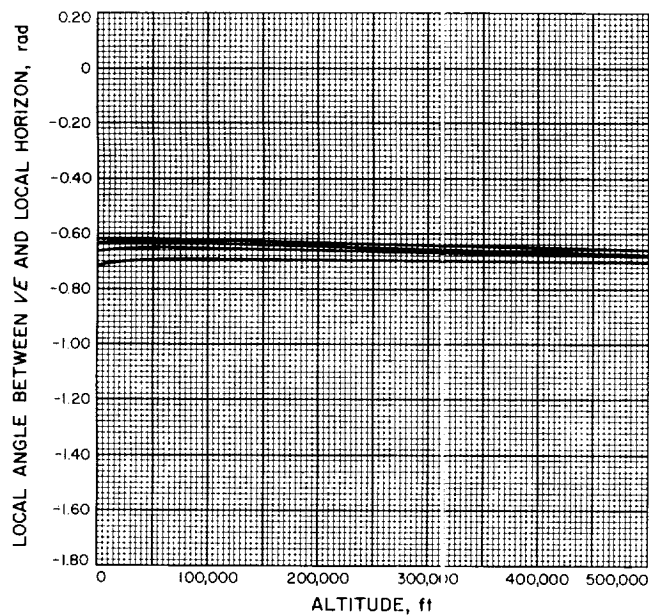
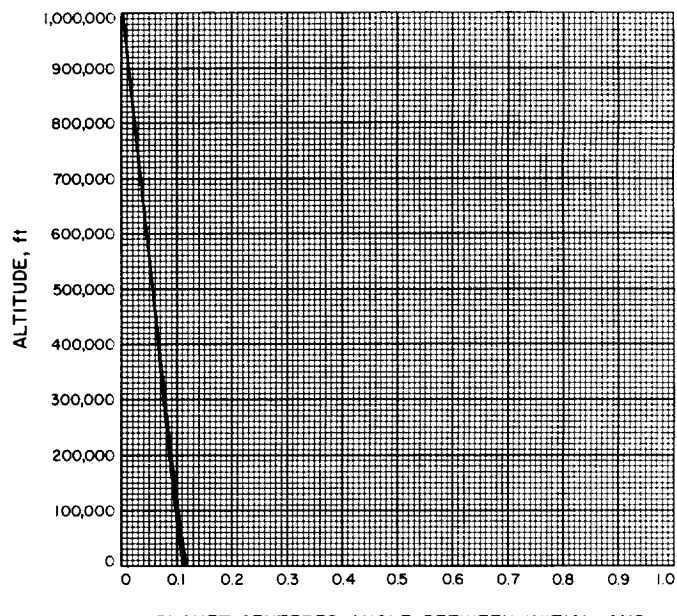


Fig. A-63



PLANET CENTERED ANGLE BETWEEN INITIAL AND
CURRENT VEHICLE POSITIONS, $\frac{\text{surface range}}{\text{Mars radius}}$

Fig. A-64

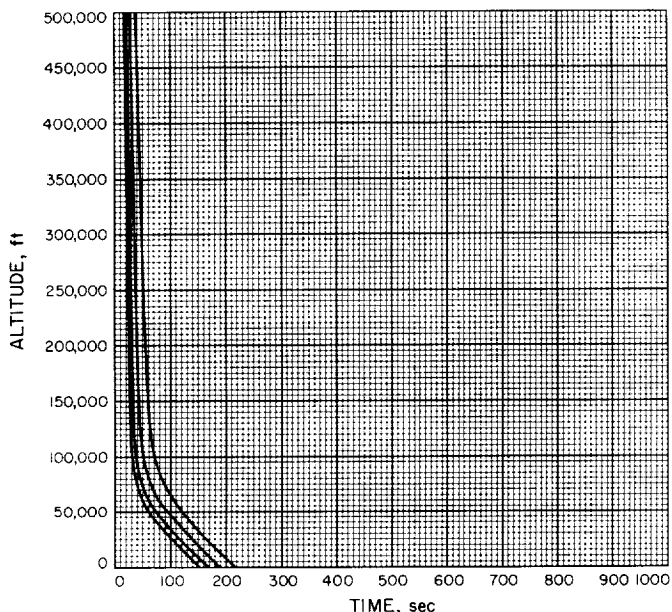


Fig. A-65

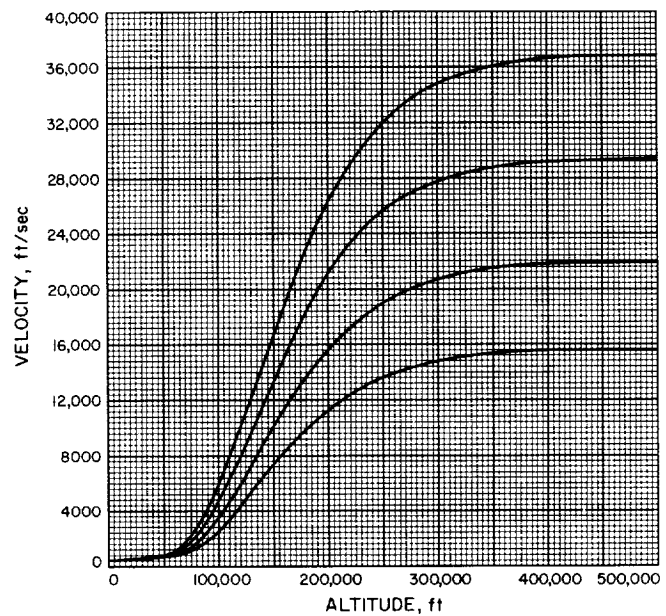


Fig. A-66

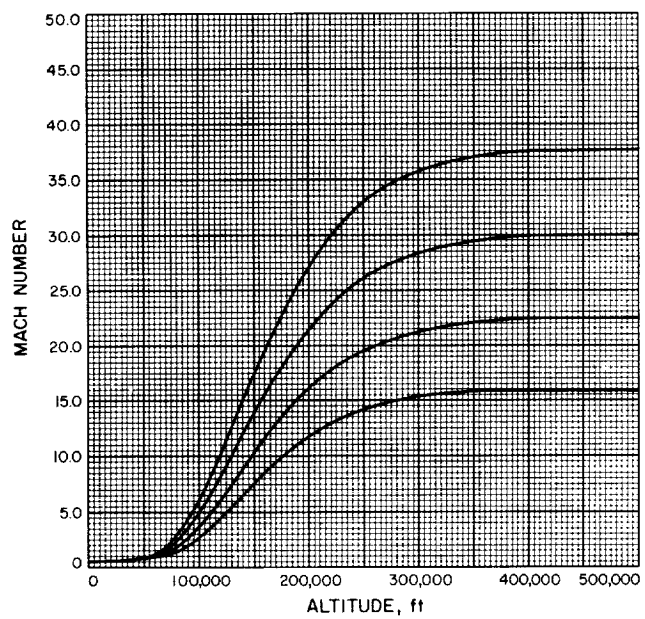


Fig. A-67

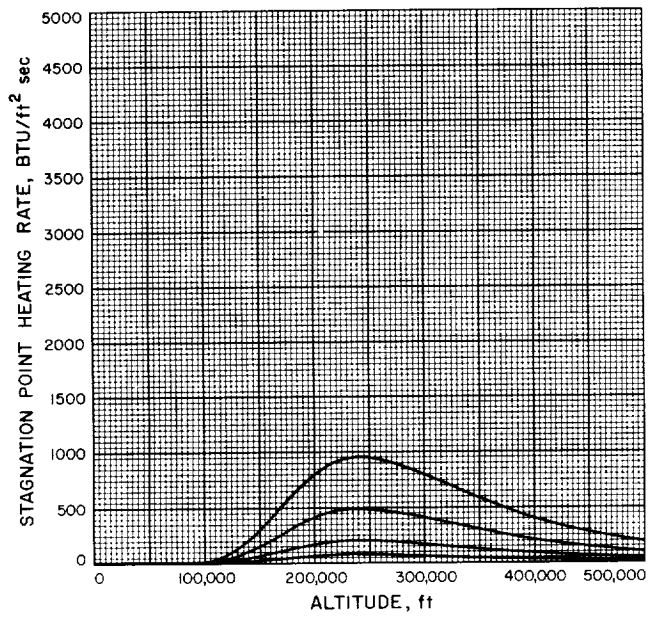


Fig. A-68

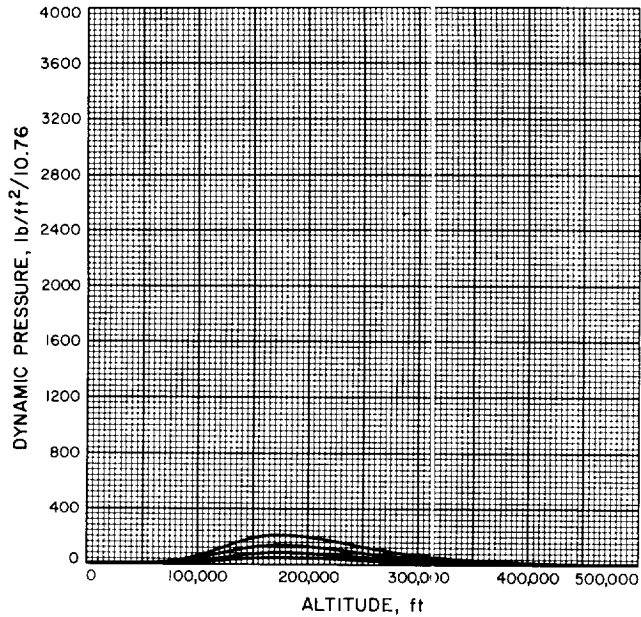


Fig. A-69

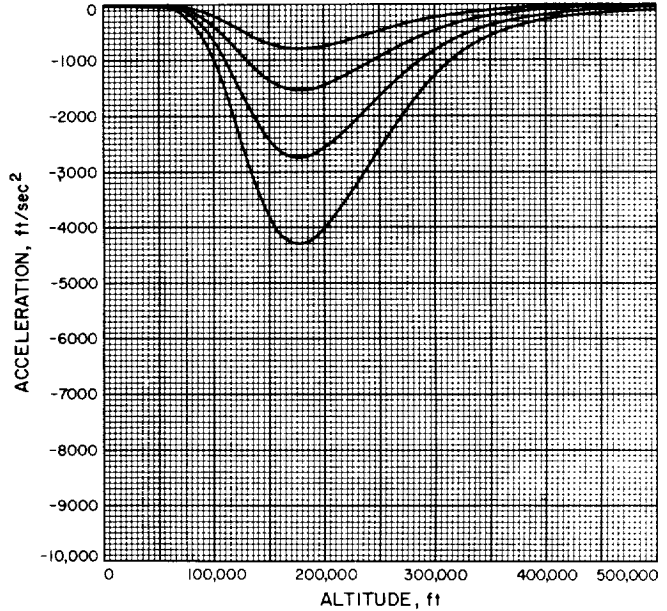


Fig. A-70

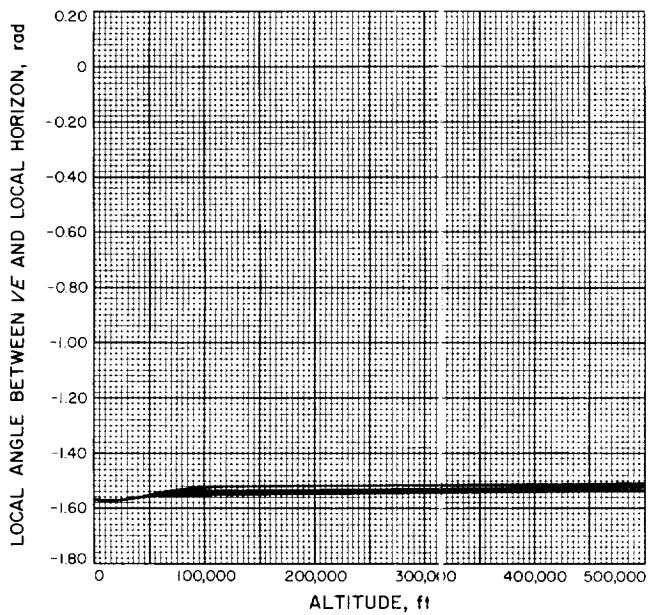
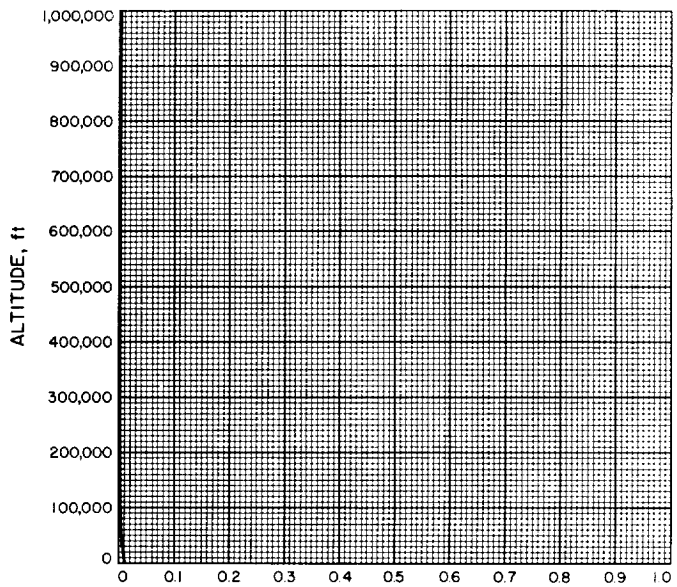


Fig. A-71



PLANET CENTERED ANGLE BETWEEN INITIAL AND
CURRENT VEHICLE POSITIONS, $\frac{\text{surface range}}{\text{Mars radius}}$

Fig. A-72

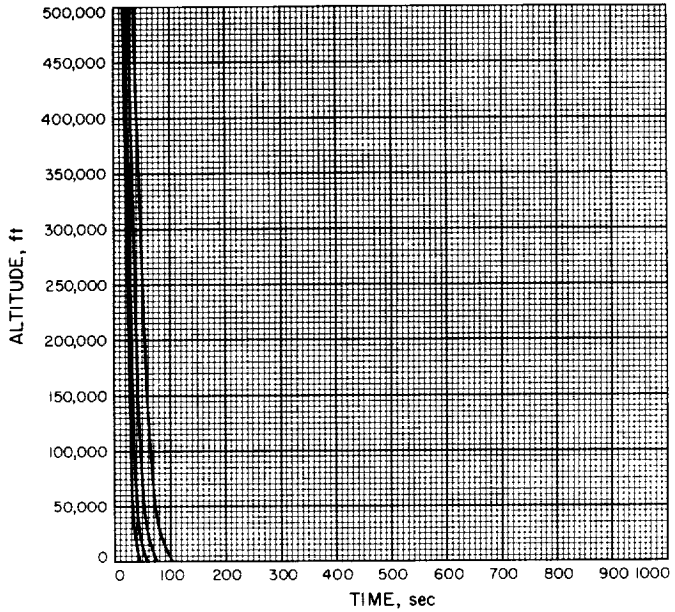


Fig. A-73

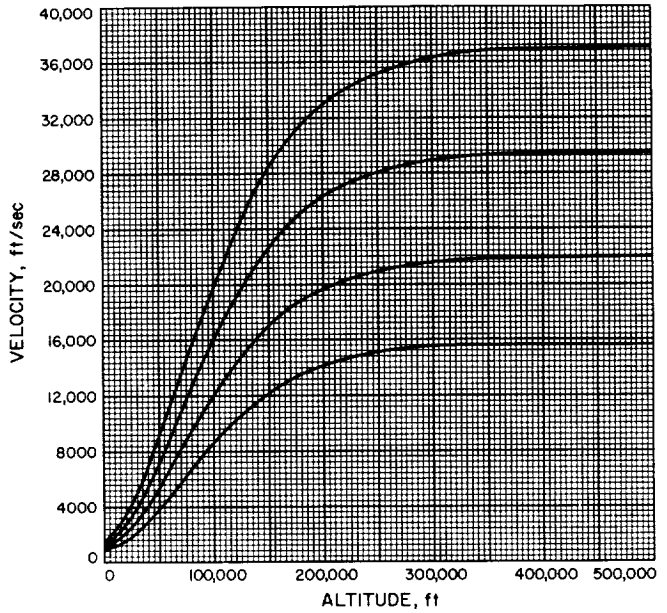


Fig. A-74

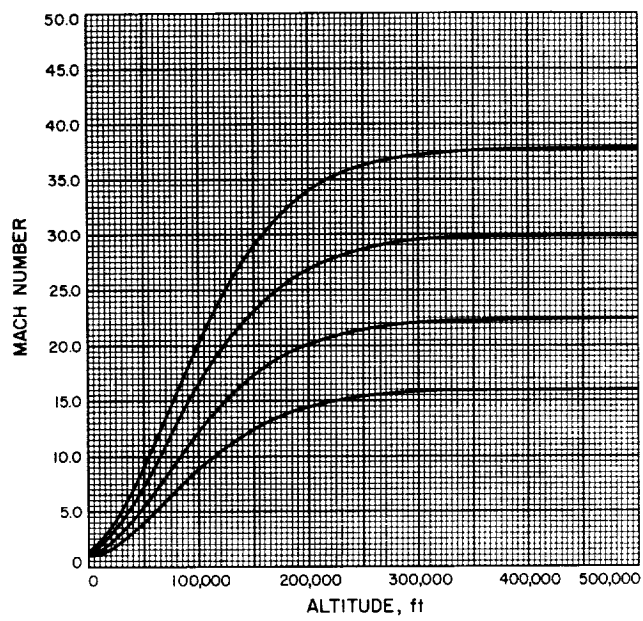


Fig. A-75

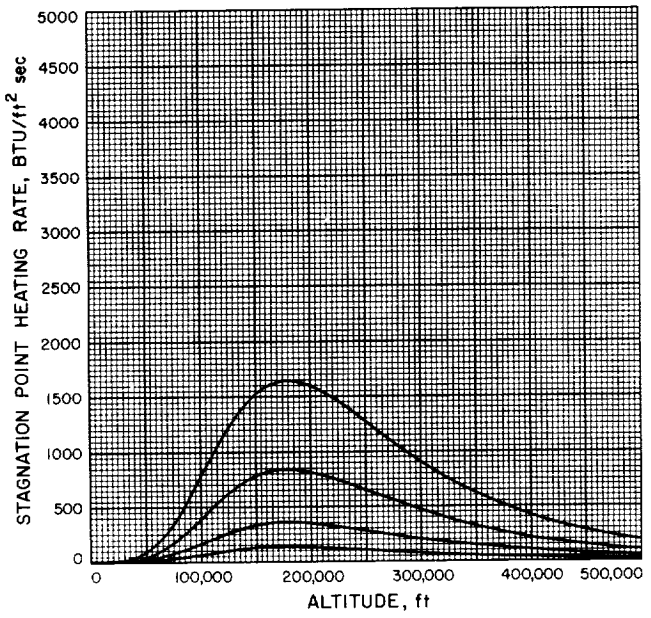


Fig. A-76

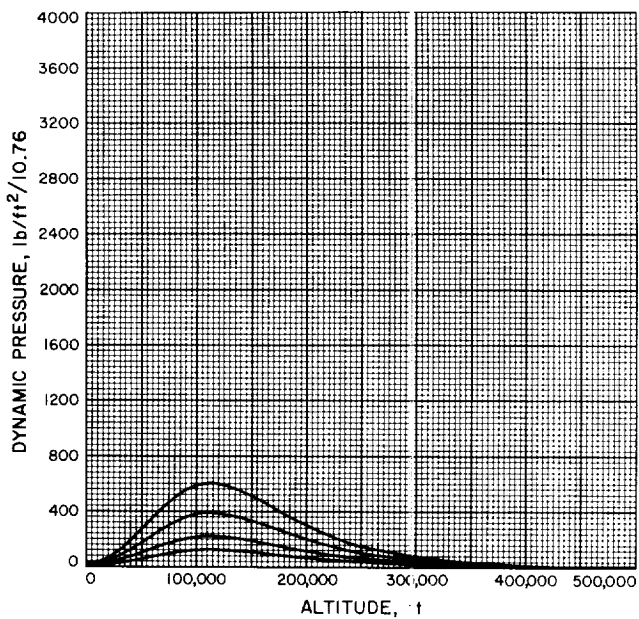


Fig. A-77

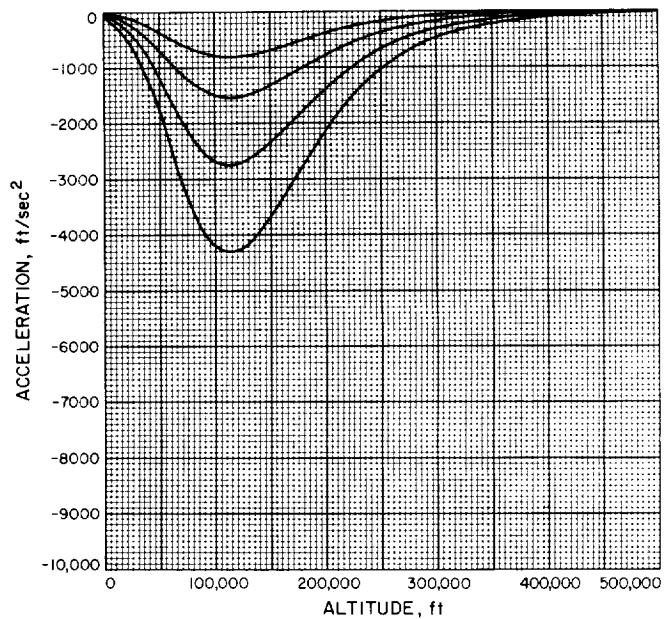


Fig. A-78

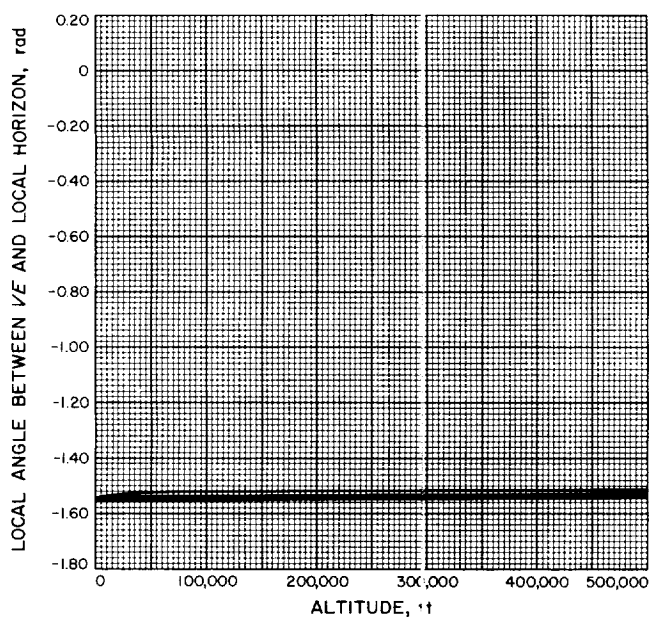


Fig. A-79

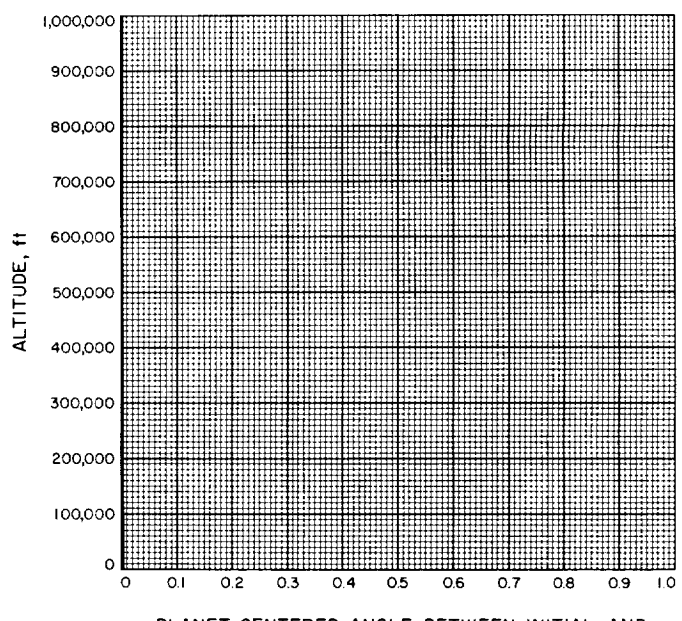


Fig. A-80

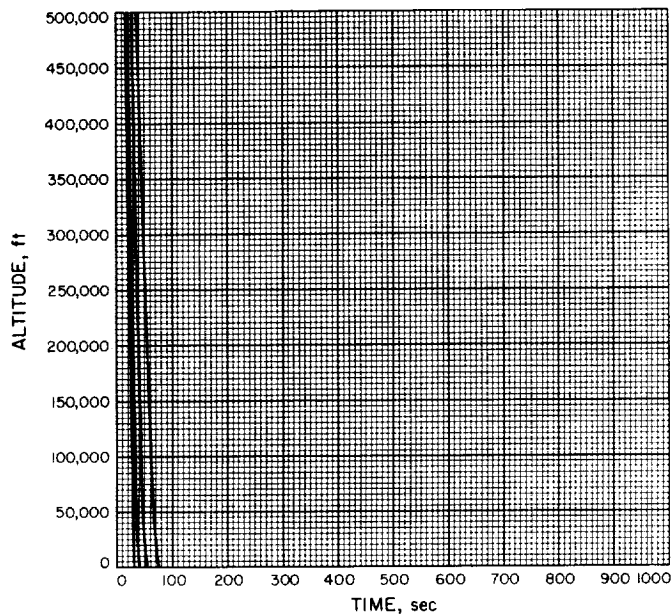


Fig. A-81

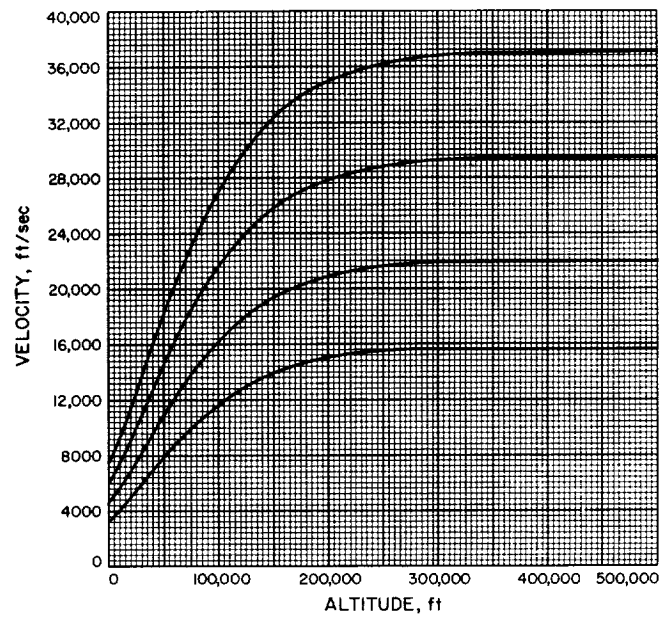


Fig. A-82

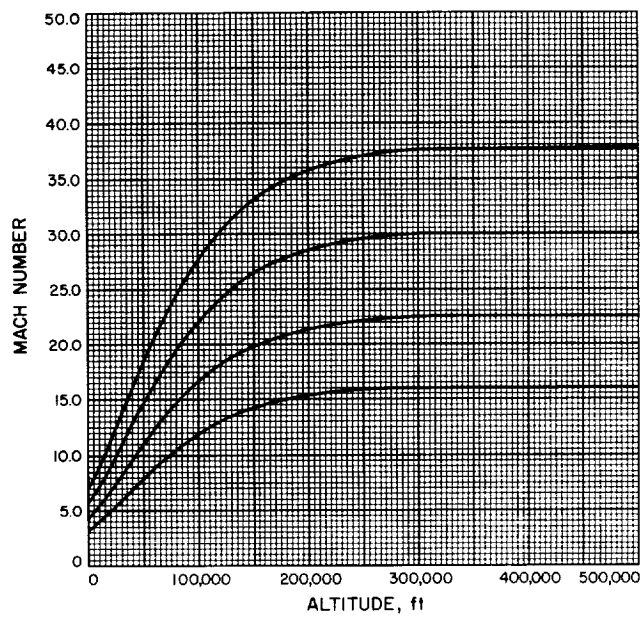


Fig. A-83

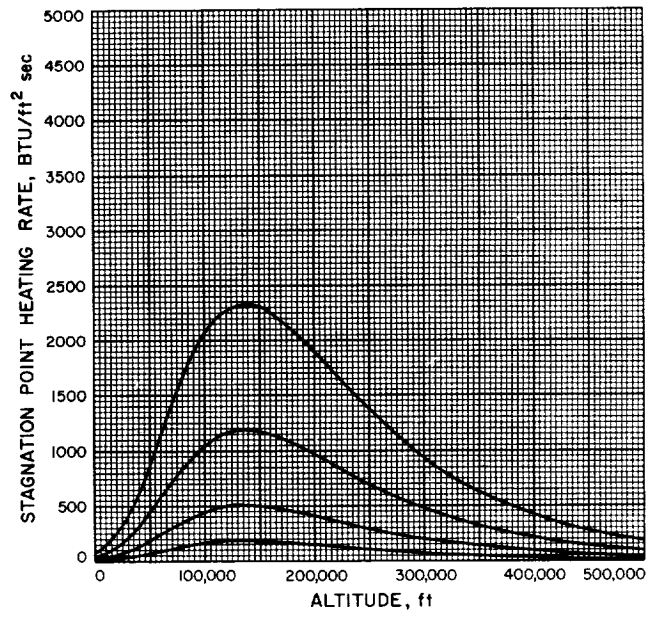


Fig. A-84

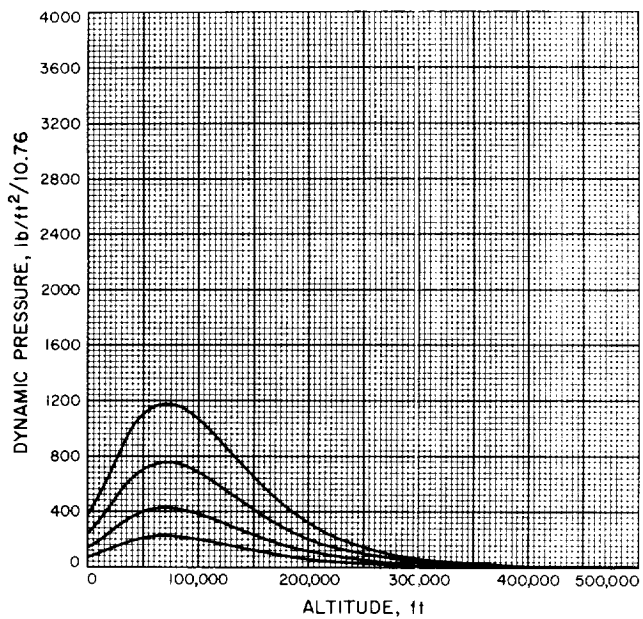


Fig. A-85

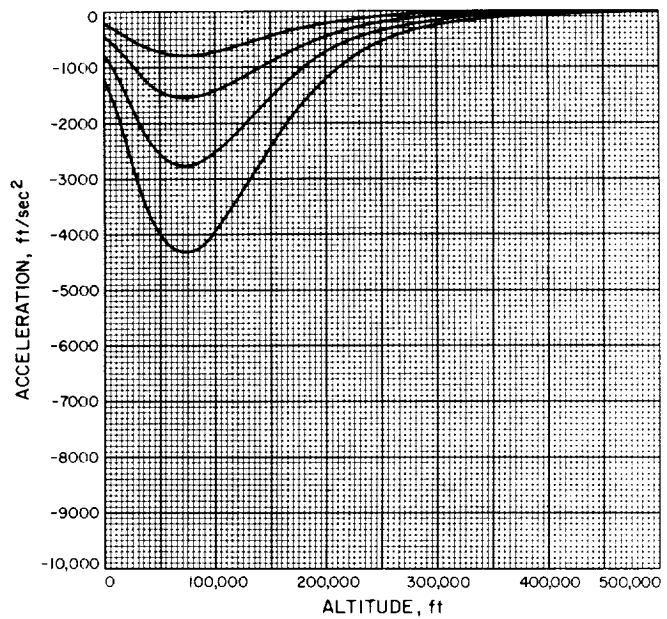


Fig. A-86

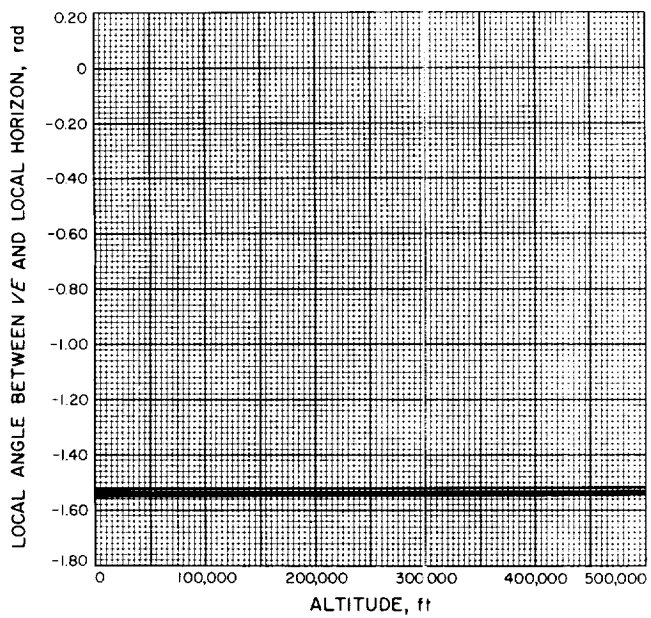


Fig. A-87

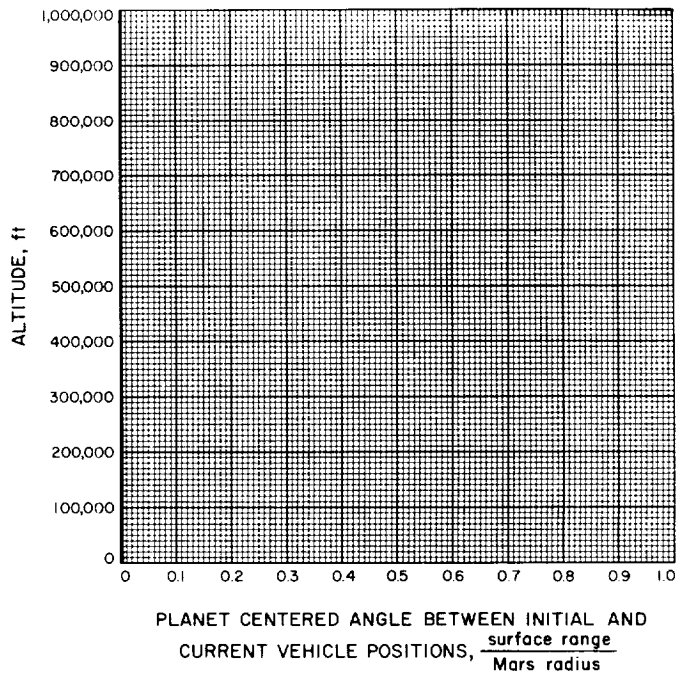


Fig. A-88

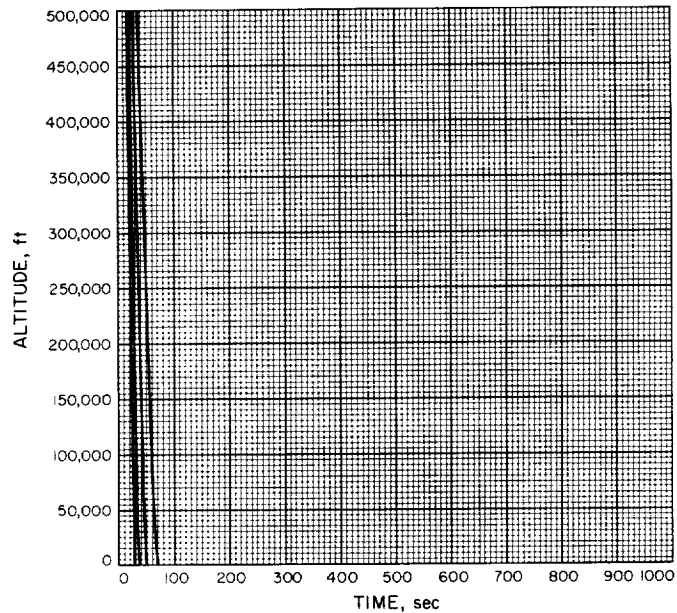


Fig. A-89

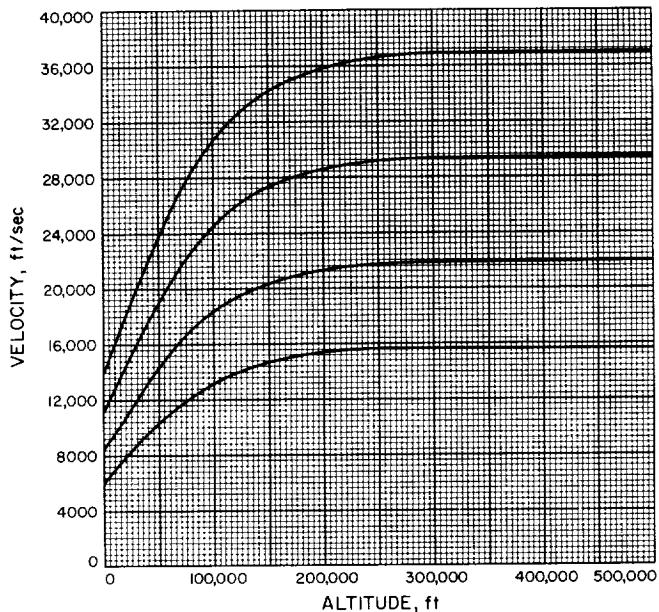


Fig. A-90

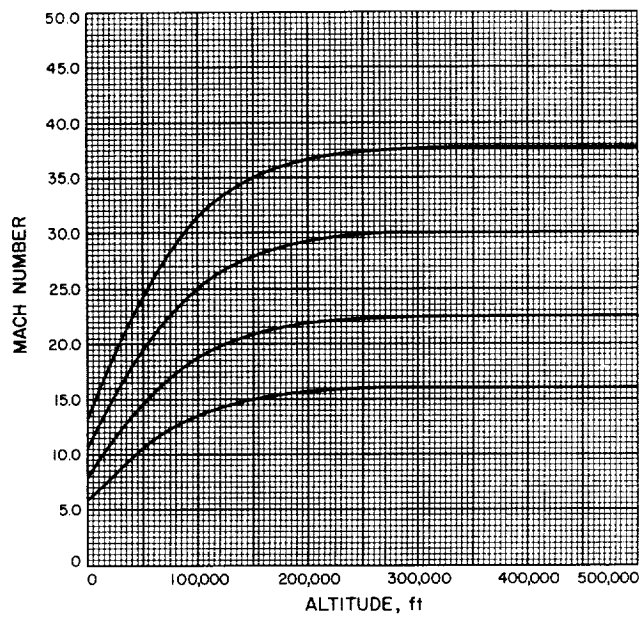


Fig. A-91

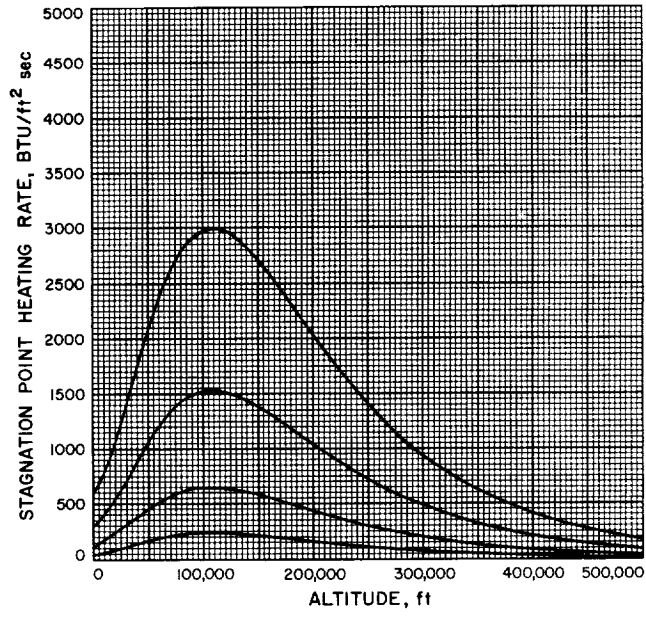


Fig. A-92

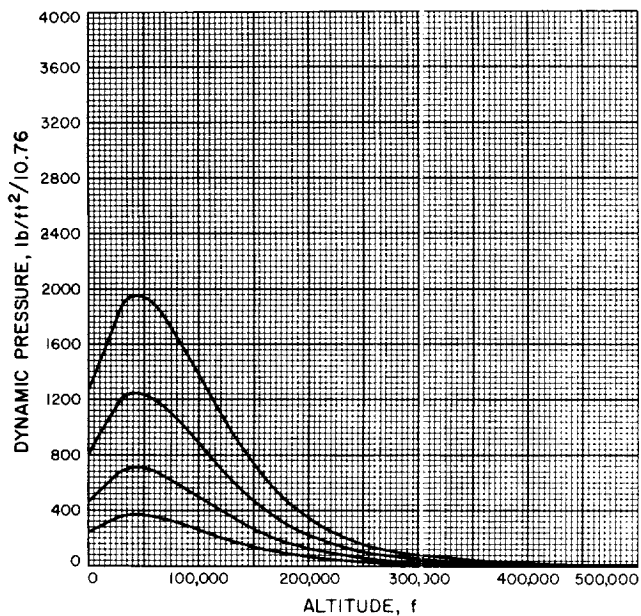


Fig. A-93

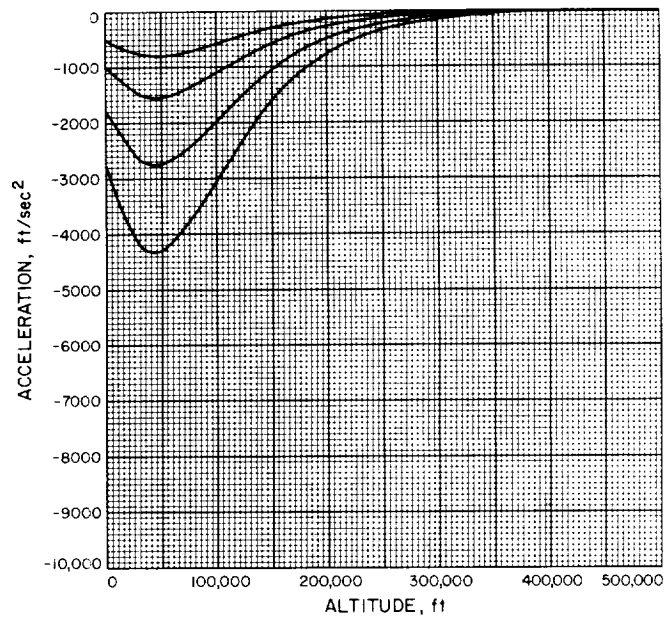


Fig. A-94

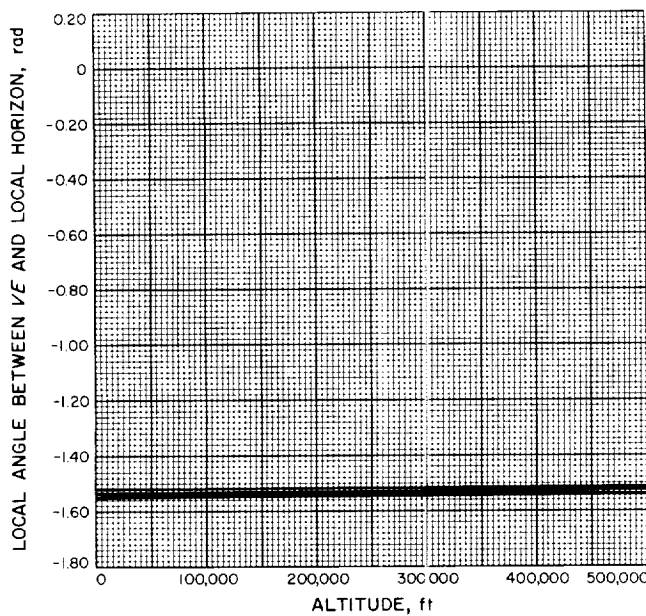


Fig. A-95

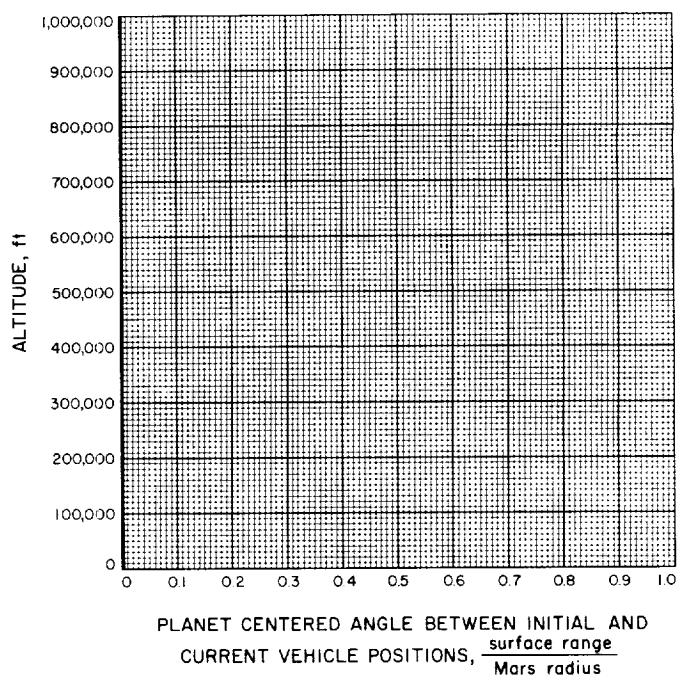


Fig. A-96

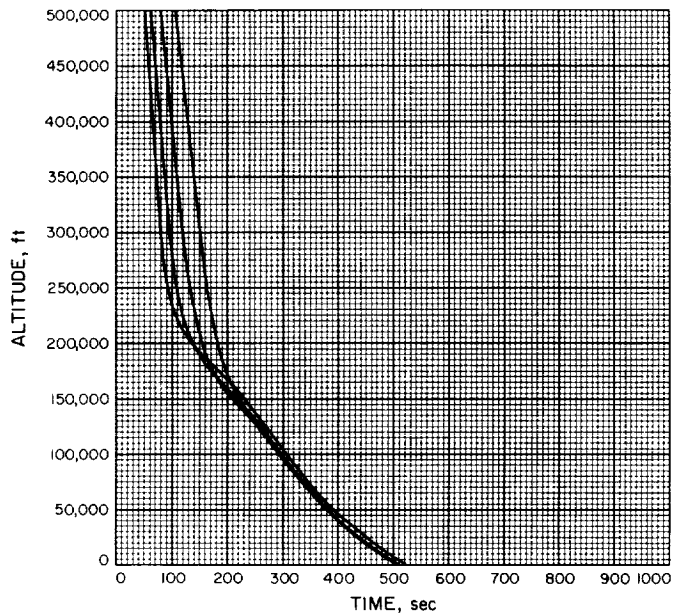


Fig. A-97

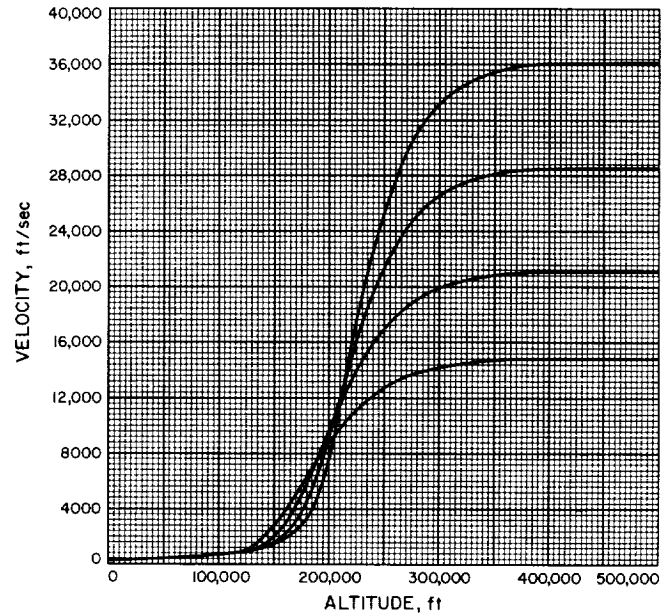


Fig. A-98

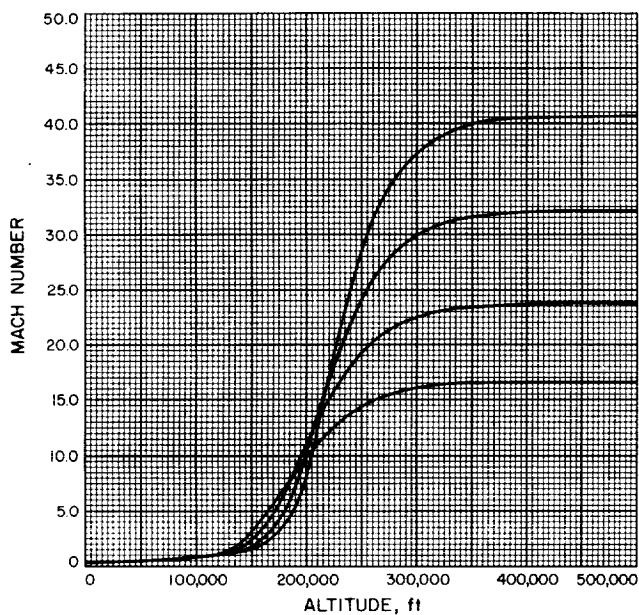


Fig. A-99

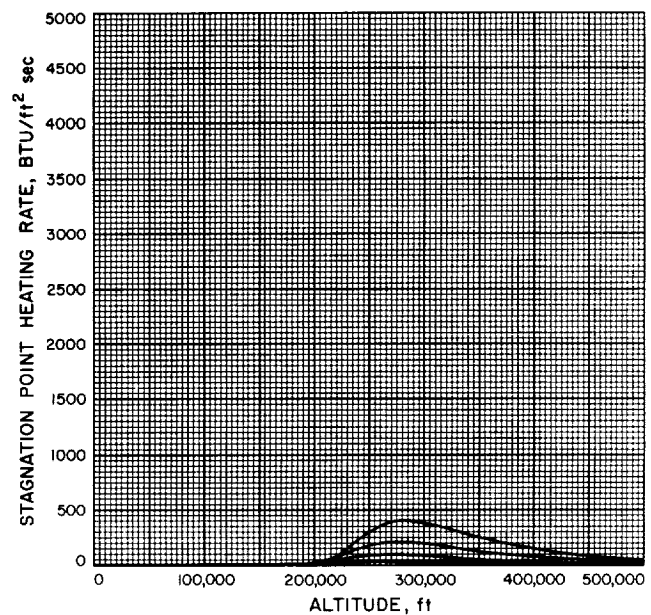


Fig. A-100

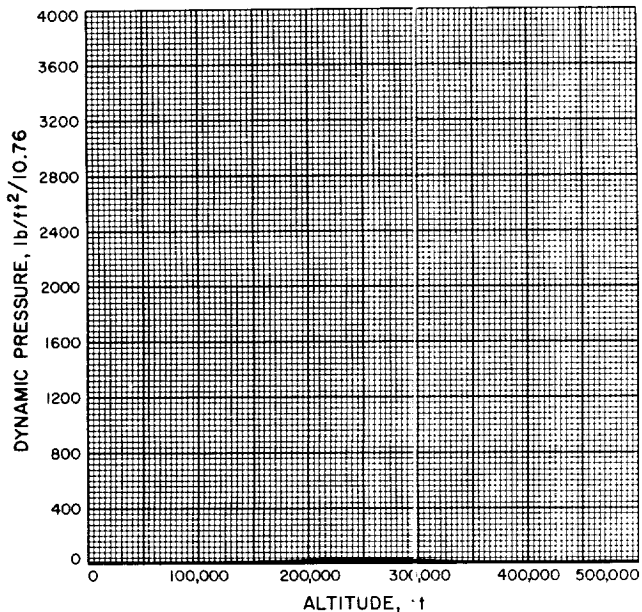


Fig. A-101

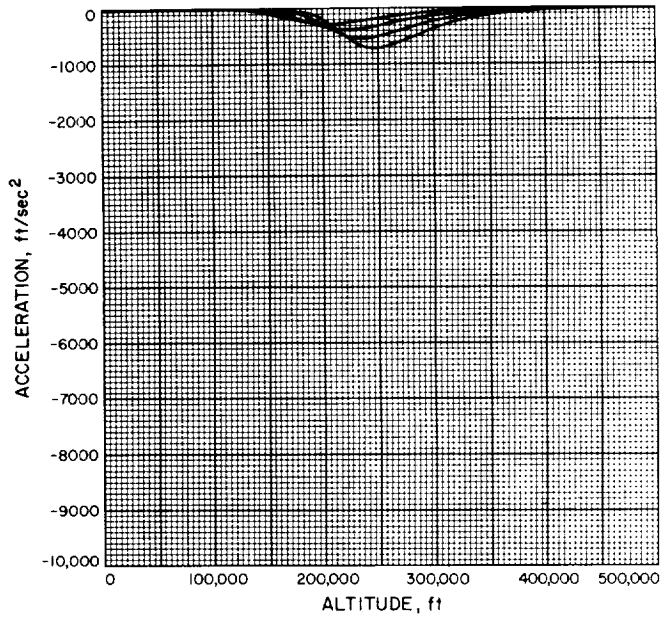


Fig. A-102

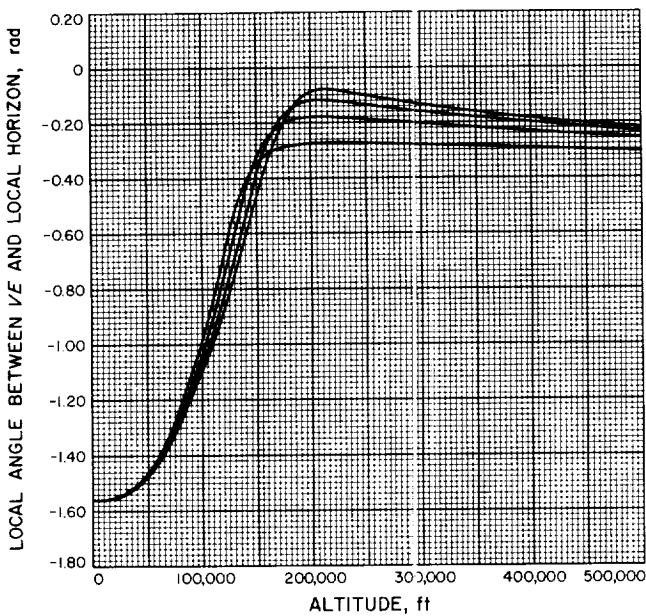


Fig. A-103

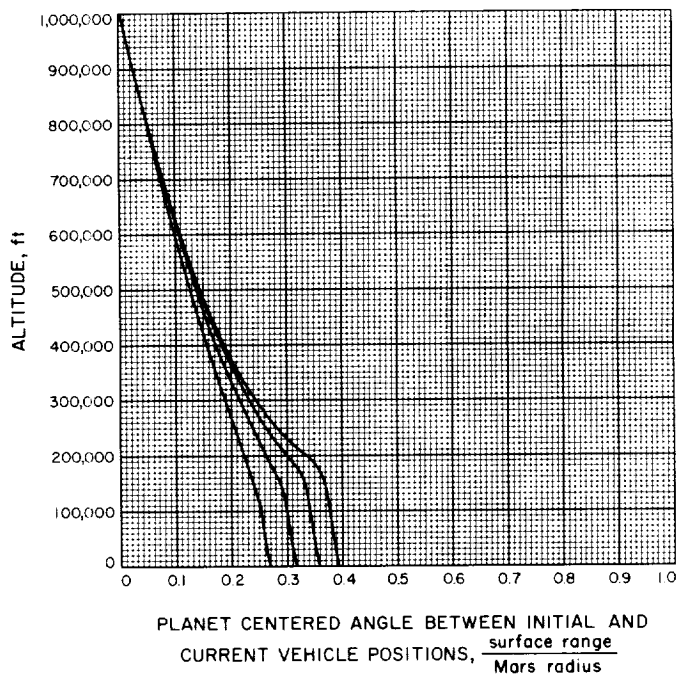


Fig. A-104

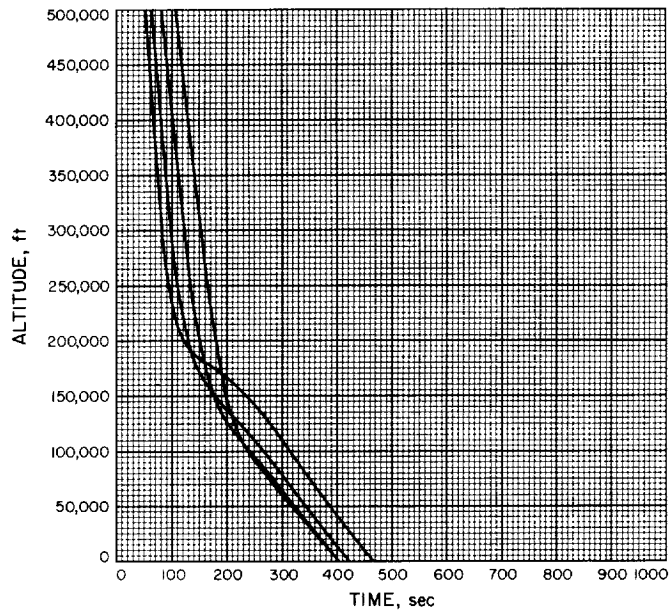


Fig. A-105

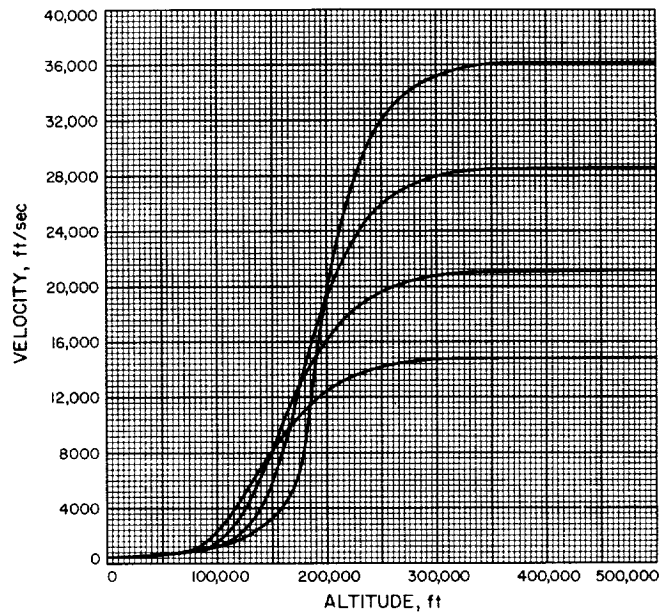


Fig. A-106

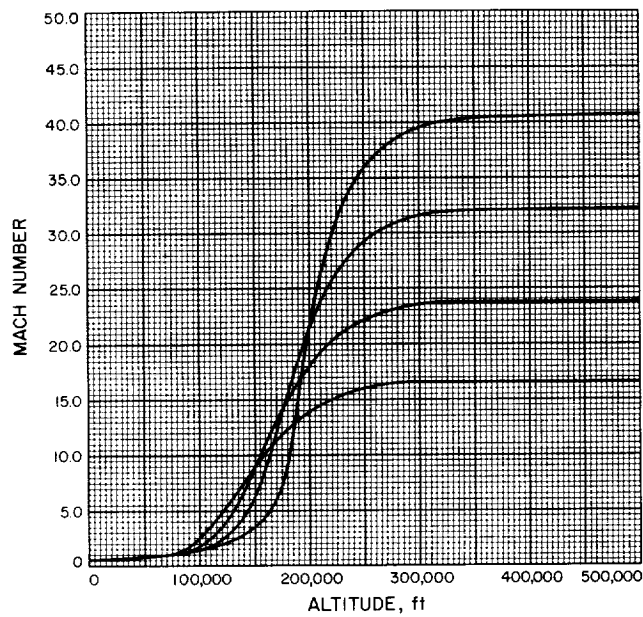


Fig. A-107

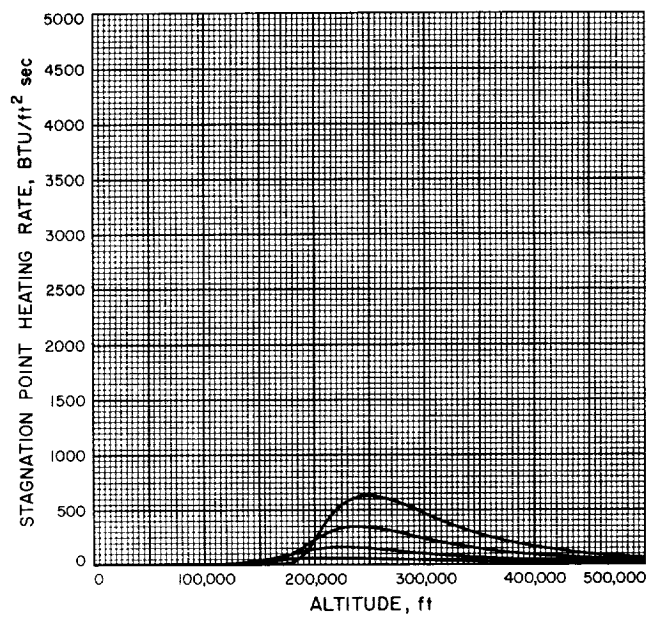


Fig. A-108

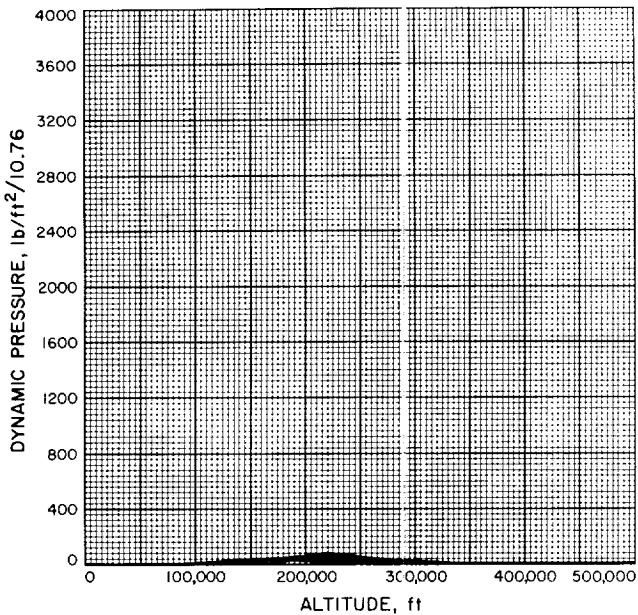


Fig. A-109

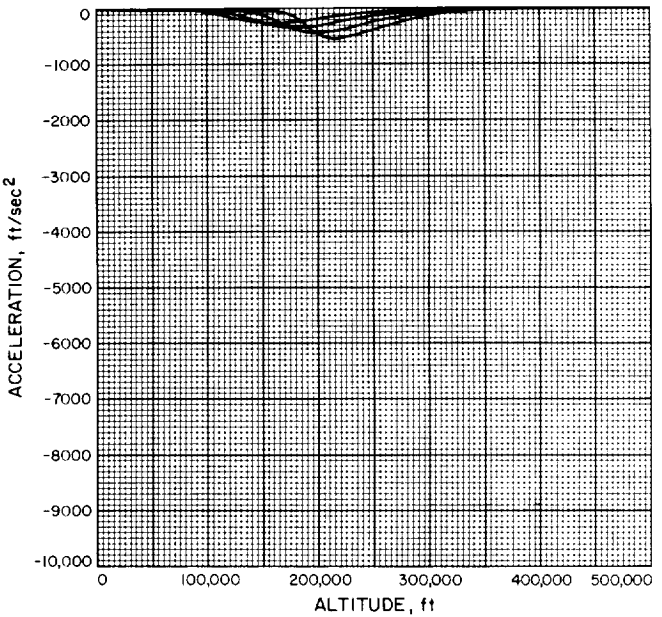


Fig. A-110

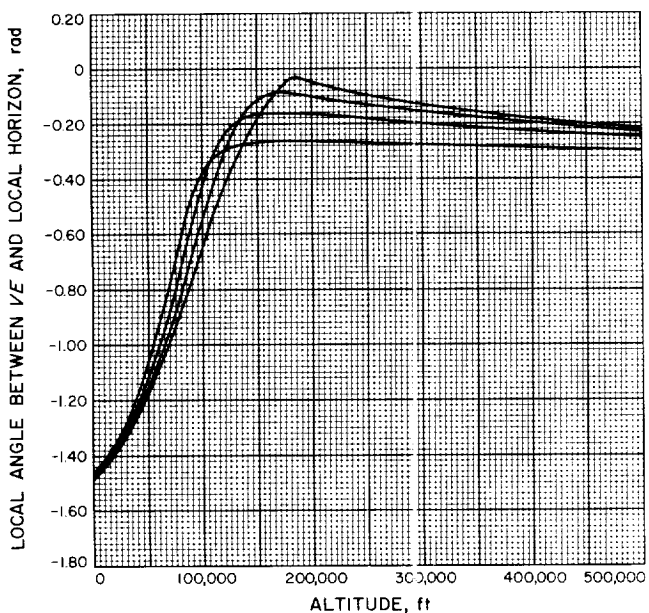
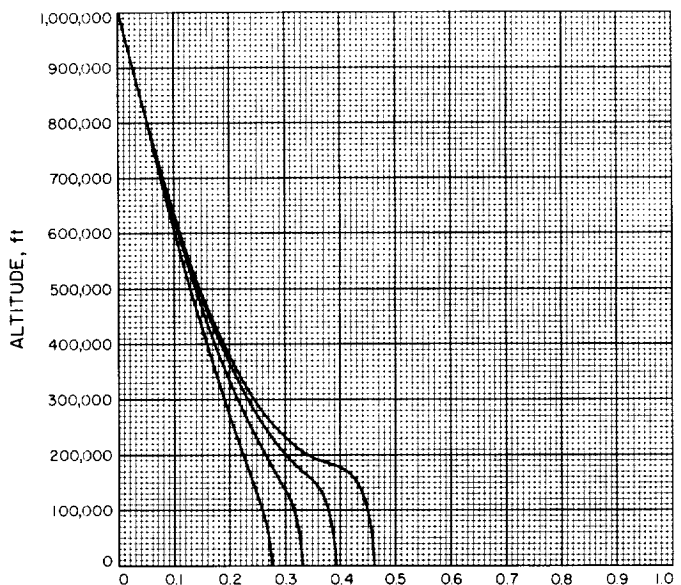


Fig. A-111



PLANET CENTERED ANGLE BETWEEN INITIAL AND
CURRENT VEHICLE POSITIONS, $\frac{\text{surface range}}{\text{Mars radius}}$

Fig. A-112

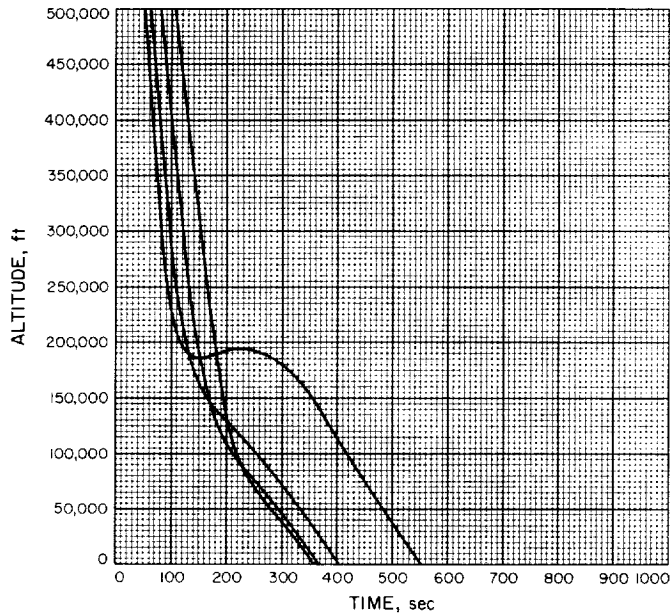


Fig. A-113

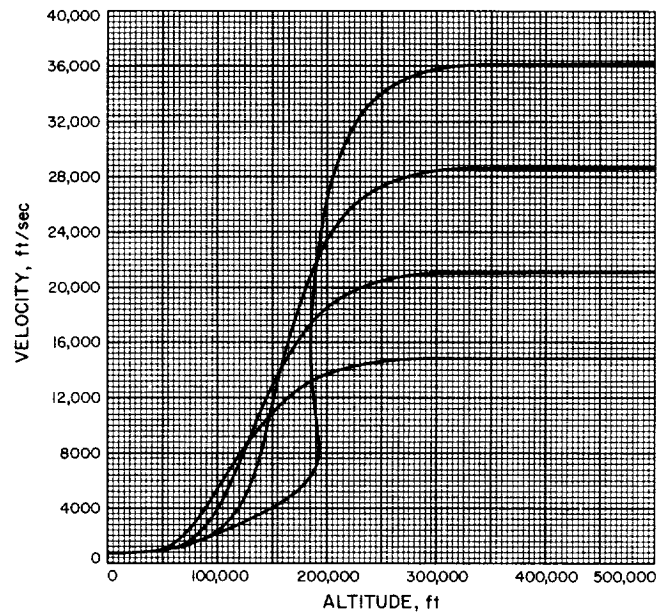


Fig. A-114

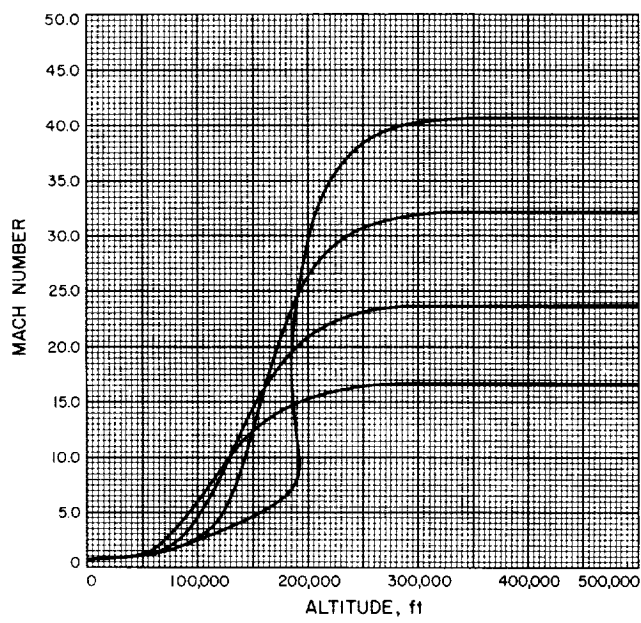


Fig. A-115

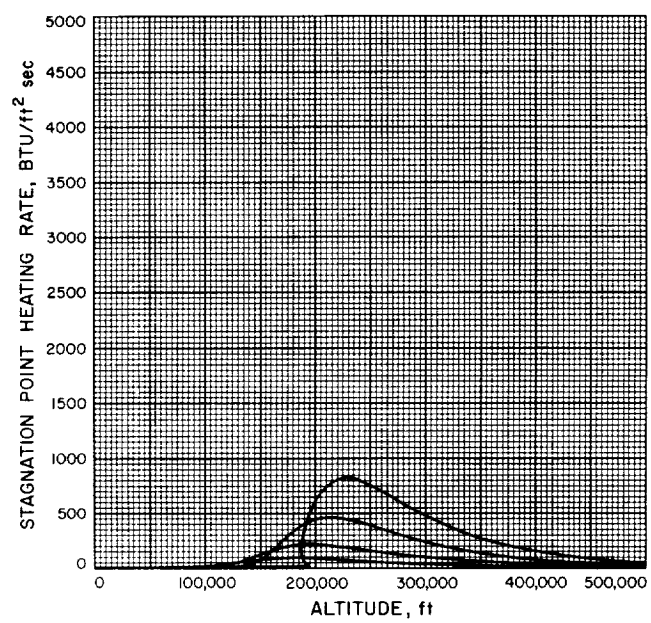


Fig. A-116

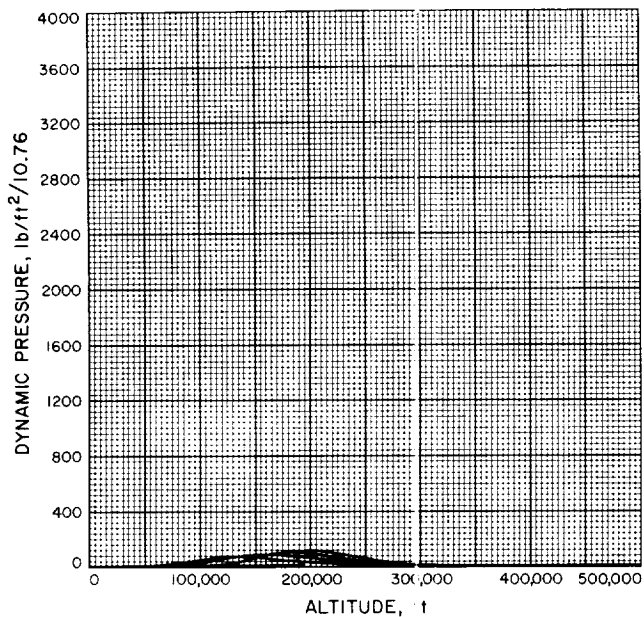


Fig. A-117

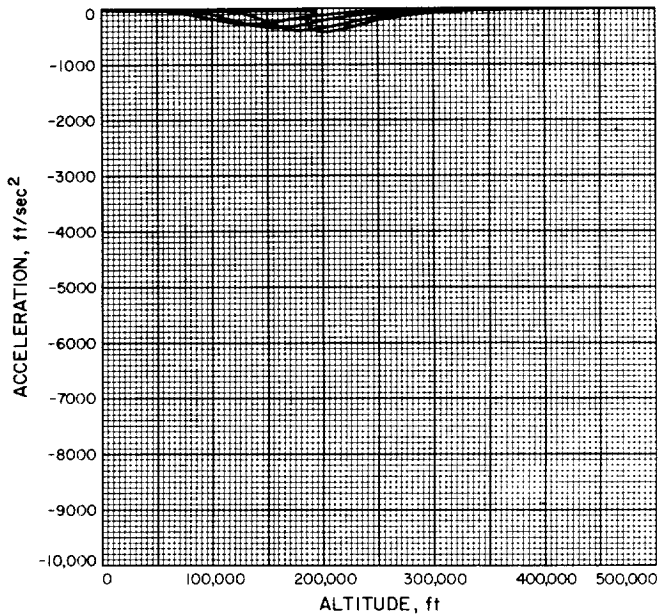


Fig. A-118

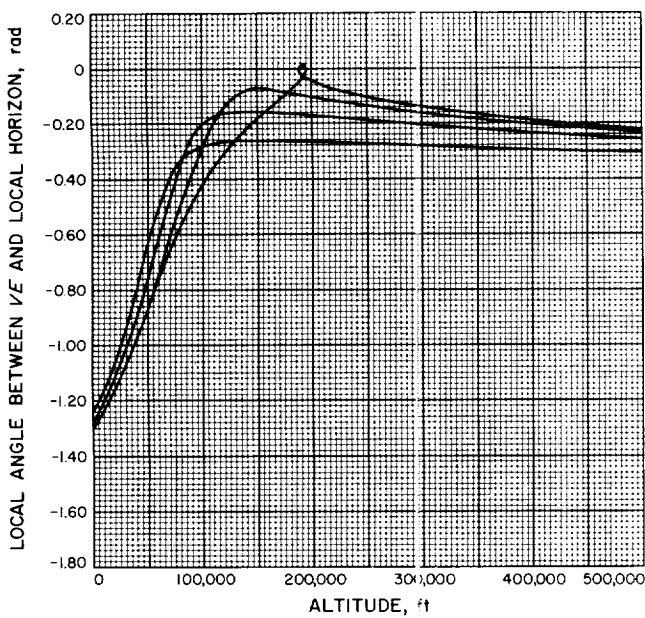
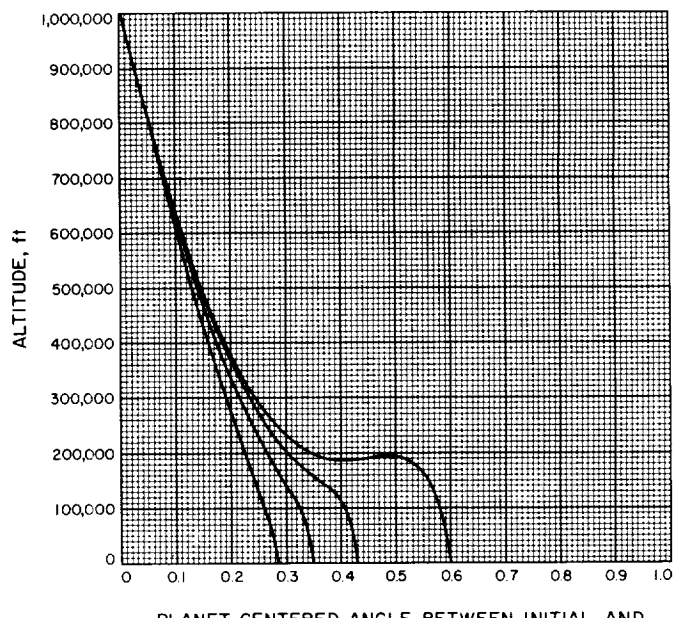


Fig. A-119



PLANET CENTERED ANGLE BETWEEN INITIAL AND
CURRENT VEHICLE POSITIONS, $\frac{\text{surface range}}{\text{Mars radius}}$

Fig. A-120

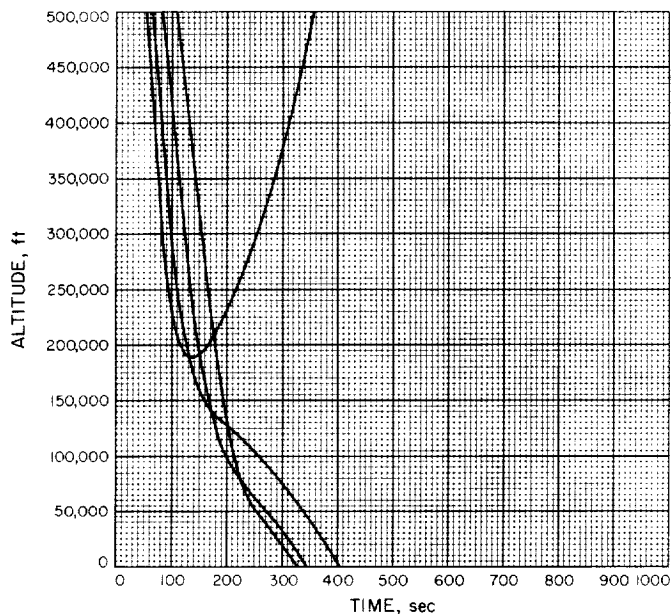


Fig. A-121

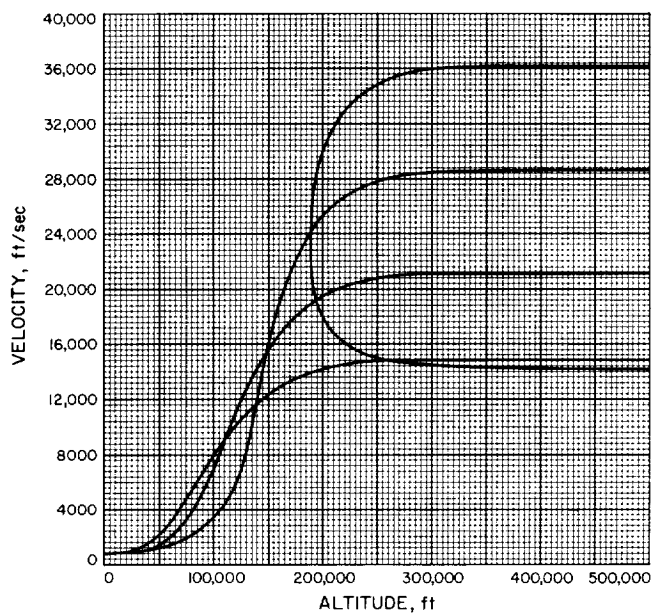


Fig. A-122

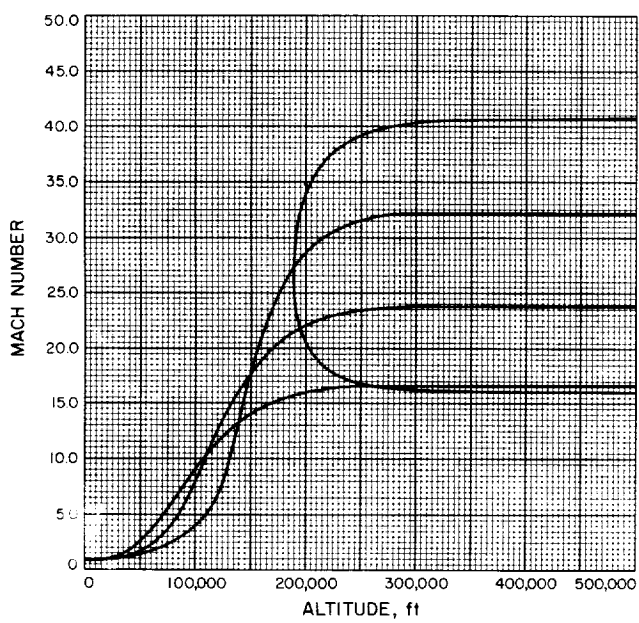


Fig. A-123

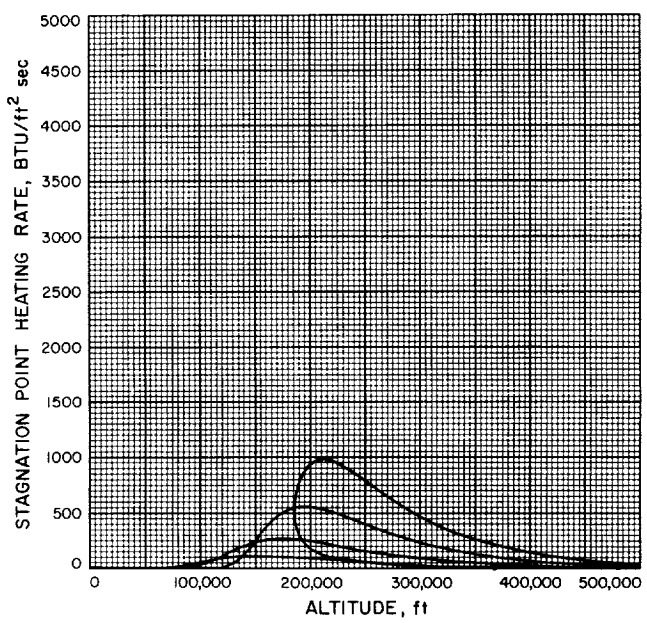


Fig. A-124

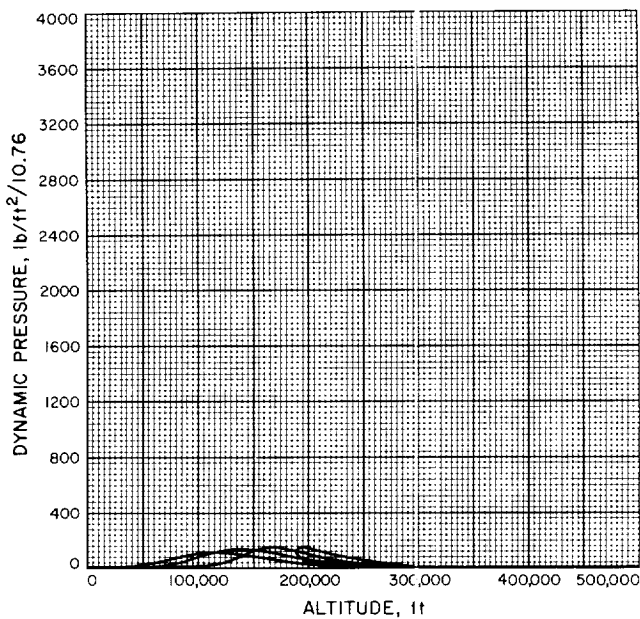


Fig. A-125

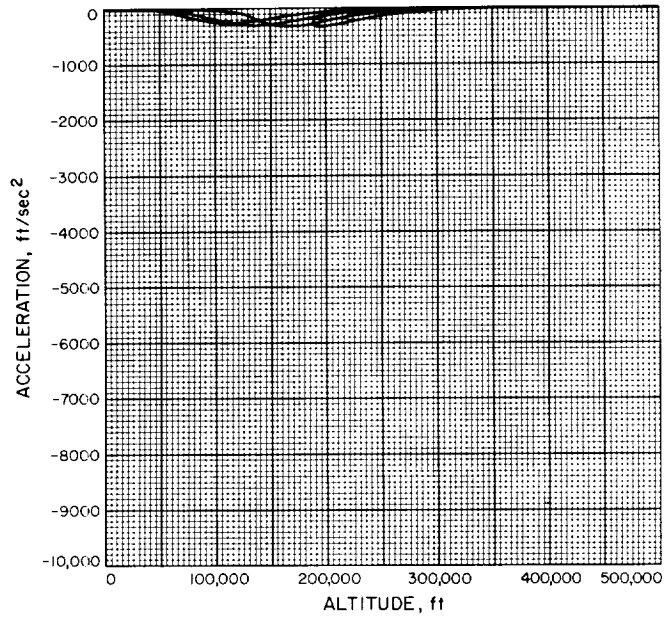


Fig. A-126

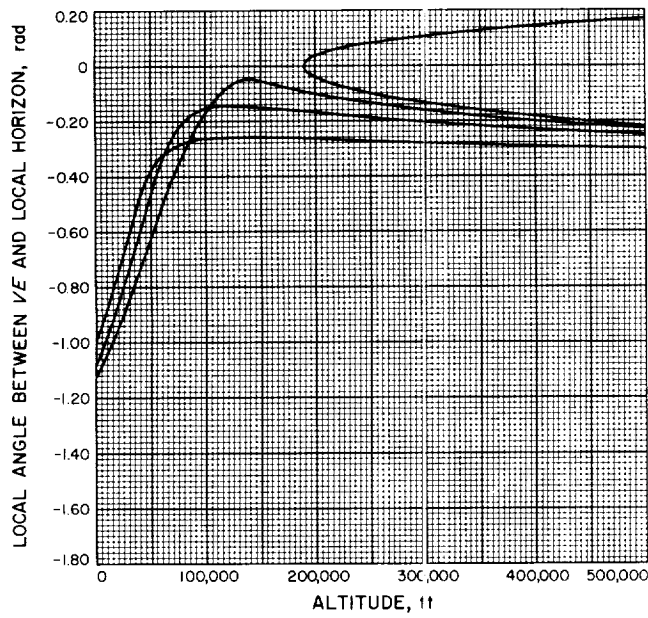
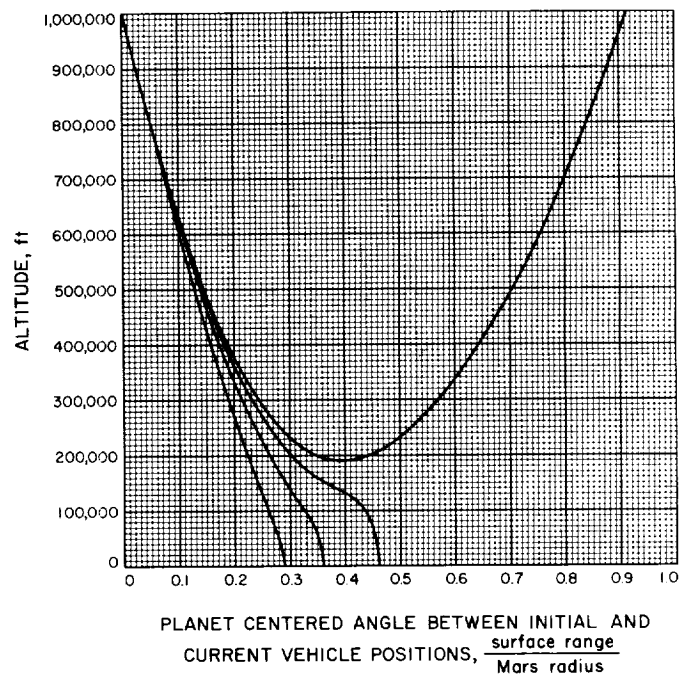


Fig. A-127



PLANET CENTERED ANGLE BETWEEN INITIAL AND

CURRENT VEHICLE POSITIONS, $\frac{\text{surface range}}{\text{Mars radius}}$

Fig. A-128

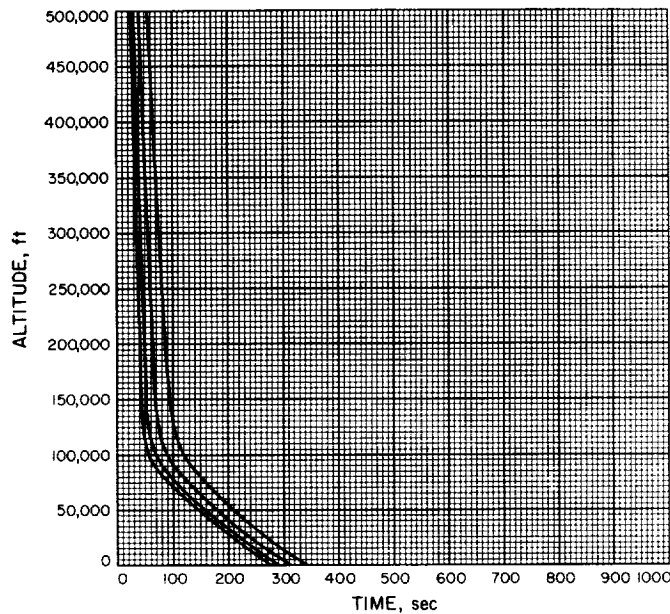


Fig. A-129

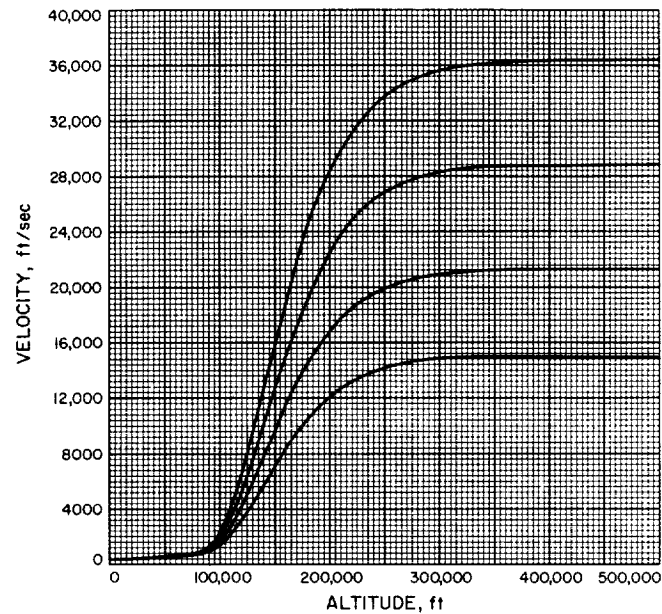


Fig. A-130

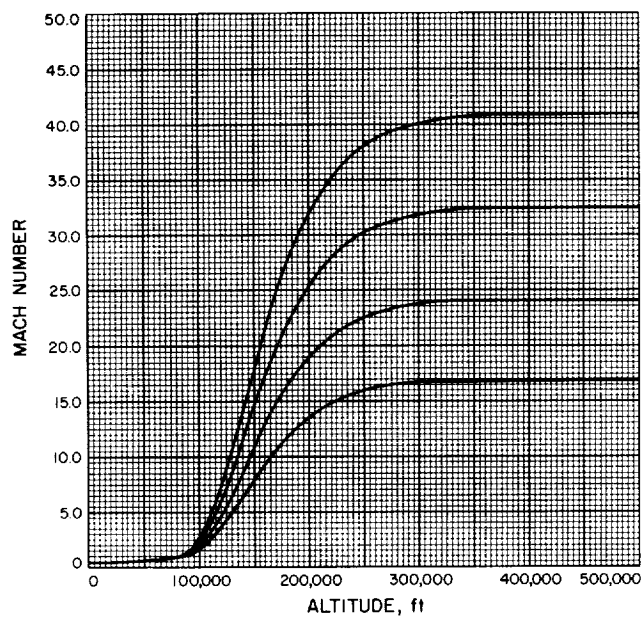


Fig. A-131

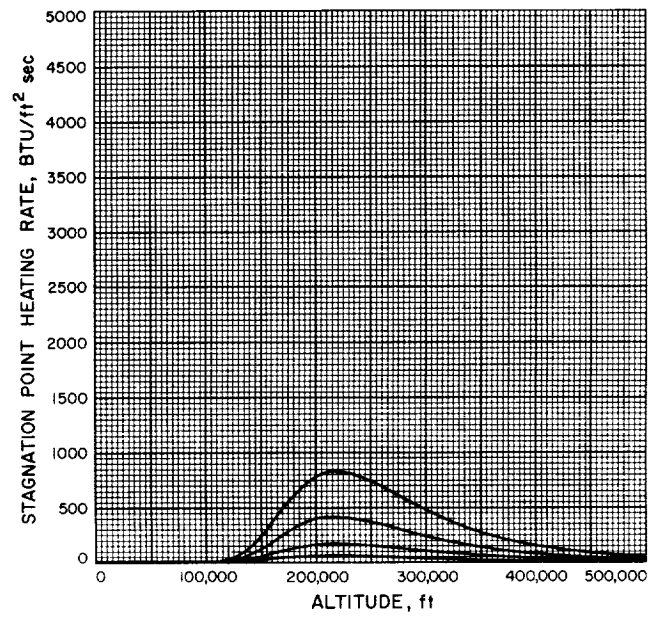


Fig. A-132

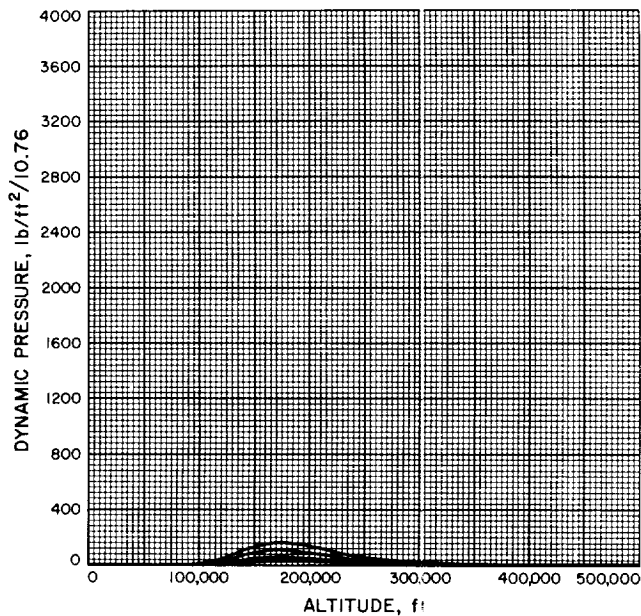


Fig. A-133

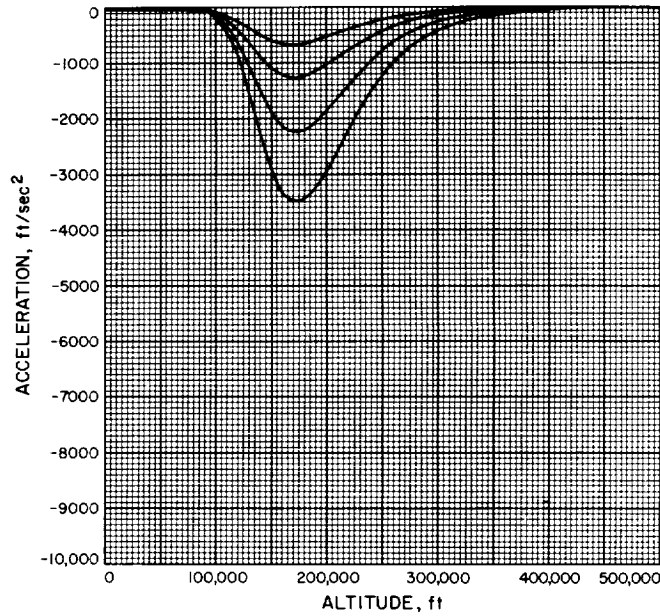


Fig. A-134

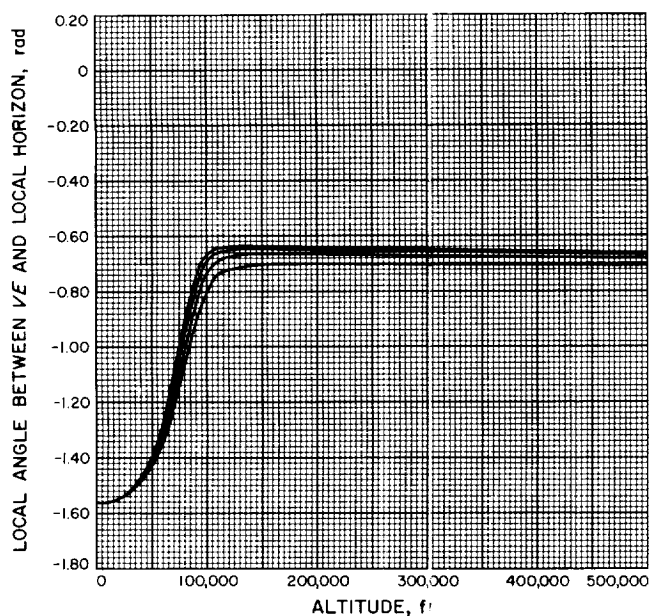


Fig. A-135

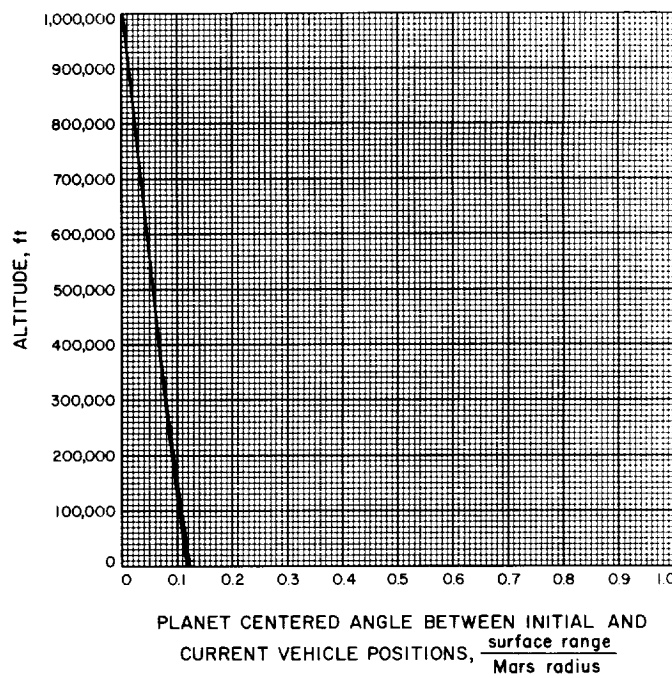


Fig. A-136

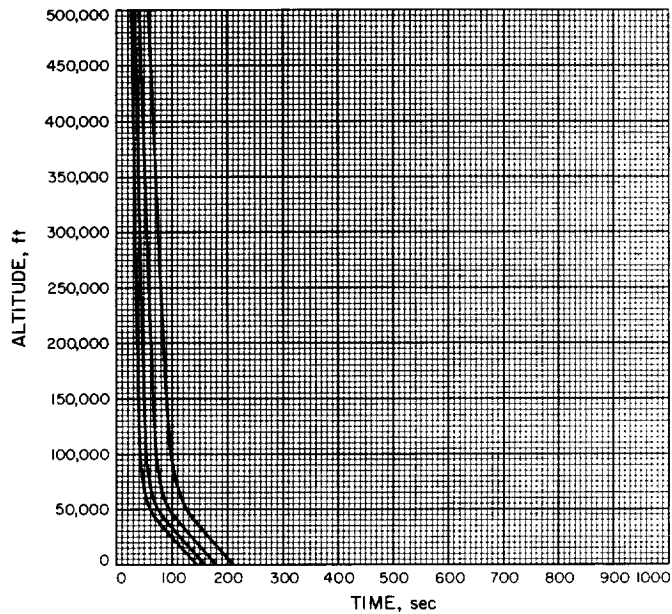


Fig. A-137

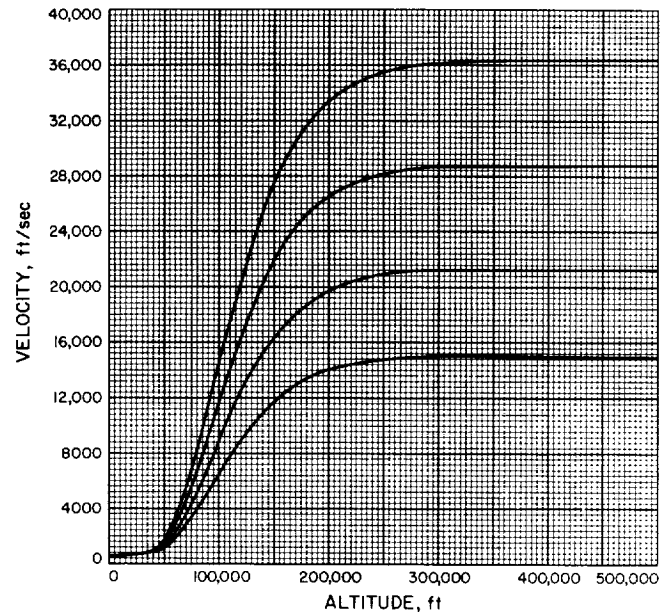


Fig. A-138

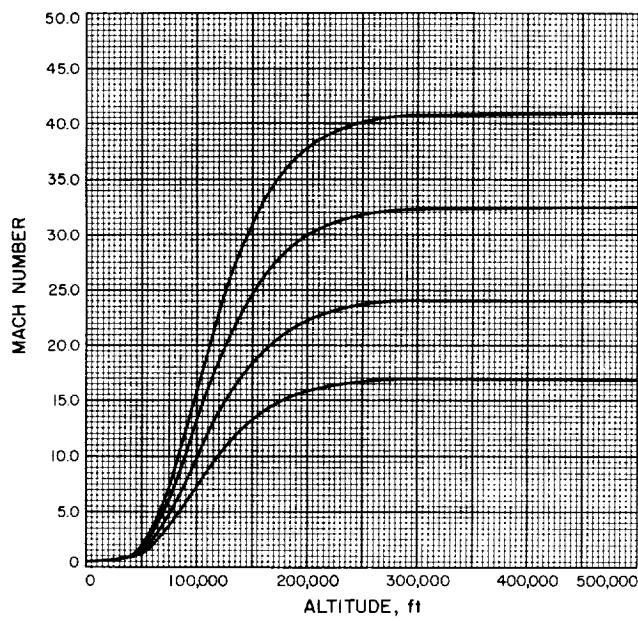


Fig. A-139

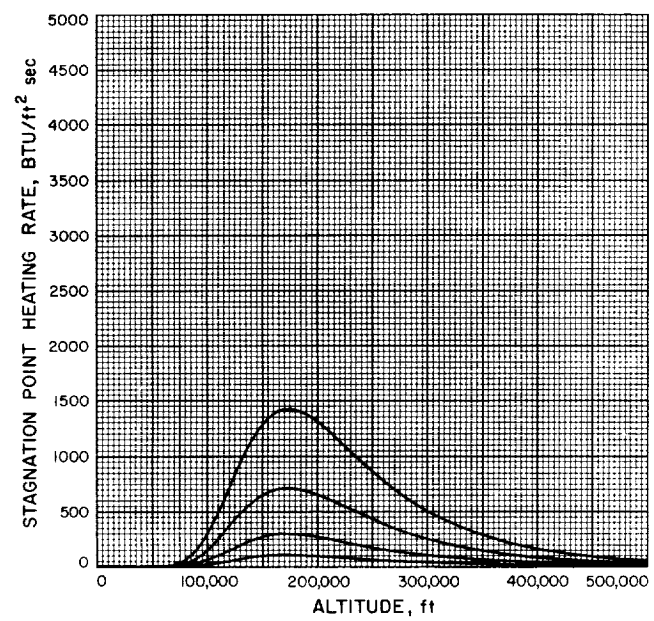


Fig. A-140

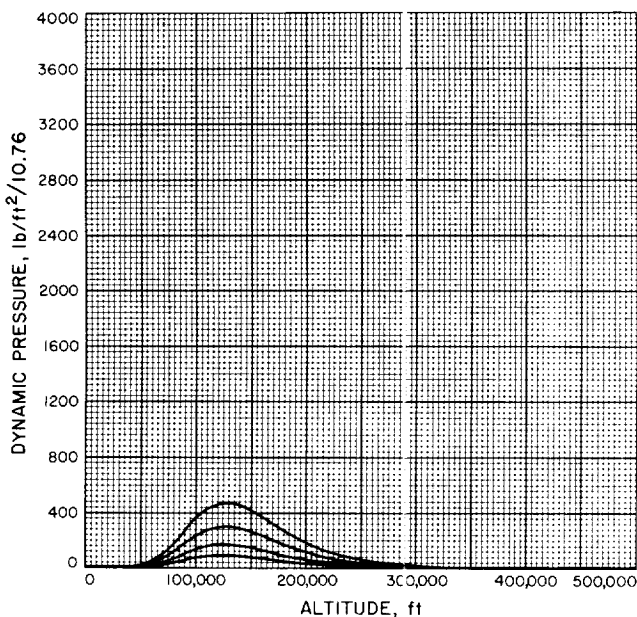


Fig. A-141

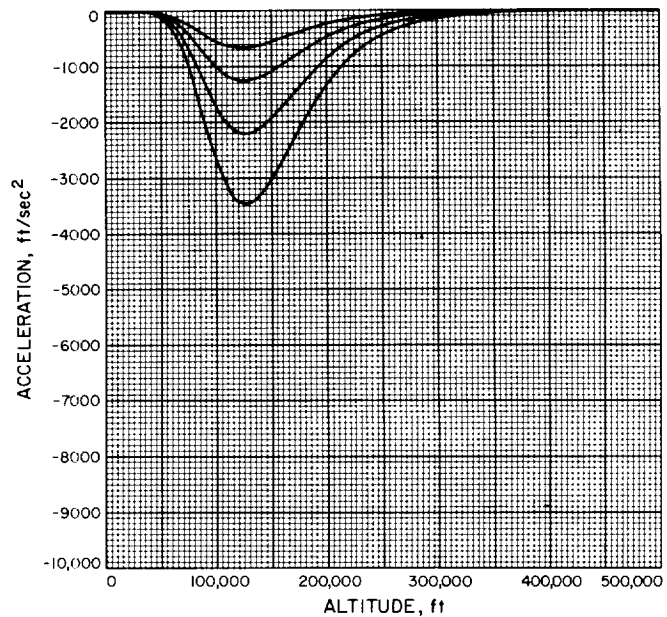


Fig. A-142

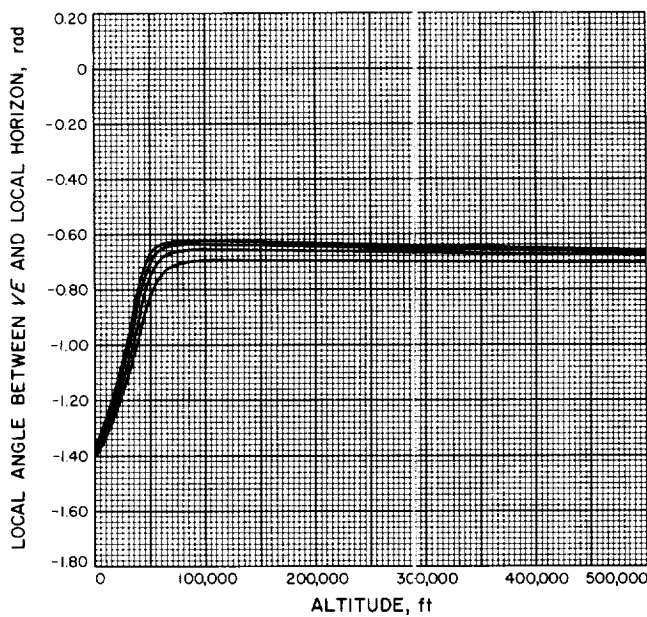


Fig. A-143

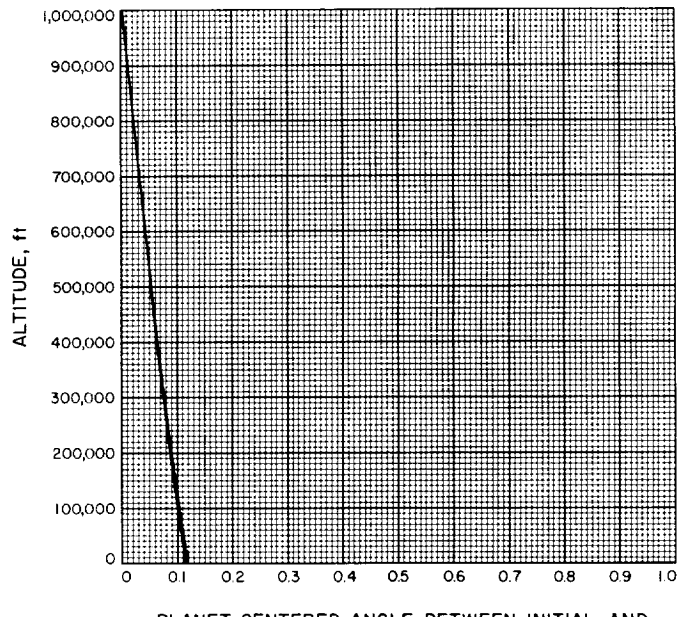


Fig. A-144

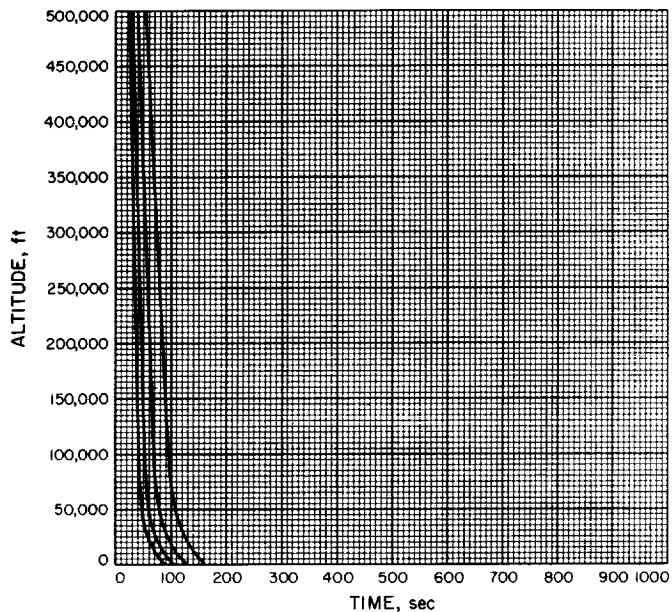


Fig. A-145

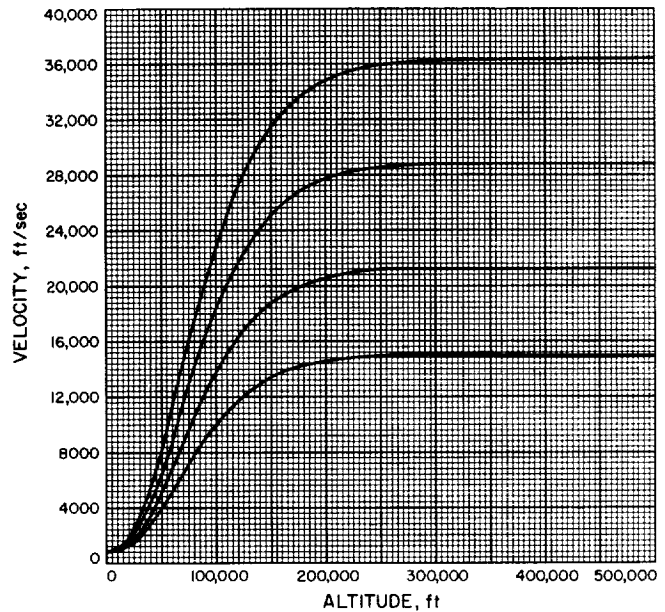


Fig. A-146

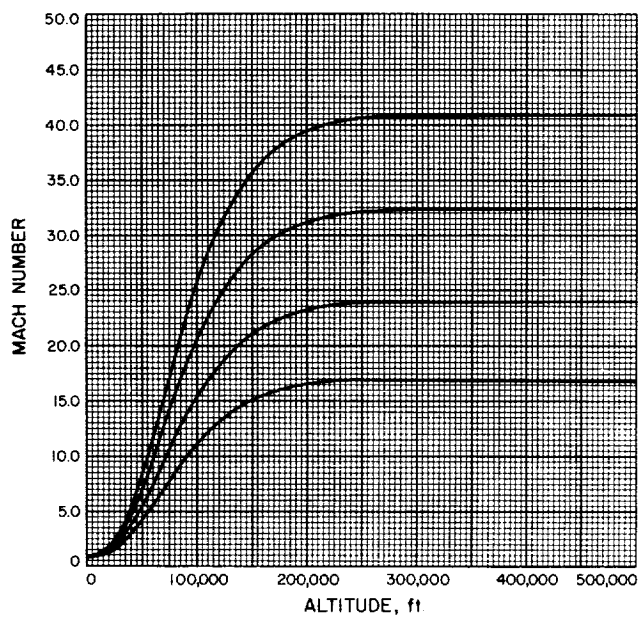


Fig. A-147

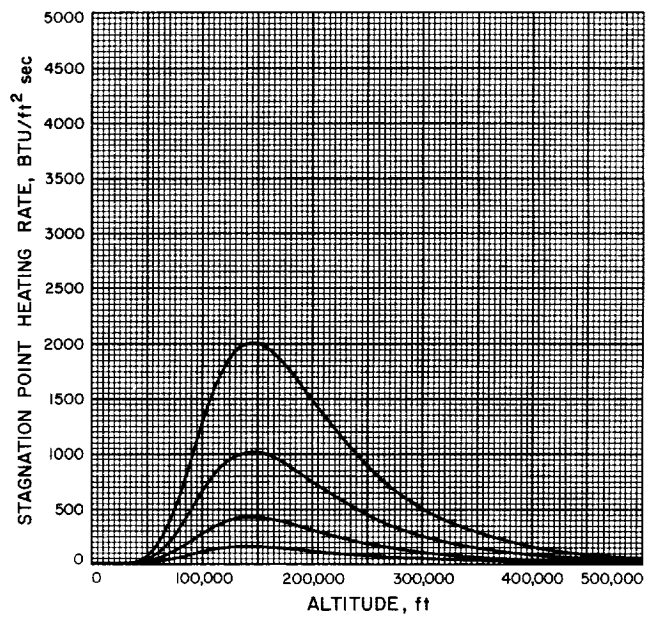


Fig. A-148

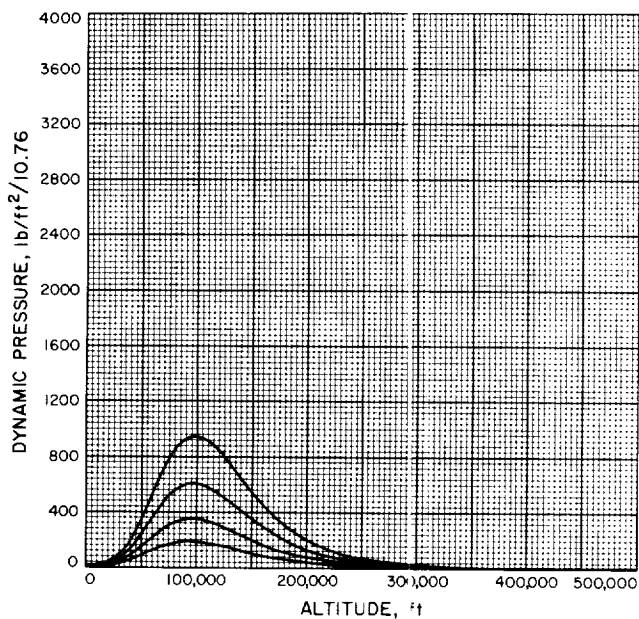


Fig. A-149

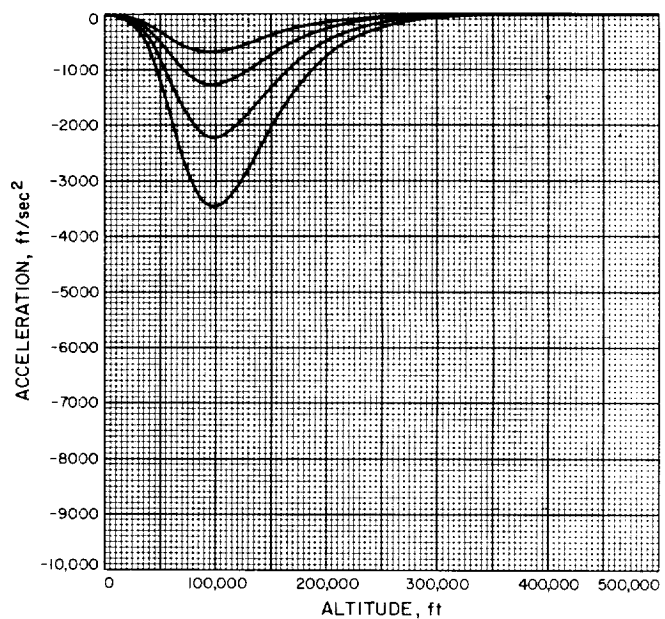


Fig. A-150

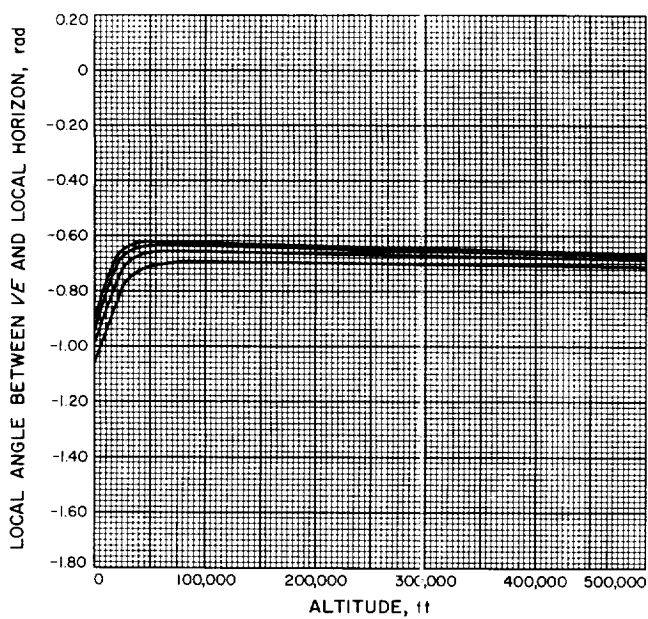
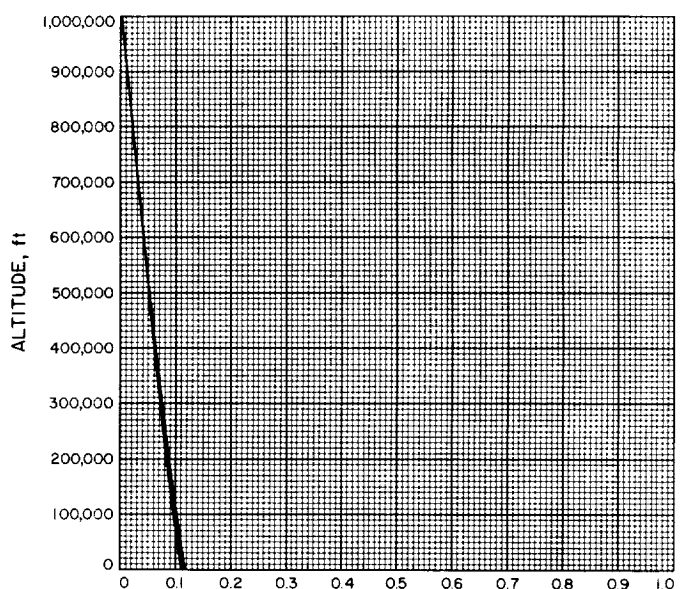


Fig. A-151



PLANET CENTERED ANGLE BETWEEN INITIAL AND
CURRENT VEHICLE POSITIONS, $\frac{\text{surface range}}{\text{Mars radius}}$

Fig. A-152

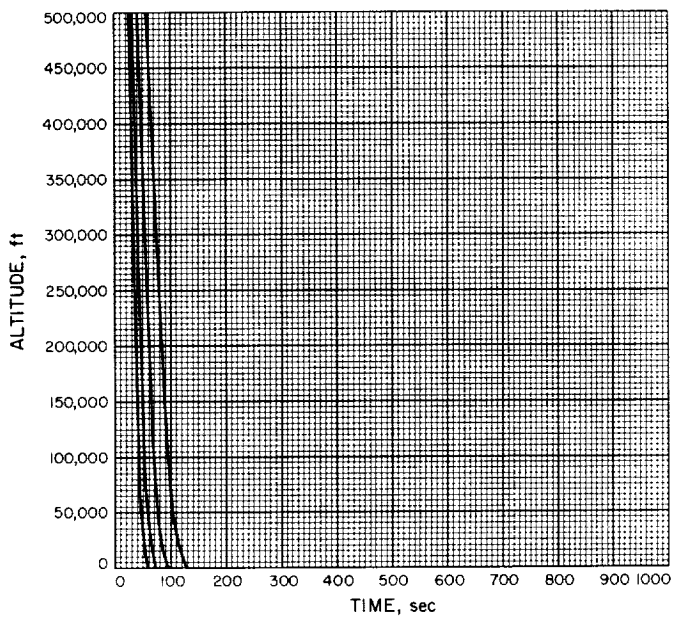


Fig. A-153

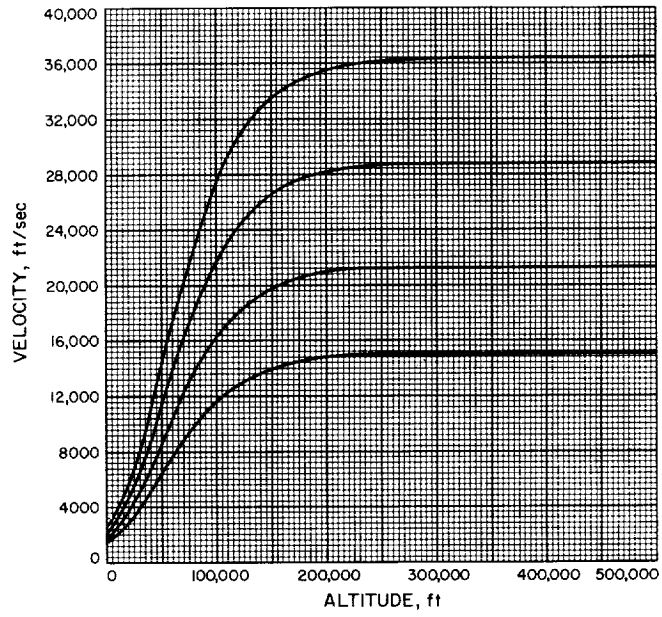


Fig. A-154

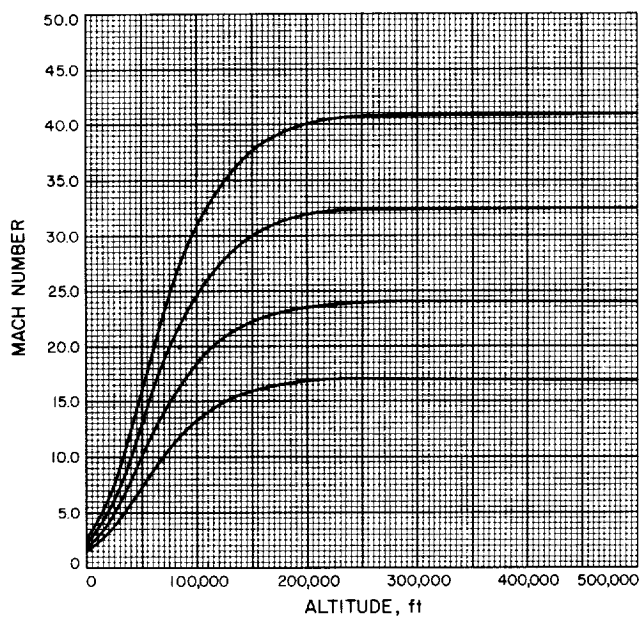


Fig. A-155

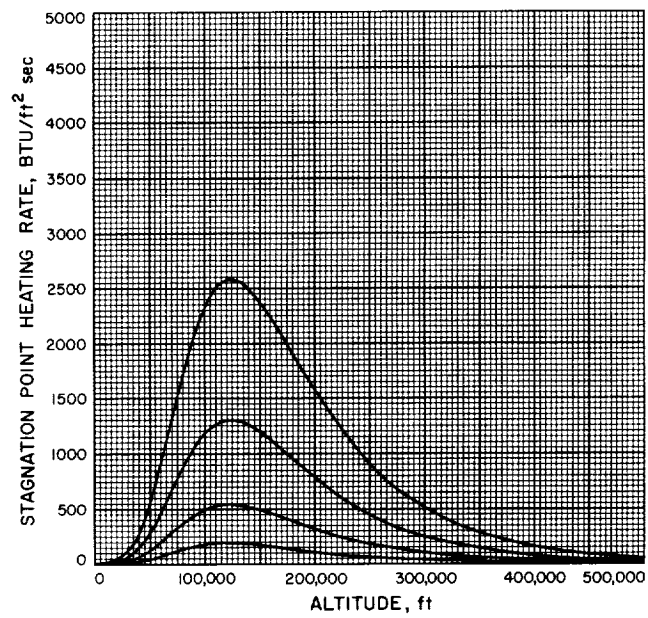


Fig. A-156

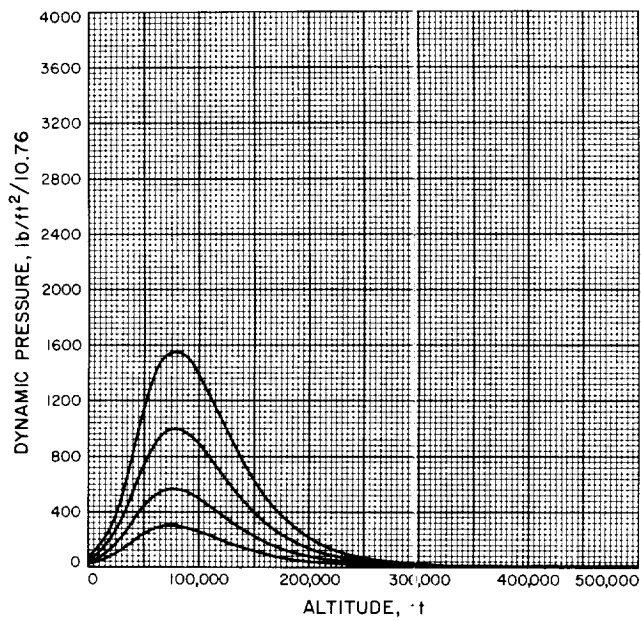


Fig. A-157

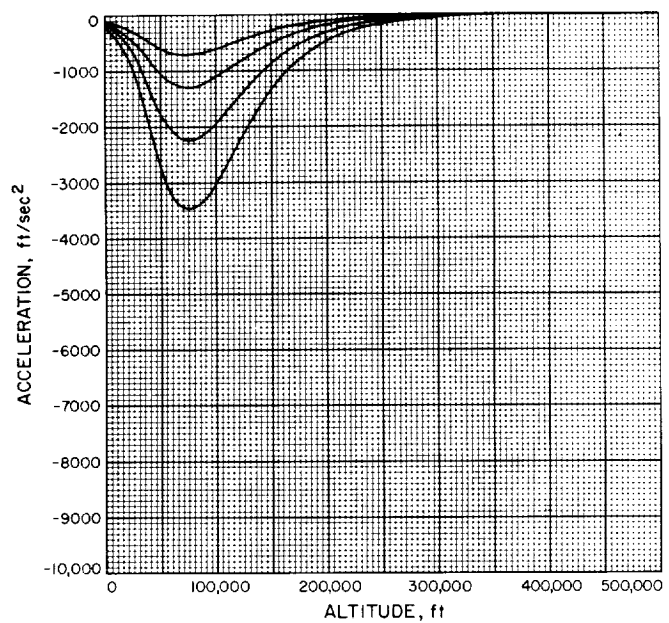


Fig. A-158

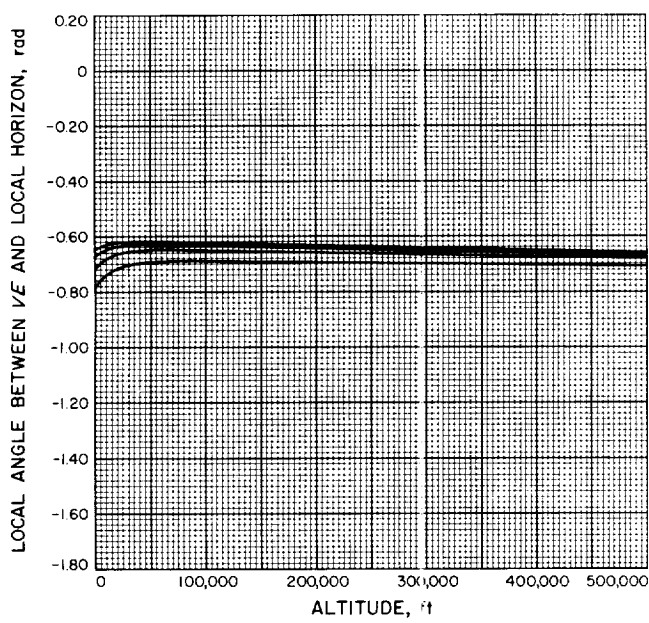


Fig. A-159

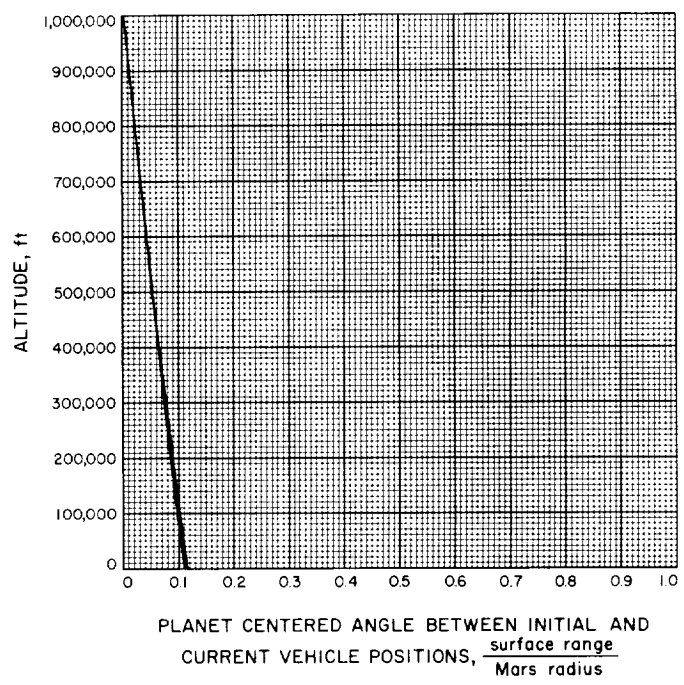


Fig. A-160

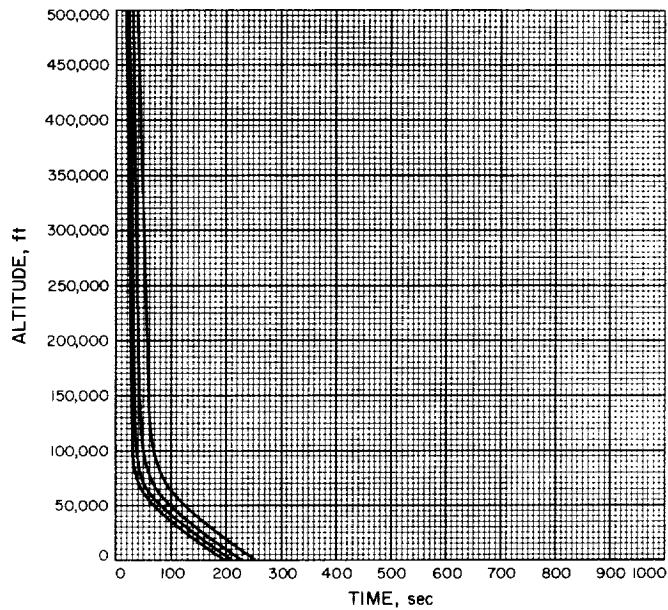


Fig. A-161

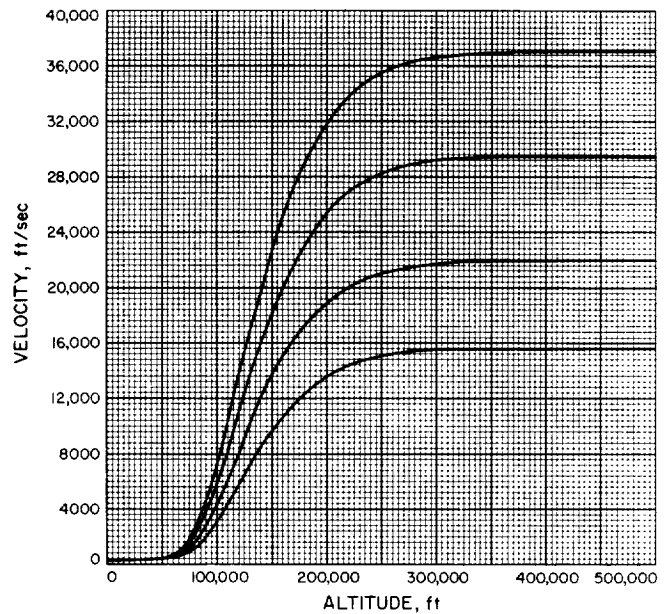


Fig. A-162

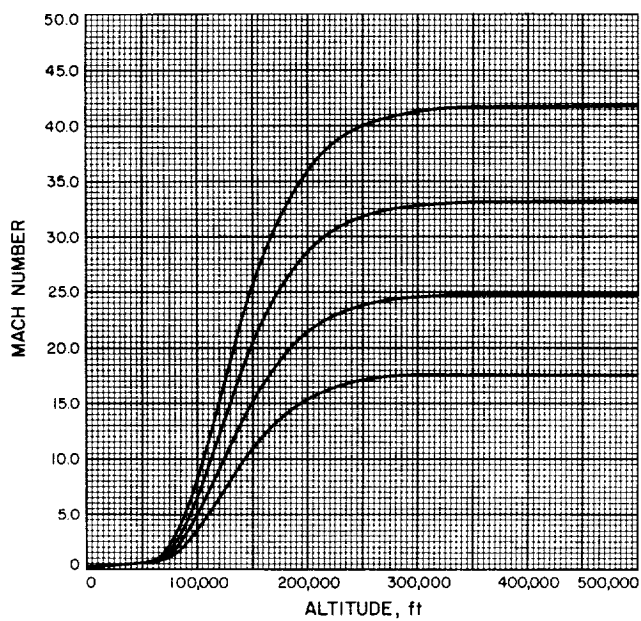


Fig. A-163

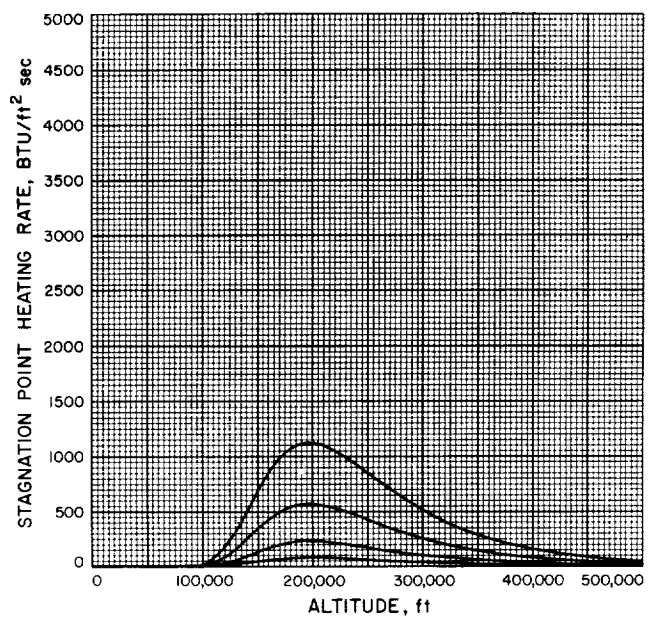


Fig. A-164

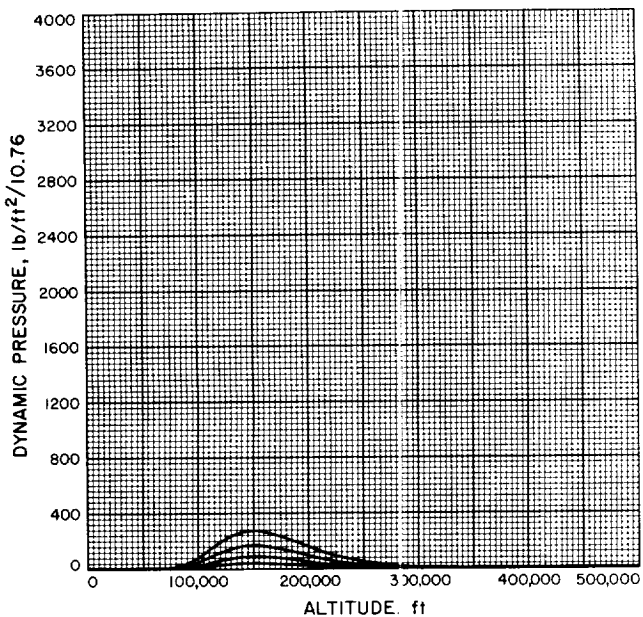


Fig. A-165

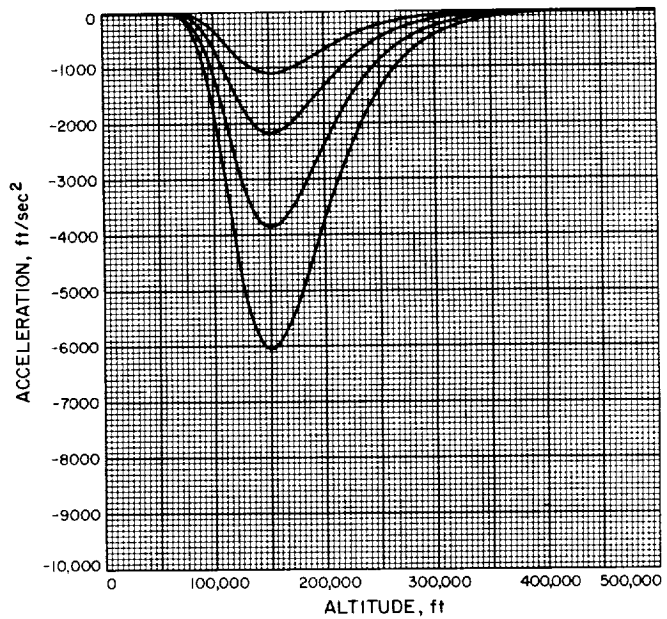


Fig. A-166

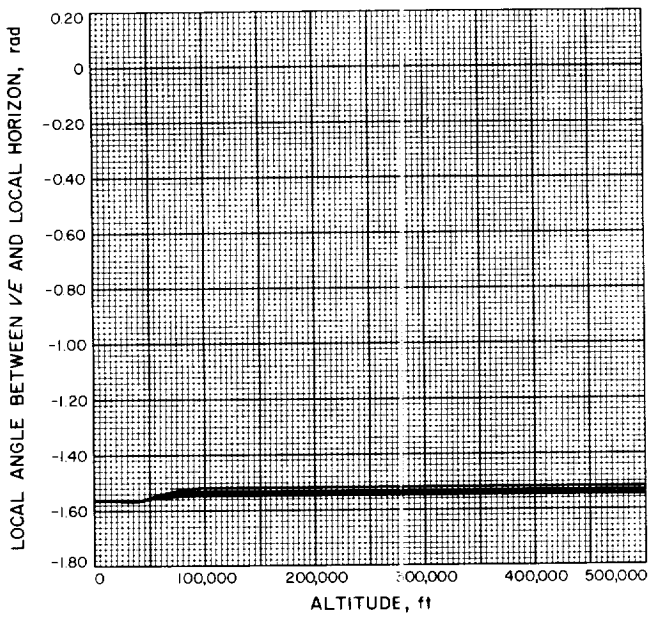


Fig. A-167

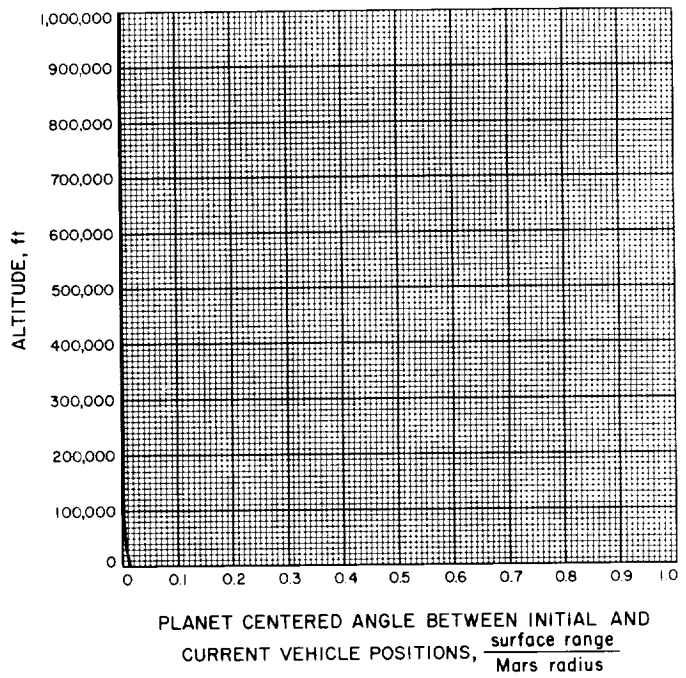
PLANET CENTERED ANGLE BETWEEN INITIAL AND
CURRENT VEHICLE POSITIONS, $\frac{\text{surface range}}{\text{Mars radius}}$

Fig. A-168

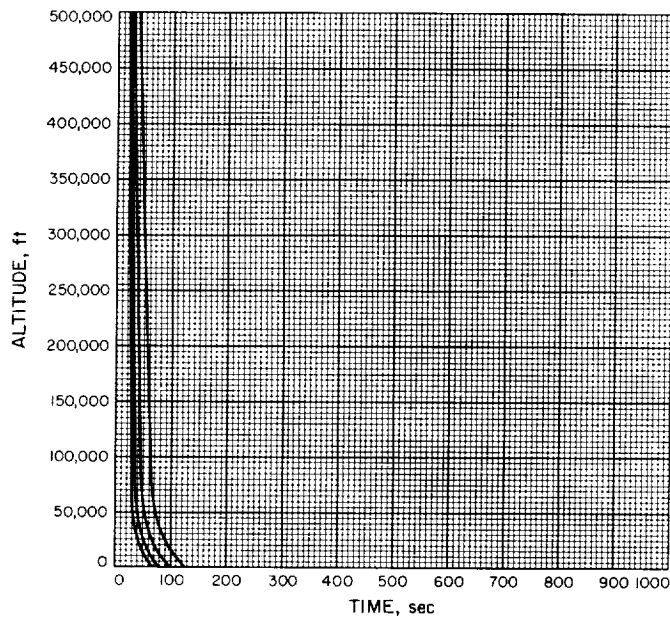


Fig. A-169

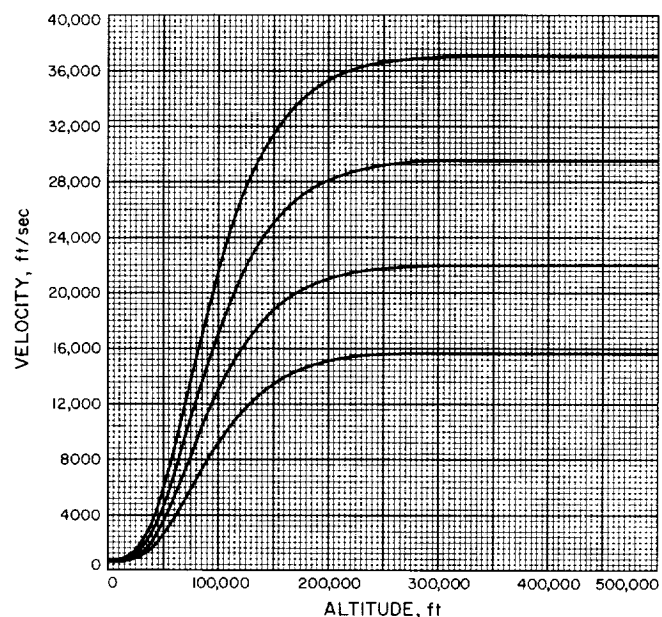


Fig. A-170

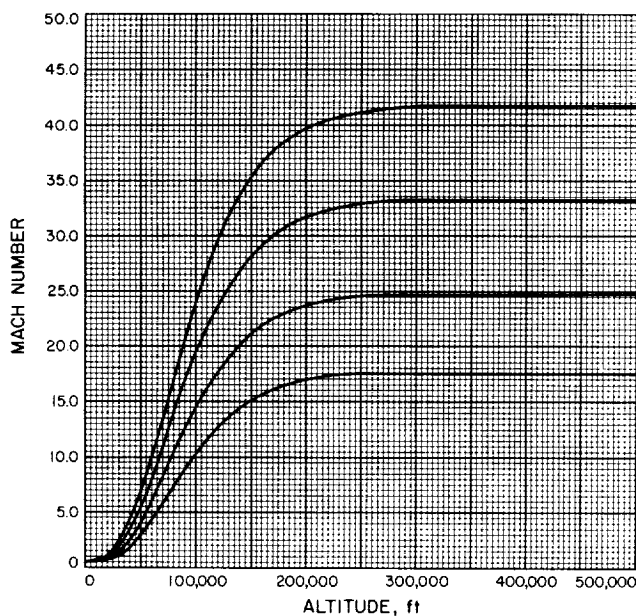


Fig. A-171

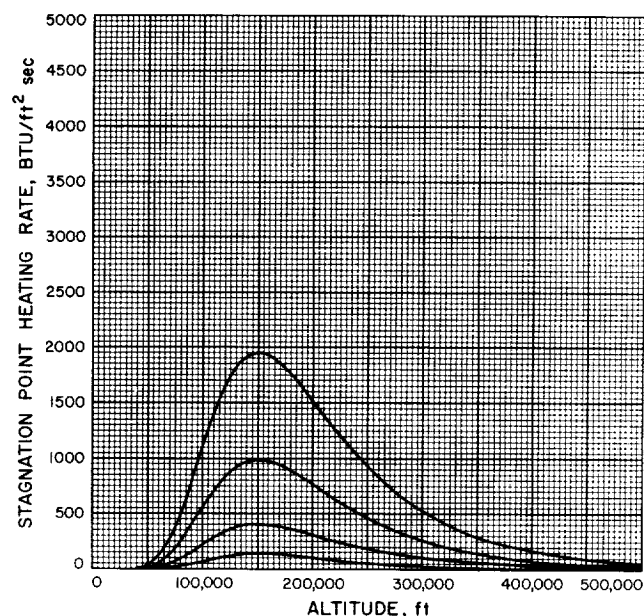


Fig. A-172

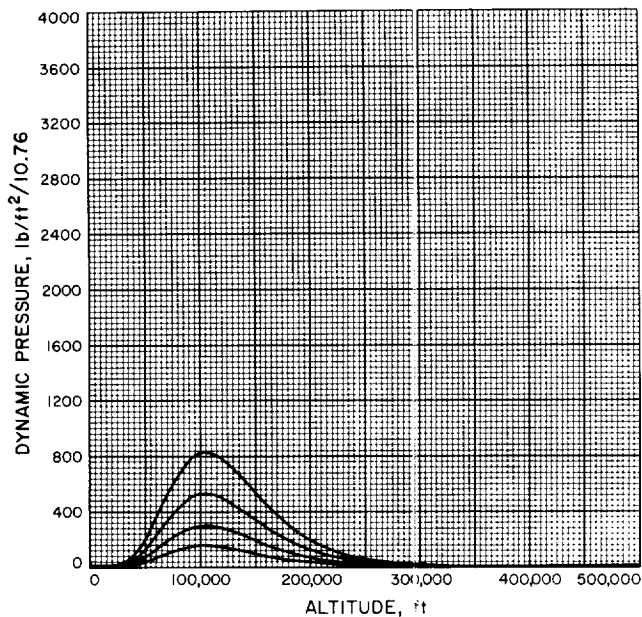


Fig. A-173

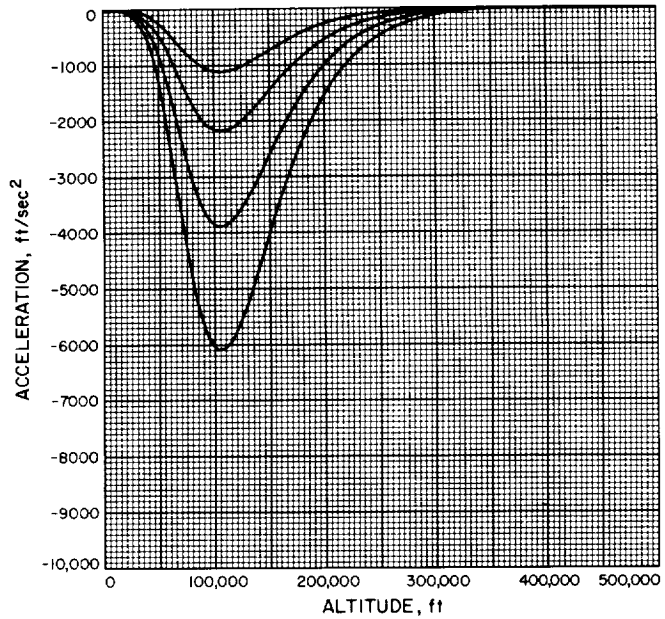


Fig. A-174

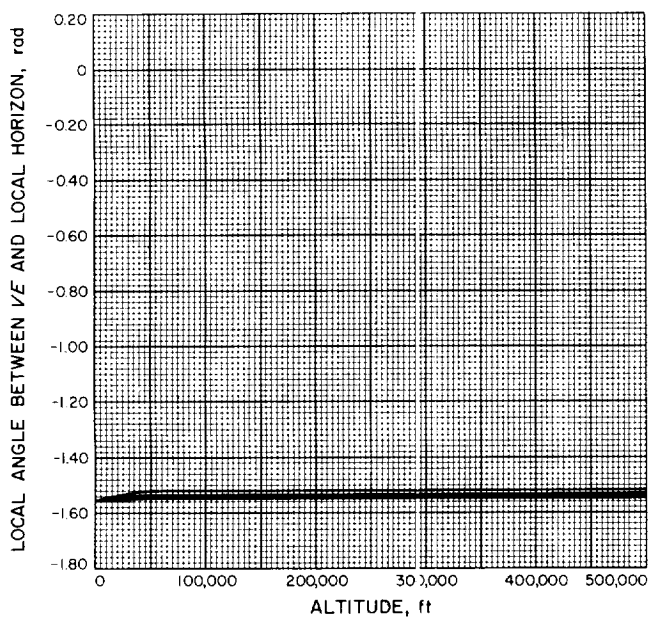


Fig. A-175

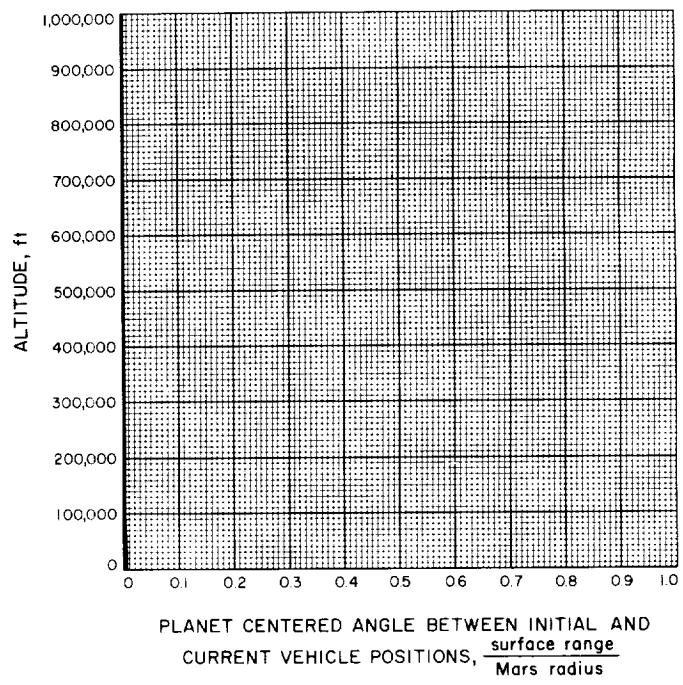


Fig. A-176

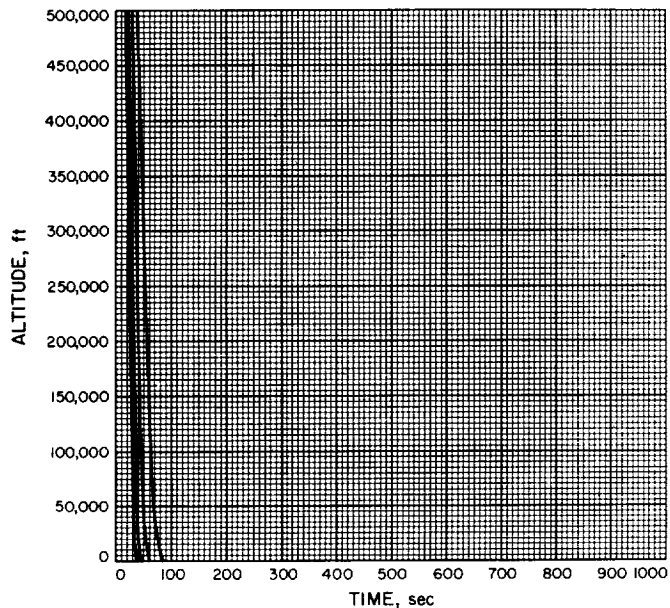


Fig. A-177

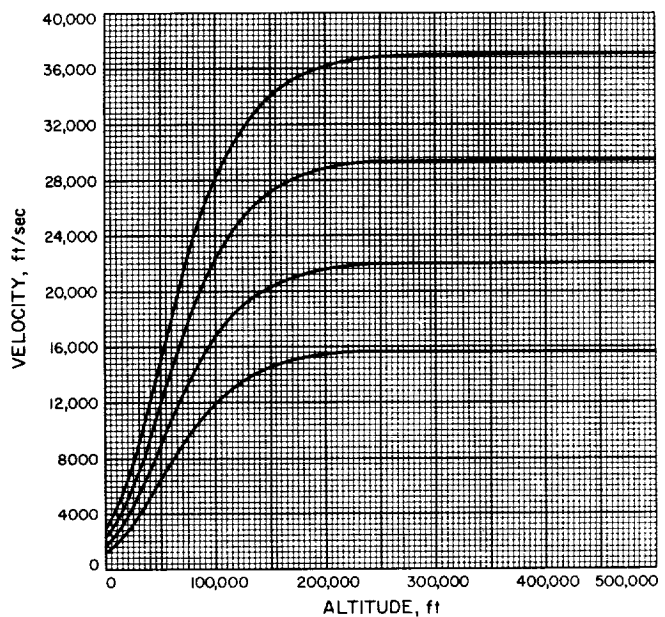


Fig. A-178

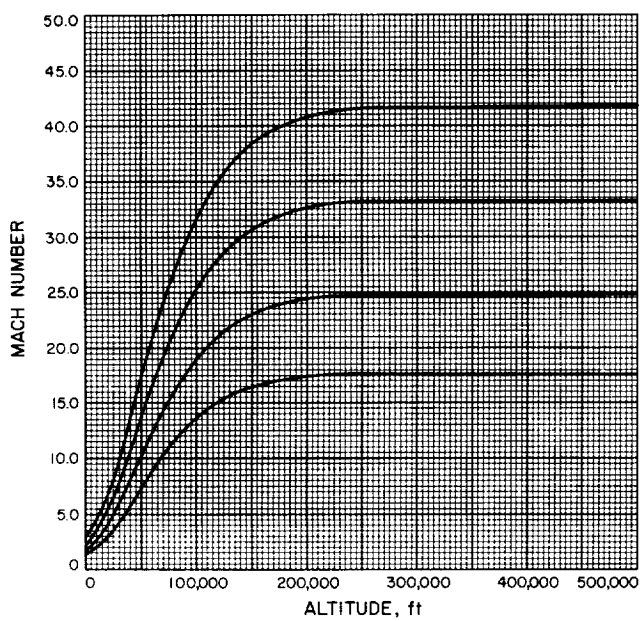


Fig. A-179

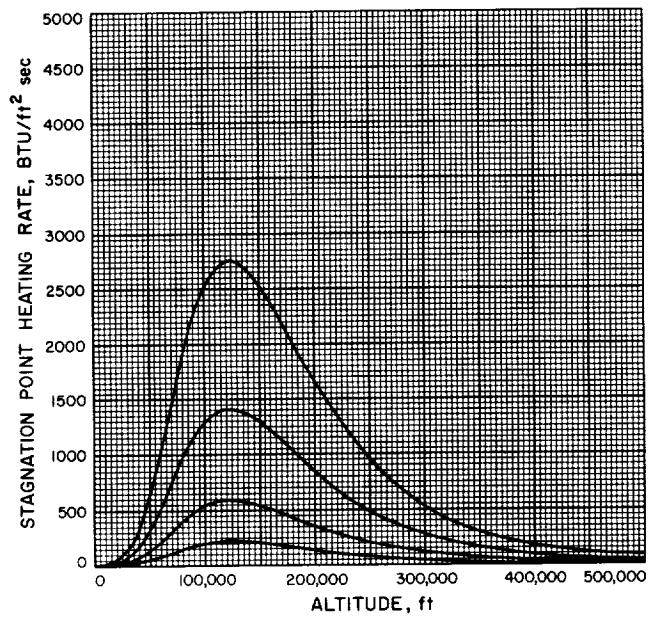


Fig. A-180

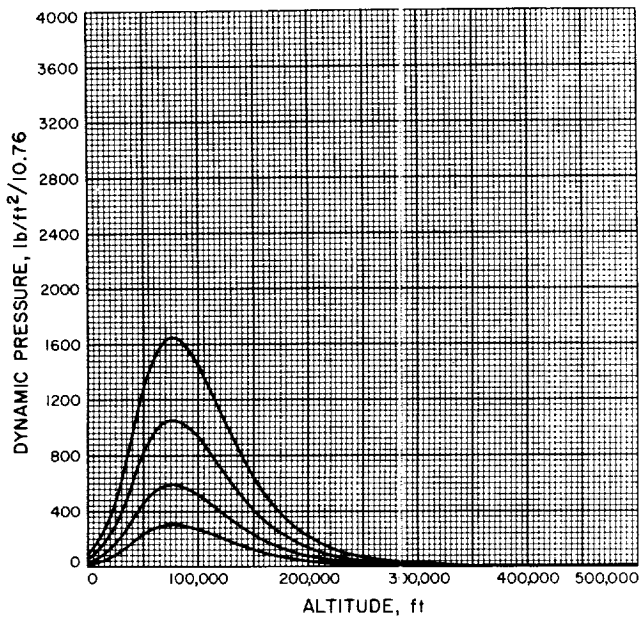


Fig. A-181

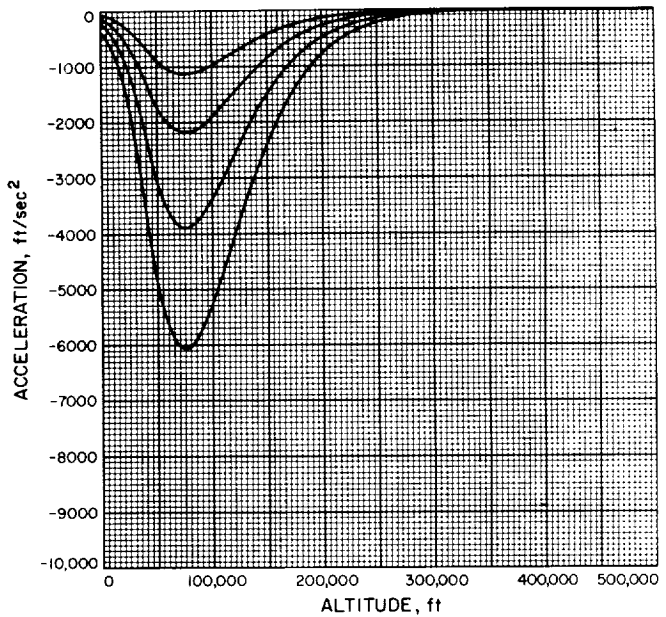


Fig. A-182

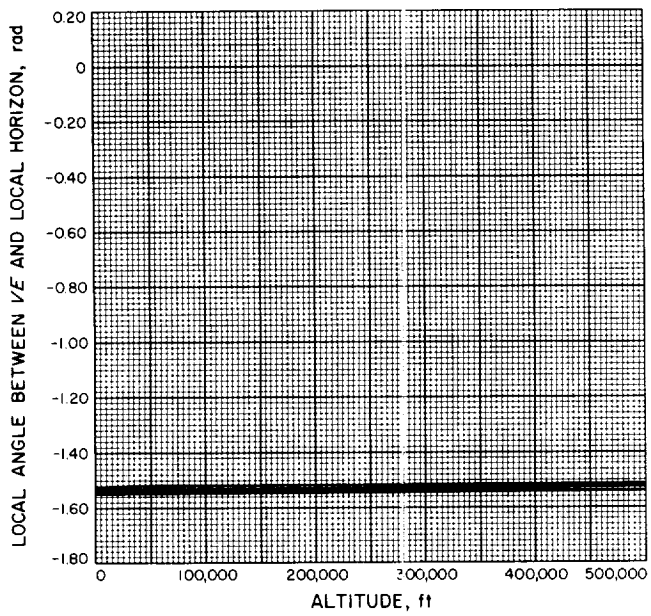
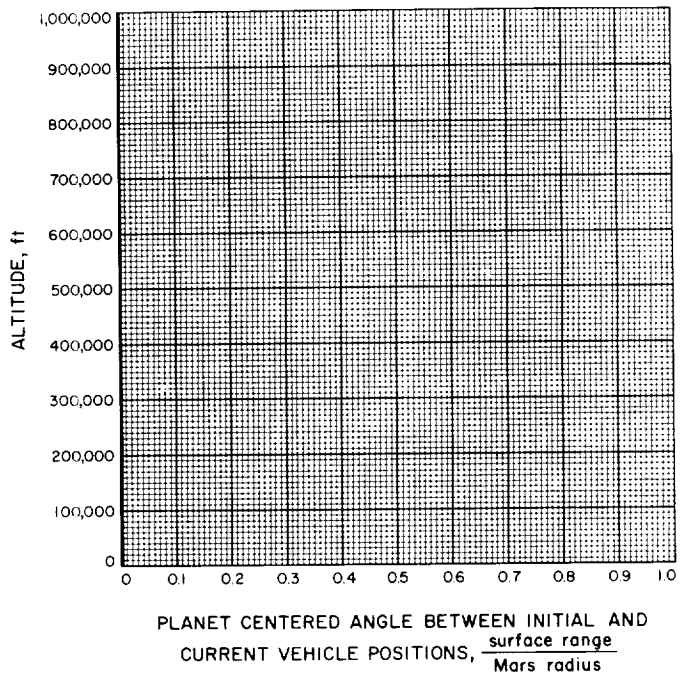


Fig. A-183



PLANET CENTERED ANGLE BETWEEN INITIAL AND

CURRENT VEHICLE POSITIONS, $\frac{\text{surface range}}{\text{Mars radius}}$

Fig. A-184

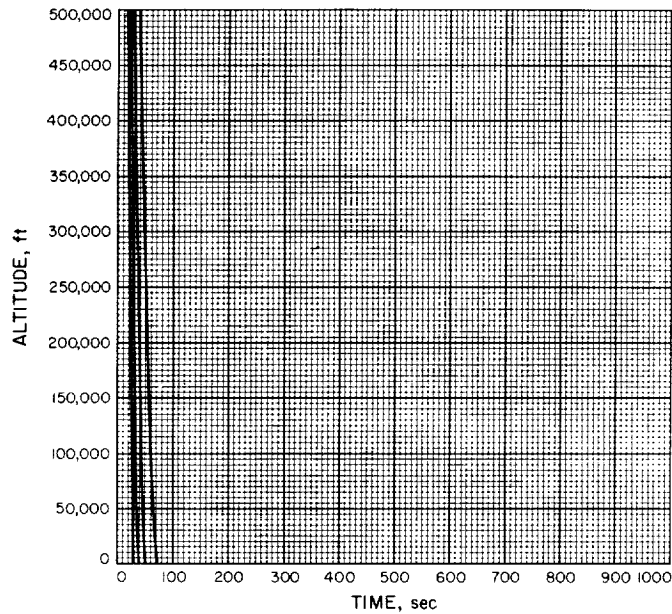


Fig. A-185

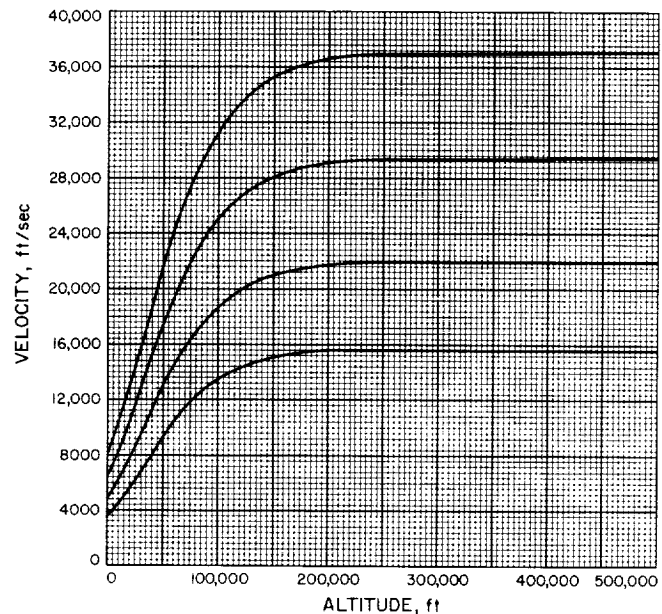


Fig. A-186

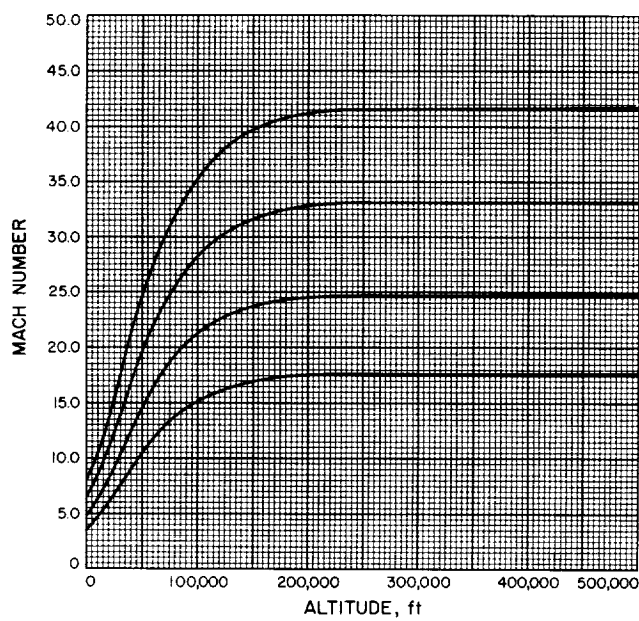


Fig. A-187

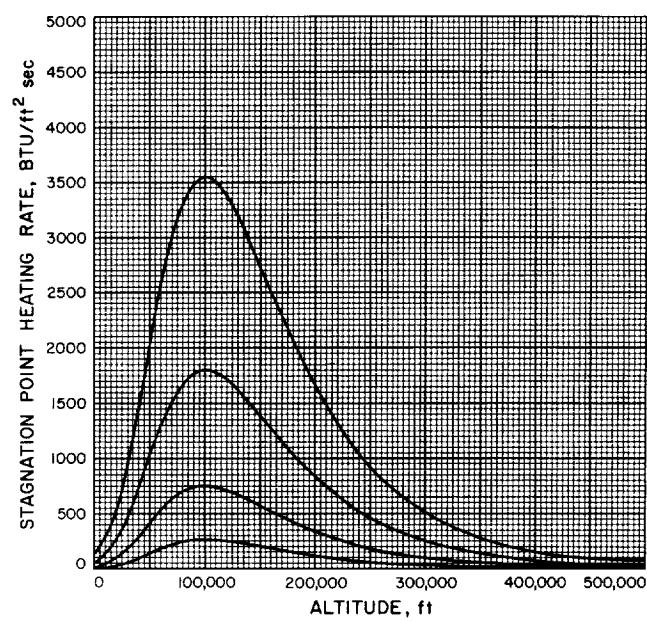


Fig. A-188

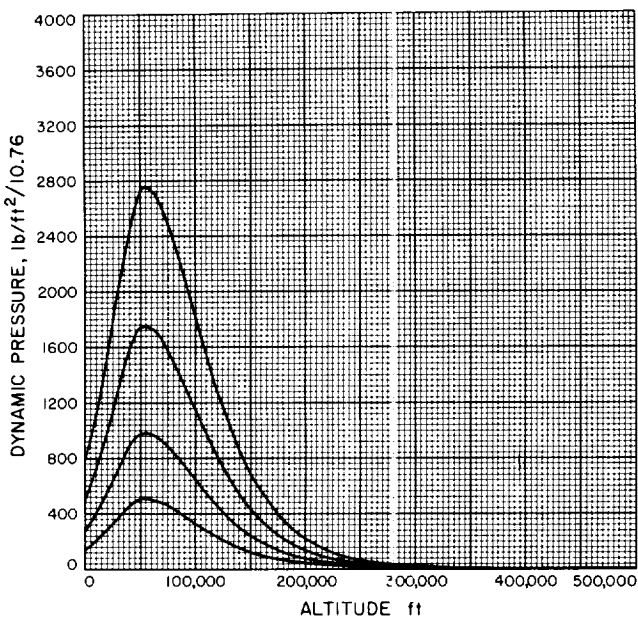


Fig. A-189

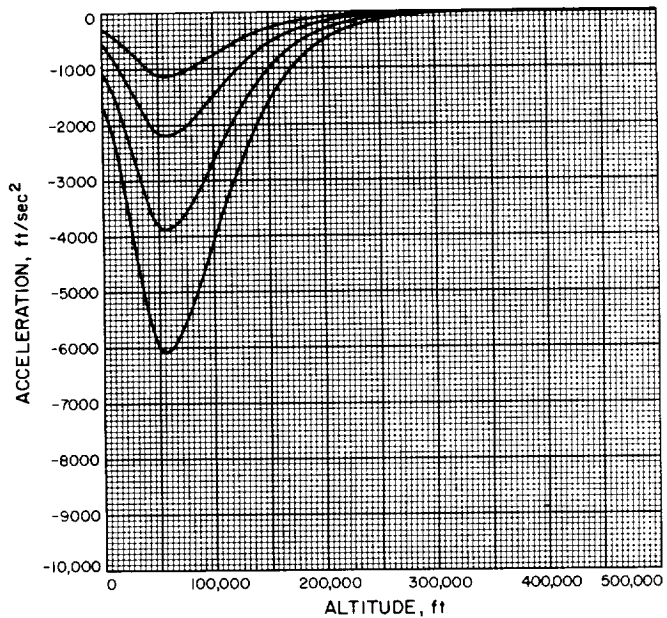


Fig. A-190

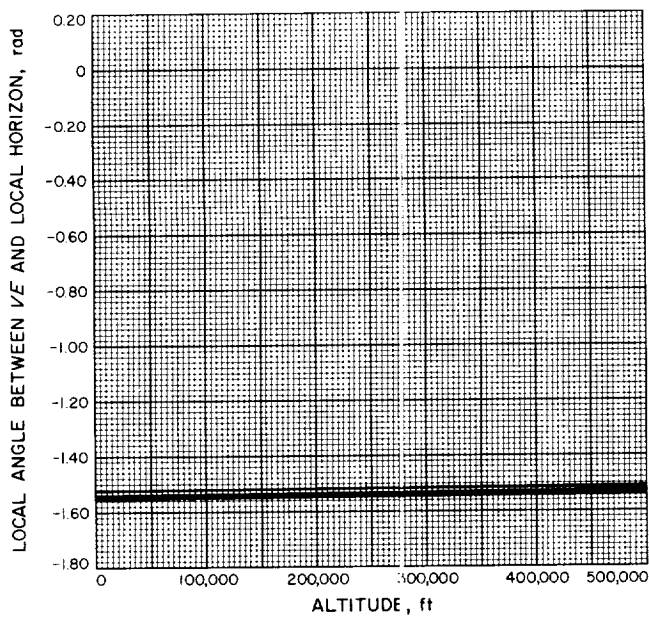


Fig. A-191

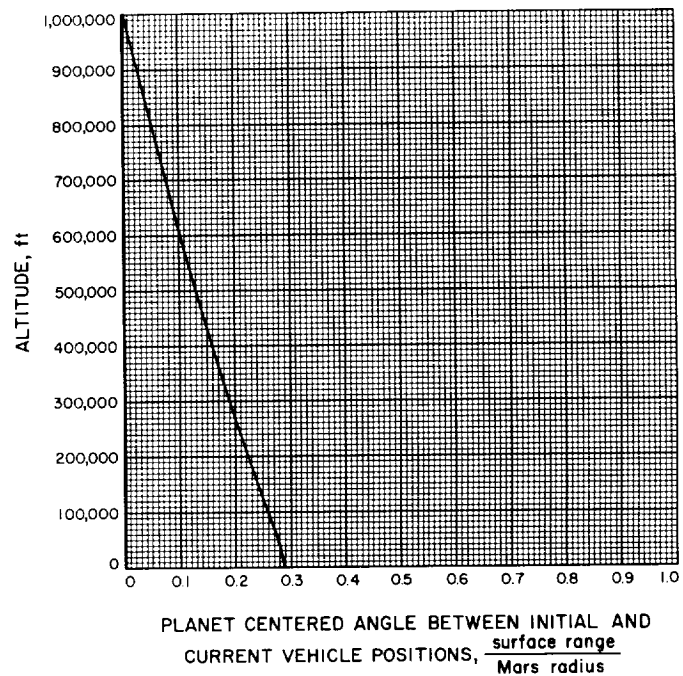


Fig. A-192

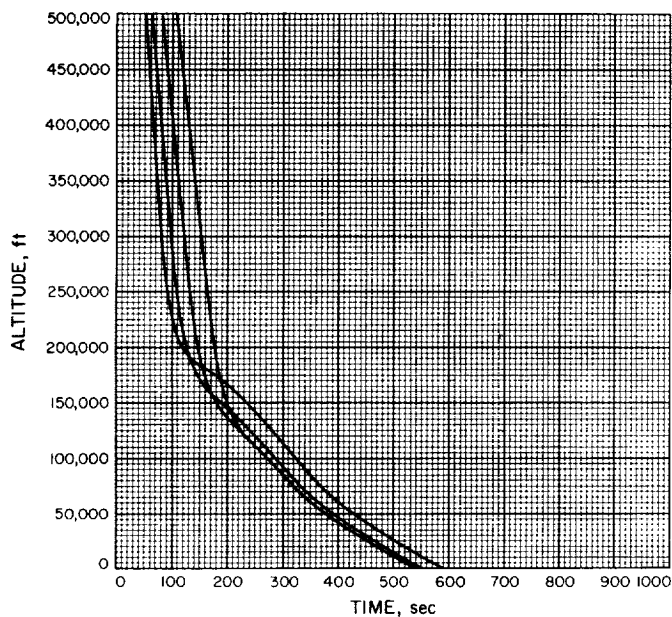


Fig. A-193

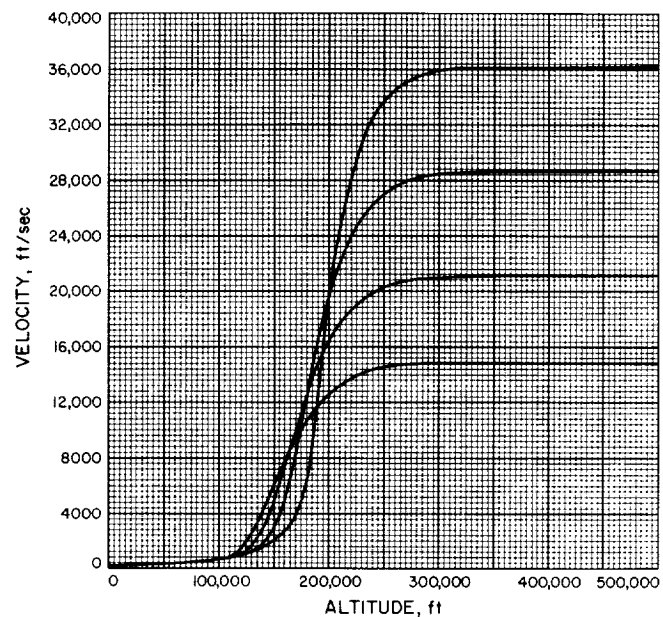


Fig. A-194

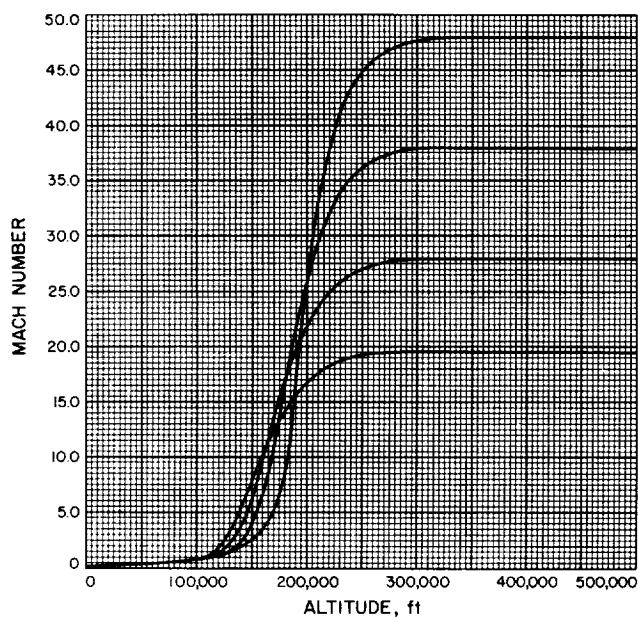


Fig. A-195

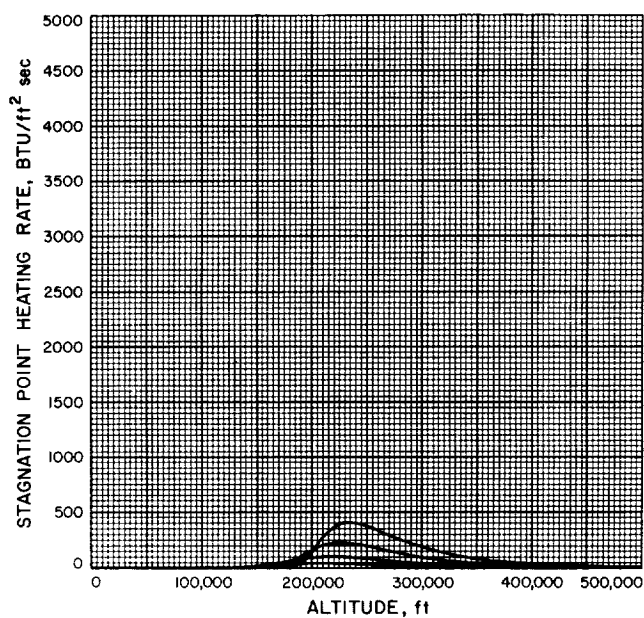


Fig. A-196

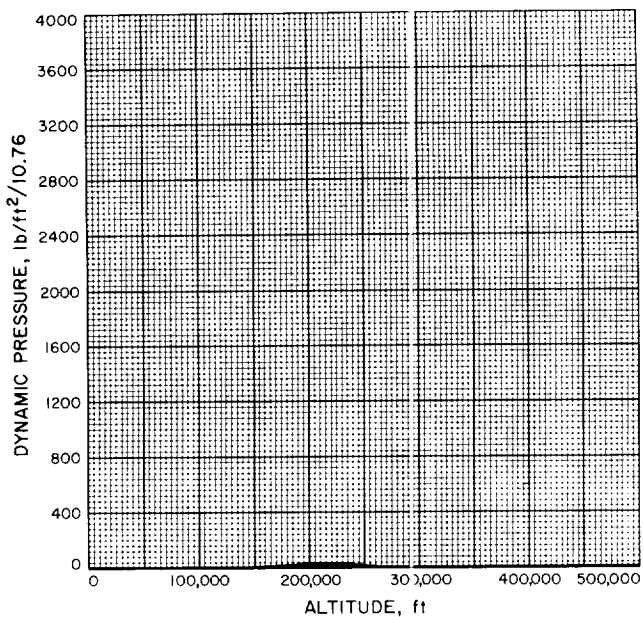


Fig. A-197

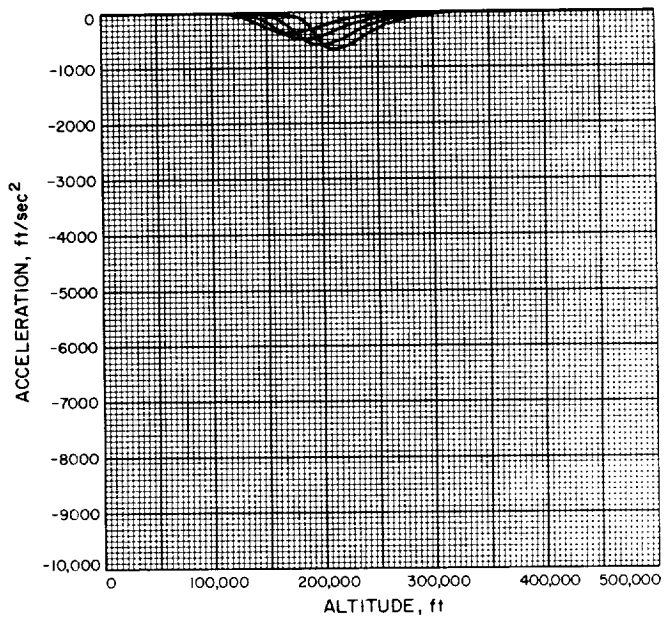


Fig. A-198

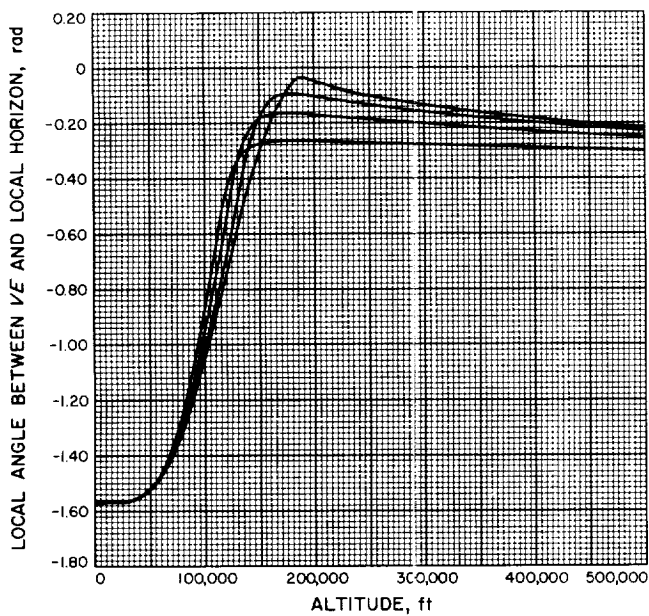


Fig. A-199

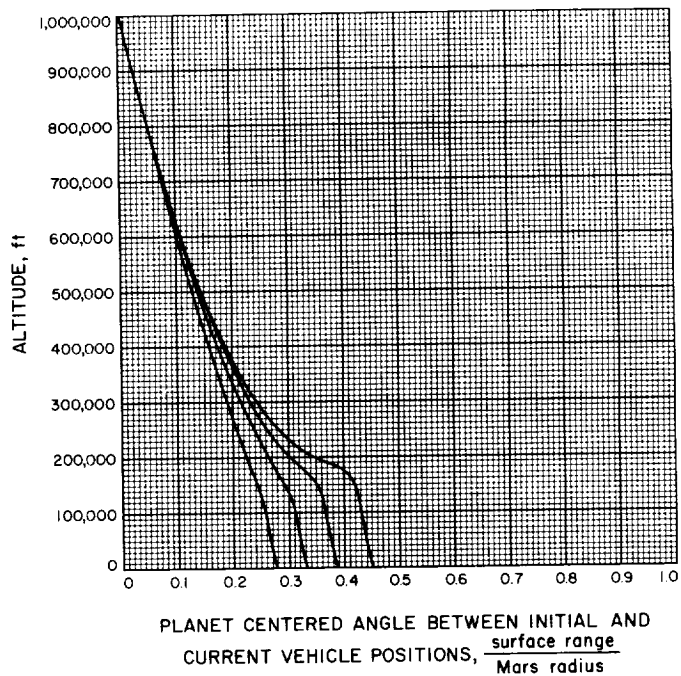


Fig. A-200

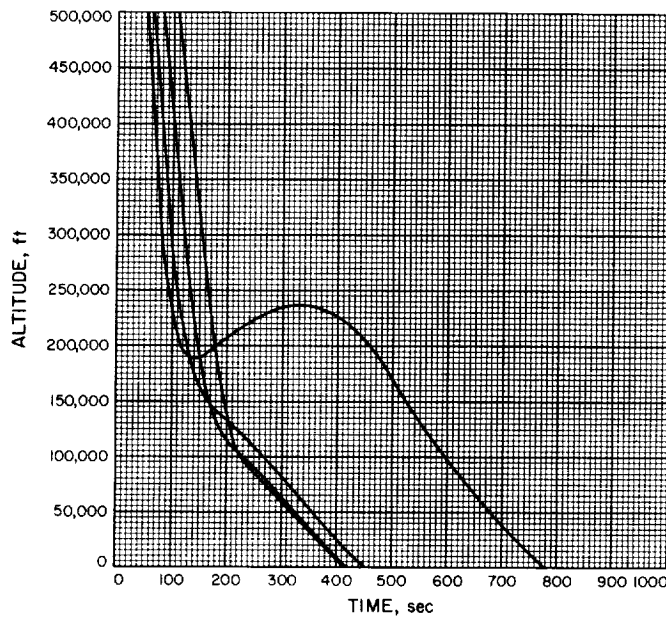


Fig. A-201

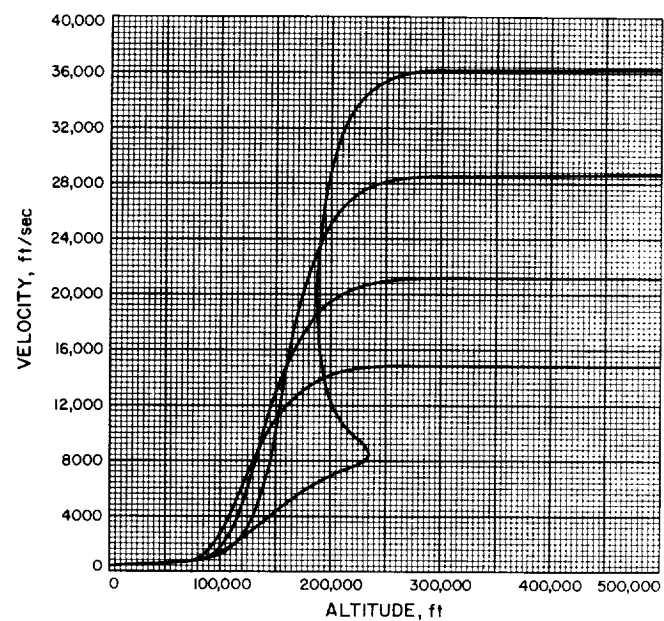


Fig. A-202

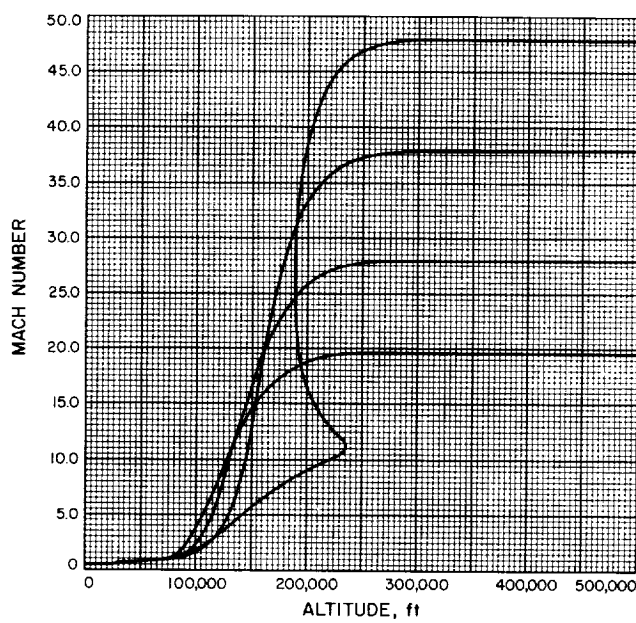


Fig. A-203

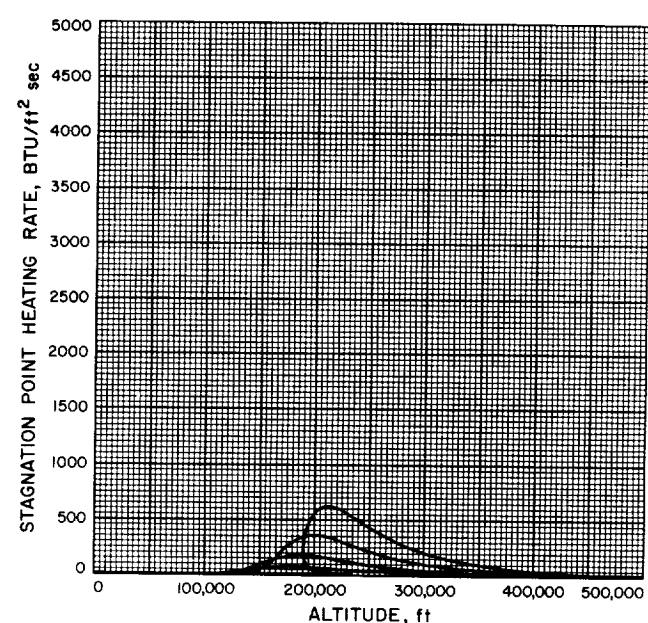


Fig. A-204

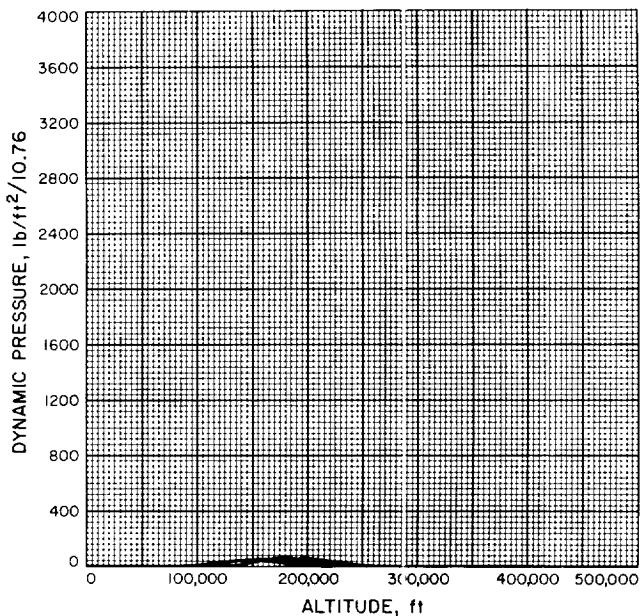


Fig. A-205

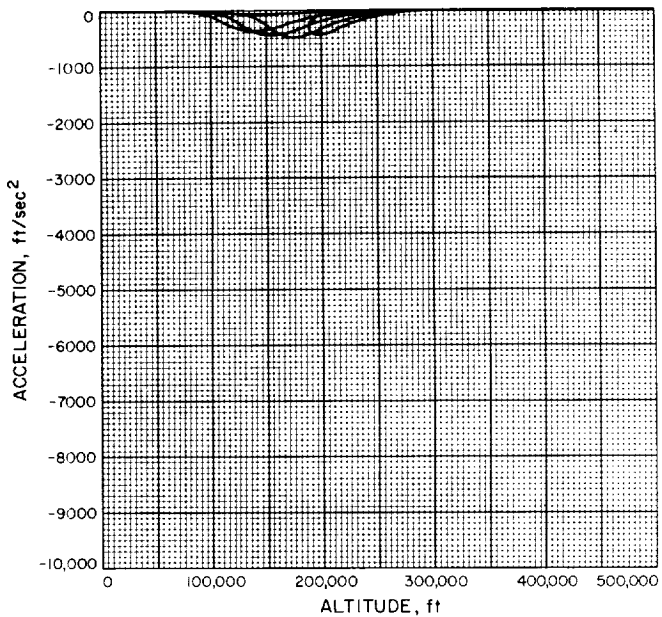


Fig. A-206

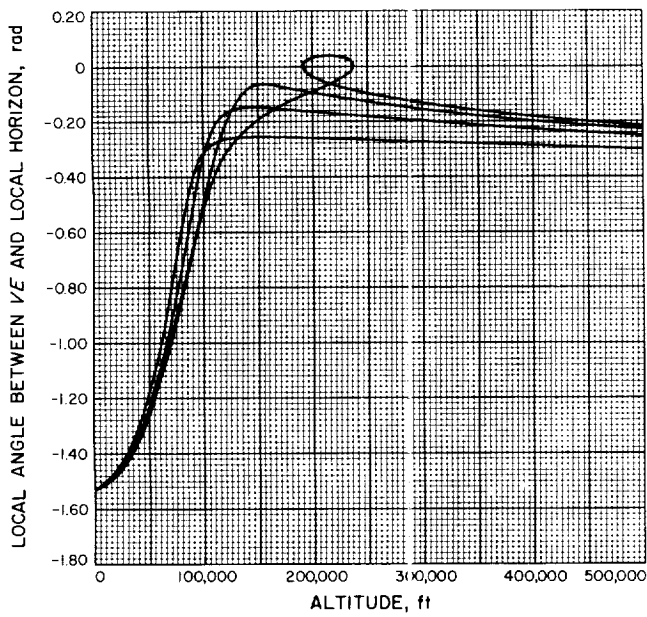
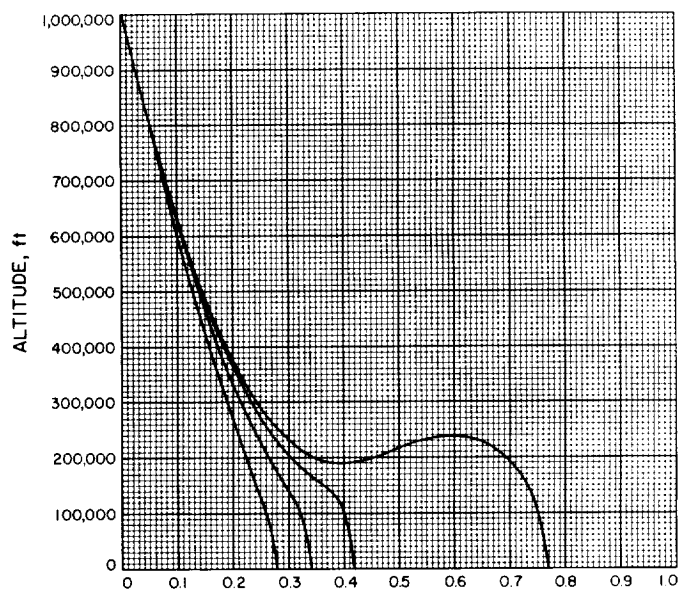


Fig. A-207



PLANET CENTERED ANGLE BETWEEN INITIAL AND
CURRENT VEHICLE POSITIONS, $\frac{\text{surface range}}{\text{Mars radius}}$

Fig. A-208

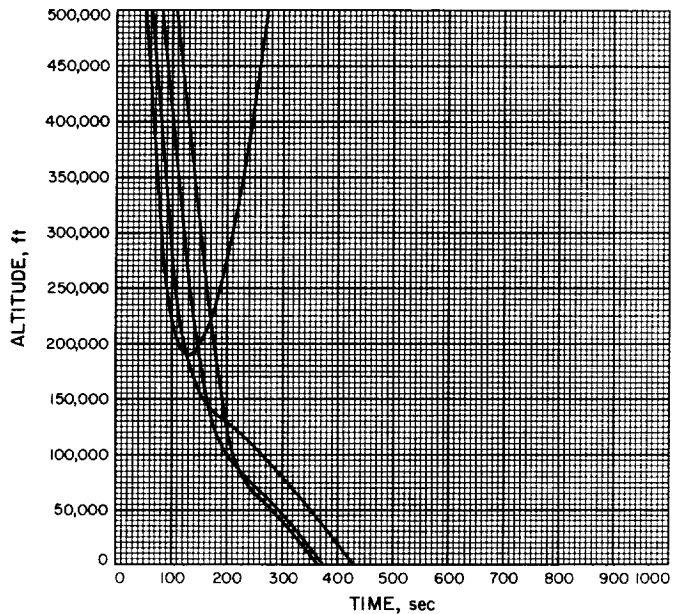


Fig. A-209

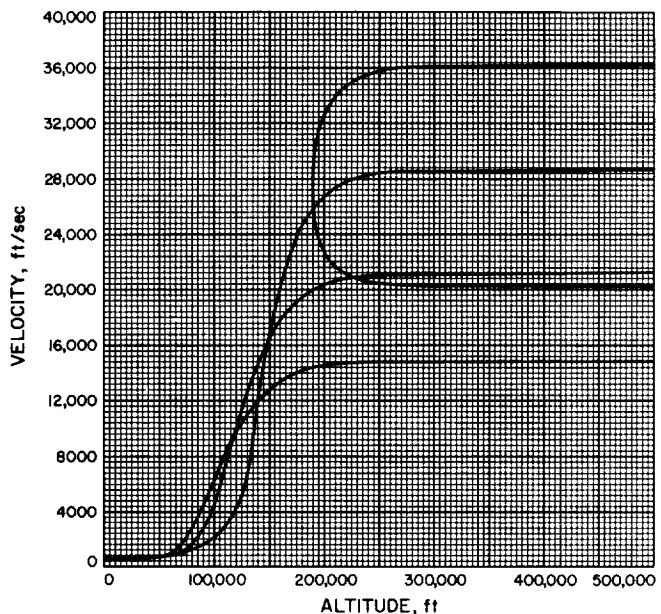


Fig. A-210

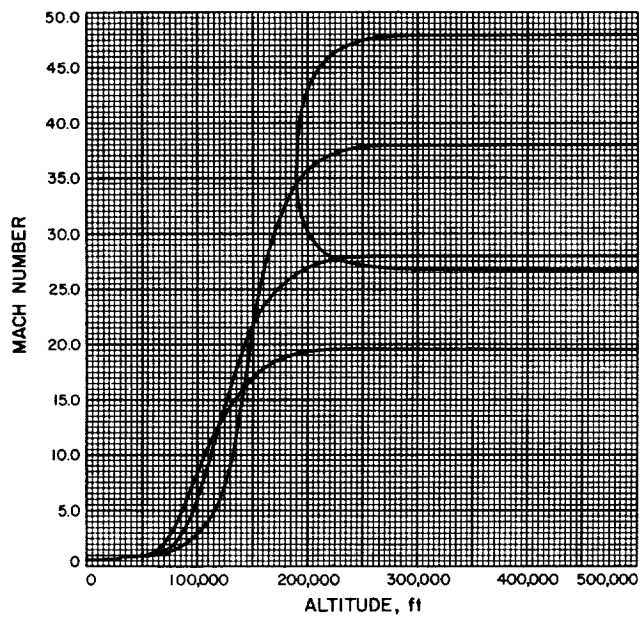


Fig. A-211

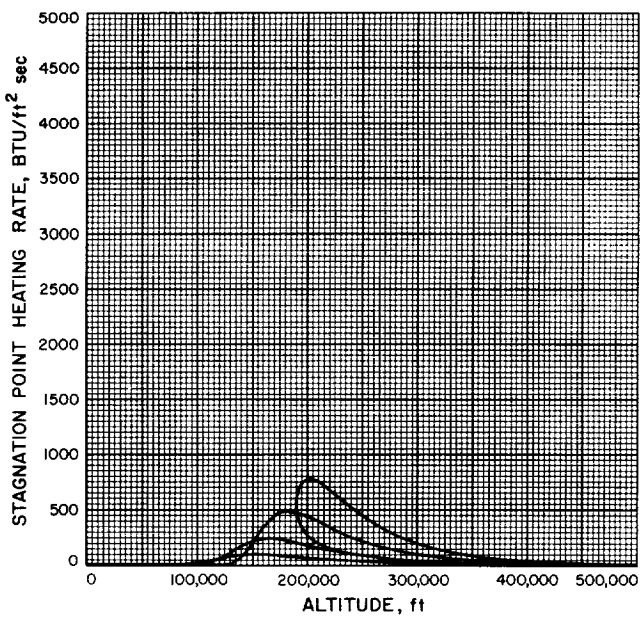


Fig. A-212

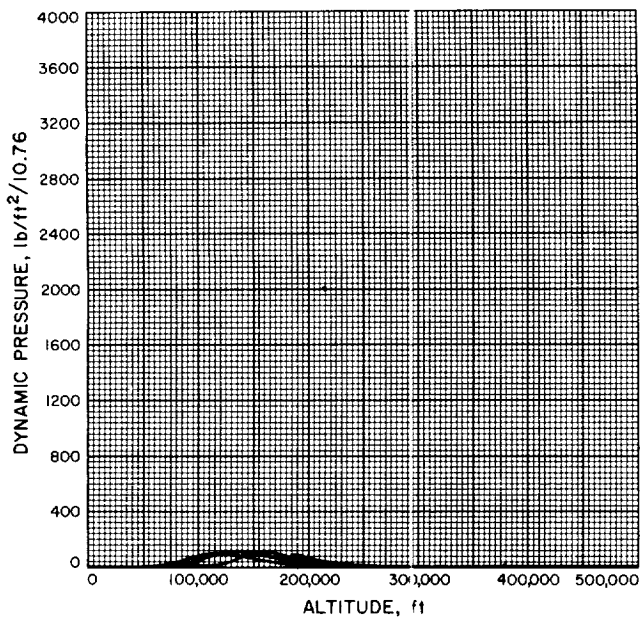


Fig. A-213

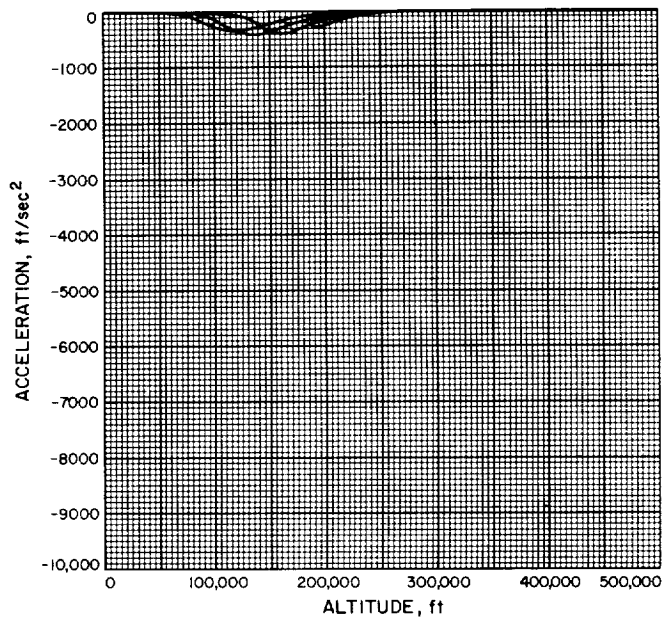


Fig. A-214

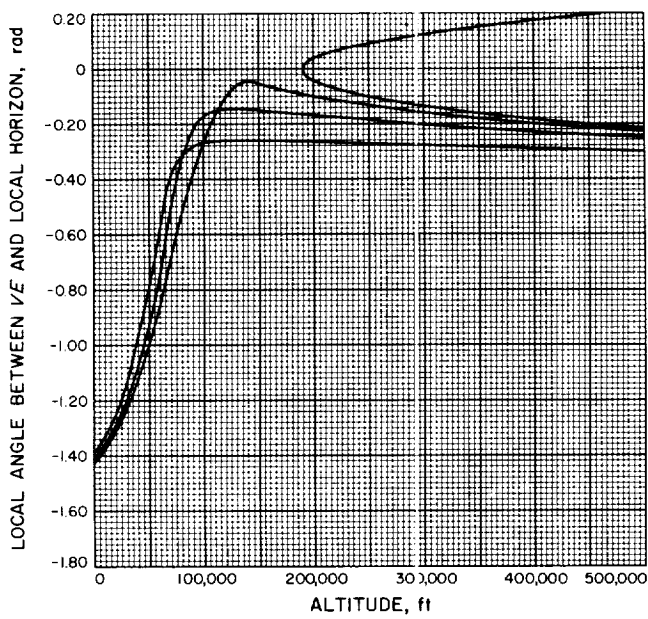


Fig. A-215

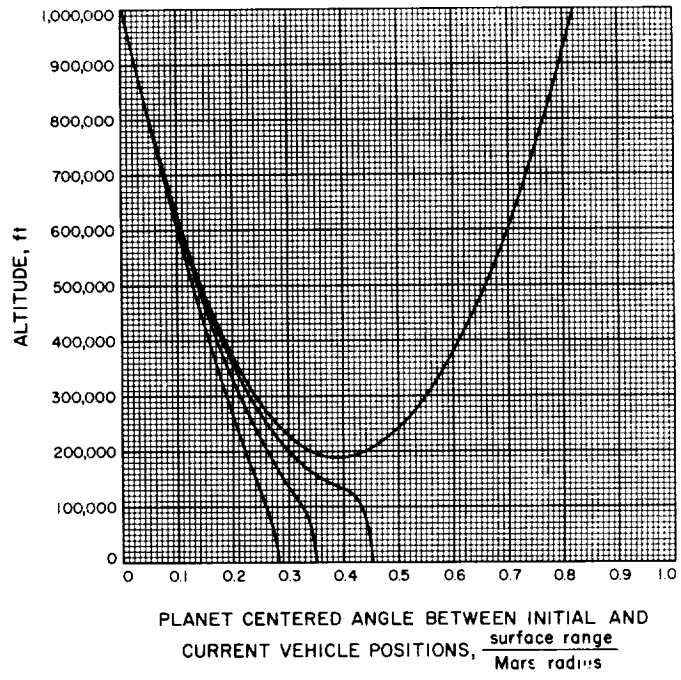


Fig. A-216

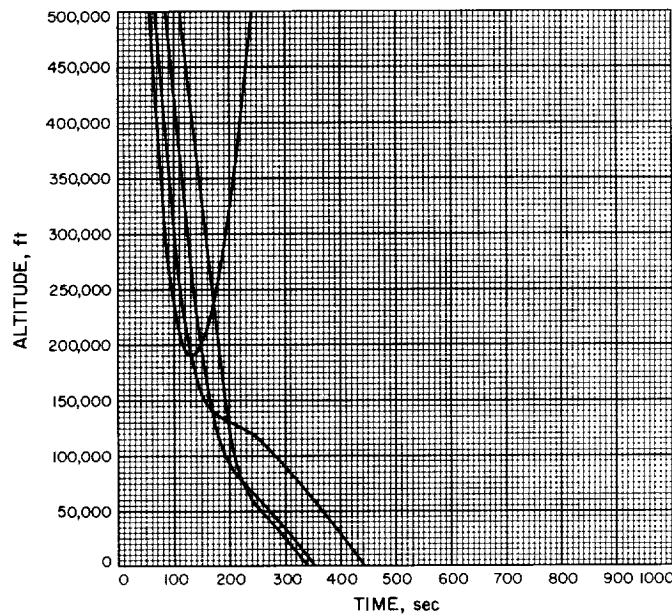


Fig. A-217

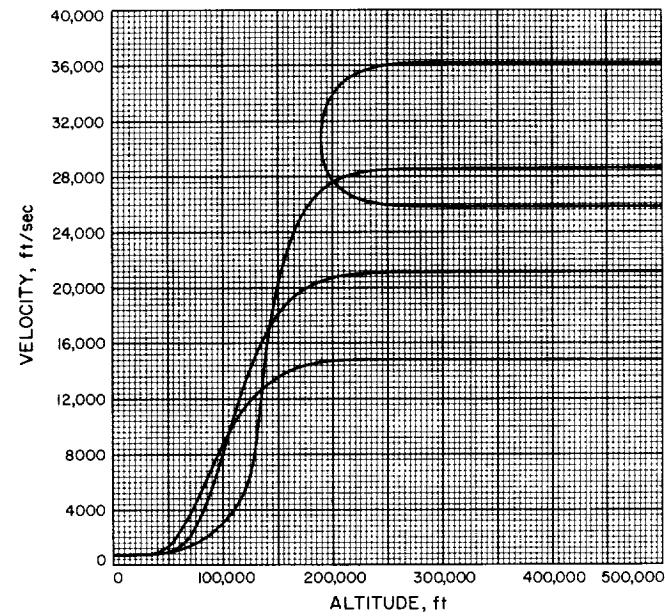


Fig. A-218

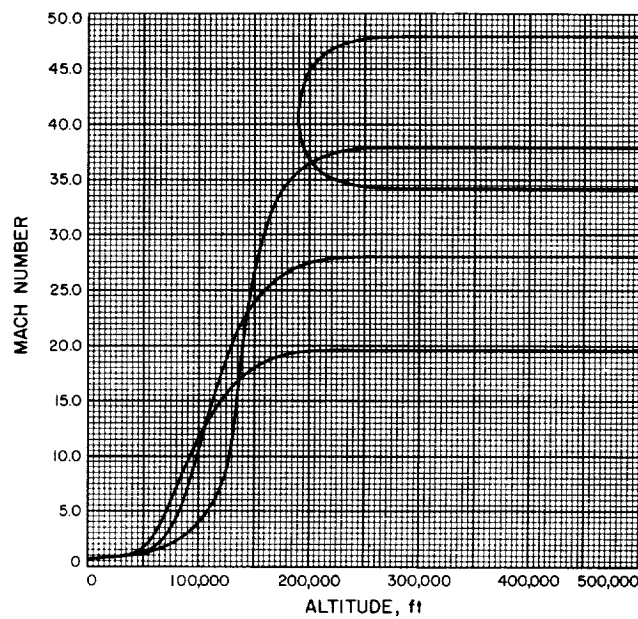


Fig. A-219

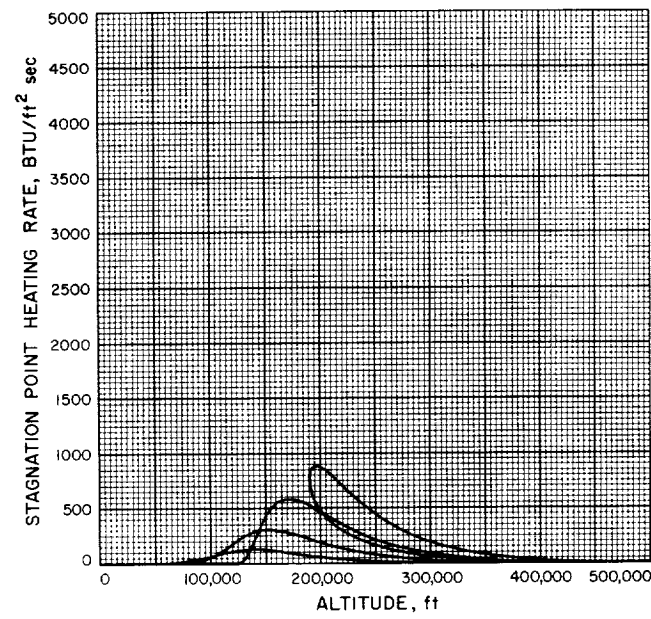


Fig. A-220

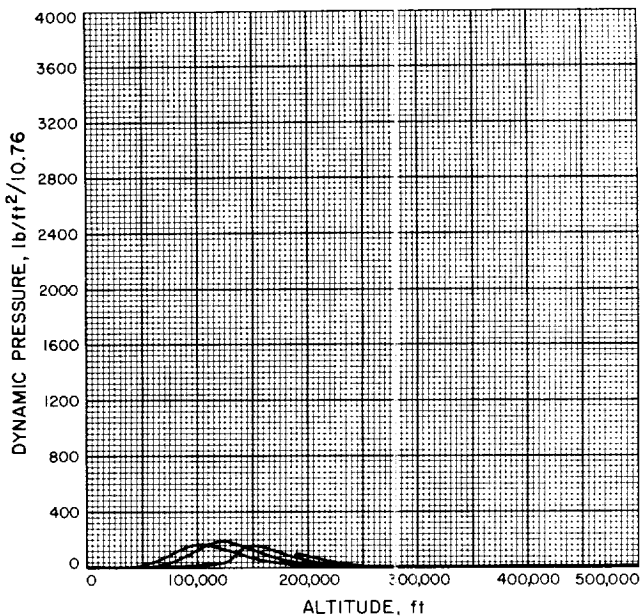


Fig. A-221

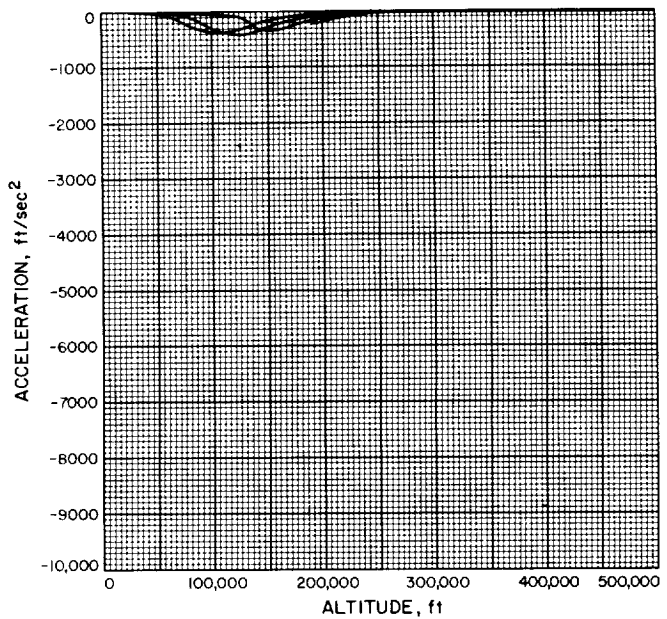


Fig. A-222

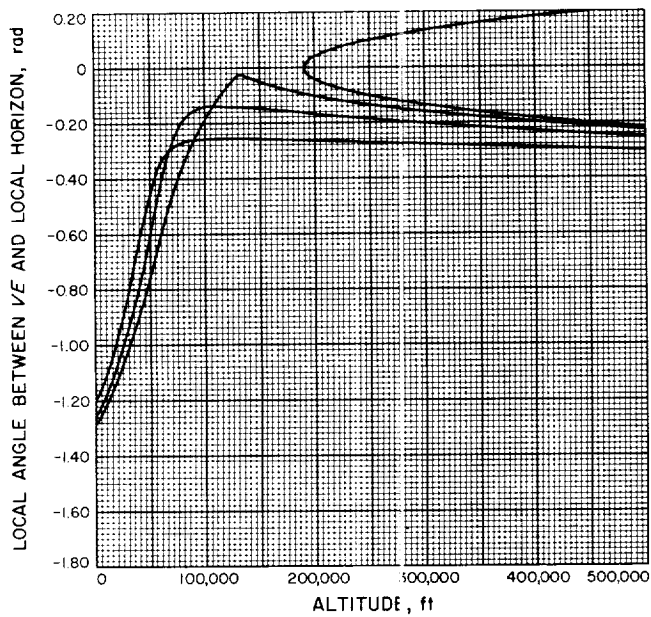


Fig. A-223

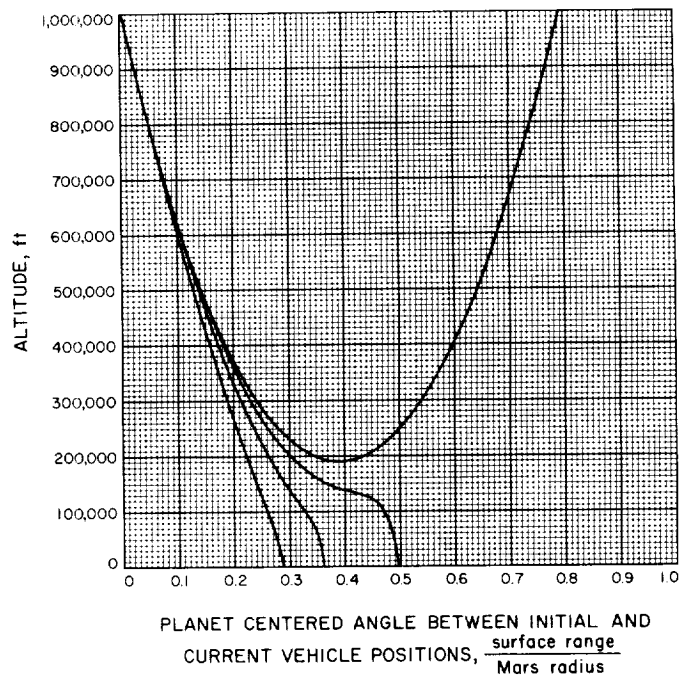


Fig. A-224

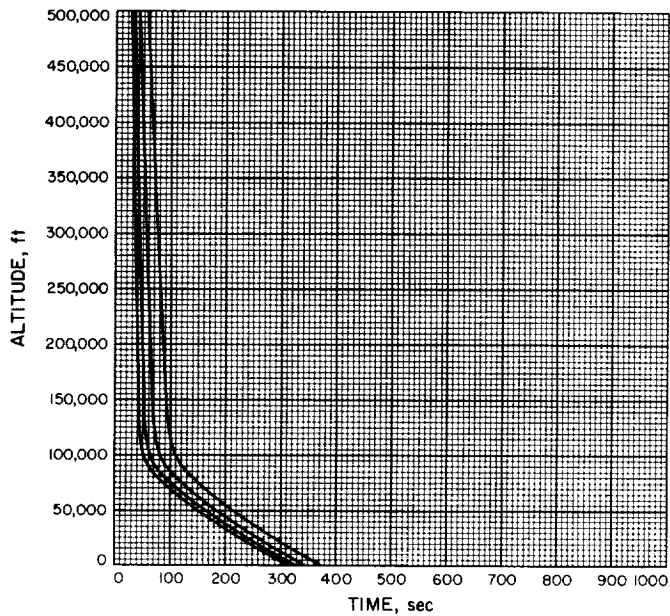


Fig. A-225

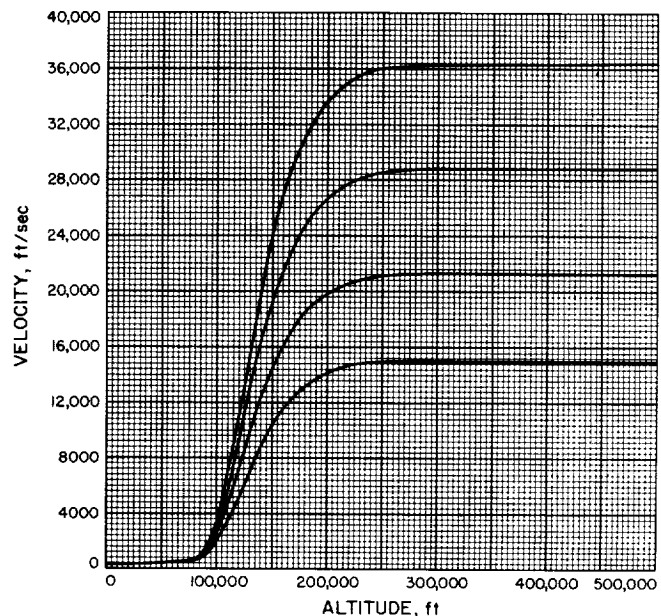


Fig. A-226

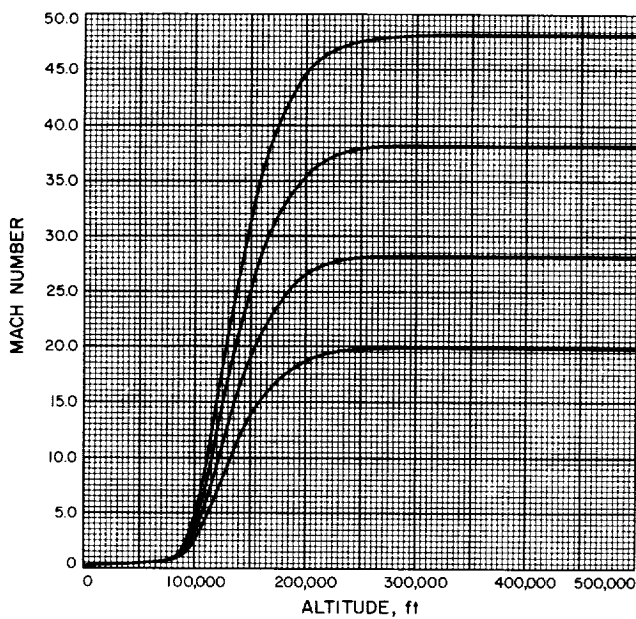


Fig. A-227

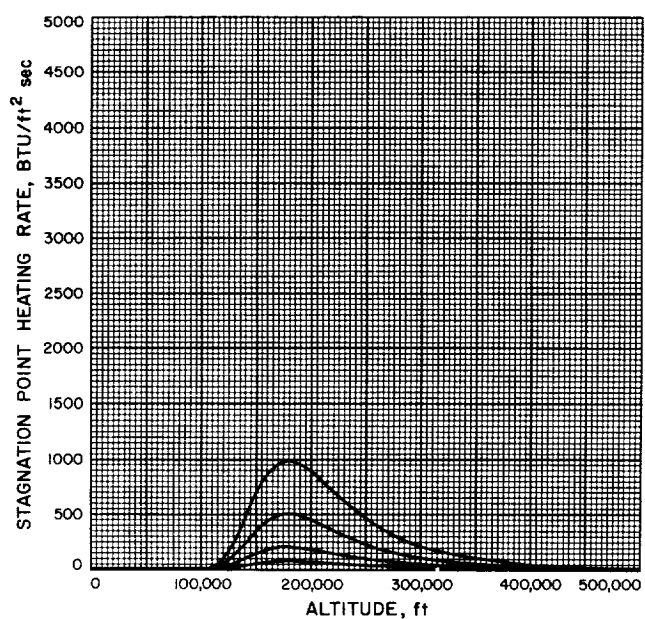


Fig. A-228

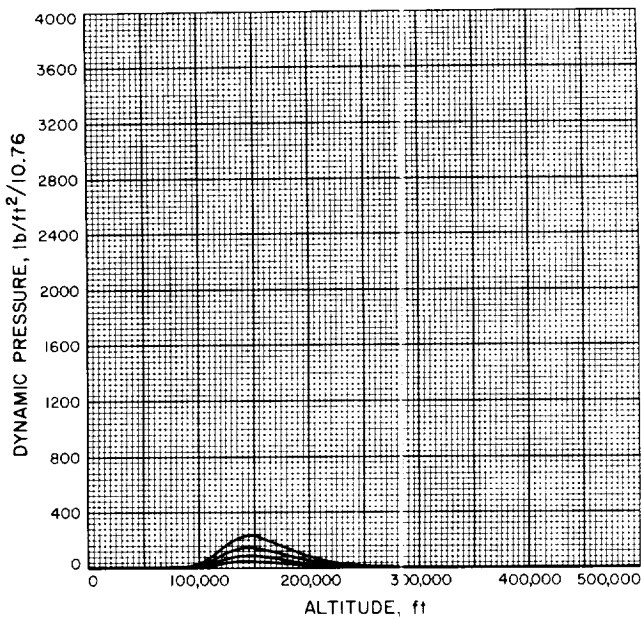


Fig. A-229

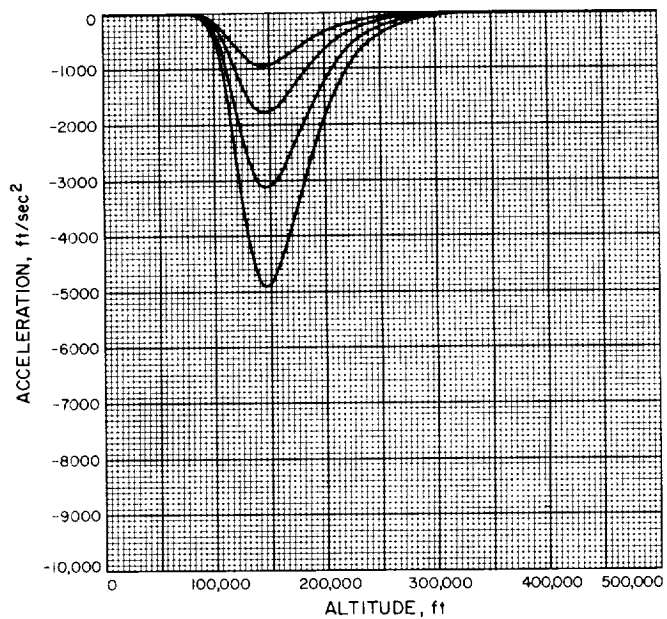


Fig. A-230

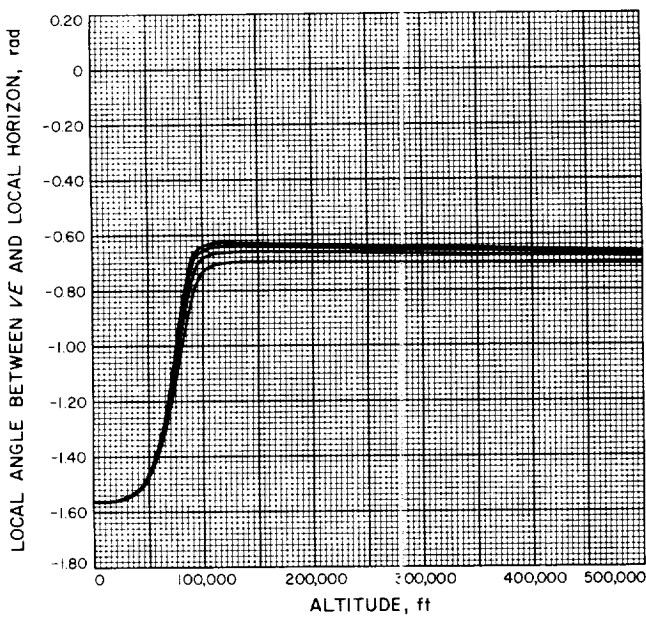


Fig. A-231

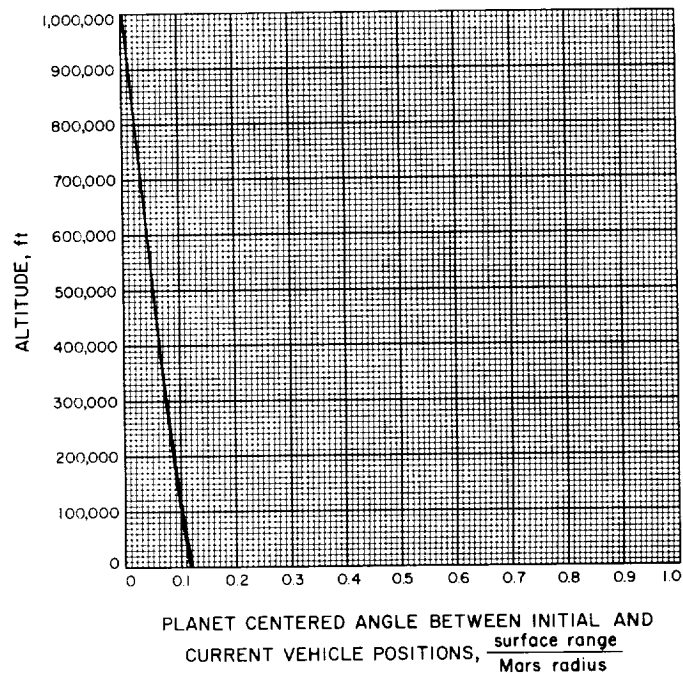


Fig. A-232

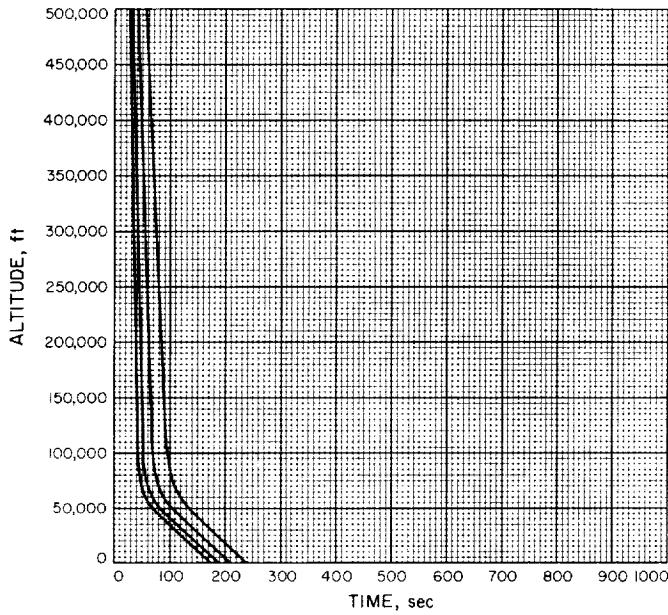


Fig. A-233

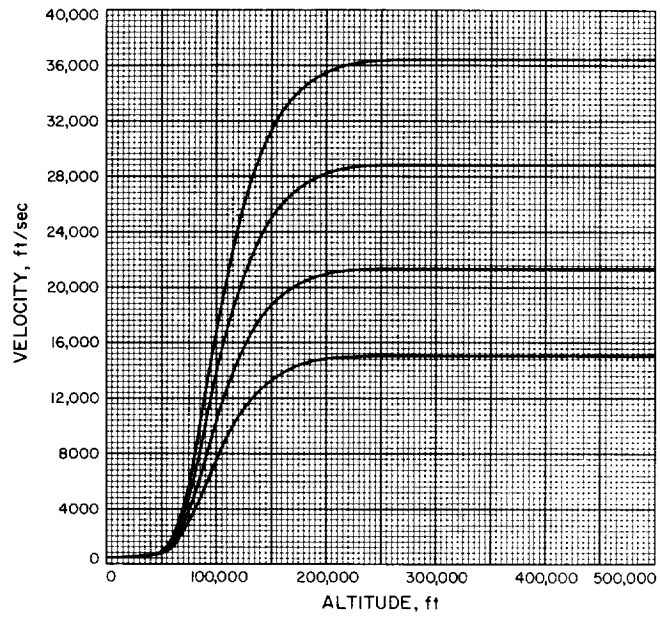


Fig. A-234

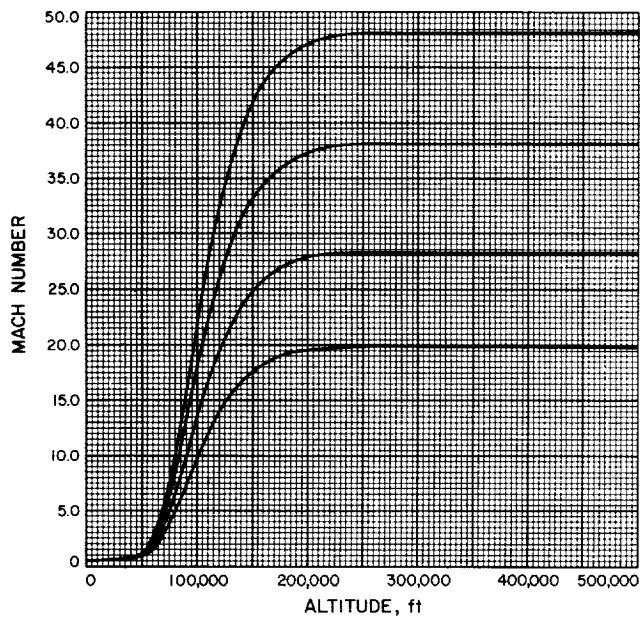


Fig. A-235

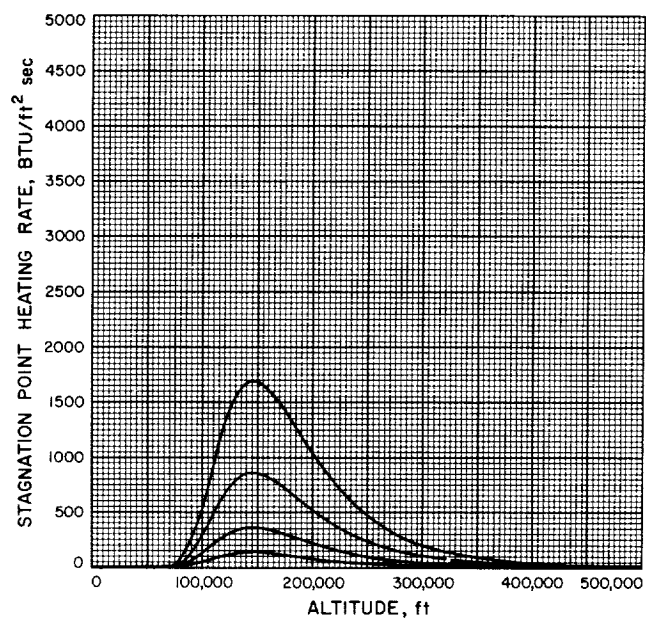


Fig. A-236

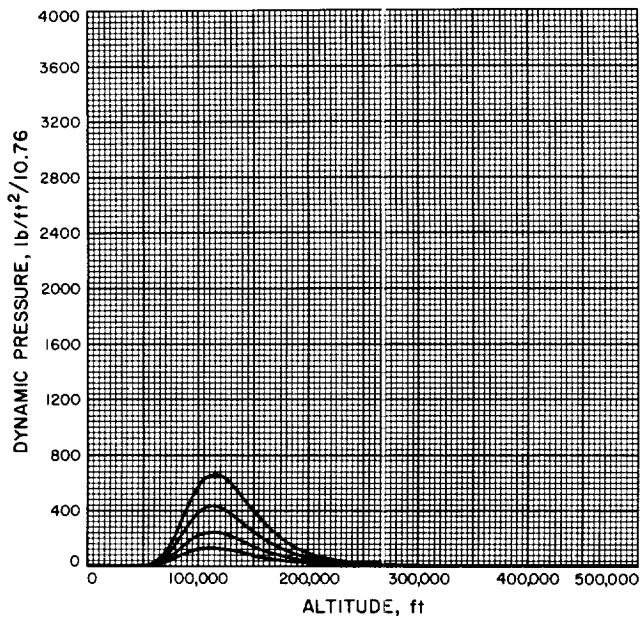


Fig. A-237

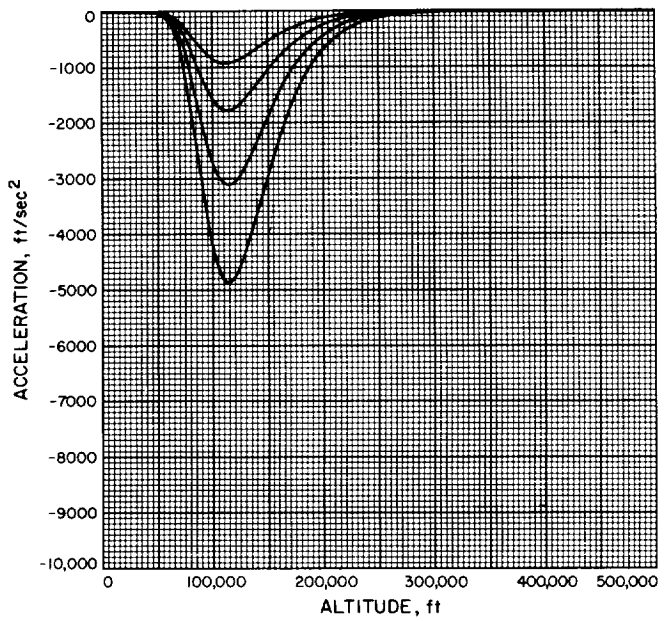


Fig. A-238

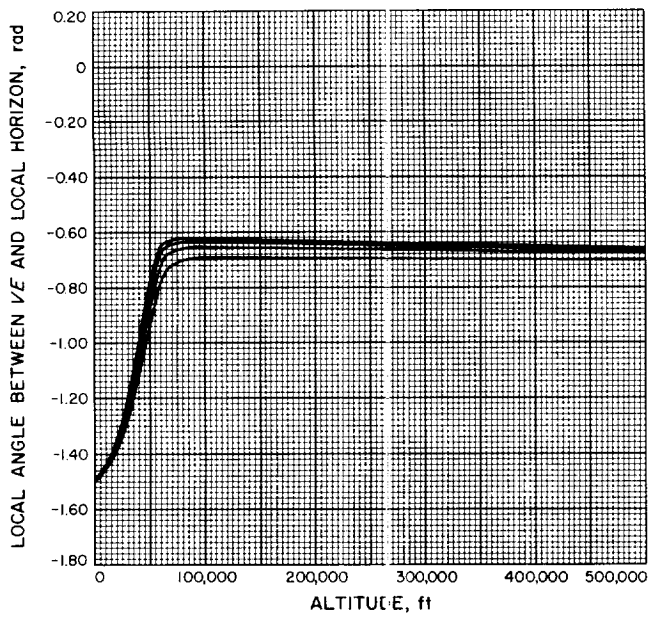


Fig. A-239

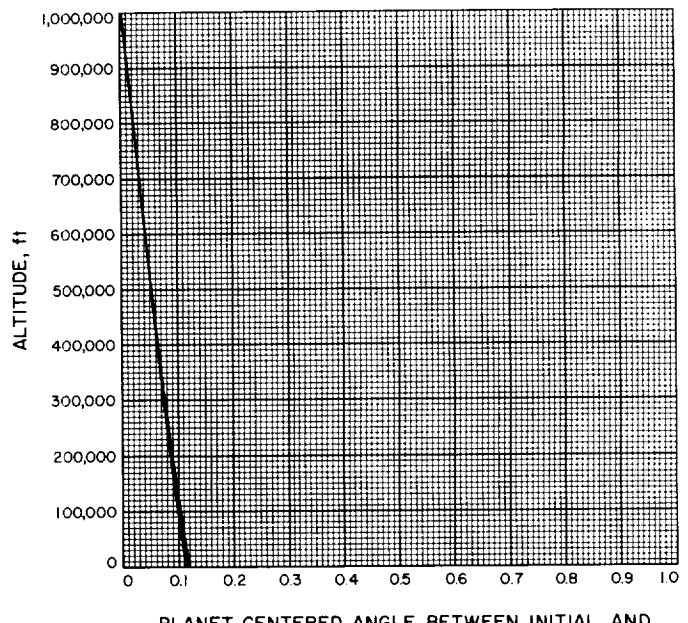


Fig. A-240

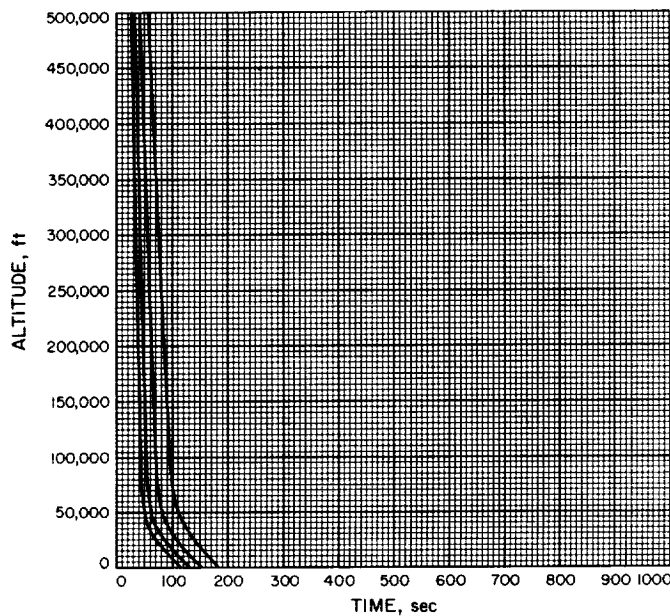


Fig. A-241

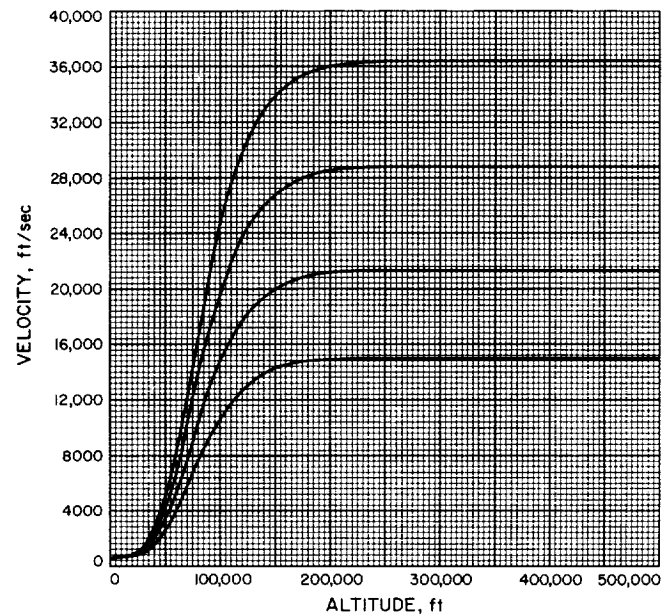


Fig. A-242

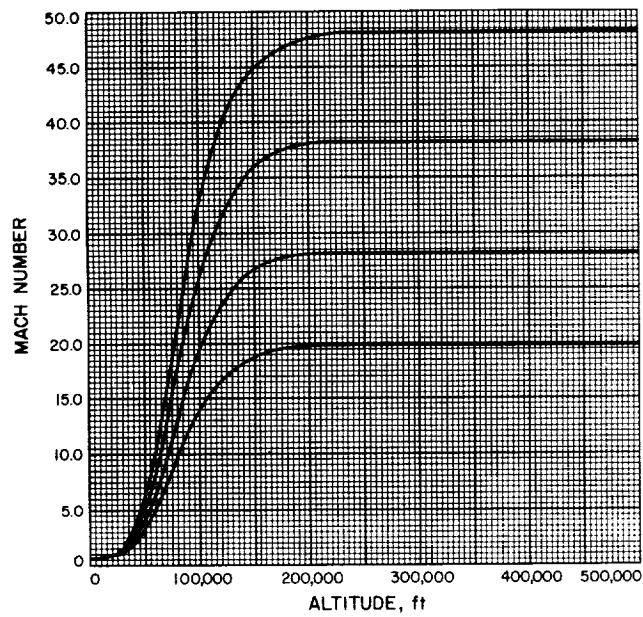


Fig. A-243

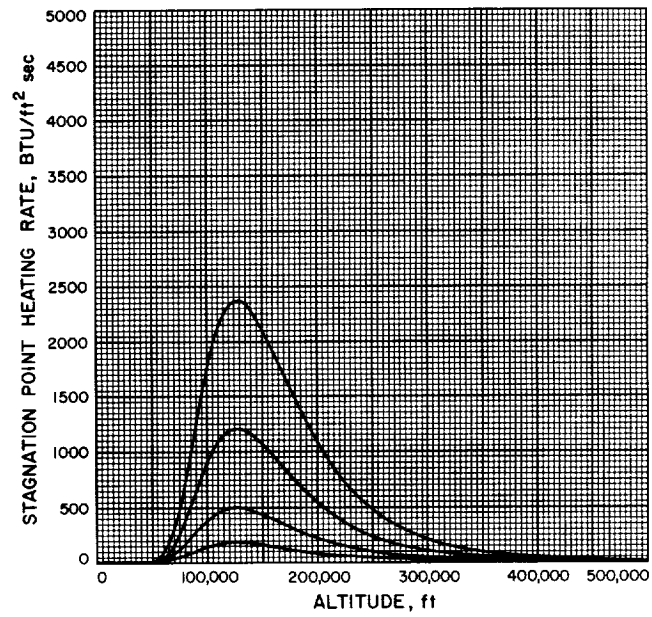


Fig. A-244

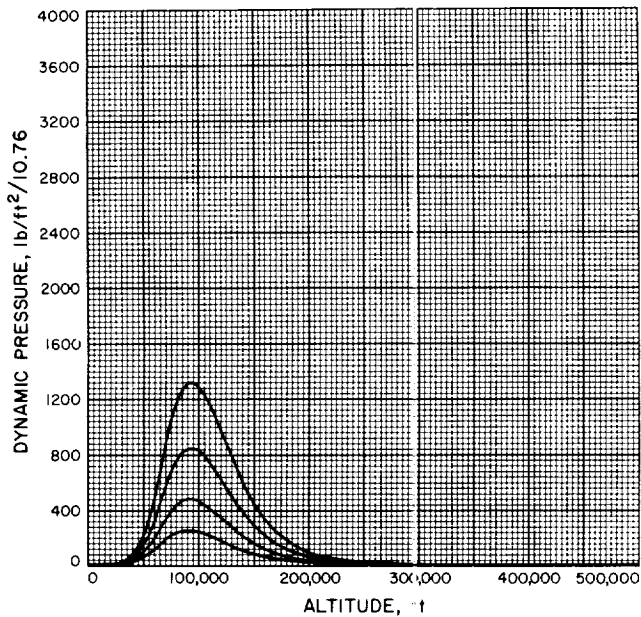


Fig. A-245

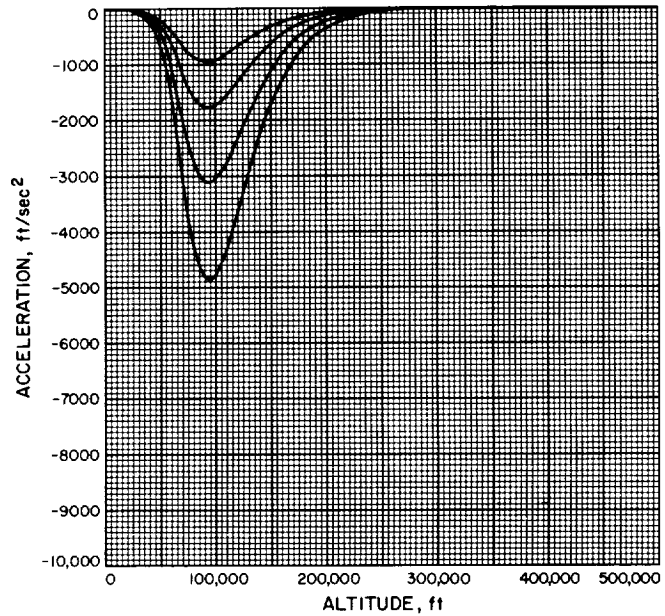


Fig. A-246

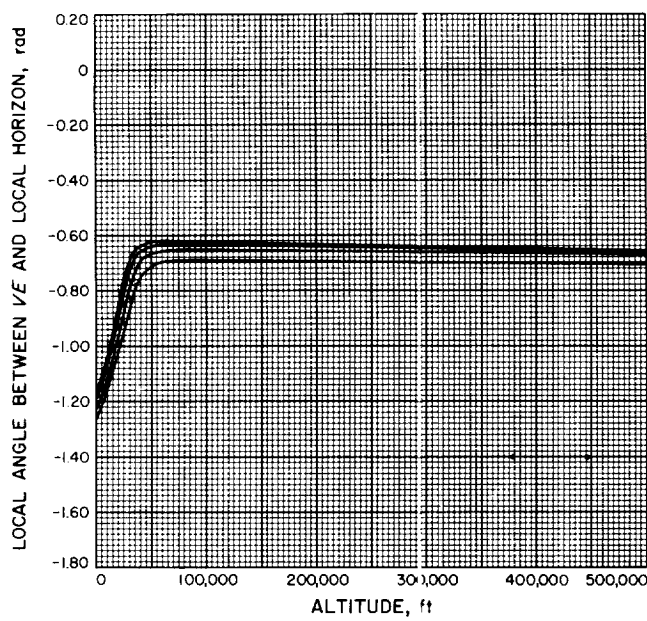
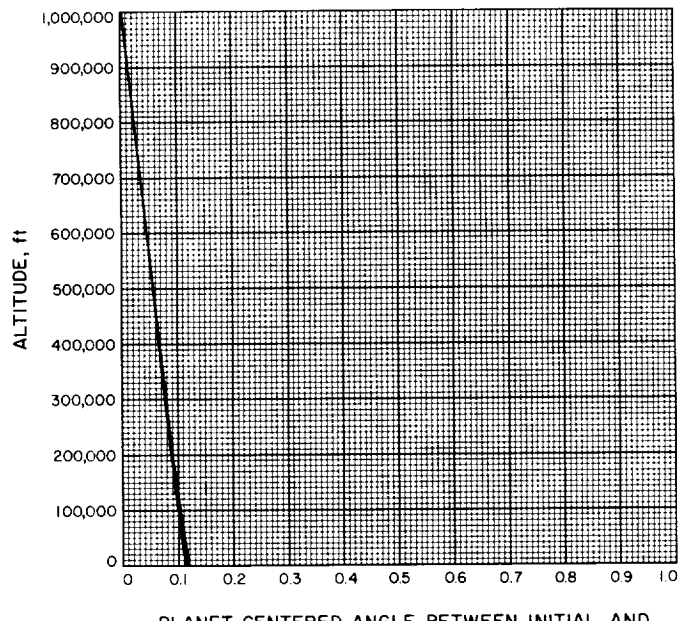


Fig. A-247



PLANET CENTERED ANGLE BETWEEN INITIAL AND
CURRENT VEHICLE POSITIONS, $\frac{\text{surface range}}{\text{Mars radius}}$

Fig. A-248

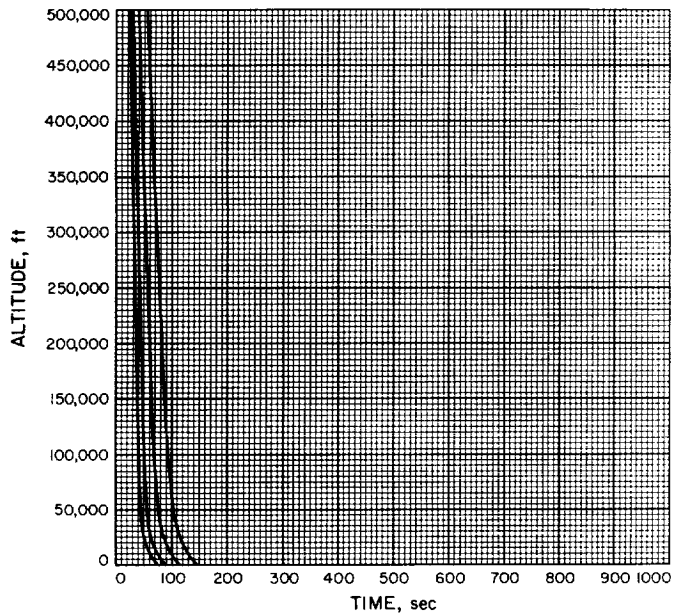


Fig. A-249

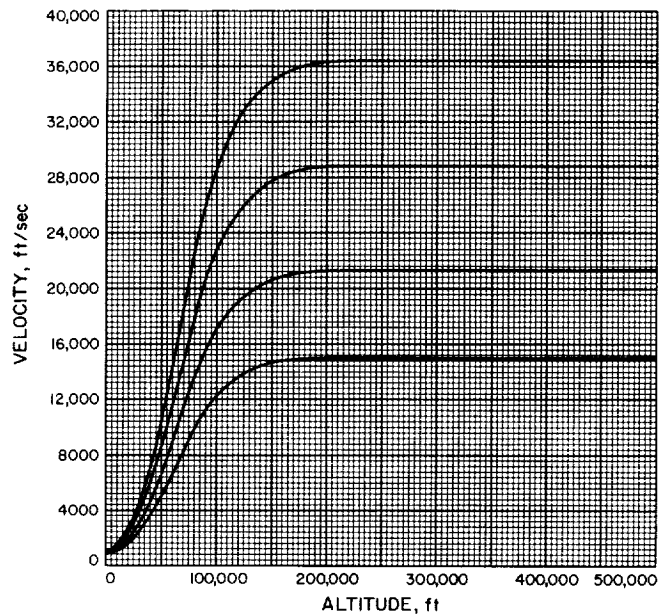


Fig. A-250

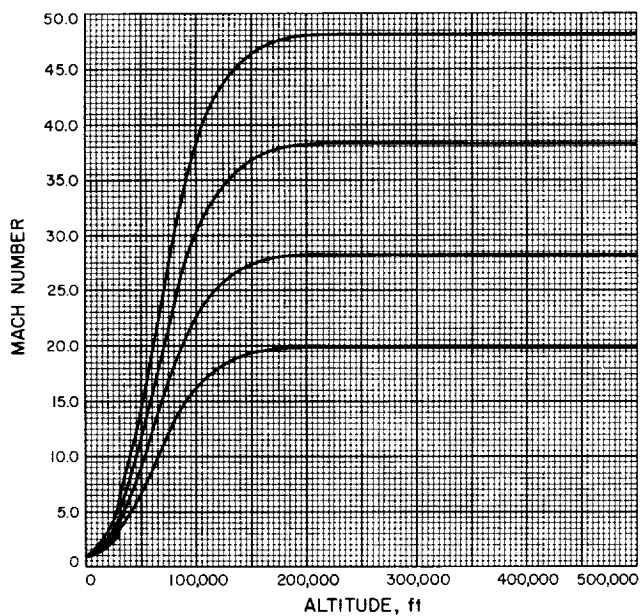


Fig. A-251

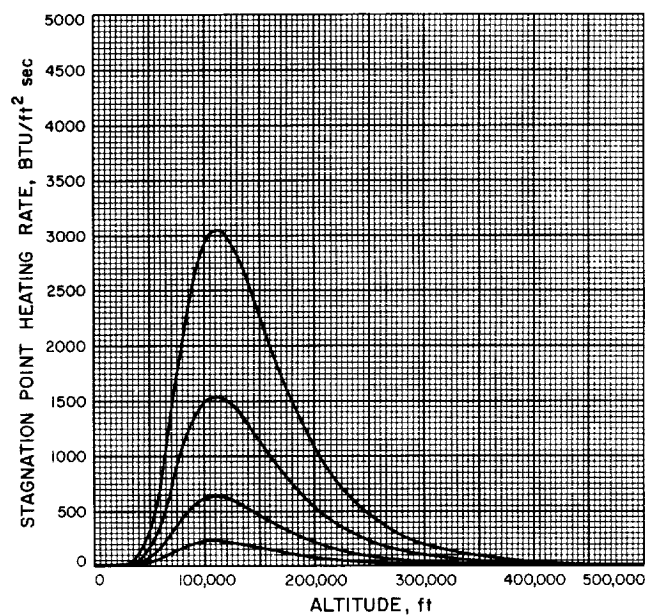


Fig. A-252

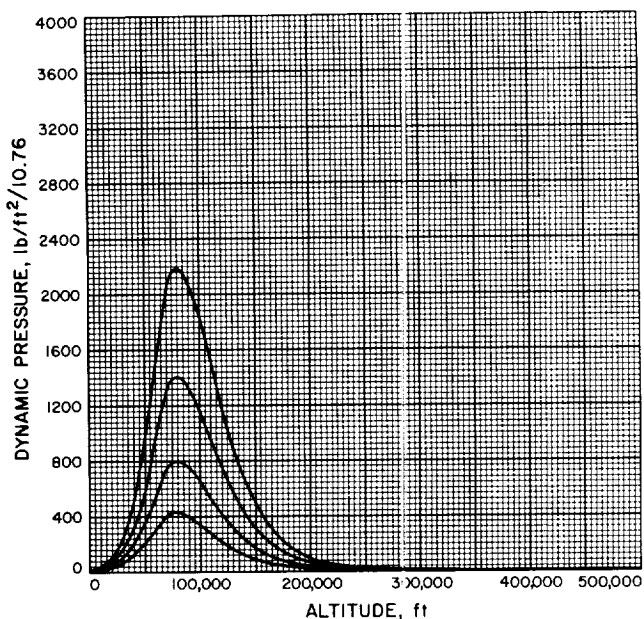


Fig. A-253

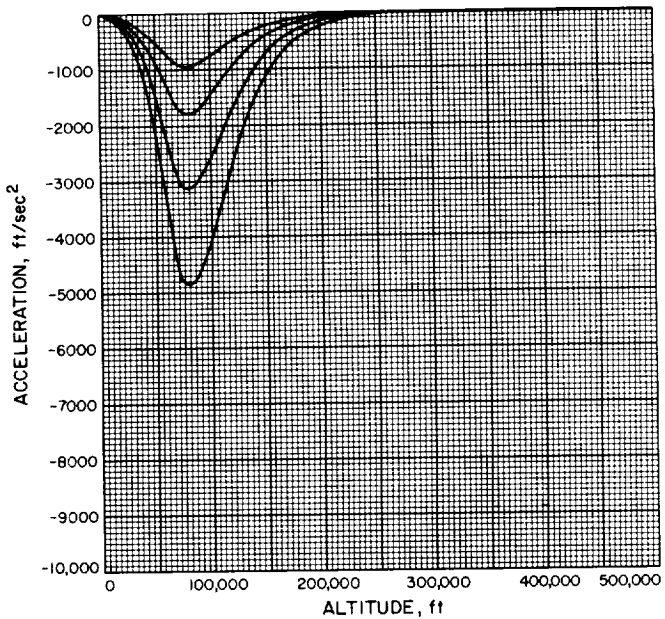


Fig. A-254

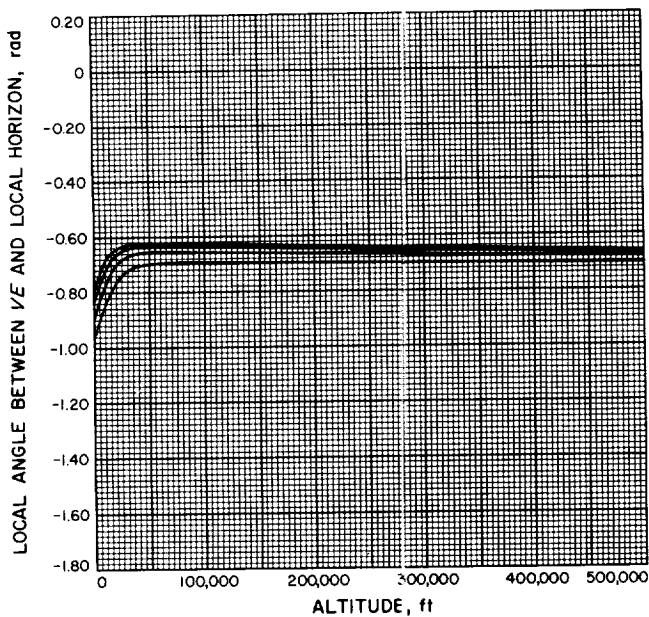


Fig. A-255

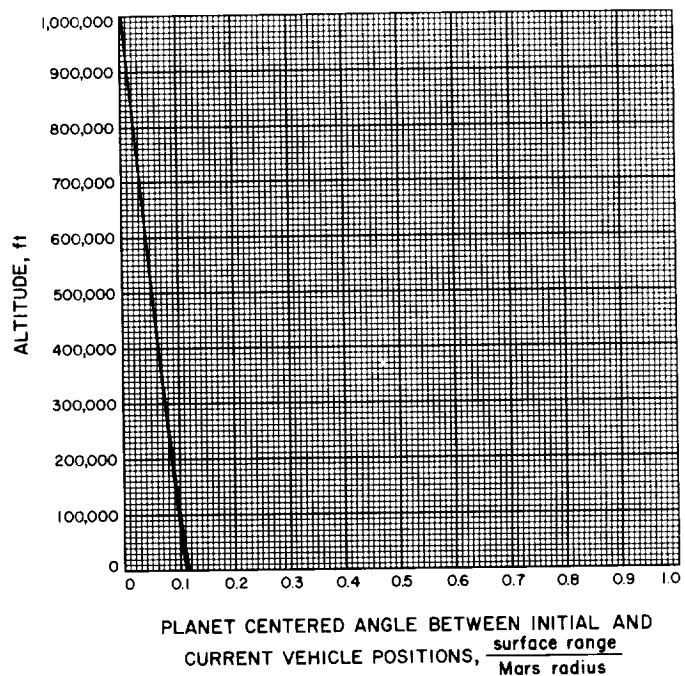


Fig. A-256

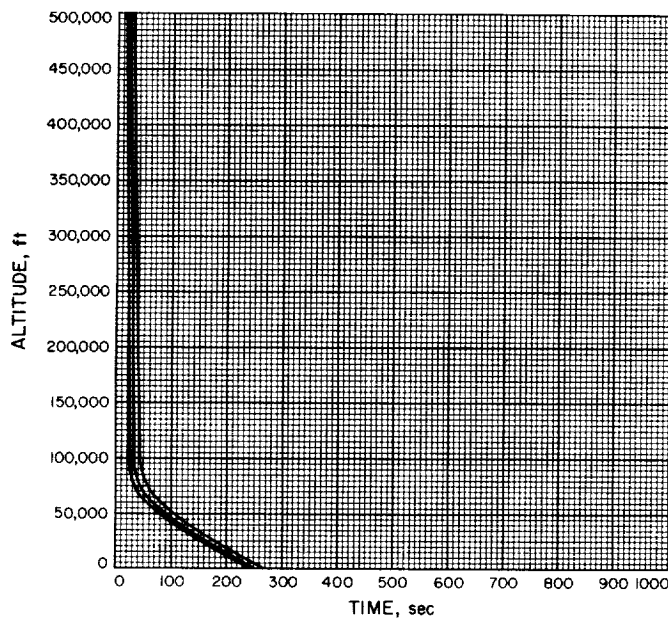


Fig. A-257

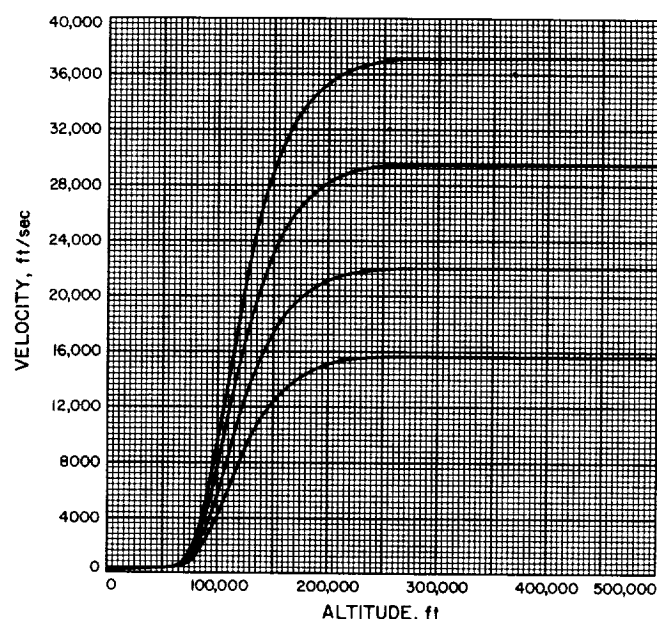


Fig. A-258

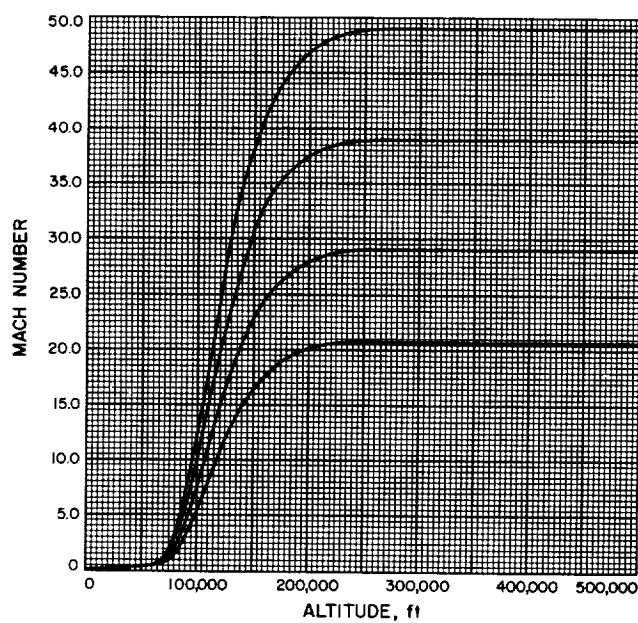


Fig. A-259

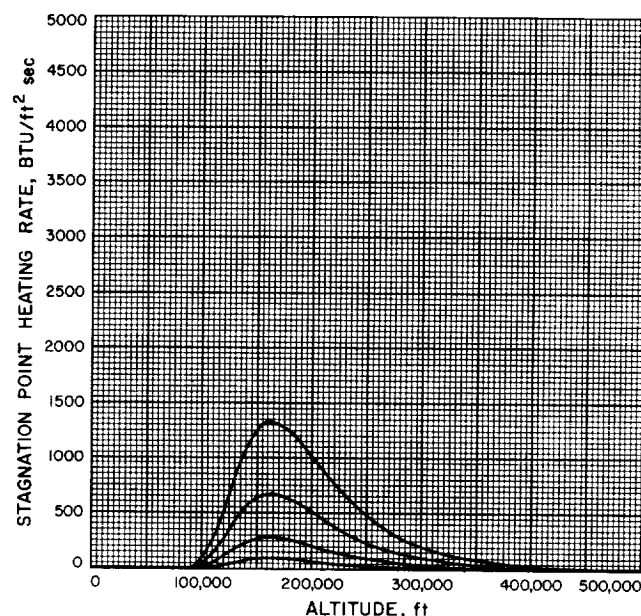


Fig. A-260

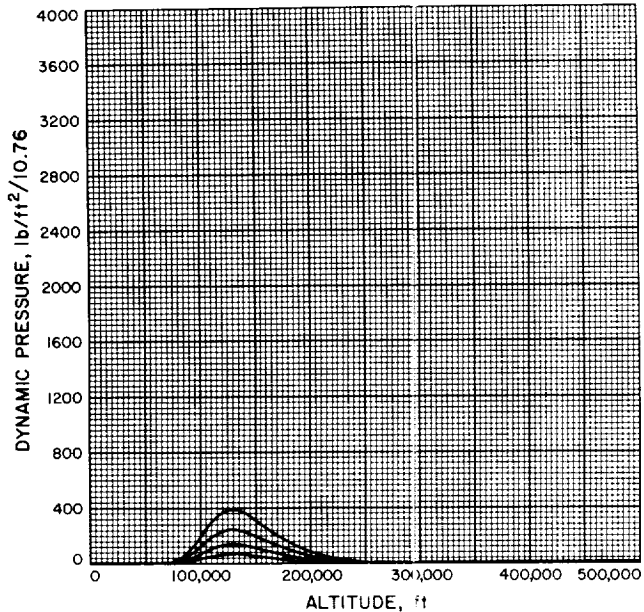


Fig. A-261

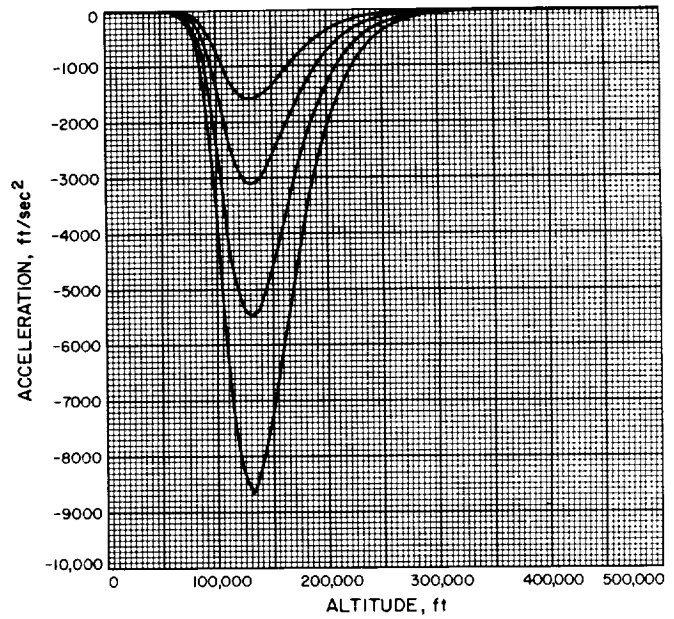


Fig. A-262

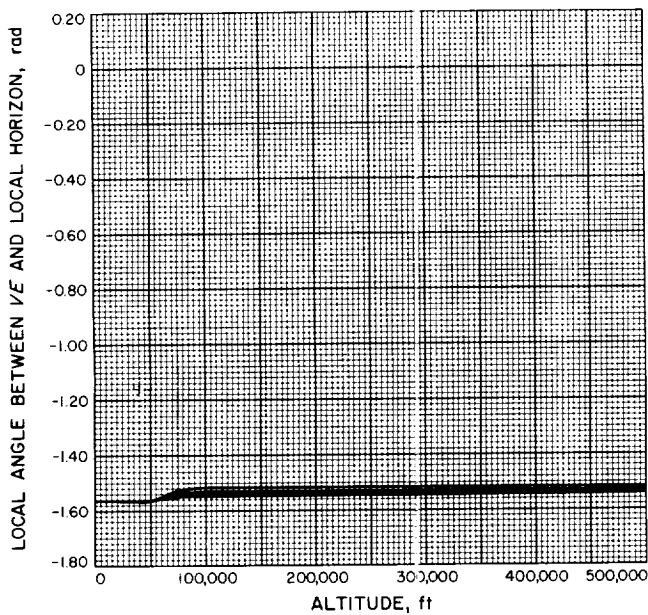


Fig. A-263

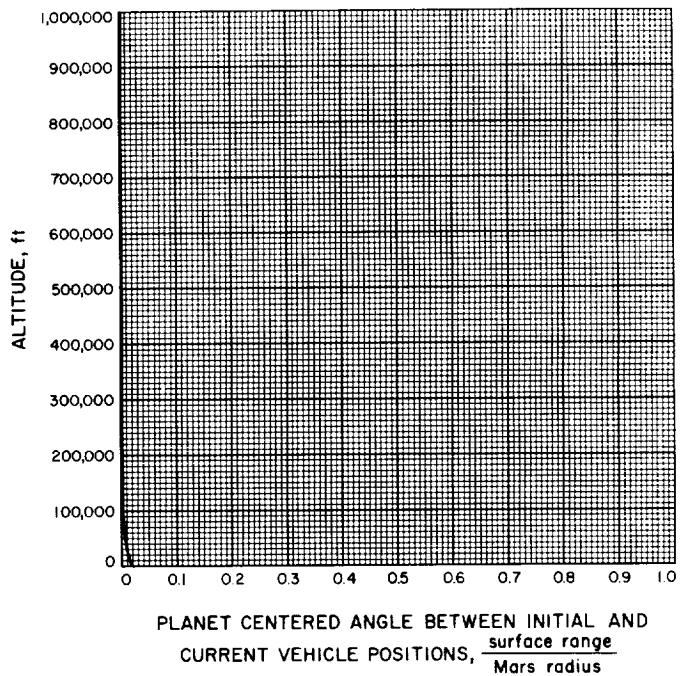


Fig. A-264

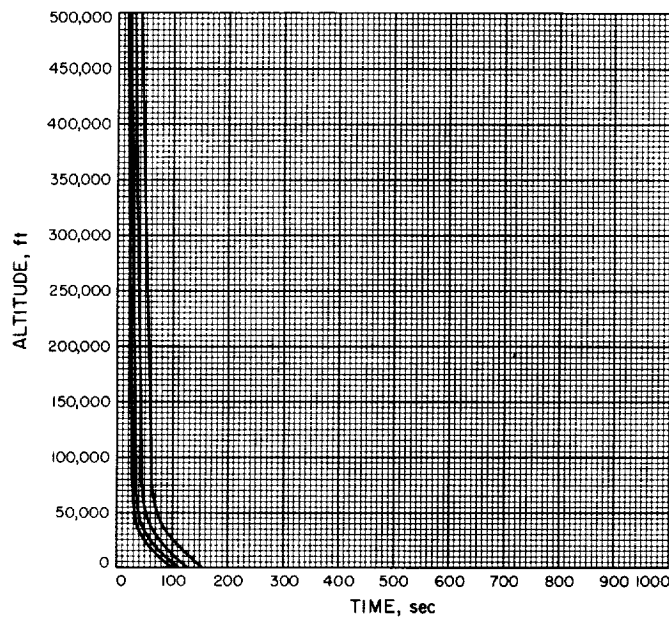


Fig. A-265

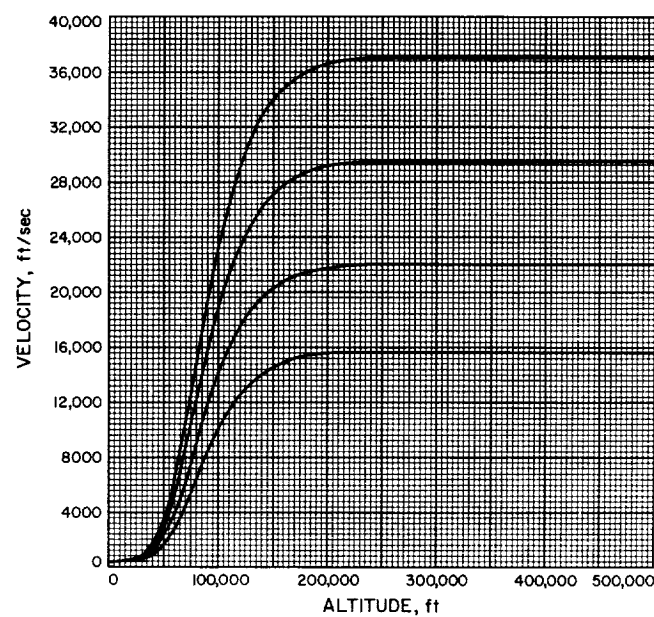


Fig. A-266

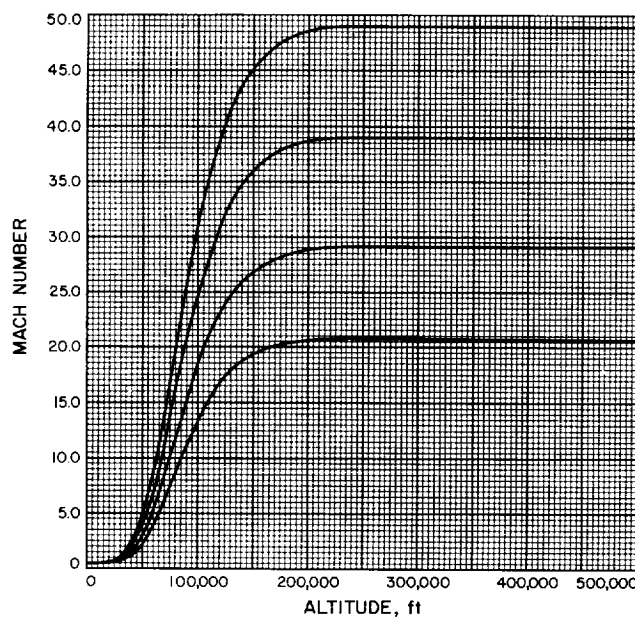


Fig. A-267

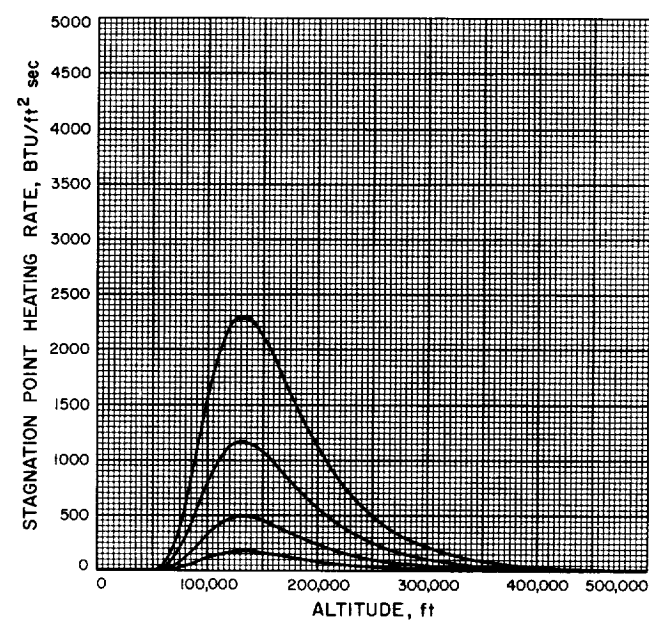


Fig. A-268

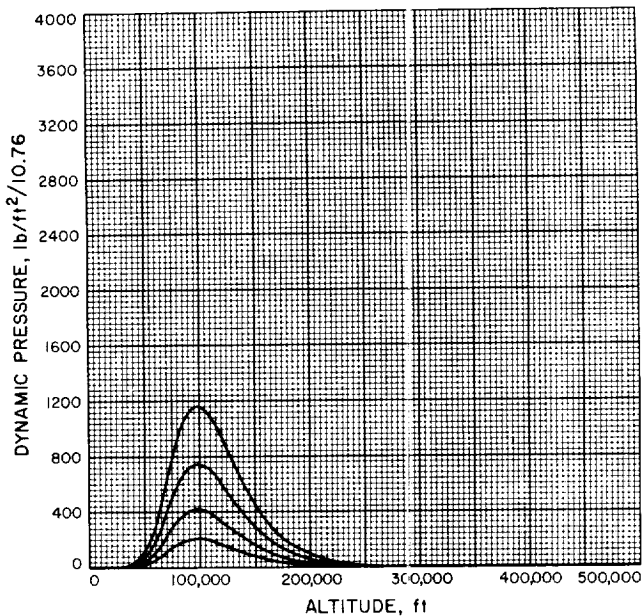


Fig. A-269

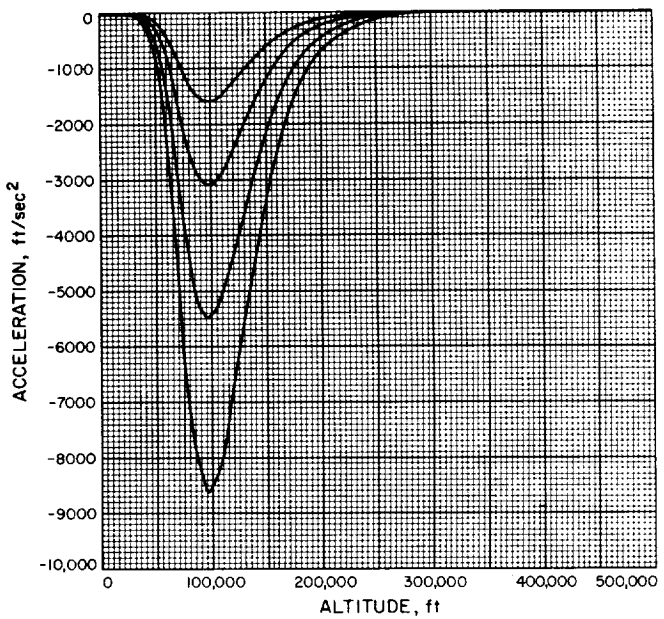


Fig. A-270

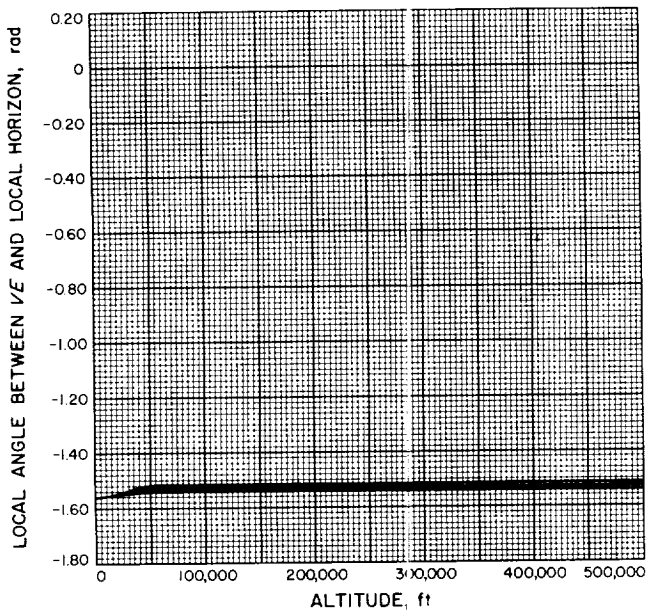


Fig. A-271

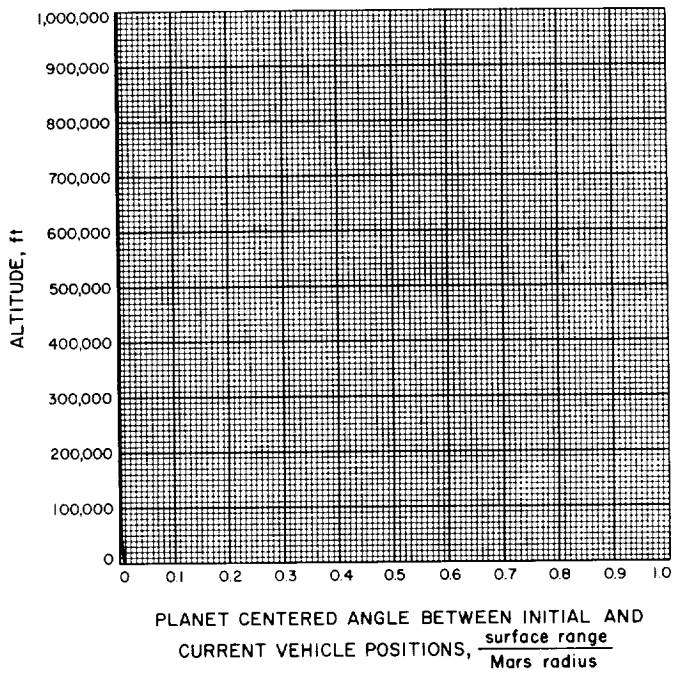


Fig. A-272

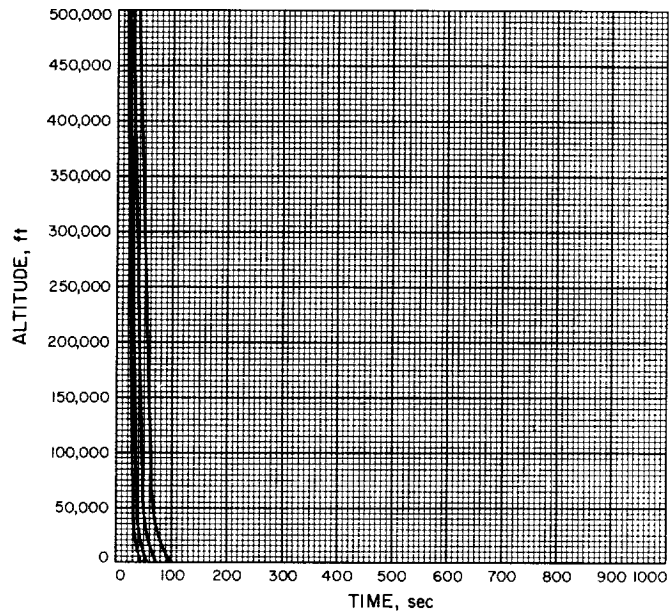


Fig. A-273

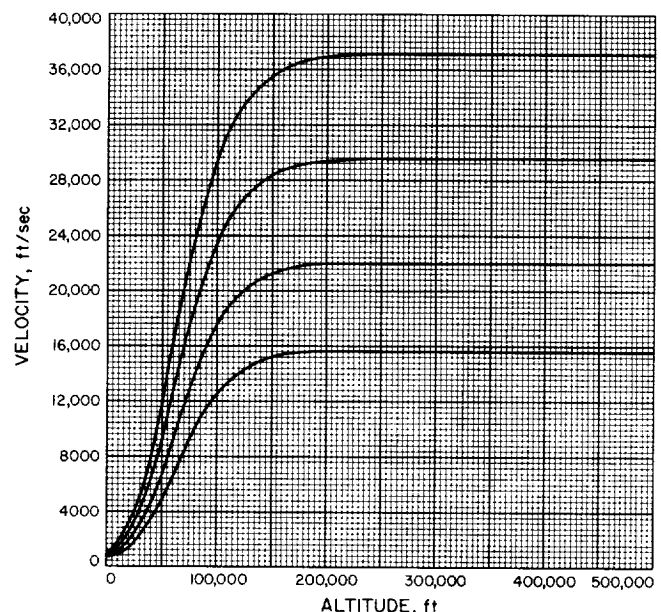


Fig. A-274

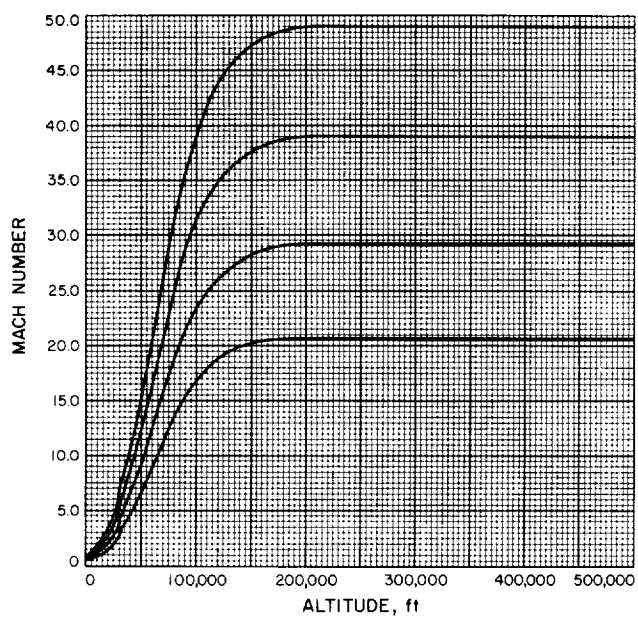


Fig. A-275

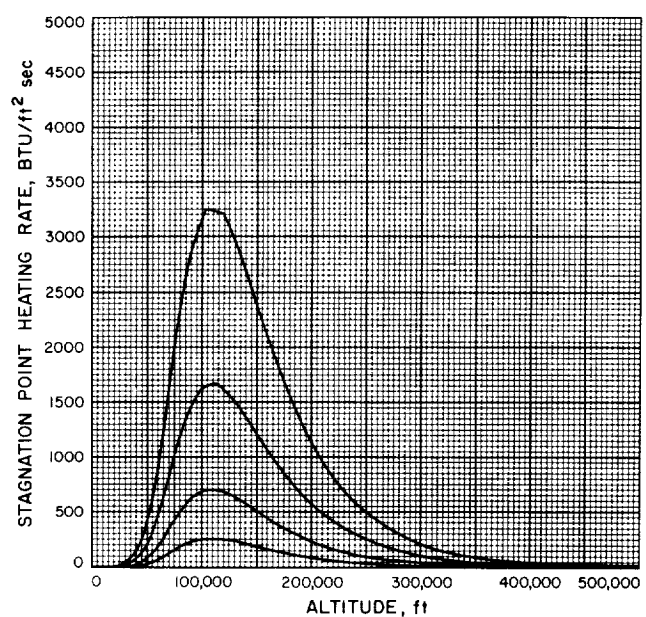


Fig. A-276

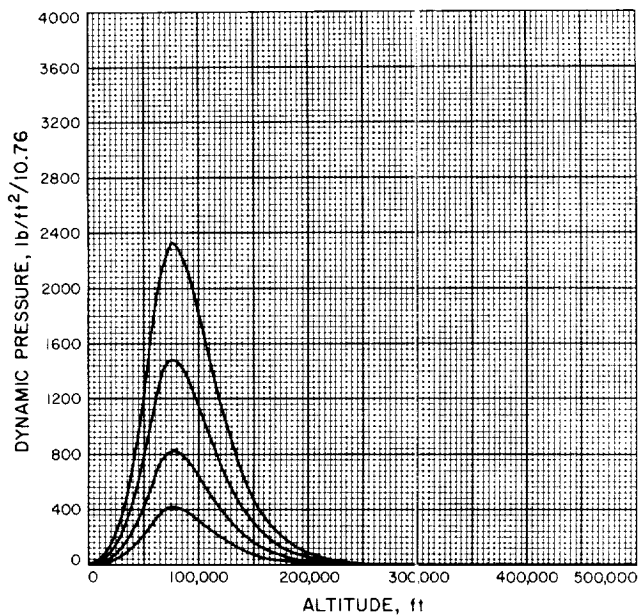


Fig. A-277

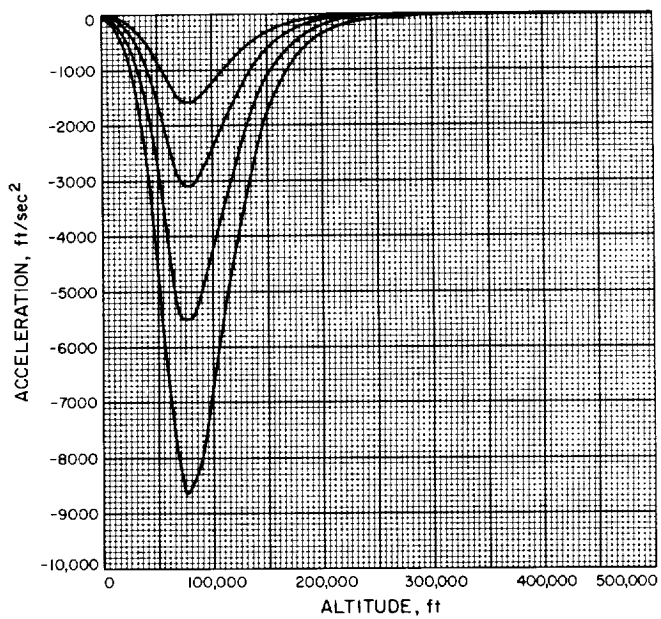


Fig. A-278

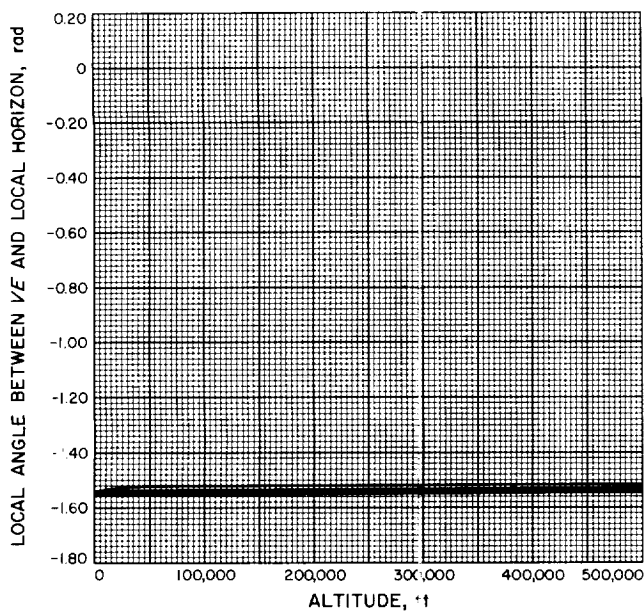


Fig. A-279

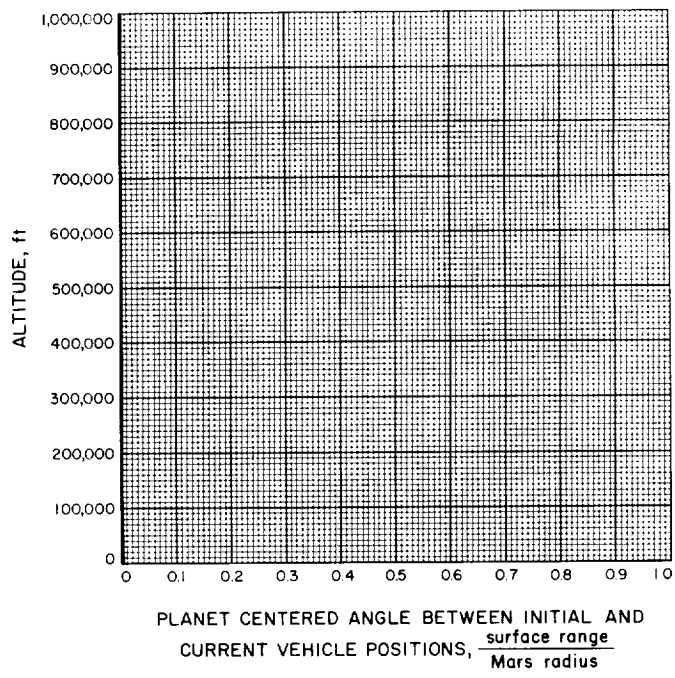


Fig. A-280

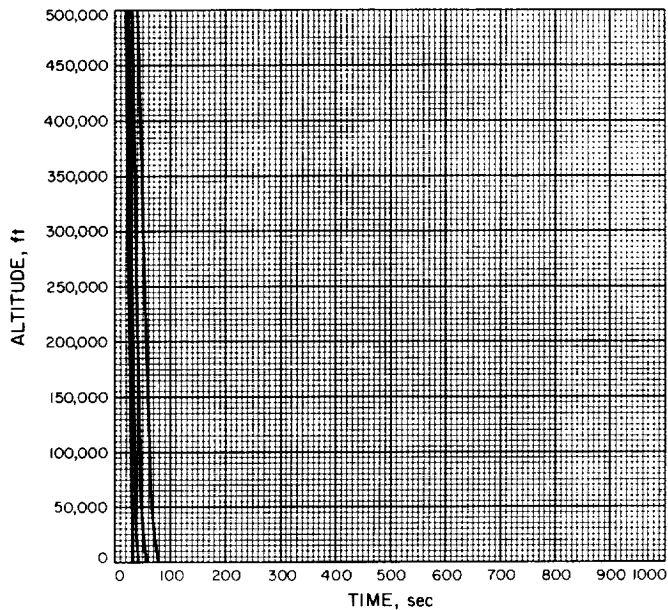


Fig. A-281

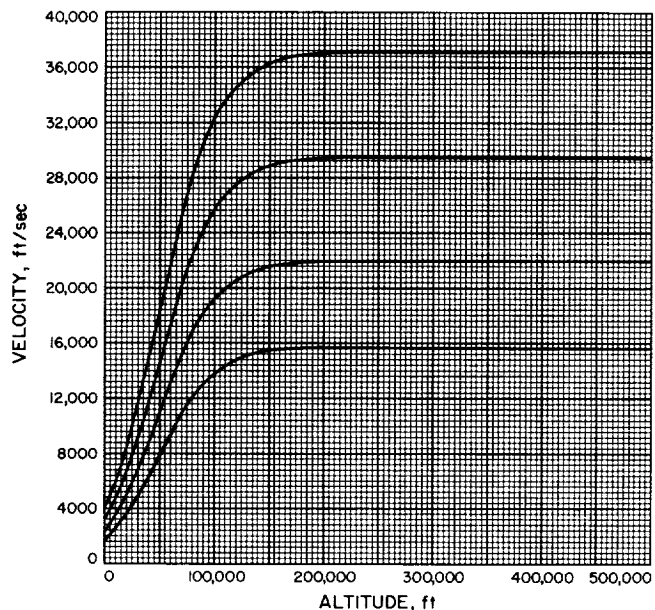


Fig. A-282

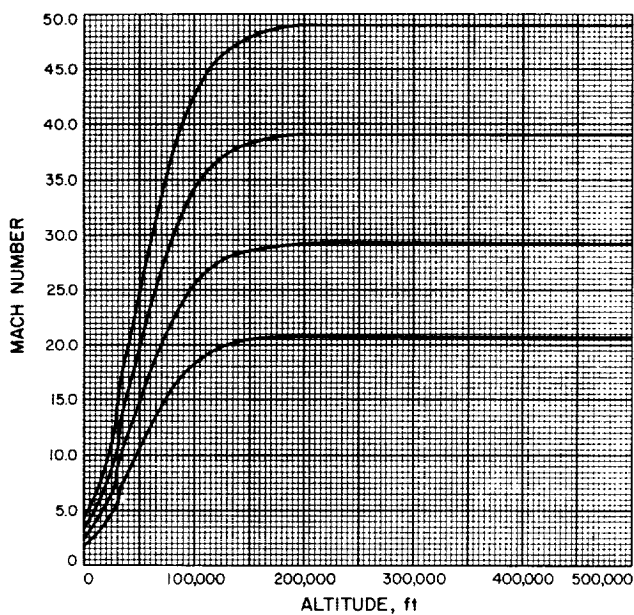


Fig. A-283

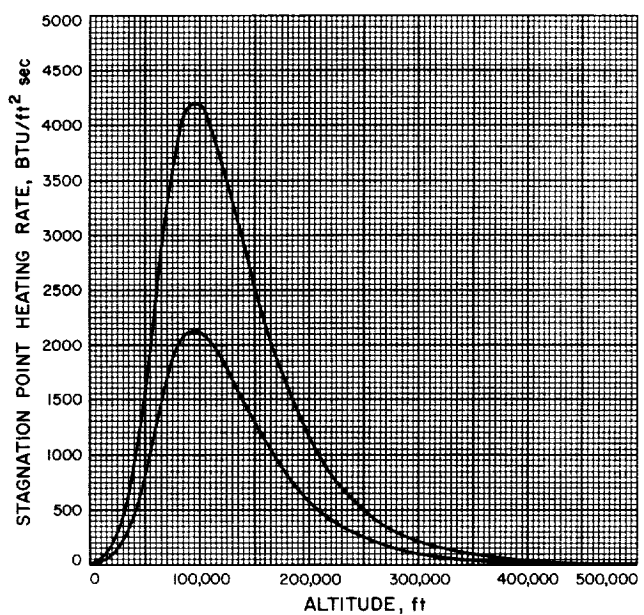


Fig. A-284

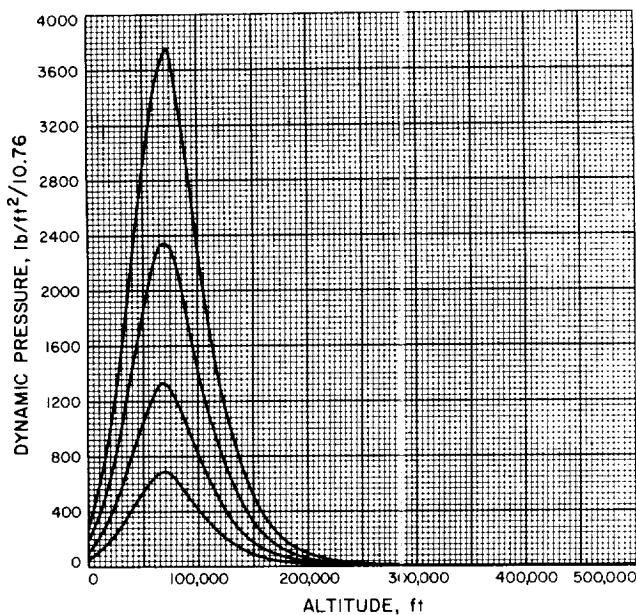


Fig. A-285

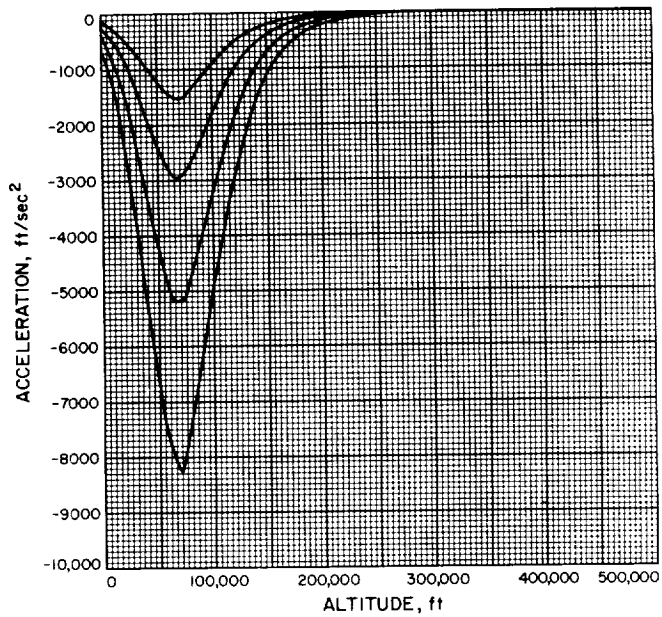


Fig. A-286

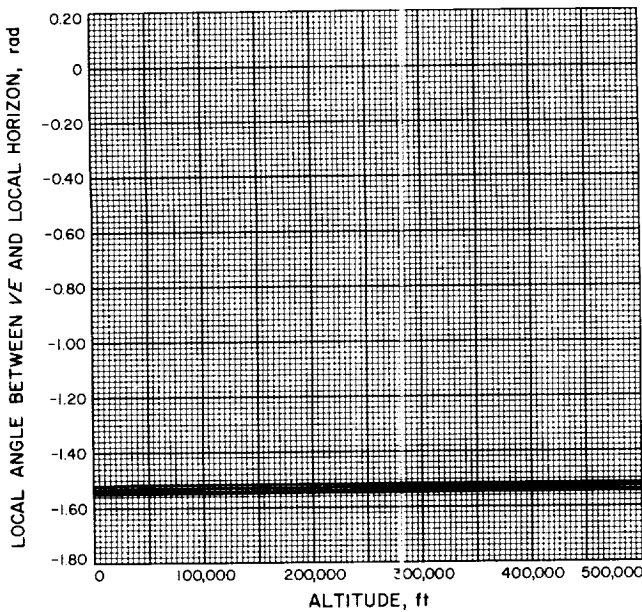


Fig. A-287

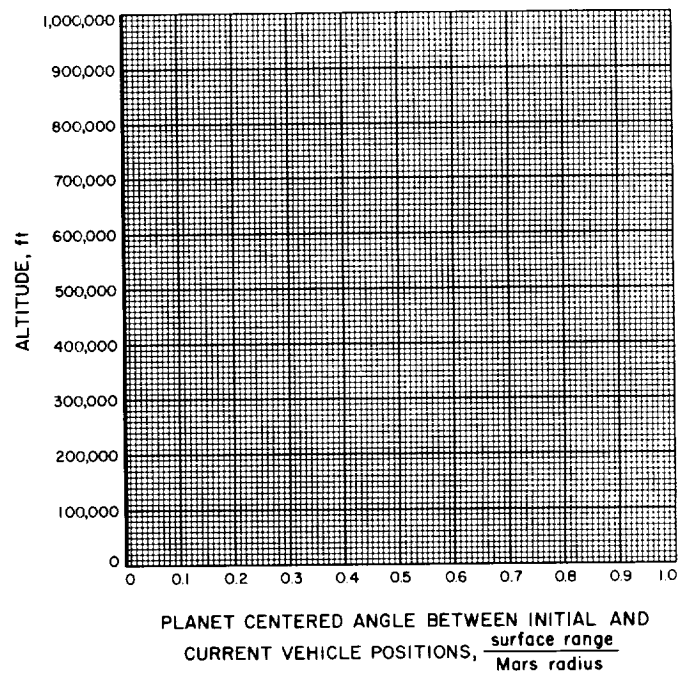


Fig. A-288

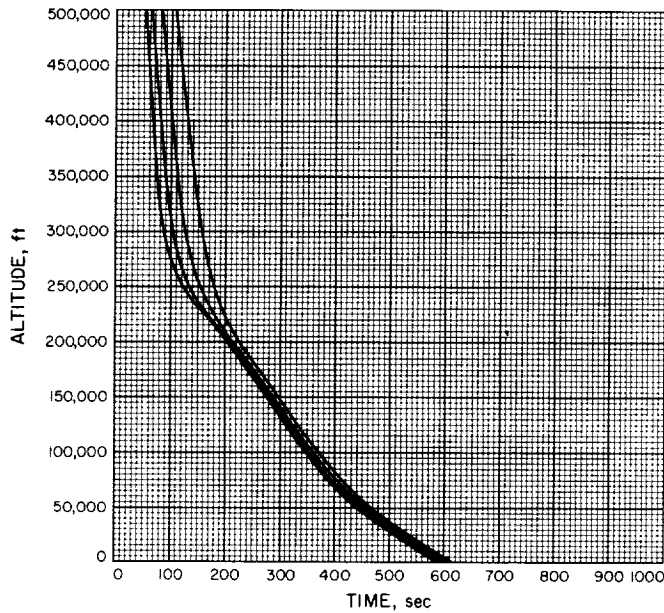


Fig. A-289

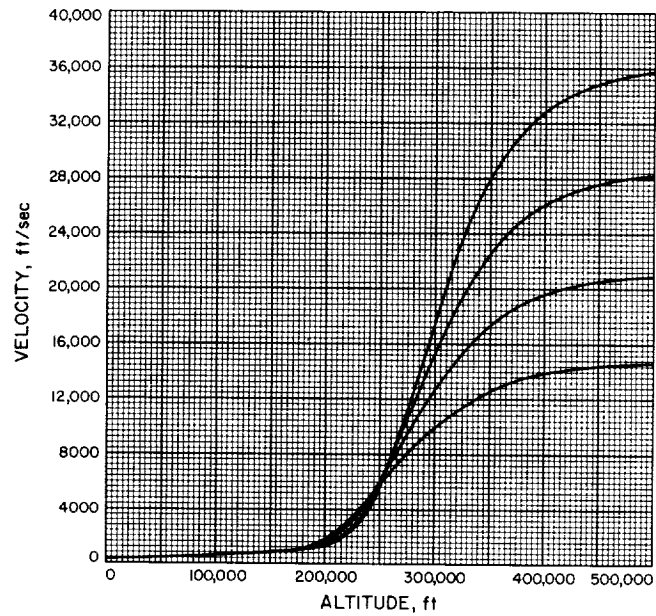


Fig. A-290

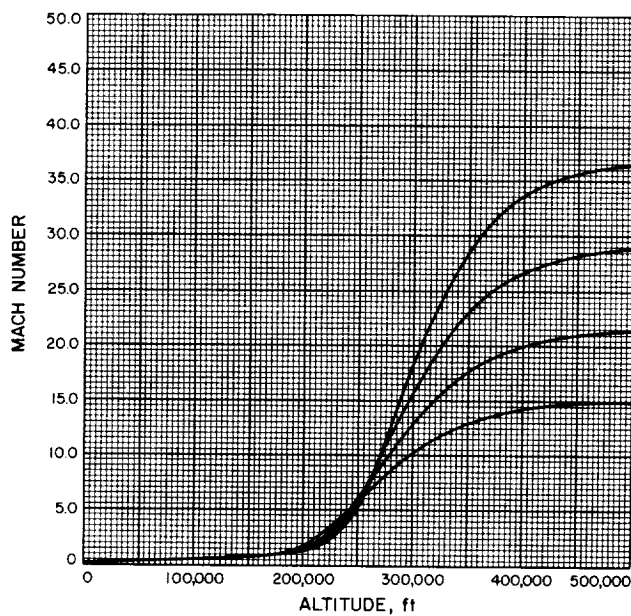


Fig. A-291

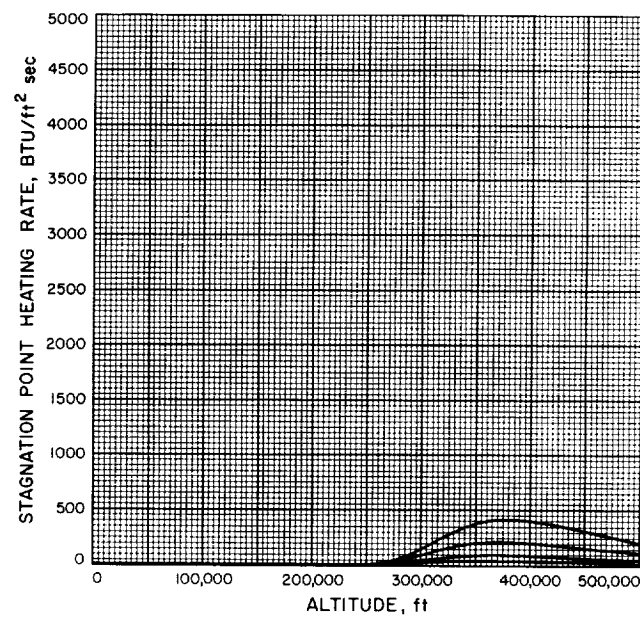


Fig. A-292

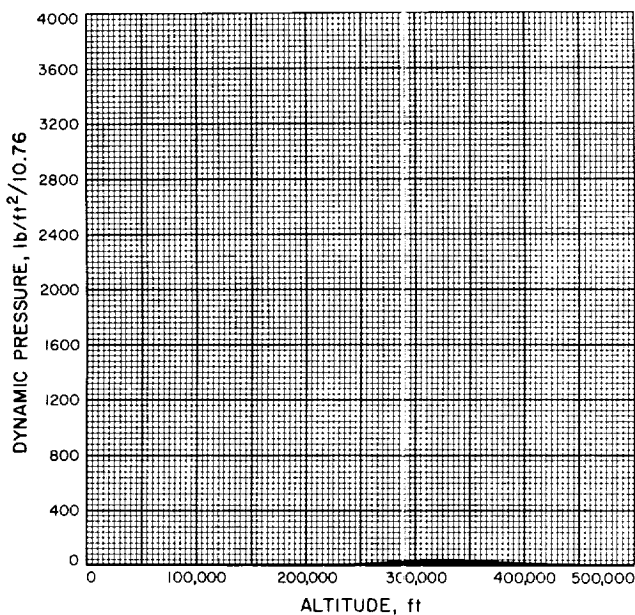


Fig. A-293

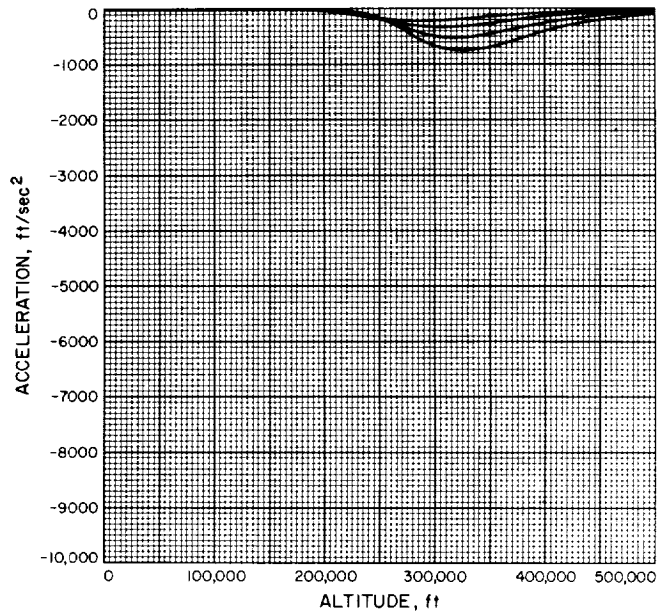


Fig. A-294

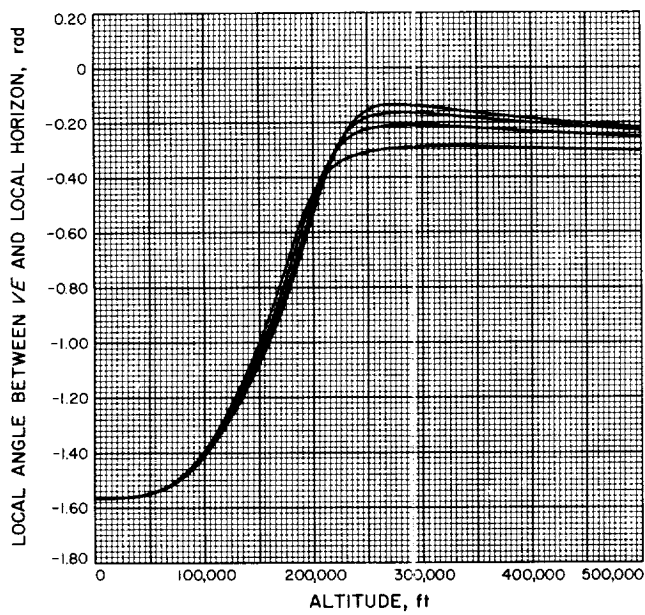


Fig. A-295

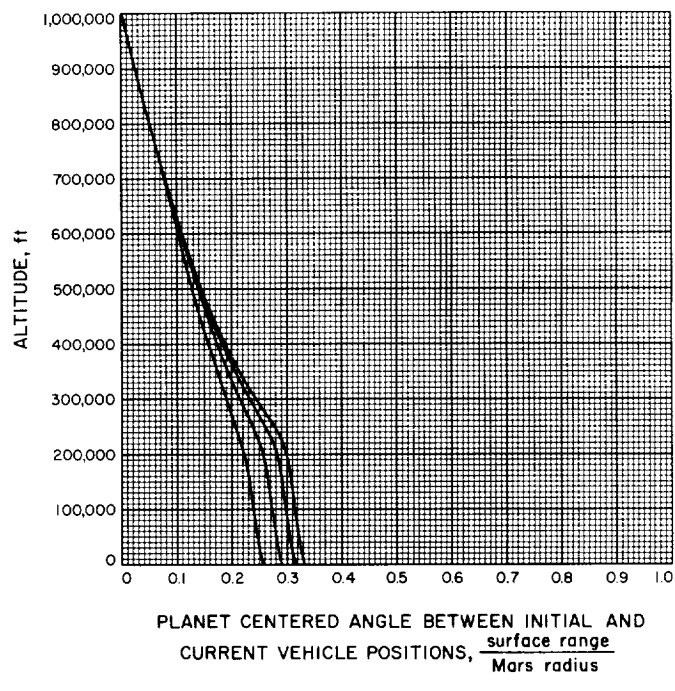


Fig. A-296

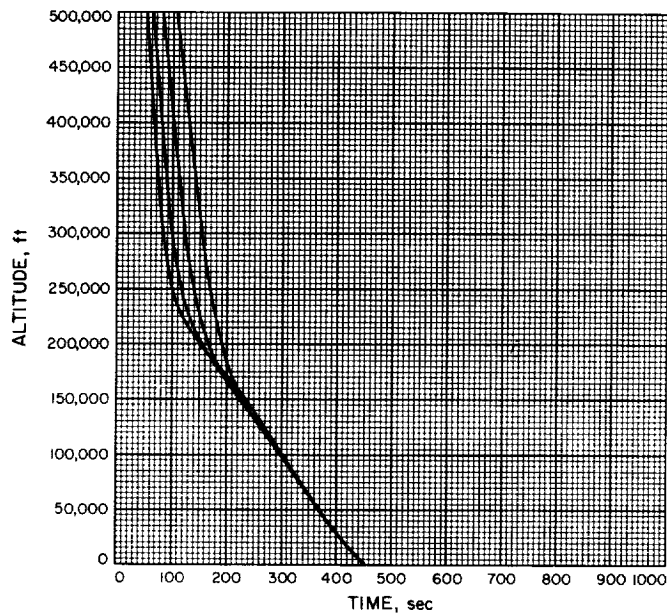


Fig. A-297

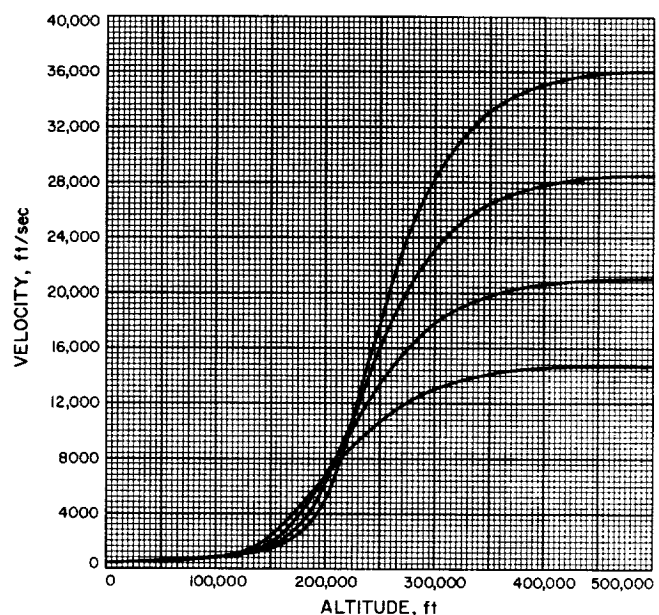


Fig. A-298

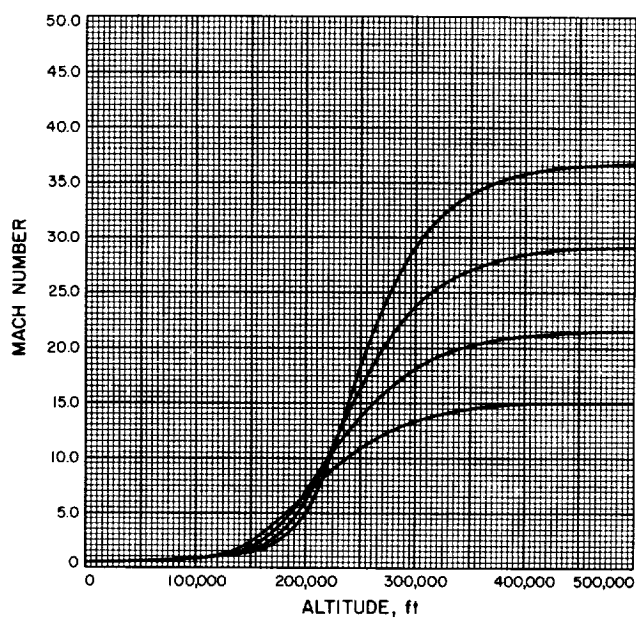


Fig. A-299

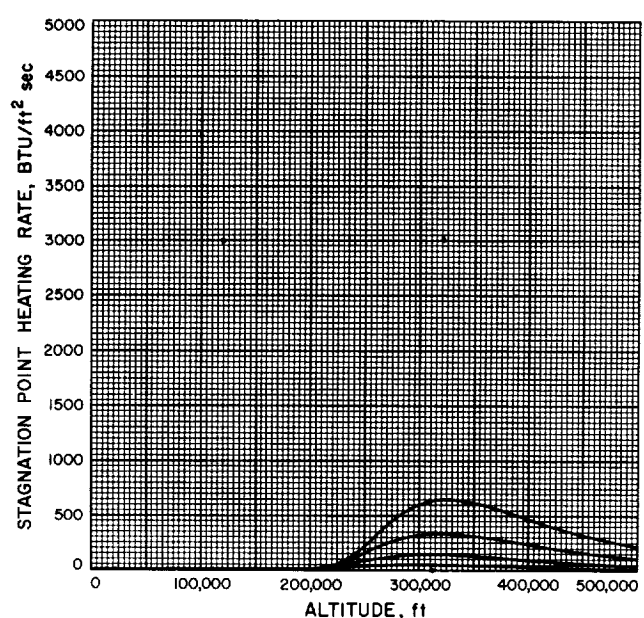


Fig. A-300

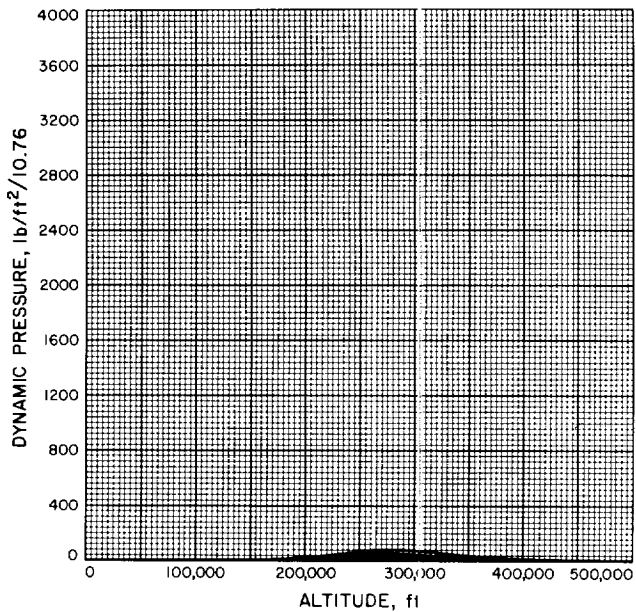


Fig. A-301

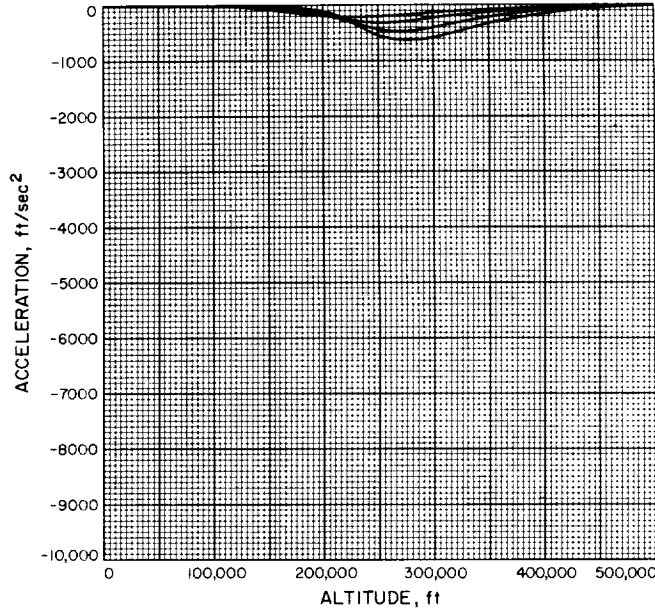


Fig. A-302

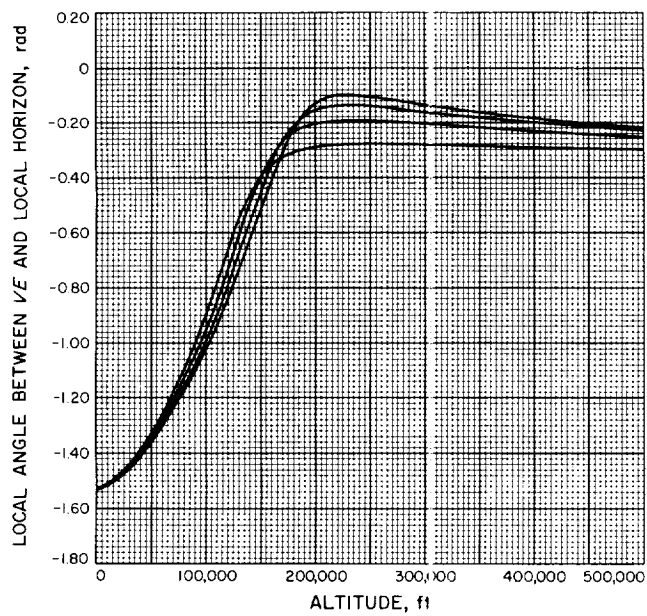


Fig. A-303

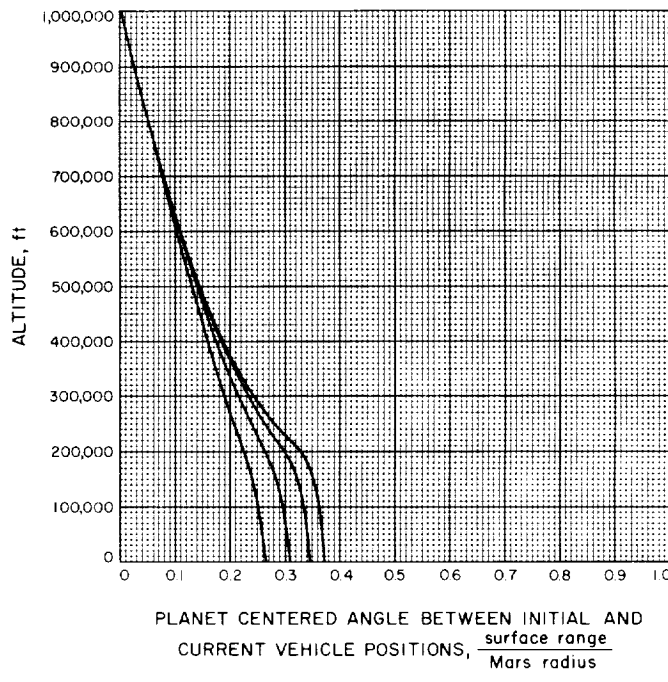


Fig. A-304

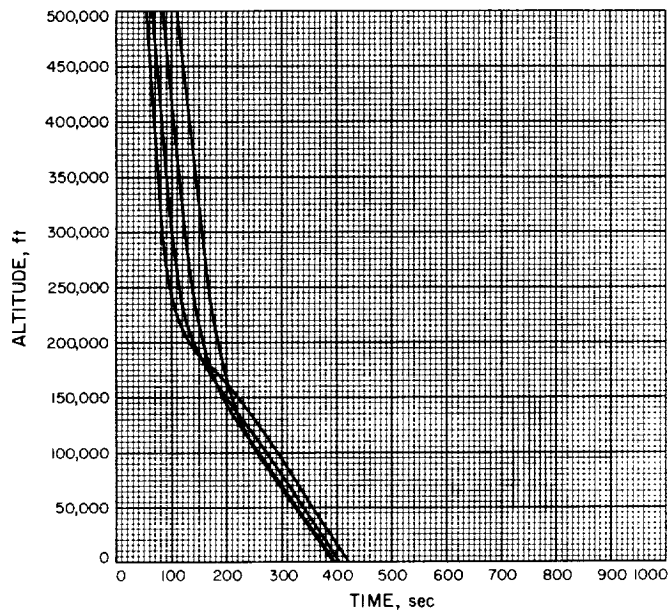


Fig. A-305

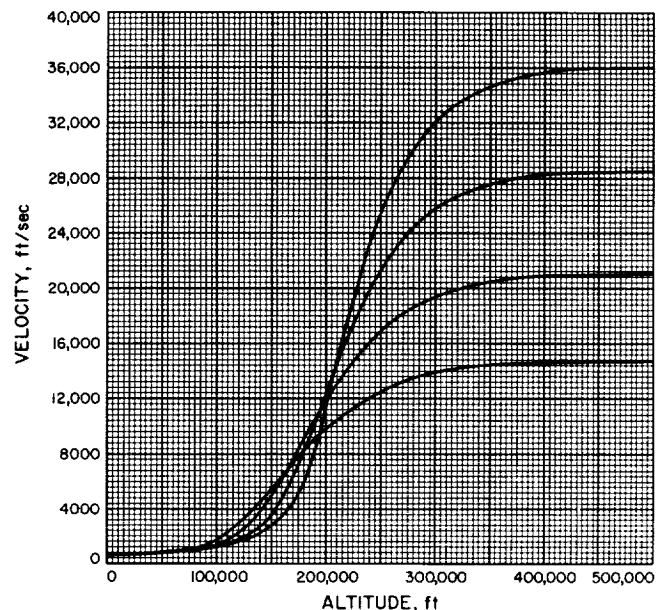


Fig. A-306

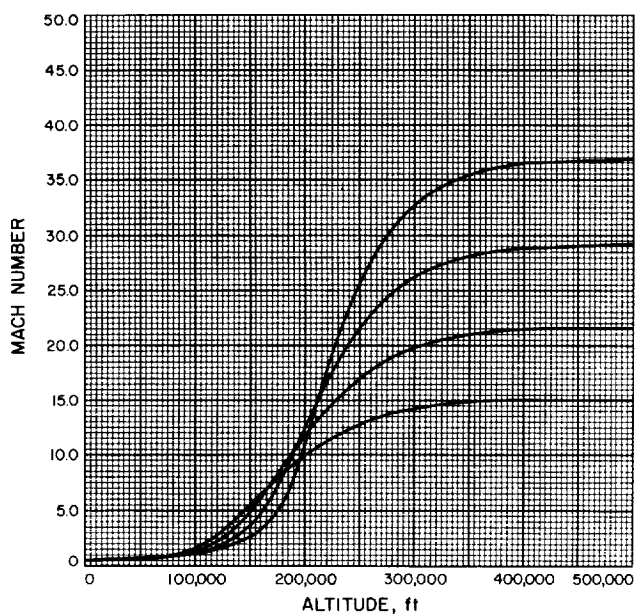


Fig. A-307

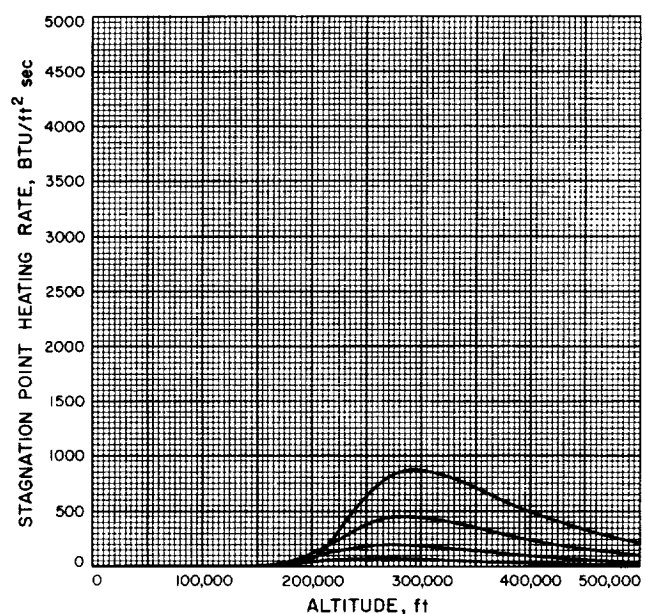


Fig. A-308

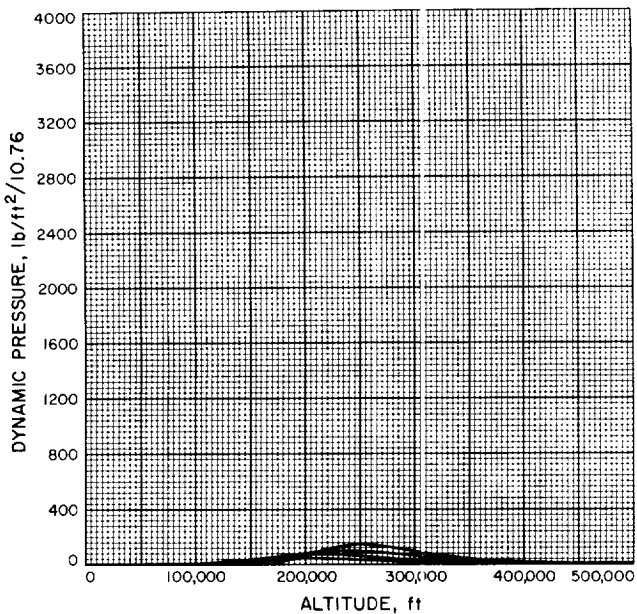


Fig. A-309

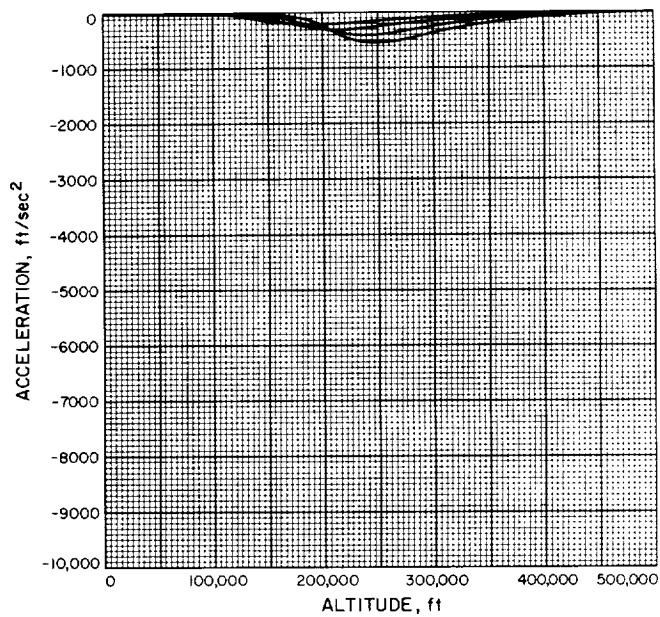


Fig. A-310

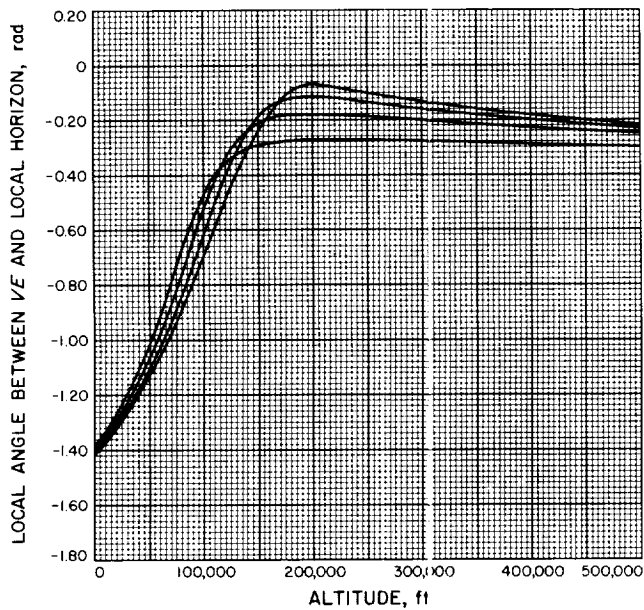


Fig. A-311

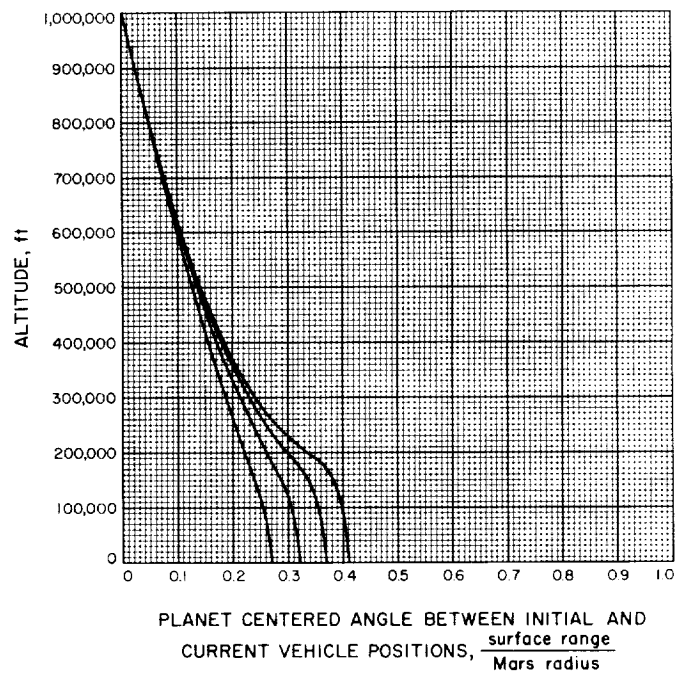


Fig. A-312

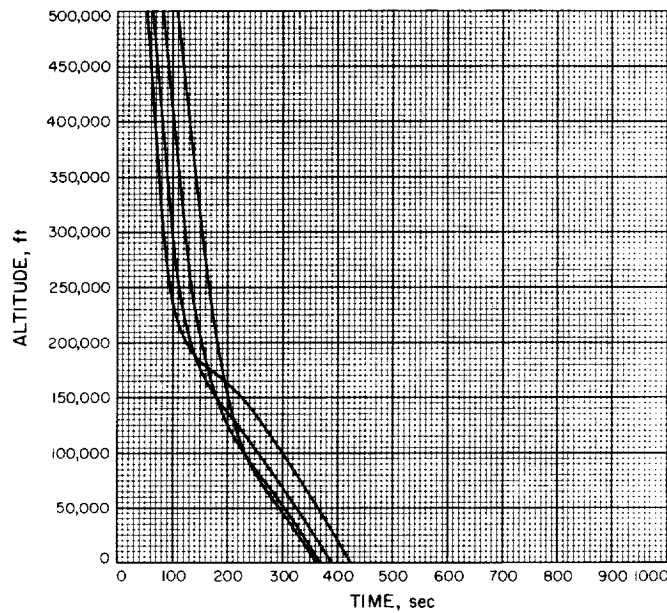


Fig. A-313

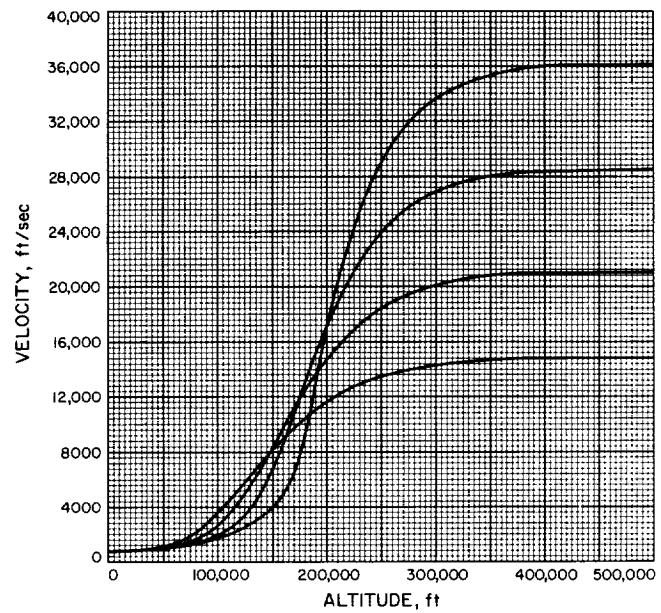


Fig. A-314

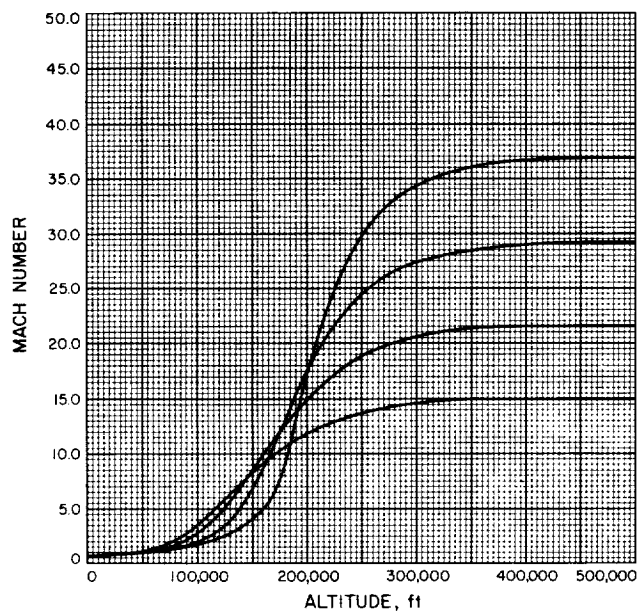


Fig. A-315

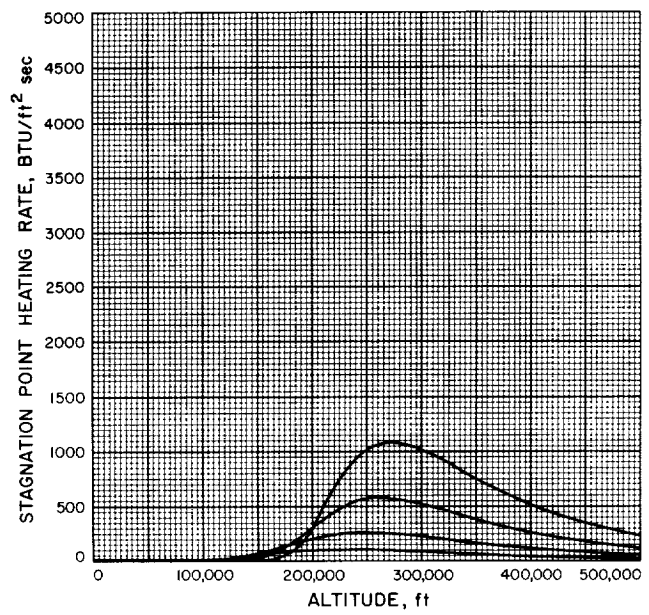


Fig. A-316

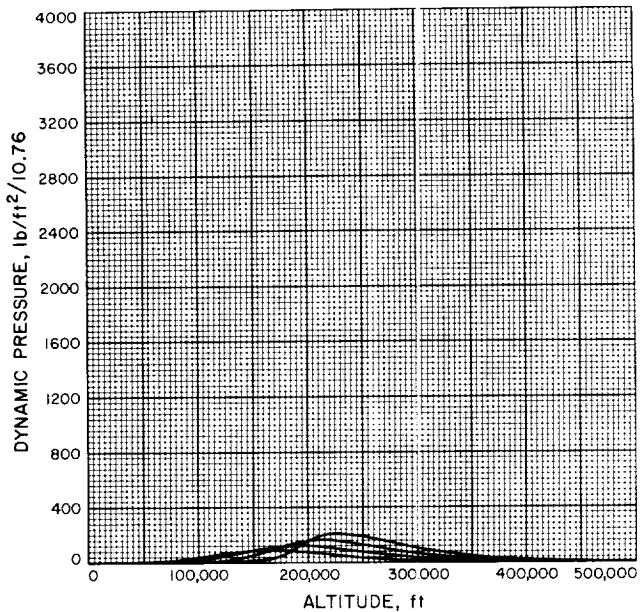


Fig. A-317

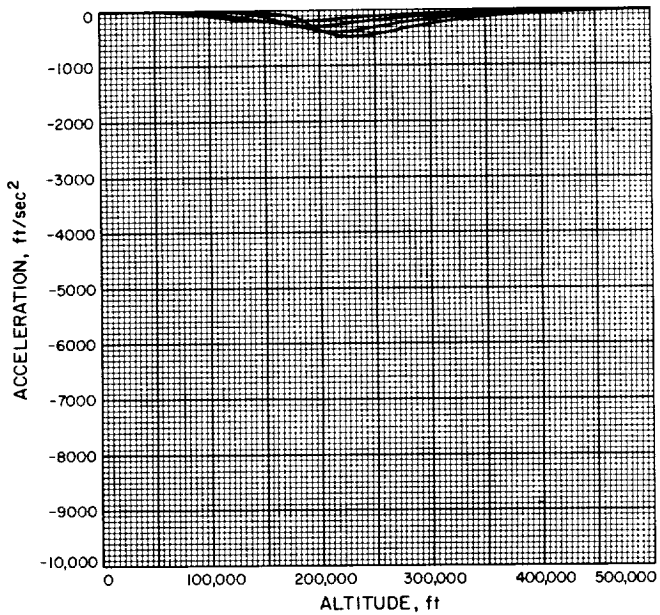


Fig. A-318

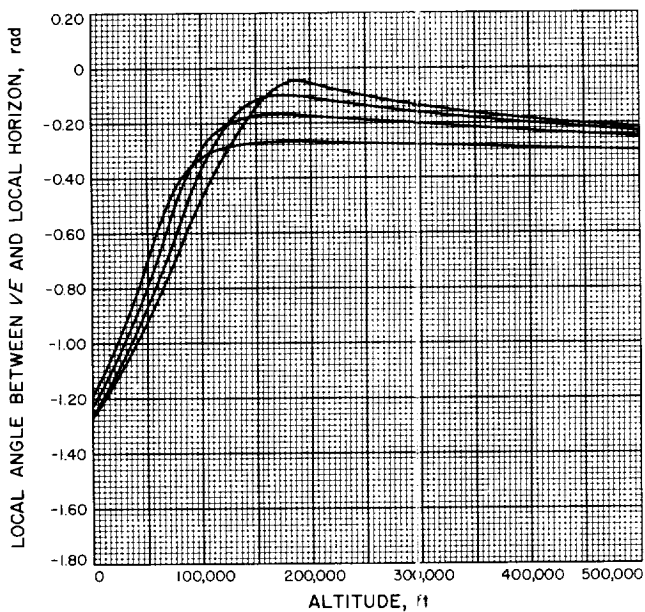


Fig. A-319

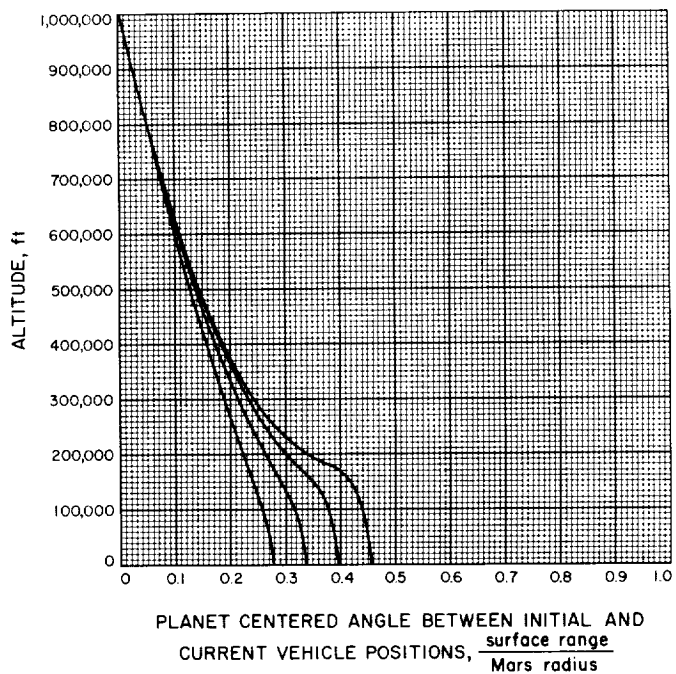


Fig. A-320

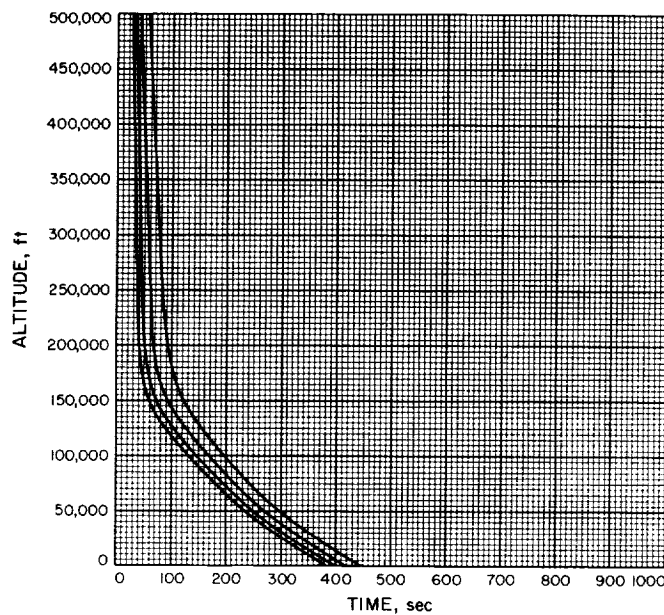


Fig. A-321

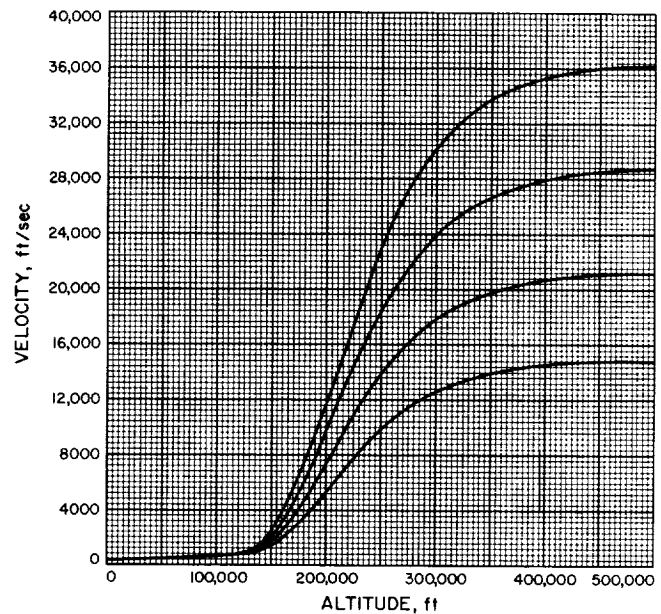


Fig. A-322

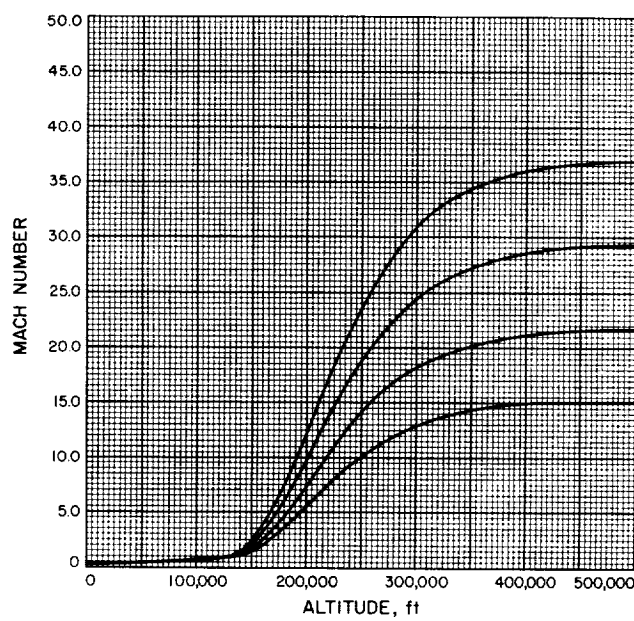


Fig. A-323

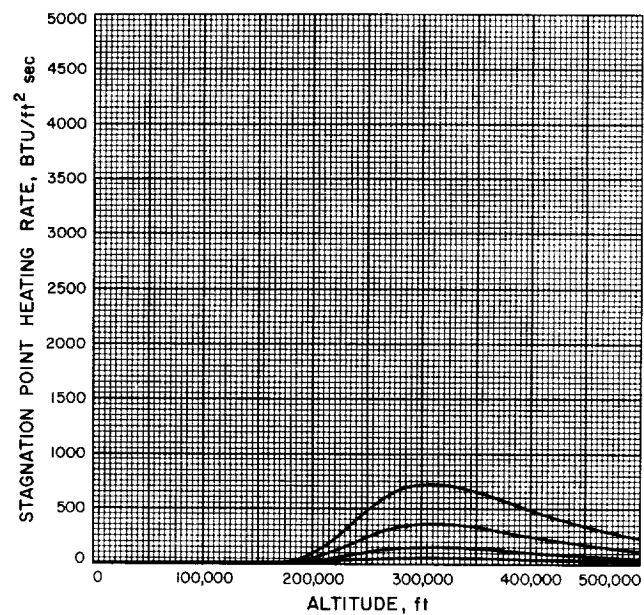


Fig. A-324

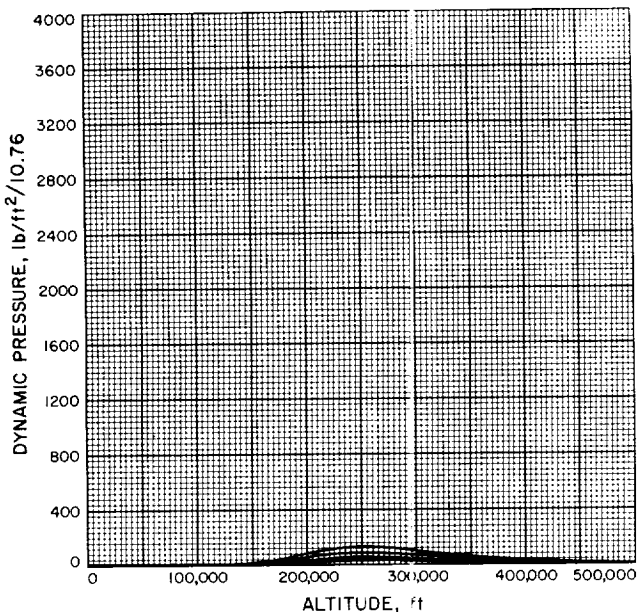


Fig. A-325

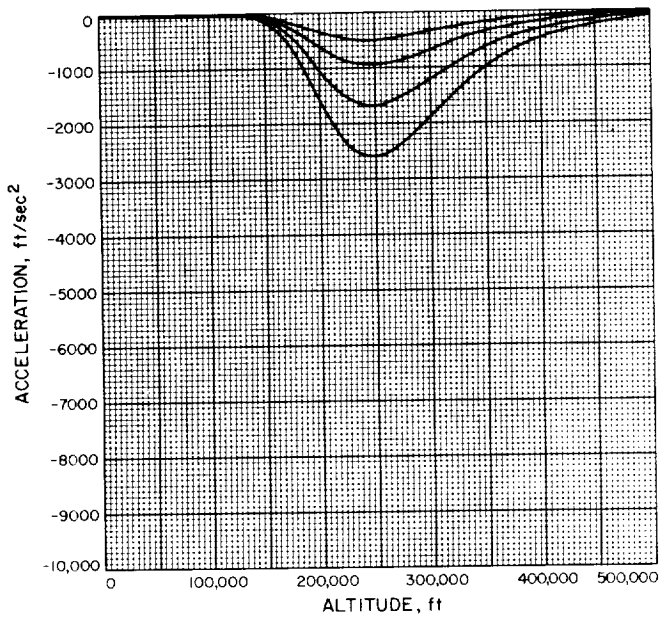


Fig. A-326

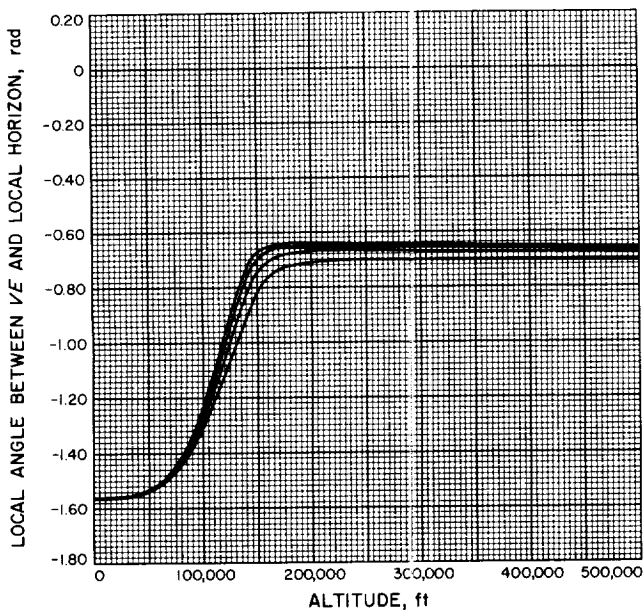


Fig. A-327

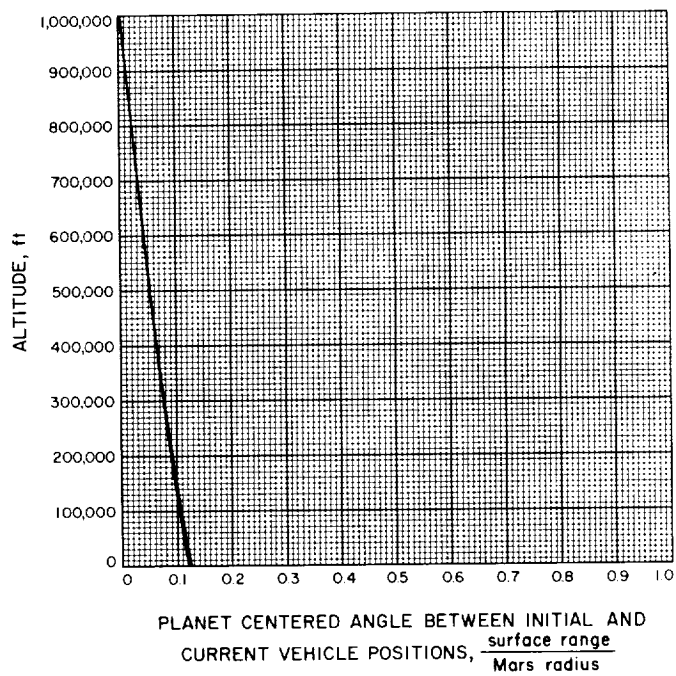


Fig. A-328

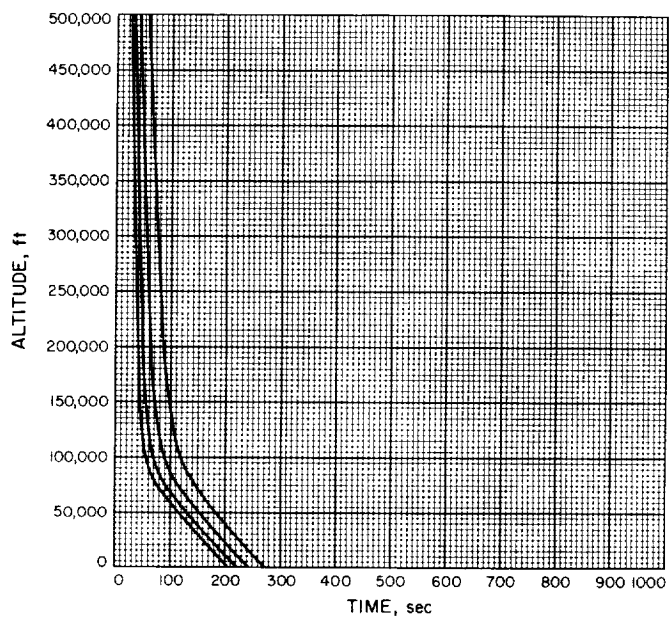


Fig. A-329

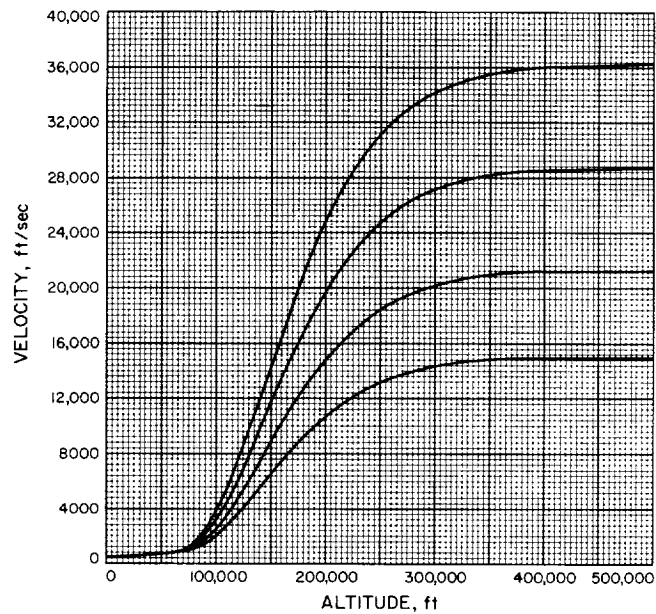


Fig. A-330

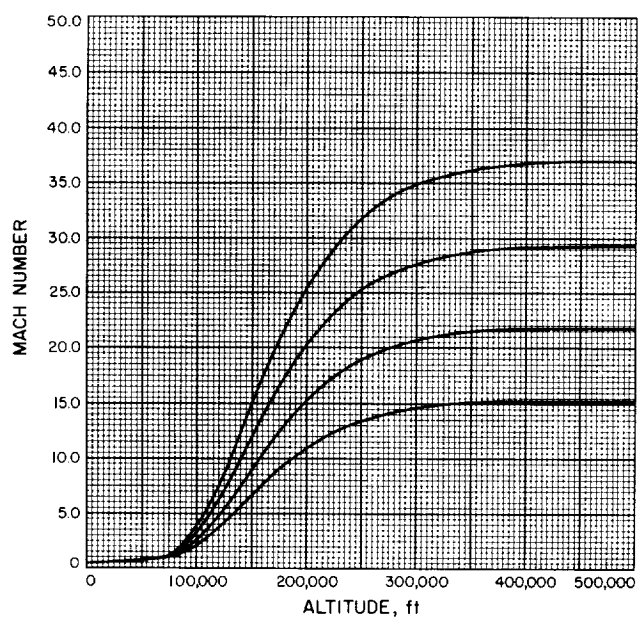


Fig. A-331

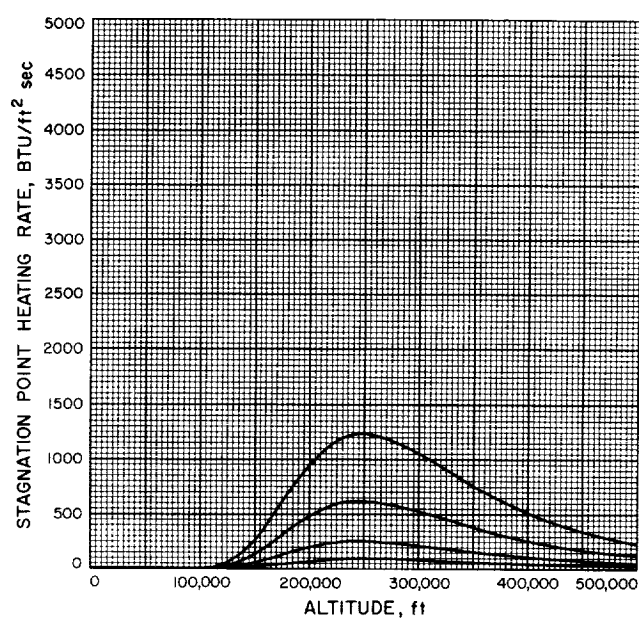


Fig. A-332

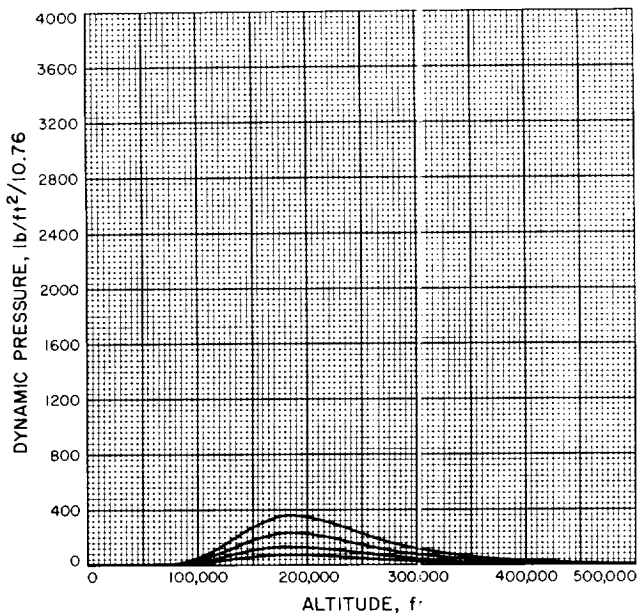


Fig. A-333

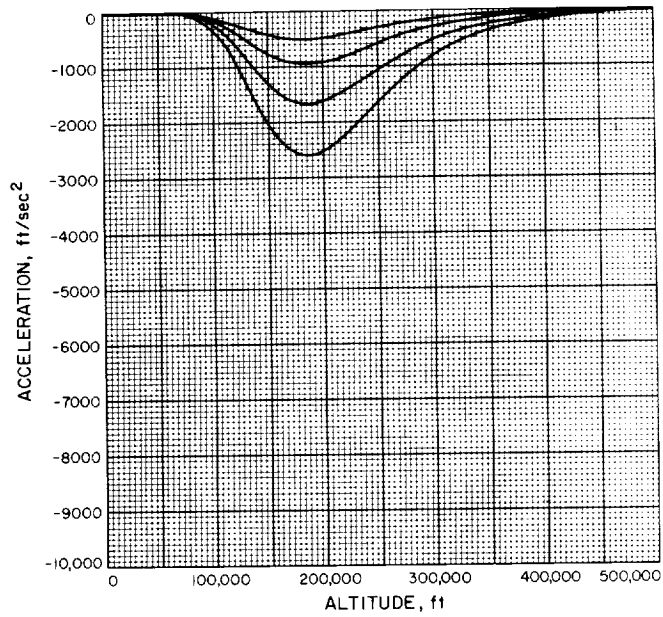


Fig. A-334

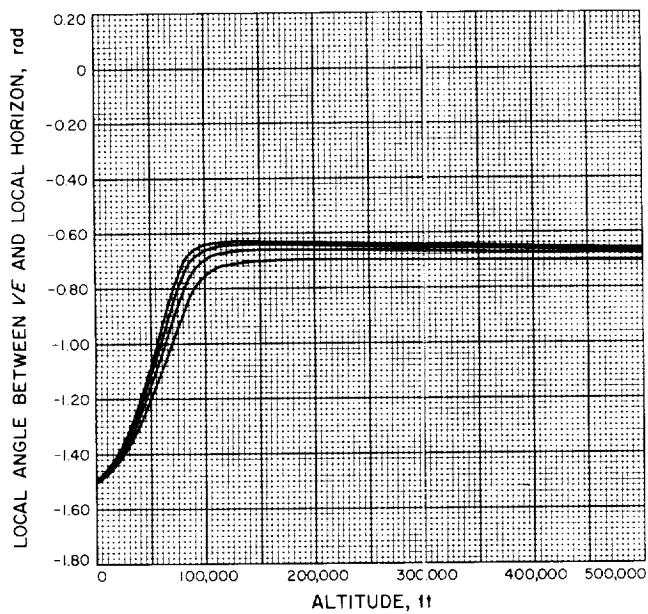


Fig. A-335

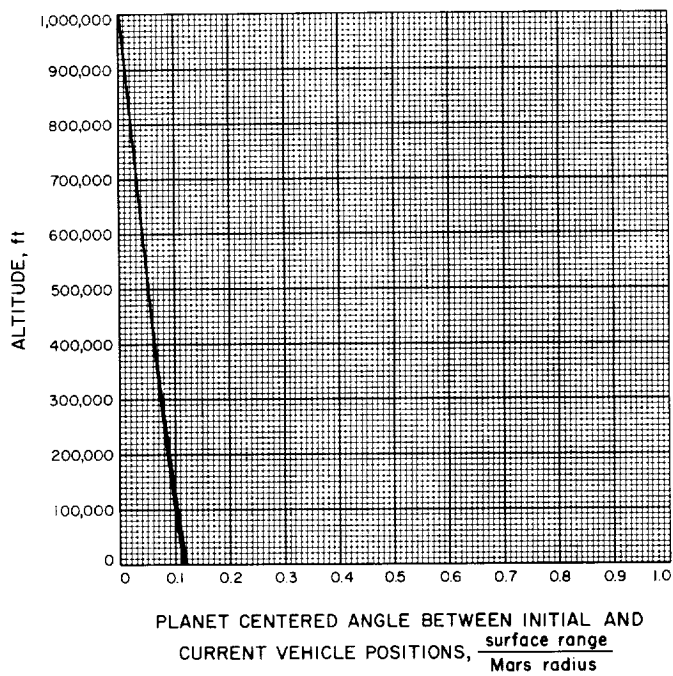


Fig. A-336

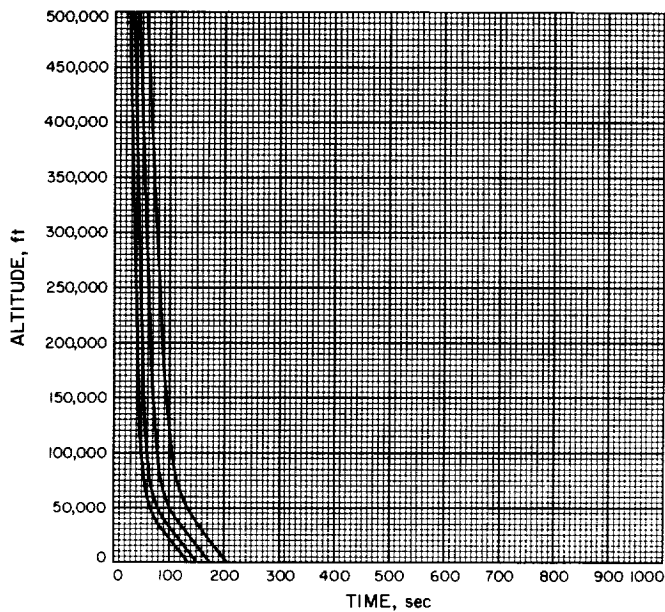


Fig. A-337

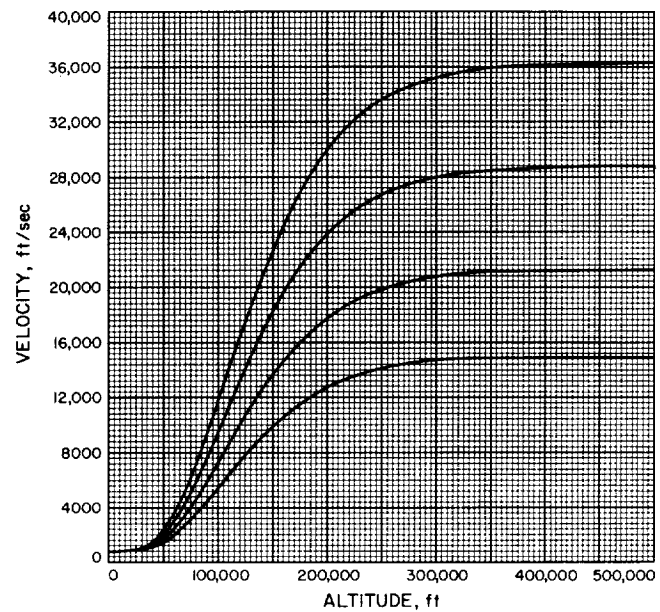


Fig. A-338

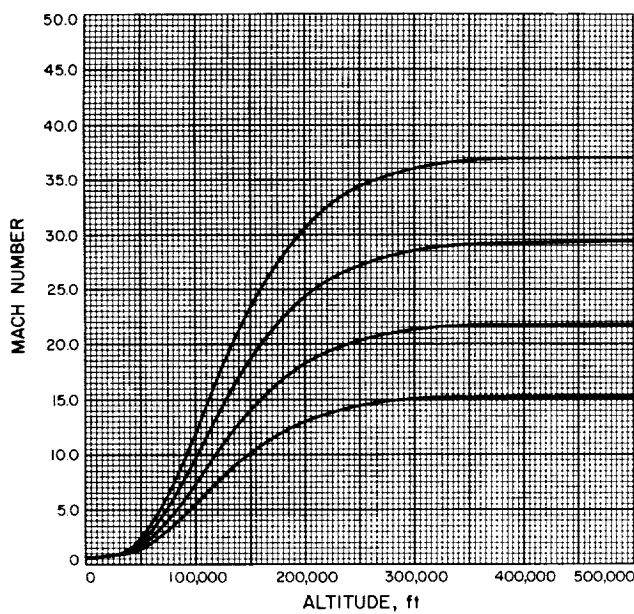


Fig. A-339

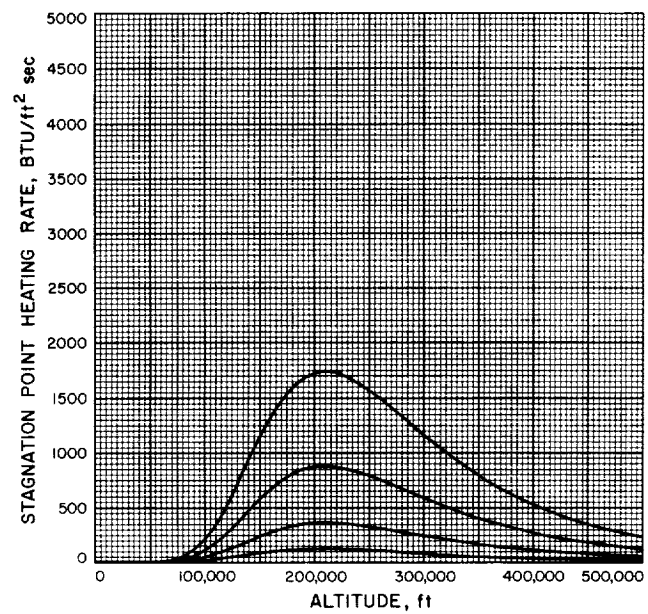


Fig. A-340

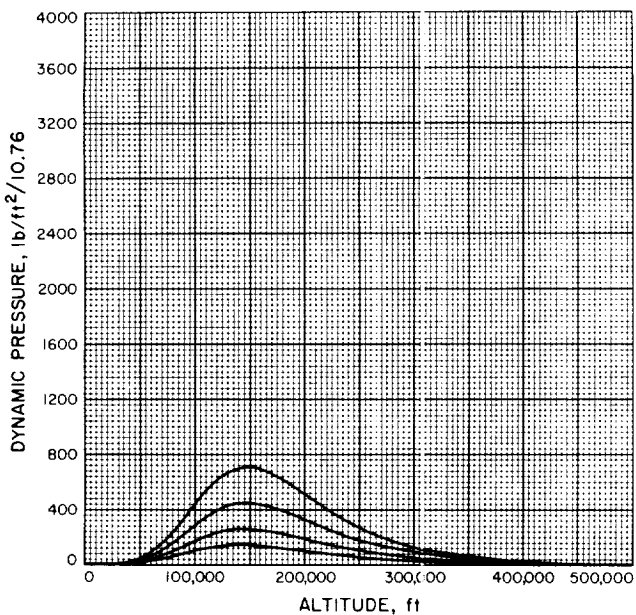


Fig. A-341

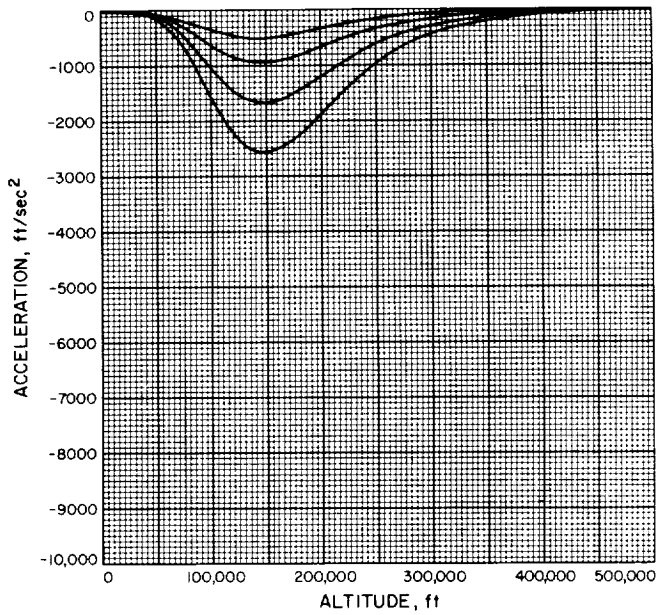


Fig. A-342

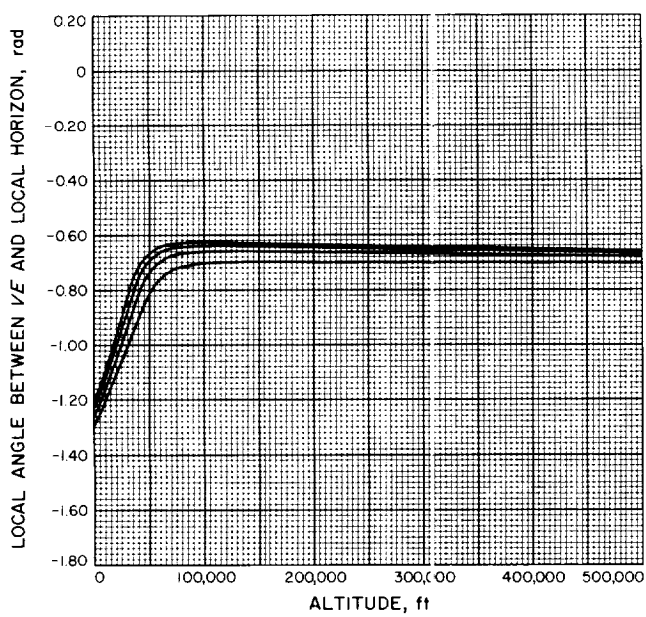


Fig. A-343

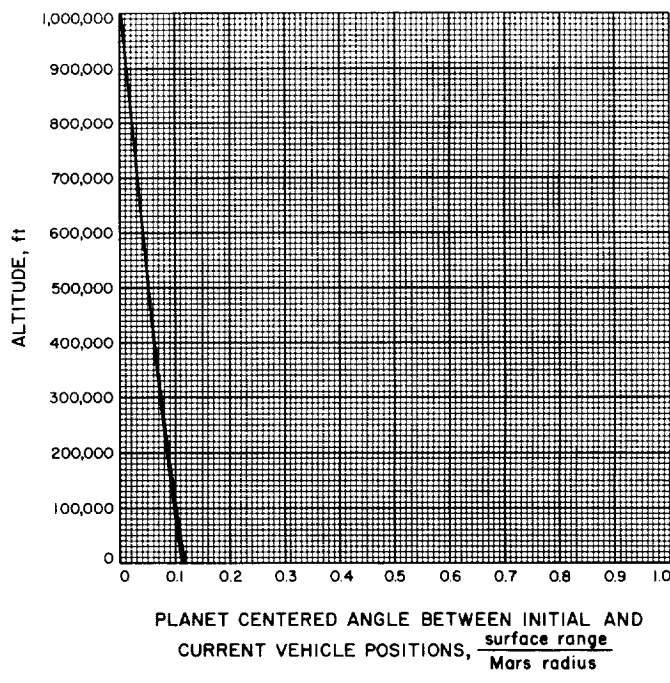


Fig. A-344

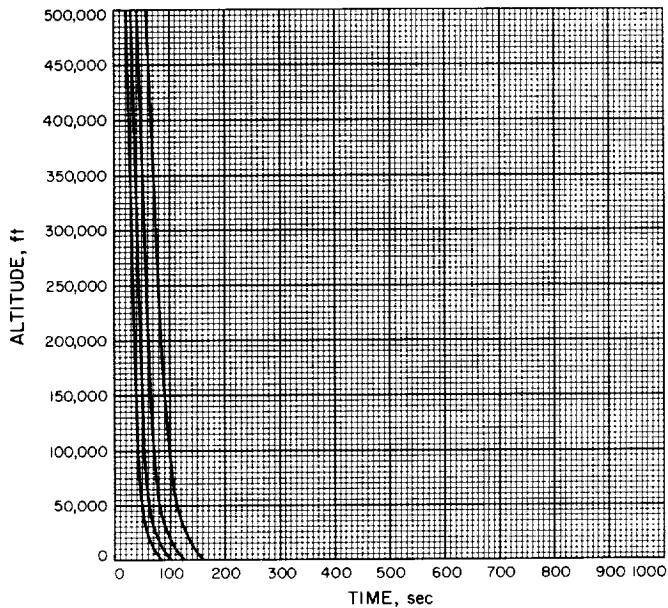


Fig. A-345

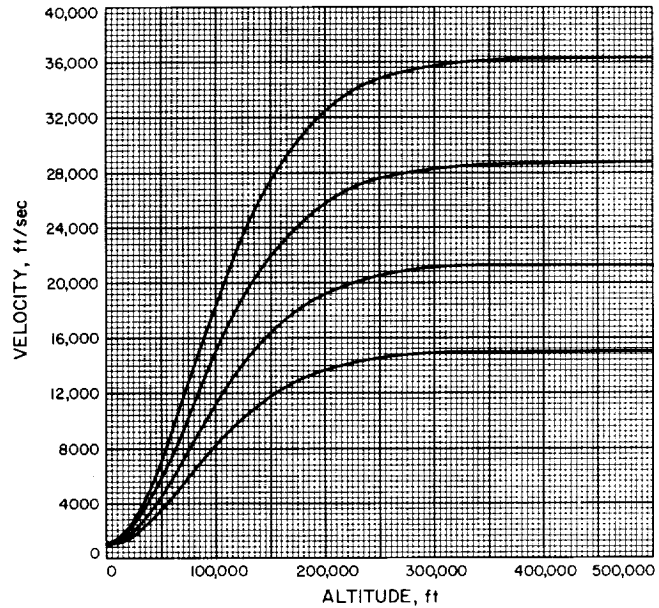


Fig. A-346

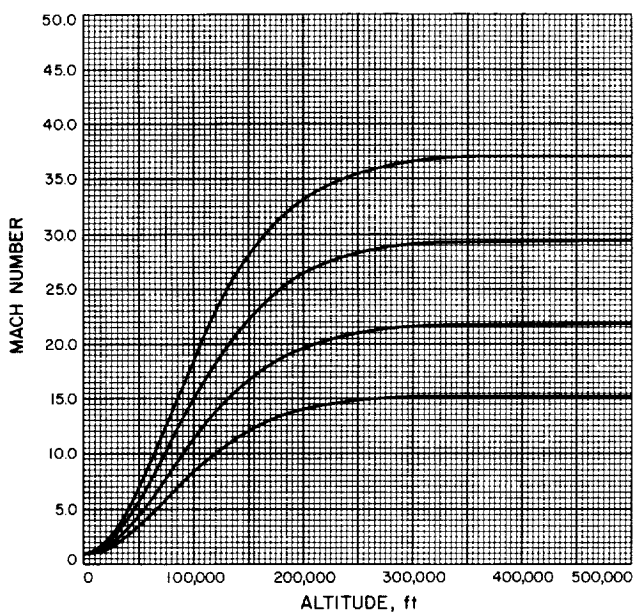


Fig. A-347

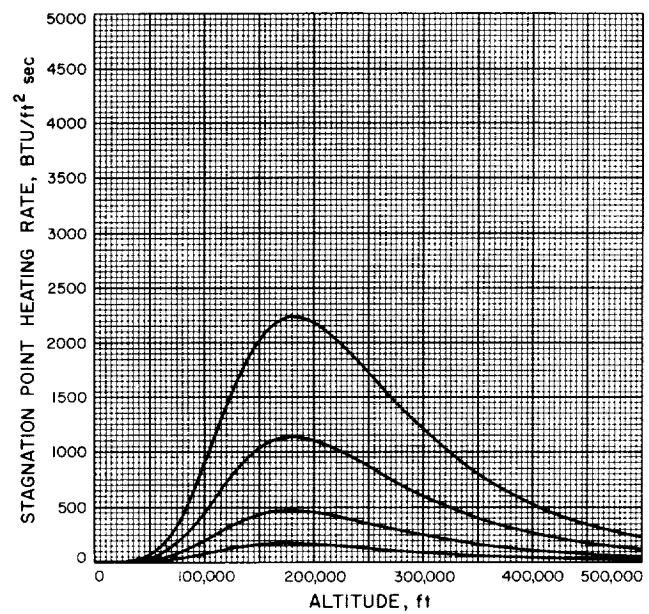


Fig. A-348

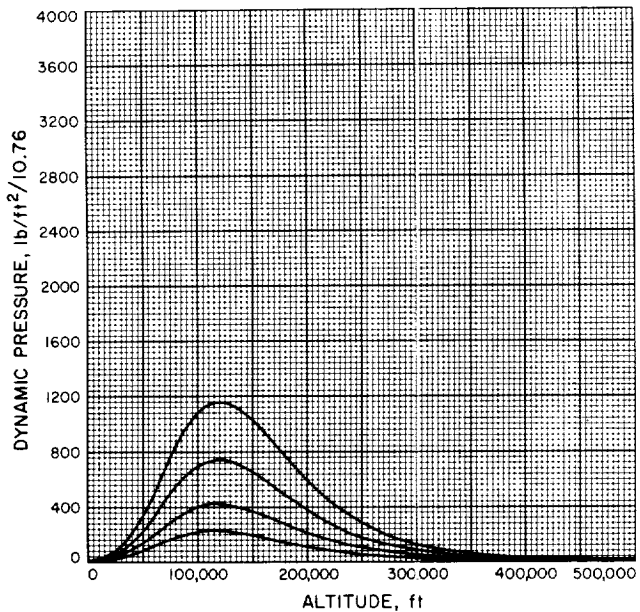


Fig. A-349

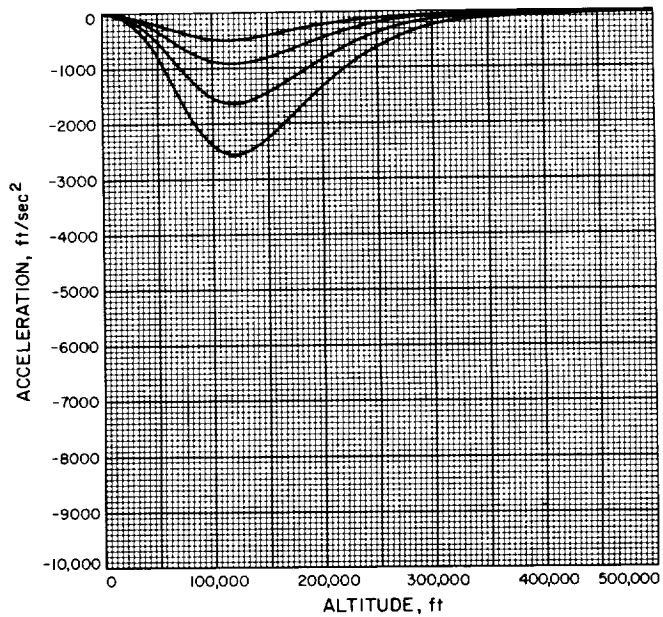


Fig. A-350

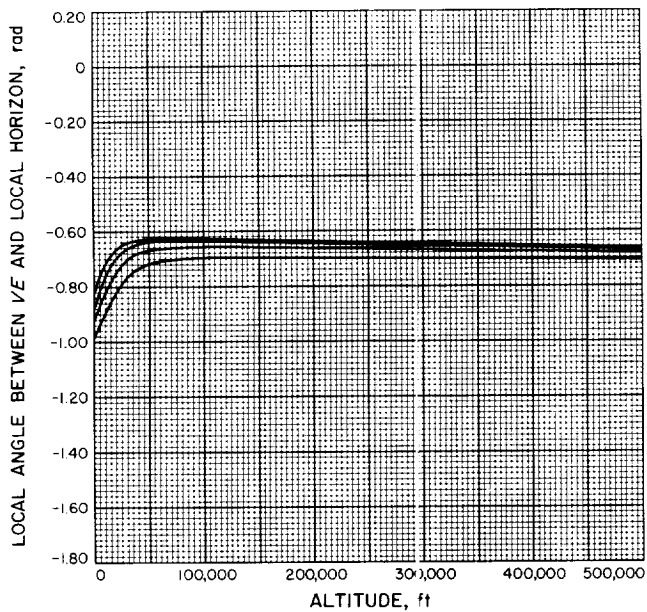
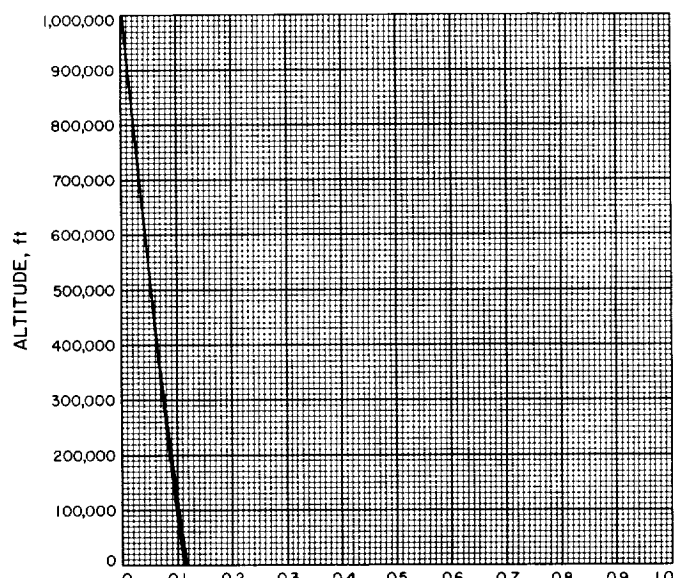


Fig. A-351



PLANET CENTERED ANGLE BETWEEN INITIAL AND
CURRENT VEHICLE POSITIONS, $\frac{\text{surface range}}{\text{Mars radius}}$

Fig. A-352

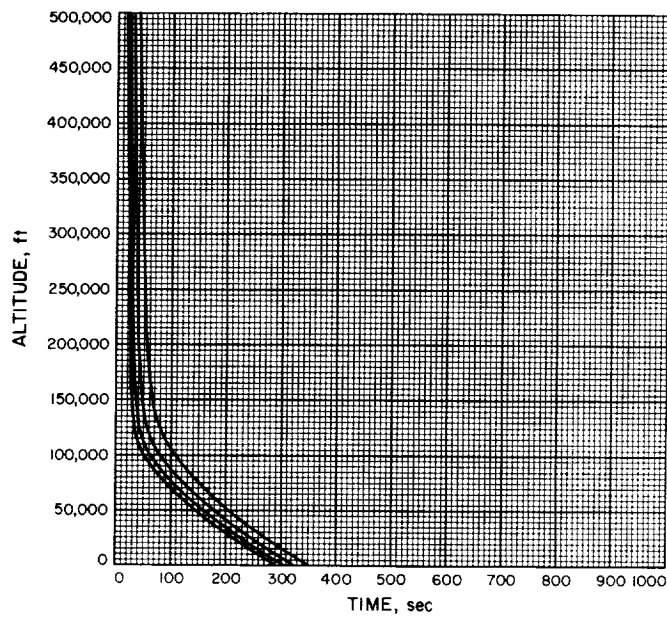


Fig. A-353

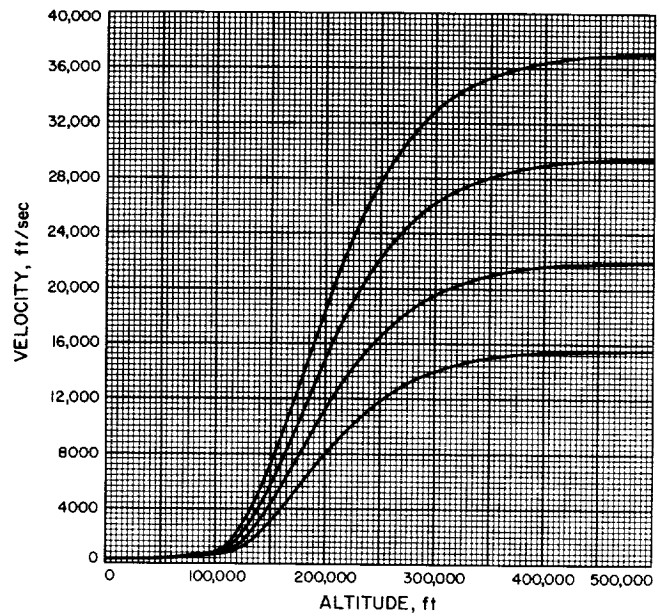


Fig. A-354

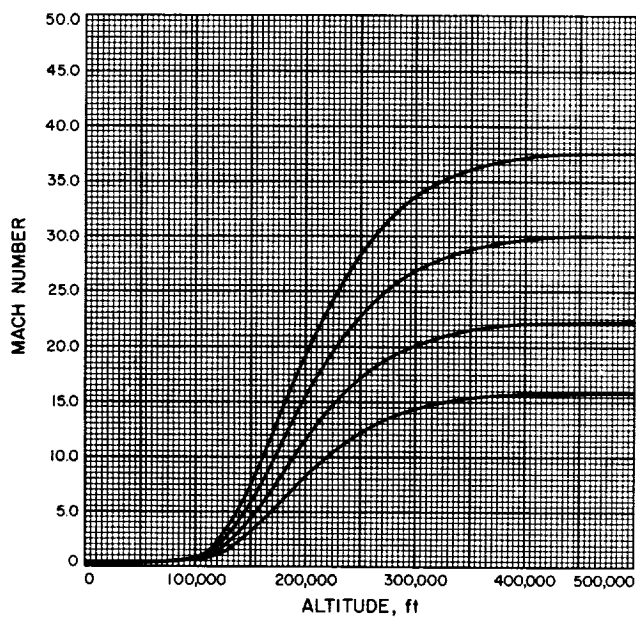


Fig. A-355

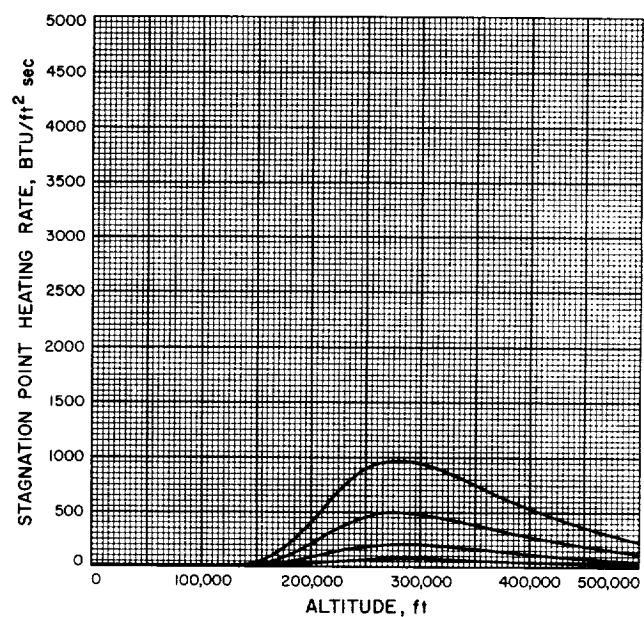


Fig. A-356

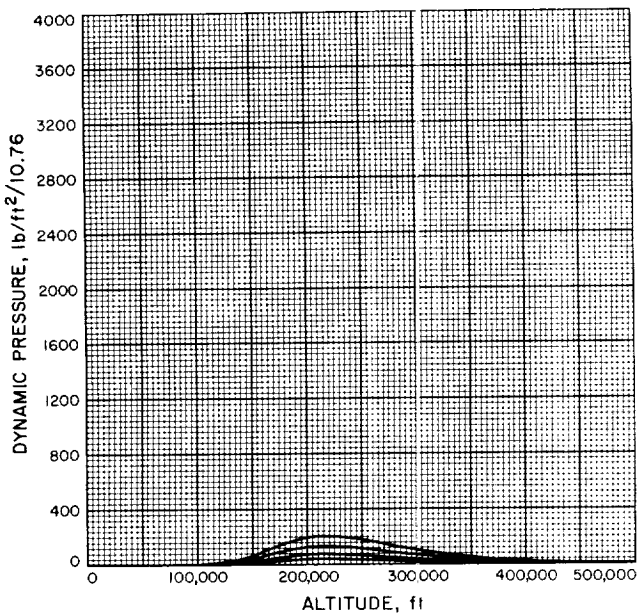


Fig. A-357

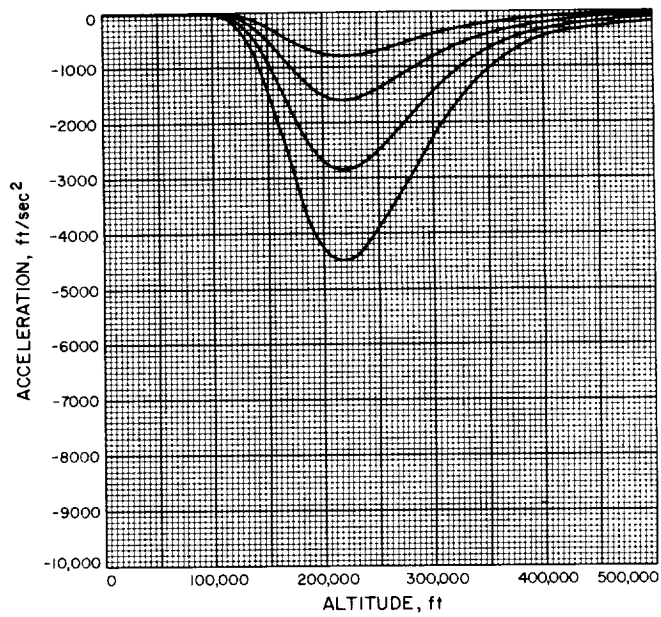


Fig. A-358

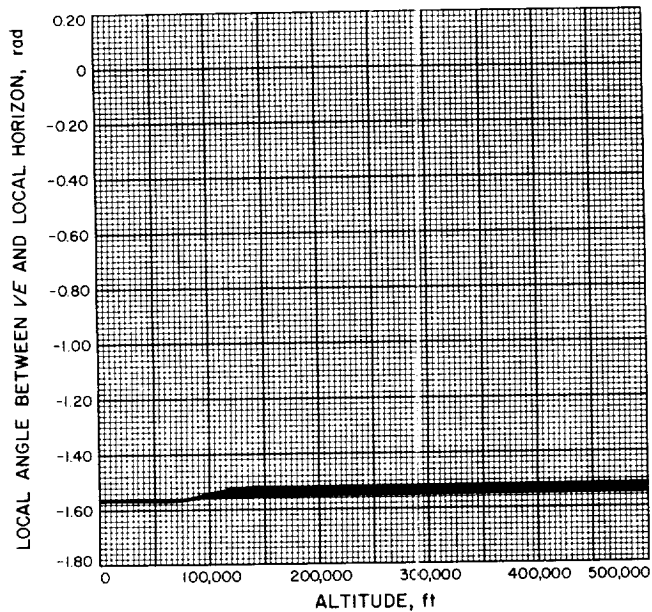


Fig. A-359

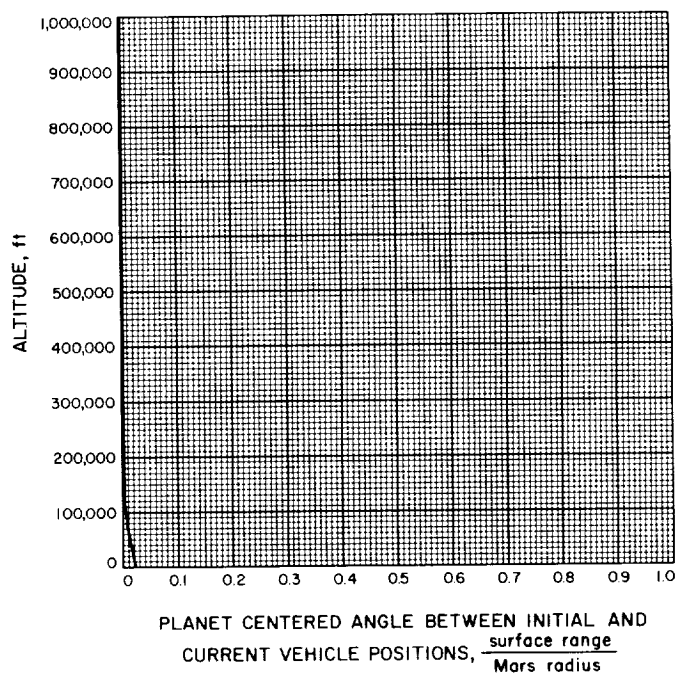


Fig. A-360

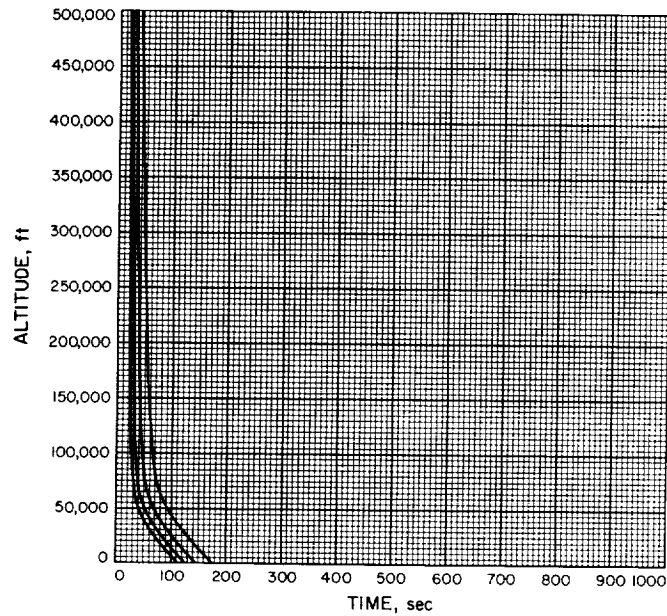


Fig. A-361

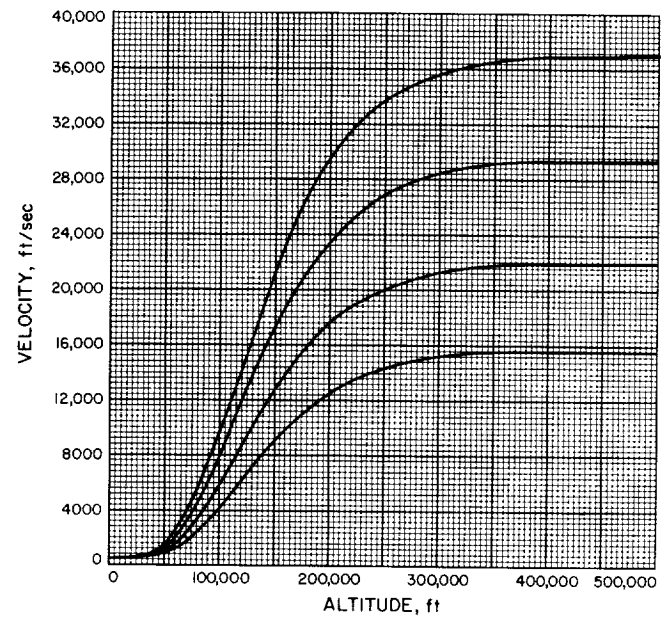


Fig. A-362

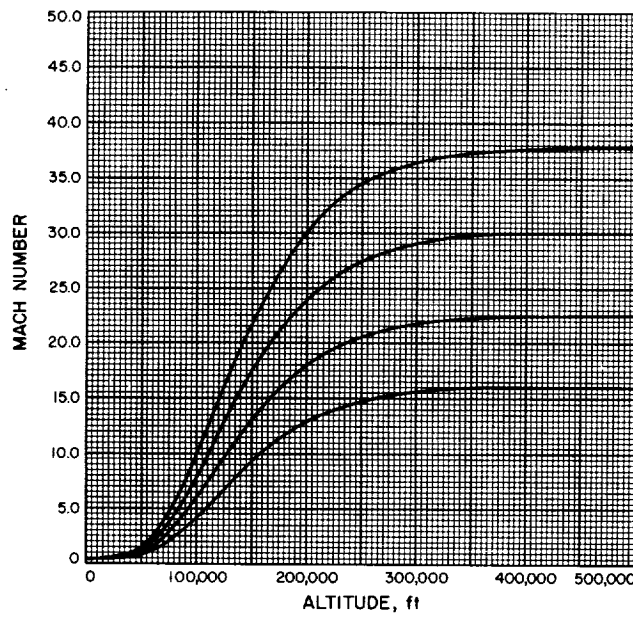


Fig. A-363

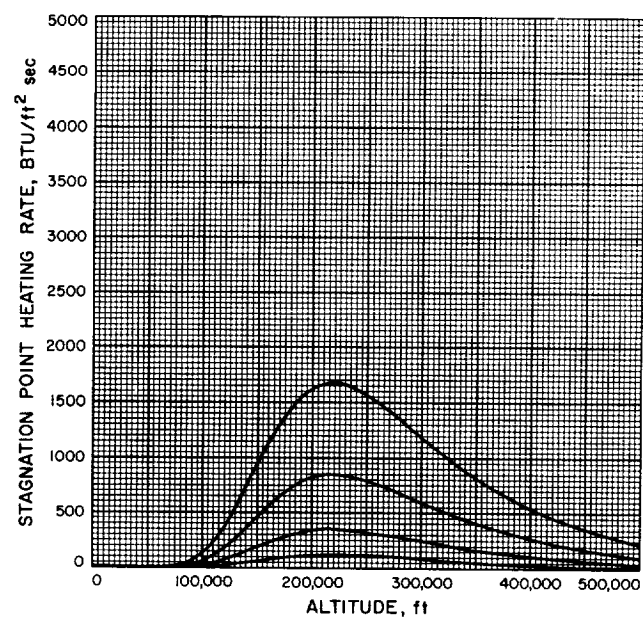


Fig. A-364

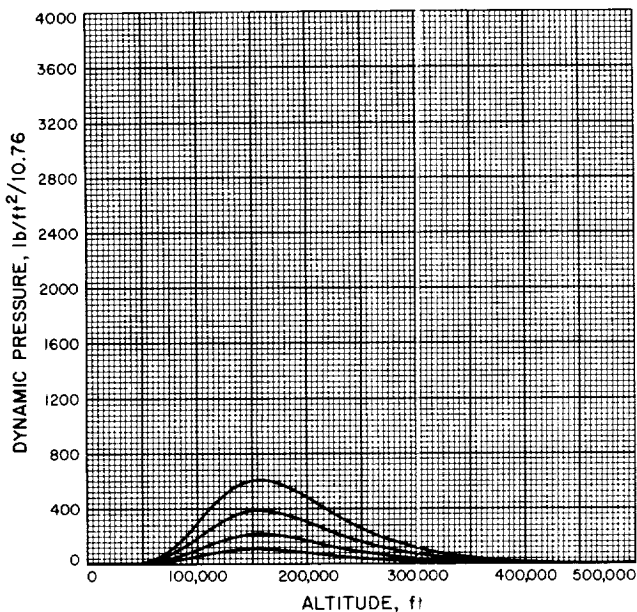


Fig. A-365

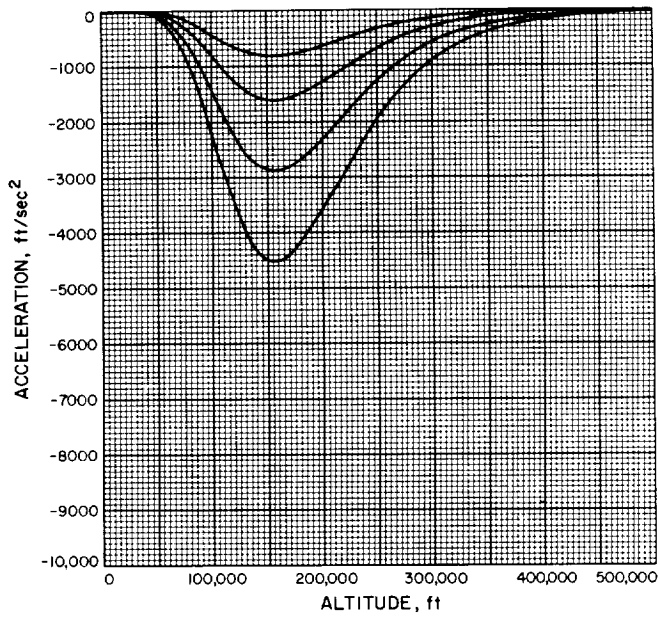


Fig. A-366

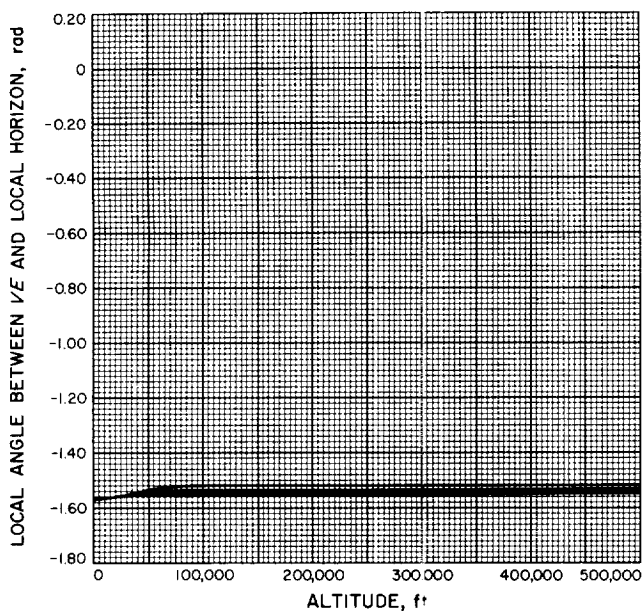


Fig. A-367

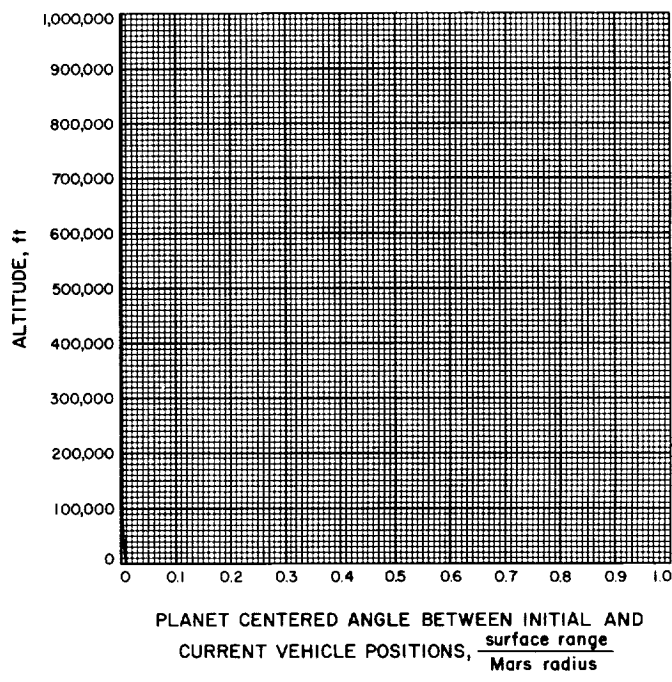


Fig. A-368

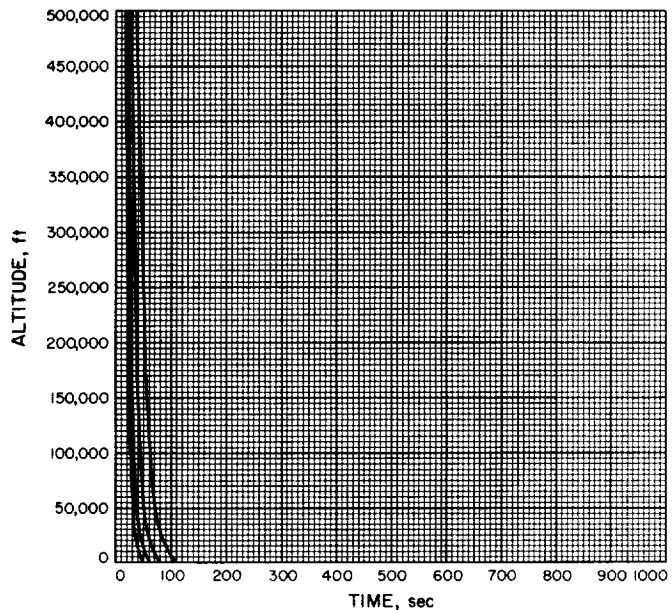


Fig. A-369

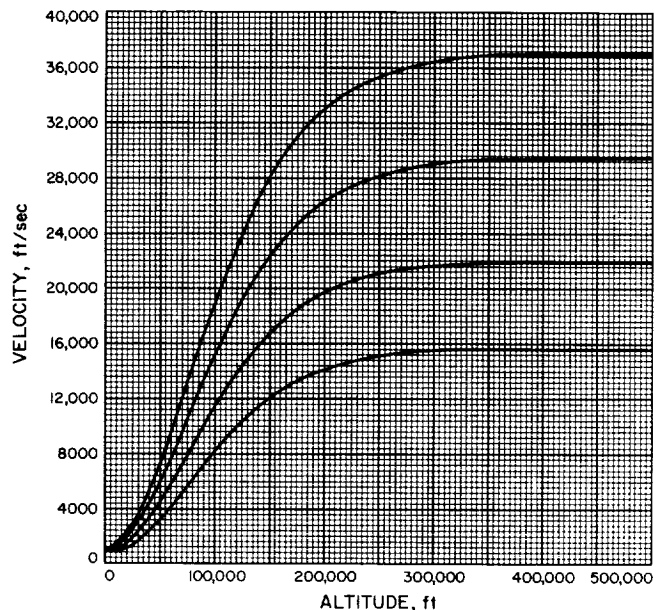


Fig. A-370

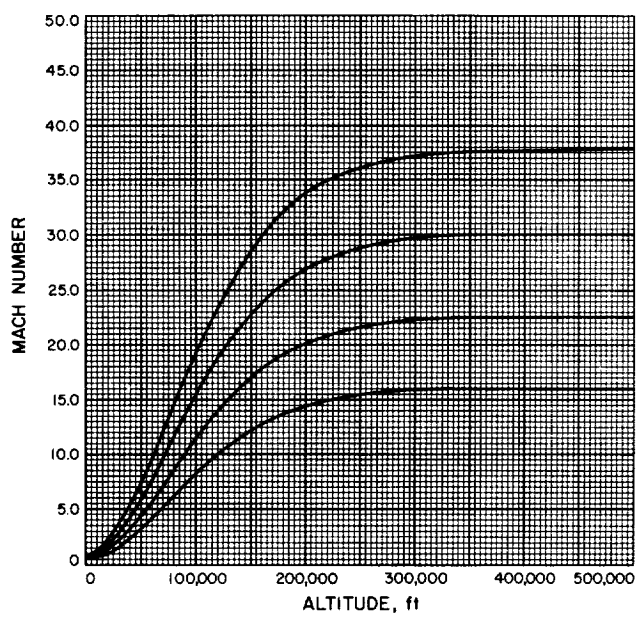


Fig. A-371

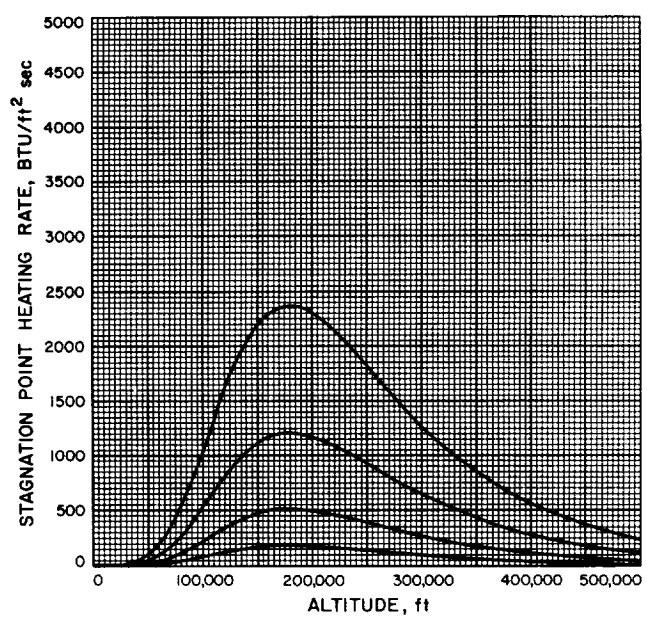


Fig. A-372

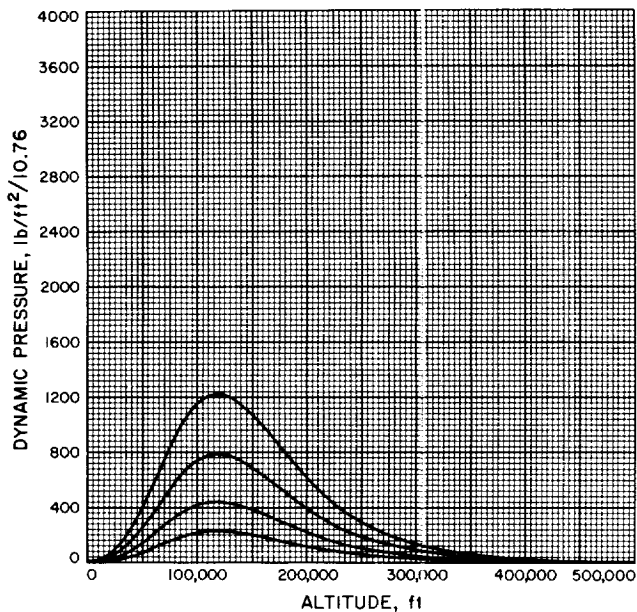


Fig. A-373

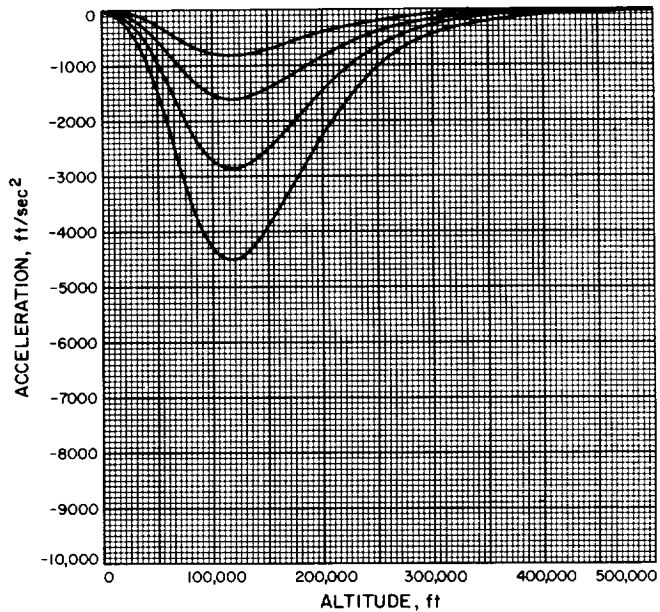


Fig. A-374

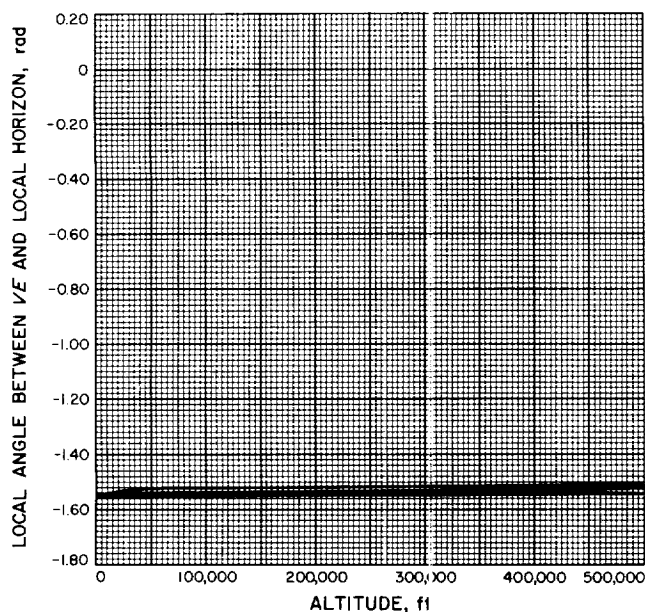


Fig. A-375

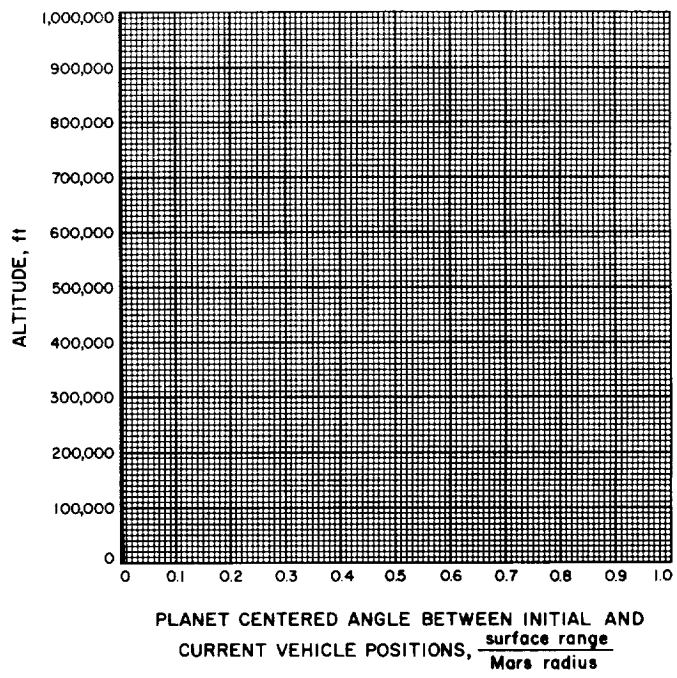


Fig. A-376

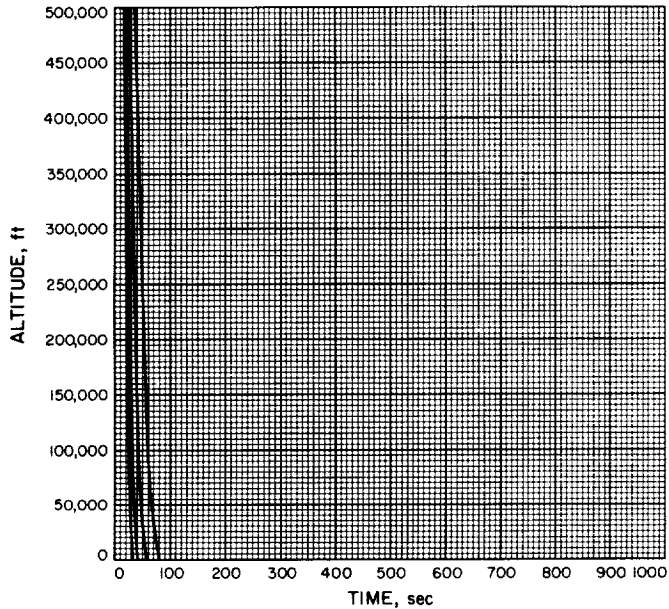


Fig. A-377

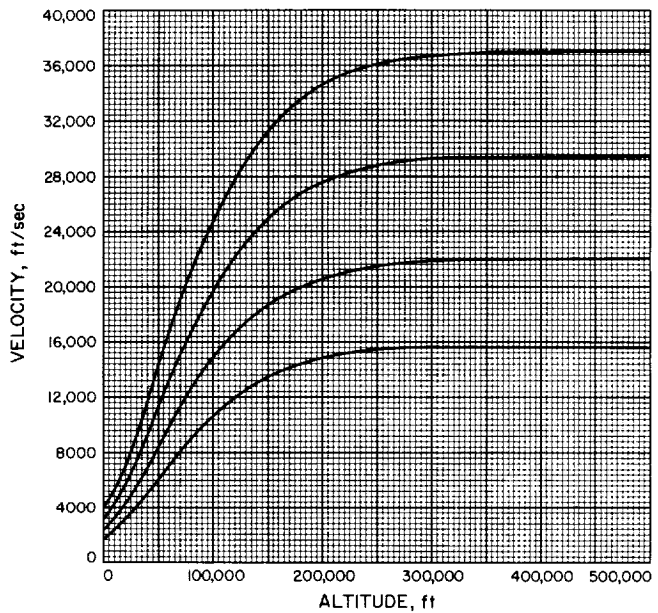


Fig. A-378

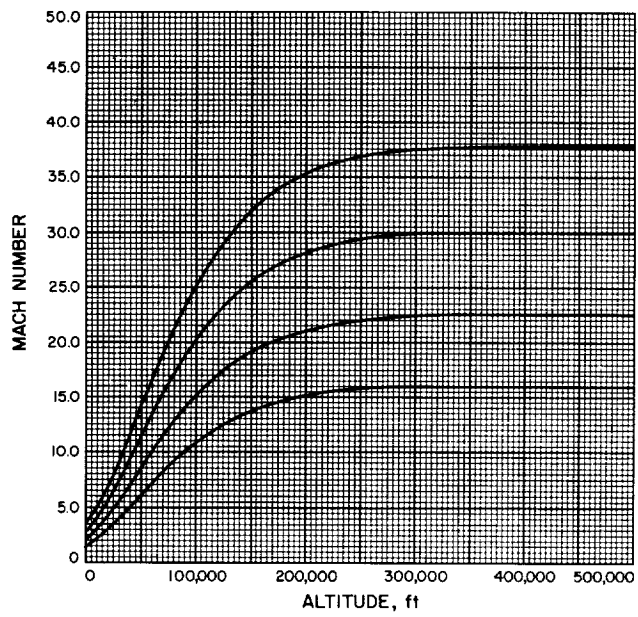


Fig. A-379

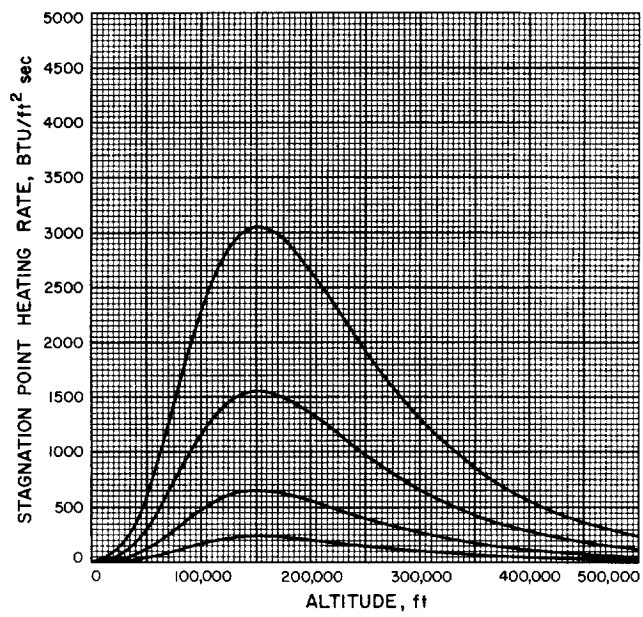


Fig. A-380

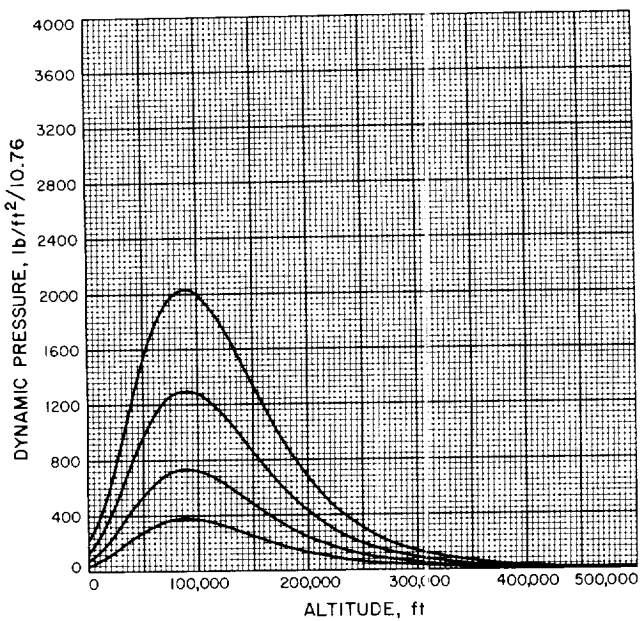


Fig. A-381

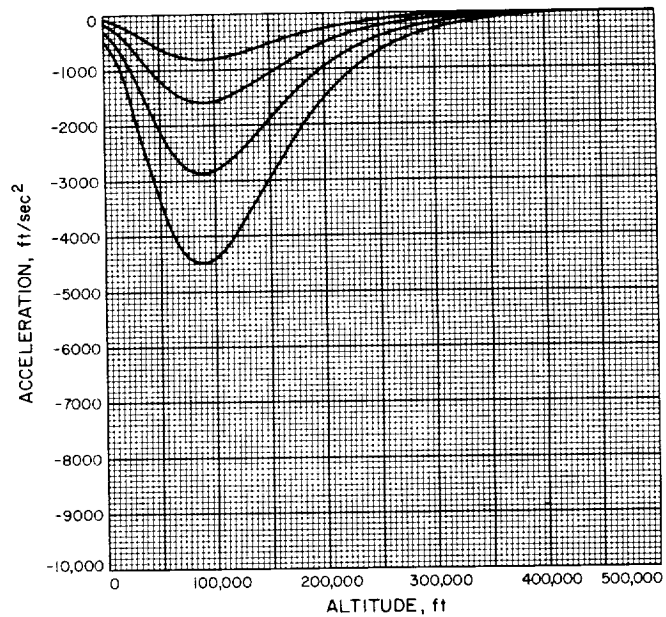


Fig. A-382

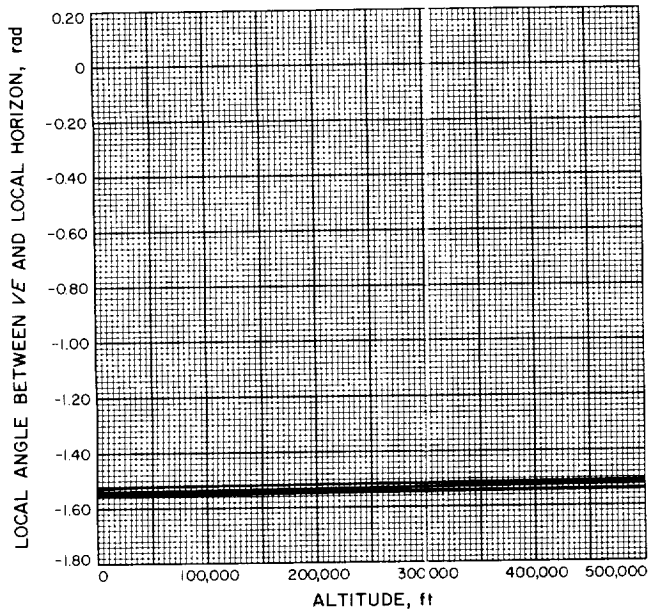


Fig. A-383

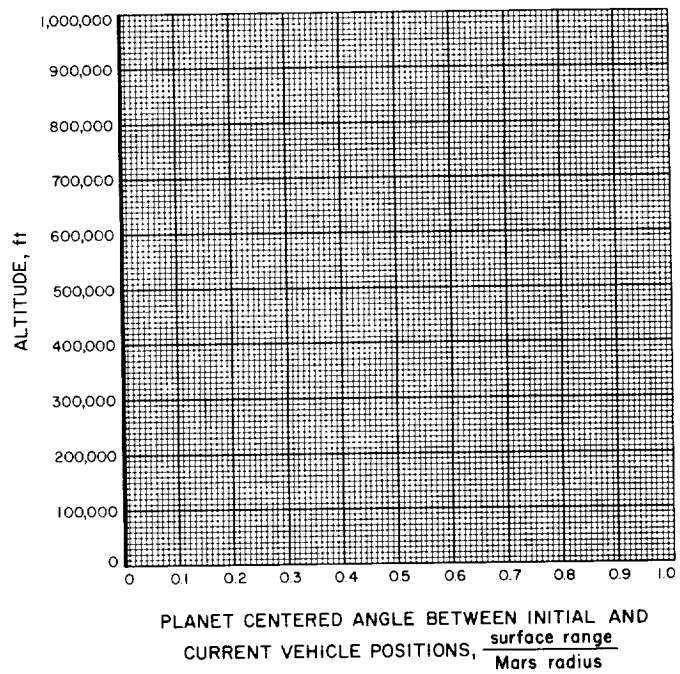


Fig. A-384

